Lecture Notes in Civil Engineering

Manish Kumar · Bikarama Prasad Yadav · Suvendu Manna · Abhishek Nandan · Rahul Silori · Somnath Fulari *Editors*

Proceedings of the International Conference on the Health, Safety, Fire and Environmental Advances

Issues, Innovations and Iterations for the Sustainable Environment

Springer

Lecture Notes in Civil Engineering 899

Series Editors

Marco di Prisco, *Politecnico di Milano, Milano, Italy*
Sheng-Hong Chen, *School of Water Resources and Hydropower Engineering, Wuhan University, Wuhan, China*
Ioannis Vayas, *Institute of Steel Structures, National Technical University of Athens, Athens, Greece*
Sanjay Kumar Shukla, *School of Engineering, Edith Cowan University, Joondalup, Australia*
Anuj Sharma, *Iowa State University, Ames, USA*
Nagesh Kumar, *Department of Civil Engineering, Indian Institute of Science Bangalore, Bengaluru, India*
Chien Ming Wang, *School of Civil Engineering, The University of Queensland, Brisbane, Australia*
Zhen-Dong Cui, *China University of Mining and Technology, Xuzhou, China*
Xinzheng Lu, *Department of Civil Engineering, Tsinghua University, Beijing, China*

Lecture Notes in Civil Engineering (LNCE) publishes the latest developments in Civil Engineering—quickly, informally and in top quality. Though original research reported in proceedings and post-proceedings represents the core of LNCE, edited volumes of exceptionally high quality and interest may also be considered for publication. Volumes published in LNCE embrace all aspects and subfields of, as well as new challenges in, Civil Engineering. Topics in the series include:

- Construction and Structural Mechanics
- Building Materials
- Concrete, Steel and Timber Structures
- Geotechnical Engineering
- Earthquake Engineering
- Coastal Engineering
- Ocean and Offshore Engineering; Ships and Floating Structures
- Hydraulics, Hydrology and Water Resources Engineering
- Environmental Engineering and Sustainability
- Structural Health and Monitoring
- Surveying and Geographical Information Systems
- Indoor Environments
- Transportation and Traffic
- Risk Analysis
- Safety and Security

To submit a proposal or request further information, please contact the appropriate Springer Editor:

– Pierpaolo Riva at pierpaolo.riva@springer.com (Europe and Americas);
– Swati Meherishi at swati.meherishi@springer.com (Asia—except China, Australia, and New Zealand);
– Wayne Hu at wayne.hu@springer.com (China).

All books in the series now indexed by Scopus and EI Compendex database!

Manish Kumar · Bikarama Prasad Yadav ·
Suvendu Manna · Abhishek Nandan ·
Rahul Silori · Somnath Fulari
Editors

Proceedings of the International Conference on the Health, Safety, Fire and Environmental Advances

Issues, Innovations and Iterations for the Sustainable Environment

Springer

Editors
Manish Kumar
School of Engineering and Sciences
Tec de Monterrey
Monterrey, Mexico

Bikarama Prasad Yadav
Sustainability Cluster
UPES
Dehradun, Uttarakhand, India

Suvendu Manna
Sustainability Cluster
UPES
Dehradun, Uttarakhand, India

Abhishek Nandan
Sustainability Cluster
UPES
Dehradun, Uttarakhand, India

Rahul Silori
Sustainability Cluster
UPES
Dehradun, Uttarakhand, India

Somnath Fulari
MAKEEN Energy
Hyderabad, Telangana, India

ISSN 2366-2557 ISSN 2366-2565 (electronic)
Lecture Notes in Civil Engineering
ISBN 978-981-92-3199-7 ISBN 978-981-92-3200-0 (eBook)
https://doi.org/10.1007/978-981-92-3200-0

© The Editor(s) (if applicable) and The Author(s), under exclusive license to Springer Nature Singapore Pte Ltd. 2026

This work is subject to copyright. All rights are solely and exclusively licensed by the Publisher, whether the whole or part of the material is concerned, specifically the rights of translation, reprinting, reuse of illustrations, recitation, broadcasting, reproduction on microfilms or in any other physical way, and transmission or information storage and retrieval, electronic adaptation, computer software, or by similar or dissimilar methodology now known or hereafter developed.
The use of general descriptive names, registered names, trademarks, service marks, etc. in this publication does not imply, even in the absence of a specific statement, that such names are exempt from the relevant protective laws and regulations and therefore free for general use.
The publisher, the authors and the editors are safe to assume that the advice and information in this book are believed to be true and accurate at the date of publication. Neither the publisher nor the authors or the editors give a warranty, expressed or implied, with respect to the material contained herein or for any errors or omissions that may have been made. The publisher remains neutral with regard to jurisdictional claims in published maps and institutional affiliations.

This Springer imprint is published by the registered company Springer Nature Singapore Pte Ltd.
The registered company address is: 152 Beach Road, #21-01/04 Gateway East, Singapore 189721, Singapore

If disposing of this product, please recycle the paper.

Contents

Influence of Addition of Various Fillers on Char Expansion of Fire-Retardant Intumescent Coatings for Steel Structures 1
Charu Mehta, A. Aravind Kumar, Mahesh Kumar Tiwari, Rakesh Kumar, and Mohammad Ahmad Shoeb

Assessment and Management of Risk on Account of Forest Fires 10
Niteen R. Yeole

Sustainable Techniques for Improvement of Black Cotton Soils 22
Guruprasad Ajay Chavan and Purnanand Savoikar

Efficient Removal of Acid Orange 7 Dye Using Acid-Activated Biochar Derived from *Averrhoa Carambola*: A Sustainable Approach for Wastewater Treatment 32
Anushree Srivastava, Atul Srivastava, and Vandana Saxena

The Sacred Art of Crafting Japamala: A Fusion of Tradition and Sustainable Innovation Though Fashion and Engineering 49
Achuthy Kottangal

Optimizing Healthcare System Performance with Smart Device Usage in Cloud-Fog Systems 64
Sumit Bansal and Sunil Kumar

Evaluation of Engineering Properties of Sandy Soil Stabilized with RBI Grade-81 Stabilizer 77
Neero Gumsar Sorum and Jinata Sanasam

Biodiesel Production with Algae Oil Blend with ANFIS, ANN and RSM Technique 88
Sunil Kumar, Siddharth Jain, and Harmesh Kumar

Prediction of Biodiesel Production from Algae Oil by Different Algorithm in Machine Learning 102
Sunil Kumar, Siddharth Jain, and Harmesh Kumar

Critical Parameters and Indicators for Assessing Soil Health 117
Srishti Sinha Ray, Dimple Bhadane, and Nishu Goyal

Comparative Analysis of Enhanced Power Yield Through Photovoltaic System Under Partial Shading Situations by Simulations and Experimental Setup 128
Divya Ahluwalia and Shahroz Anjum

Circular-Core PCF Employing Different Materials of Nano-rods for Sensing Enhancement 138
Simarpreet Kaur, Vikas Wasson, and Ruchi

Status of CCUS Project Viability for Mumbai Offshore and Cambay Basins, Western India 149
Rahul Kumar Singh and Atul Kumar Patidar

The Serious 2018 Summer Water Crisis in Shimla 160
Navjot Hothi

Reviving Tradition: Exploring the Craft of "Chindi Dari" of Uttarakhand for Sustainable Textile Upcycling and Wearable Innovations 168
Priyanka Sharma and Nilakshi Yein

Industrial Waste Utilization in Concrete: Towards Sustainable Green Materials for Achieving Net Zero Emissions and Improving Indoor Air Quality 175
J. S. Sudarsan, Swati Sinha, R. Padmapriya, and N. Sunmathi

Multiple-Degradation CID:IQ Dataset 191
Vikas Wasson, Bikrampal Kaur, Suniti Dutt, and Simarpreet Kaur

Author Index 207

Influence of Addition of Various Fillers on Char Expansion of Fire-Retardant Intumescent Coatings for Steel Structures

Charu Mehta[1(✉)], A. Aravind Kumar[1], Mahesh Kumar Tiwari[2], Rakesh Kumar[1], and Mohammad Ahmad Shoeb[1]

[1] Fire Research Division, CSIR-Central Building Research Institute, Roorkee, Uttarakhand, India
charumehta.009@gmail.com

[2] Associate Professor, Centre for Excellence Occupational Health, Safety, Fire & Environment (C-OHSFE), GD Goenka University, Gurgaon, Haryana, India

Abstract. When steel reaches temperatures above 500 °C during accidental fires, it loses its mechanical strength. Fire safety of steel structures is one of the important factors to consider when designing construction infrastructure because it can save human lives and valuable property. An Intumescent coating acts as a protective layer on the steel structures at high temperatures, as it produces a carbonaceous char on reaction to fire. The char layer formed acts as insulation during fire accidents, protecting the steel structures physically and thermally. The coating composition is formulated to produce an effective carbonaceous char. An Intumescent coating is made up of fire-retardant additives and fillers combined with a binder and a solvent. The incorporation of fire-retardant fillers in the coating composition results in a variety of alterations to the produced char layer, including increased fire resistance, altered char layer growth rate, and strengthened char structure. This chapter presents the char expansion results that occur when various fillers are added to water-based fire-retardant Intumescent coating compositions.

Keywords: Coatings · Intumescence · Char layer · Steel structures · Fillers

1 Introduction

Steel is commonly used in building construction either as the primary structural material or as reinforcement for concrete structures. In the case of a fire, unprotected steel constructions might not have the requisite fire resistance. This is because, in a fire, the temperature of exposed steel components rises rapidly due to steel's strong heat conductivity. Abbas Rezaeian studied the behaviour of welded members and connections in fire-induced steel structures. He discovered that when exposed to temperatures above 400 °C, the strength of steel welds decreased rapidly. At 600 °C and 800 °C, the welds lost 50% and 8% of their initial ultimate strength, respectively (Rezaeian et al. 2020). Because the load-bearing capacity of a steel structure is related to its strength, the structure may eventually be damaged or collapse if its strength is reduced to a critical level

© The Author(s), under exclusive license to Springer Nature Singapore Pte Ltd. 2026
M. Kumar et al. (Eds.): HSFEA 2023, LNCE 899, pp. 1–9, 2026.
https://doi.org/10.1007/978-981-92-3200-0_1

that cannot handle the loads imposed on it. As a result, steel structures are susceptible to fire attacks.

According to studies, applying fire-retardant coatings to steel structures' surfaces can successfully protect them from high temperatures, keep their temperature below their critical point, increase the length of time that they resist fire, and effectively lower fire loss. Fire-retardant coatings on steel structures are classified as intumescent or non-intumescent based on their fire-prevention method. Intumescent coatings are being widely used in fire safety procedures as the most effective approach for the reactive fire protection of building steel. These coatings are well-known for their ability to provide efficient fire safety measures without compromising the visual appeal or architectural integrity of steel buildings (Lucherini and Maluk 2019). Intumescent coatings are usually composed of an acid source (also known as a "catalyst"), a carbonaceous compound (sometimes known as "carbonific"), a blowing agent (also known as "spumific"), binders, and additives (Puri and Khanna 2017). In the event of a fire, an acid-releasing catalyst, such as ammonium polyphosphate (APP), is used to initiate the process. When exposed to temperatures above 250 °C, the catalyst releases acid that reacts with the carbon source, like penta-erythritol (PER), to form char. Meanwhile, the spumific agent, such as melamine (MEL), decomposes to liberate gases, causing foaming. This foam ultimately solidifies to form a barrier against heat transfer (Gu et al. 2007). In the study conducted by Yew Ming Chian, it was found that flame-retardant additives improved the fire protection and thermal properties of water-based intumescent coatings on steel structures. The coating with a 2:1:1 ratio of APP, MEL, and PER demonstrated good water resistance, adhesion strength, uniform char layer formation, and thermal stability, making it an effective option for fire protection performance (Kun et al. 2018).

Binders play an important role in the formation of the char structure. It develops the film and binds all the components together. The polymer binder serves as a shield for the substrate and the components inside the film. It ensures that the fillers, additives, and resin are distributed evenly. The type of binder employed determines whether an intumescent coating is solvent-based or water-based. Solvent-based coatings make use of polymer binders, which evaporate to form a hard film. During this process, the thinner solvent evaporates, increasing the molecular mass of the polymer and resulting in the formation of a three-dimensional molecule. The 3D molecule then solidifies, forming a strong, chemically resistant protection. However, one significant disadvantage of solvent-based coatings is their toxicity. This is due to the existence of volatile organic compounds (VOCs), which evaporate quickly and have the potential to harm individuals and the environment. Water-based coatings, on the other hand, distribute the resin by using water as a solvent. These coatings are resilient to heat and abrasion, have strong adhesion, and are low in toxicity. In contrast to solvent-based coatings, they have a longer drying time and a worse resistance to hydrolysis. Although water-based coatings are easier to use and less harmful to the environment than solvent-based coatings, they are not as weather-resistant. Solvent-based coatings work best outside, whereas water-based coatings are generally more appropriate for indoor use.

1.1 Effect of Various Fillers on Fire Retardant Intumescent Coatings

The use of fire-retardant fillers in intumescent coating greatly improves its ability to protect against fire. By adding these fillers, we can significantly reduce the flammability and burning of the polymer in the coating. Additionally, the filler has an impact on the polymer's melt rheology, which can affect the way it drips. The effect of expandable graphite (EG) on the fire protection properties of epoxy-based intumescent fire-retardant coating for steel buildings was investigated by Sami Ullah. The results indicated that the formulation containing 9.8% EG exhibited the highest residual mass and largest char expansion among the formulations (Ullah et al. 2021). M.C. Yew researched the effects of different combinations and individual flame-retardant fillers on the mechanical and fire-retardant properties of coatings. The findings of the study showed that the choice of suitable filler combinations had a significant impact on the coatings' chemical and physical properties (Yew et al. 2015). Ying Zeng investigated the effects of five ingredients on the fire-resistance properties of epoxy-based intumescent coatings: ammonium polyphosphate, melamine, TiO_2, $CaCO_3$, and vitreous silicate fiber. She found that increasing the amount of any one of the three fillers reduced the expansion of the coatings while enhancing the mechanical stability of the char (Zeng et al. 2020). Using various filler combinations, Mohammadreza Nasirzadeh developed an intumescent coating, and several test techniques were used to evaluate its characteristics. When vermiculite, celite, and ATH were evaluated, the findings indicated that the intumescent paint containing 3% vermiculite performed better (Nasirzadeh et al. 2023).

2 Materials and Methods

2.1 Sample Preparation

The intumescent coatings (W1–W10) with varying compositions in weight% %, as indicated in Table 1, were developed by using an acid source, a carbon source, a blowing agent, and a fire-retardant filler (water-based polyvinyl acetate) as well as fire-retardant additives. Before the testing, a mixture consisting of water-based binder, fillers, and additives was put on the steel sheet and allowed to dry for a full day. The difference in the coatings was due to the addition of various fillers. As shown in Table 1, specimen W1 did not contain any filler, and different fillers—TiO_2, $CaCO_3$, sodium silicate, calcium silicate, Mg $(OH)_2$, silica gel, aluminum hydroxide, gypsum, and expandable graphite were added to W2 to W10, respectively.

2.1.1 Preliminary Test

In the initial testing phase, the thickness of the char layer was measured to determine the effectiveness of the coating samples in protecting against fire. Sheets with a coating thickness of approximately 1 mm were coated with the different formulations and subjected to a preliminary test using a non-luminous premixed flame gas torch with a flame temperature of almost 1000 °C, as depicted in Fig. 1. The compositions were specifically designed to achieve a thicker and stronger char layer to protect the underlying steel sheet. The thickness of the char layer was quantified using a metric scale.

Table 1. Coating formulations (weight%)

	W1	W2	W3	W4	W5	W6	W7	W8	W9	W10
Acid source	23.70	23.70	23.70	23.70	23.70	23.70	23.70	23.70	23.70	23.70
Carbon source	14.81	14.81	14.81	14.81	14.81	14.81	14.81	14.81	14.81	14.81
Blowing agent	14.81	14.81	14.81	14.81	14.81	14.81	14.81	14.81	14.81	14.81
Binder	11.11	11.11	11.11	11.11	11.11	11.11	11.11	11.11	11.11	11.11
Solvent	29.63	29.63	29.63	29.63	29.63	29.63	29.63	29.63	29.63	29.63
TiO_2	–	5.93	–	–	–	–	–	–	–	–
$CaCO_3$	–	–	5.93	–	–	–	–	–	–	–
Sodium-meta-Silicate	–	–	–	5.93	–	–	–	–	–	–
Calcium silicate	–	–	–	–	5.93	–	–	–	–	–
Mg $(OH)_2$	–	–	–	–	–	5.93	–	–	–	–
Silica gel	–	–	–	–	–	–	5.93	–	–	–
Al $(OH)_3$	–	–	–	–	–	–	–	5.93	–	–
Gypsum	–	–	–	–	–	–	–	–	5.93	–
Expandable graphite	–	–	–	–	–	–	–	–	–	5.93



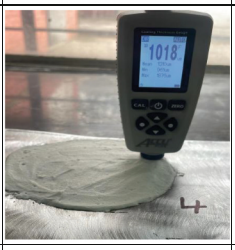
Fig. 1. **a** Gas torch preliminary test, **b** GI sheet showing samples for preliminary test, **c** flame temperature- 927.2 °C

3 Results

3.1 Appearance and Expansion of Intumescent Coatings

The char expansion was observed after the preliminary test, and the effect of the addition of various fillers on char expansion and char structure was compared in the various specimens of intumescent coatings in Table 2. Also, Table 2 shows the average coating thickness of the specimens. As shown in the table, a char thickness of 20 mm was found when no filler was added to the composition, i.e., specimen W1.

Table 2. Coating thickness, char thickness, and the char structure of various specimens.

	Coating thickness	Char thickness	Char structure
W1			
W2			
W3			
W4			
W5			

(*continued*)

Table 2. (*continued*)

W6			
W7			
W8			
W9			
W10			

The filler TiO_2 was added to specimen W2, which increased the char thickness to 25 mm and improved the char structure. TiO_2 adds porosity and expands the volume, leading to improved flame retardancy, insulation, and height expansion. TiO_2 can improve the foam structure of char residue, increase the weight of coating residues,

and improve the anti-oxidation characteristics of char layers. These effects lead to a lower flame-spread rate, as explained by Mohd Sabee (2022).

On addition of $CaCO_3$ as filler in specimen W3, char thickness was found to be 20 mm, like W1, which showed that there was no increase in char layer due to the addition of $CaCO_3$ as filler. There was an improvement in the char structure as it was observed to show more strength as compared to W1. This was following the results of the study done by K. Md Nasir in which the intumescent system was improved by the addition of various fillers (TiO_2, aluminum tri-hydroxide, magnesium hydroxide, and calcium carbonate) (Nasir 2018).

Alkali silicates as fillers were added to specimens W4 and W5, which contributed to an increase in char thickness to 25 mm and 28 mm, respectively. K. Md Nasir's study developed an inorganic flame-retardant coating by using sodium silicate as a ceramizable binder and meta-kaolin (9:1) with additional ingredients. The coating resulted in the formation of a protective carbon char on top of silicon dioxide networks that provided fire resistance at high temperatures (Chen 2021). Hence, alkali silicates prove to increase intumescence potential as they can self-intumescence at lower temperatures, which is associated with the release of H_2O (Ahmadi et al. 2024).

Hydroxides (magnesium hydroxide and aluminum tri-hydroxide) as fillers were added as fillers to specimens W6 and W8, which are non-toxic and environmentally friendly chemicals that are effective in reducing smoke, absorbing toxic fumes, and showing flame retardant behavior by releasing water vapors in their dehydration process. The water vapors released during their decomposition can absorb toxic fumes, cool the surface, and form a protective layer of MgO and Al_2O_3 (Scionti et al. 2023). As seen from Table 2, Mg $(OH)_2$ in W6 did not contribute to char expansion (char thickness-10 mm), but its degradation helps absorb smoke and toxic fumes. Al $(OH)_3$ in W8 contributed to char expansion (char thickness-30 mm) and is an environmentally friendly filler, which reduced smoke on its decomposition.

Adding silica as filler in specimen W7 increased the char thickness to 30 mm. The char foam was found to be hard, and a uniform char layer was formed. Also, good char adhesion with the substrate was observed in the specimen. Hence, silica as filler contributes to providing resistance to fire by forming a hard and thick char layer. In a study by Ming Chian Yew, silica fumes were used as a binder to synthesize a fire-retardant intumescent coating, and the study revealed that adding silica fumes increased the residual weight, dense structure, and thermal stability of coatings (Yew and Sulong 2012).

Gypsum, as a fire-retardant filler, was added to specimen W9, which showed an increase in char expansion to 30 mm. Gypsum-calcium sulphate di-hydrate has shown promising effects on the morphology of char formed by fire-retardant intumescent coatings. Gypsum occurs naturally in the form of crystals containing two water molecules within the crystal structure. When gypsum is heated, water molecules are gradually released, lowering the polymer matrix's temperature. As a result, the formed calcium sulphate settles onto the surface and forms a protective layer that acts as a fire-resistant barrier against the transfer of heat (Bhoite et al. 2022).

W10 was found to increase the char thickness to 30 mm due to the addition of expandable graphite as filler. Expandable graphite acts as a fire-retardant filler as graphite

expands on heating to form an intumescent layer on the surface, which can slow the flame spread. It acts both as a carbonific agent and as a spumific agent in the intumescence mechanism. On heating, its structure forms porous voids, allowing cooling by flow of air, which can increase the time of ignition (Sabee 2022).

4 Conclusion

Various fillers contribute to char expansion in intumescent coatings, as shown in Fig. 2. A char expansion of 20 mm was found in specimen W1, and a thick char of a maximum of 30 mm was achieved on the addition of various fillers. Hence, it can be concluded that various fillers contribute to char expansion, absorb smoke, and improve char structure. The residue left behind after the filler breaks down could play a crucial role in creating a thermal barrier that prevents heat transfer from the external heat source to the underlying substrate. This makes it a highly significant aspect to consider in terms of providing insulation.

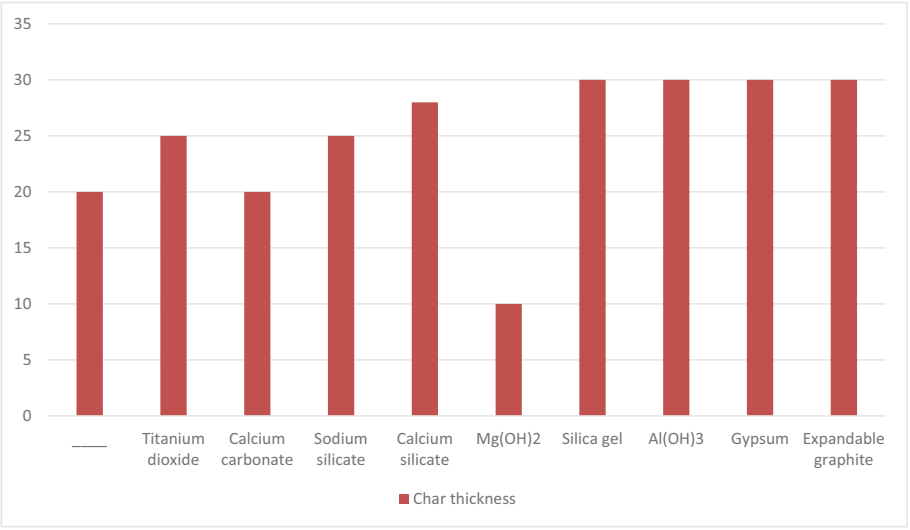


Fig. 2. Char expansion on the addition of various fillers

References

1. Rezaeian, A., Keshavarz, M., Hajjari, E.: Mechanical properties of steel welds at elevated temperatures. J. Constr. Steel Res. **167**, 105853 (2020). https://doi.org/10.1016/j.jcsr.2019.105853
2. Lucherini, A., Maluk, C.: Intumescent coatings used for the fire-safe design of steel structures: a review. J. Constr. Steel Res. **162**, 105712 (2019). https://doi.org/10.1016/j.jcsr.2019.105712
3. Puri, R.G., Khanna, A.S.: Intumescent coatings: a review on recent progress. J. Coat. Technol. Res. **14**, 1–20 (2017)

4. Gu, J.W., Zhang, G.C., Dong, S.L., Zhang, Q.Y., Kong, J.: Study on preparation and fire-retardant mechanism analysis of intumescent flame-retardant coatings. Surf. Coat. Technol. **201**(18), 7835–7841 (2007). https://doi.org/10.1016/j.surfcoat.2007.03.020
5. Kun, Y.M., Chian, Y.M., Huat, S.L., Han, B.J., Durairaj, R., Ching, N.T.: Optimization of flame-retardant additives on fire protection performance and thermal properties of water-based intumescent coating. J. Adv. Res. Appl. Mech. **49**(1), 12–23 (2018)
6. Ullah, S., et al.: Effects of expandable graphite on char morphology and pyrolysis of epoxy-based intumescent fire-retardant coating. J. Appl. Polym. Sci. **138**(41), 51206 (2021). https://doi.org/10.1002/app.51206
7. Yew, M.C., Sulong, N.R., Yew, M.K., Amalina, M.A., Johan, M.R.: Influences of flame-retardant fillers on fire protection and mechanical properties of intumescent coatings. Prog. Org. Coat. **78**, 59–66 (2015). https://doi.org/10.1016/j.porgcoat.2014.10.006
8. Zeng, Y., Weinell, C.E., Dam-Johansen, K., Ring, L., Kiil, S.: Effects of coating ingredients on the thermal properties and morphological structures of hydrocarbon intumescent coating chars. Progress Organic Coatings **143**, 105626 (2020). https://doi.org/10.1016/j.porgcoat.2020.105626
9. Nasirzadeh, M., Yahyaei, H., Mohseni, M.: Effects of inorganic fillers on the performance of the water-based intumescent fire-retardant coating. Fire Mater. **47**(1), 51–61 (2023)
10. Mohd Sabee, M.M.S., et al.: Flame retardant coatings: additives, binders, and fillers. Polymers **14**(14), 2911 (2022). https://doi.org/10.3390/polym14142911
11. Md Nasir, K., Ramli Sulong, N.H., Johan, M.R., Afifi, A.M.: An investigation into waterborne intumescent coating with different fillers for steel application. Pigm. Resin Technol. **47**(2), 142–153 (2018). https://doi.org/10.1108/PRT-09-2016-0089]
12. Chen, S.N., Li, P.K., Hsieh, T.H., Ho, K.S., Hong, Y.M.: Enhancements on flame resistance by inorganic silicate-based intumescent coating materials. Materials **14**(21), 6628 (2021). https://doi.org/10.3390/ma14216628
13. Ahmadi, H., Ulusoy, B., Fu, A., Dalmau, G., Wu, H., Dam-Johansen, K.: Inorganic intumescing alkali silicate particles. Ceram. Int. (2024). https://doi.org/10.1016/j.ceramint.2023.12.407
14. Scionti, G., Piperopoulos, E., Atria, M., Calabrese, L., Proverbio, E.: Effect of magnesium hydroxide and aluminum hydroxide as thermal barriers on the flame-retardant behavior of acrylic-based coating. Coatings **13**(9), 1517 (2023). https://doi.org/10.3390/coatings13091517
15. Yew, M.C., Sulong, N.R.: Fire-resistive performance of intumescent flame-retardant coatings for steel. Mater. Des. **34**, 719–724 (2012). https://doi.org/10.1016/j.matdes.2011.05.032
16. Bhoite, S.P., et al.: Understanding the influence of gypsum upon a hybrid flame retardant coating on expanded polystyrene beads. Polymers **14**(17), 3570 (2022)

Assessment and Management of Risk on Account of Forest Fires

Niteen R. Yeole(✉)

Department of Chemical Engineering, Energy Cluster, School of Advanced Engineering, UPES, Energy Acres, Dehradun, Uttarakhand, India
nryeole@ddn.upes.ac.in

Abstract. A major issue on a global scale is the spread of wildfires. Things will only become worse in the future. Climate change and human activity are the main contributing factors. Forest fires are a serious threat to human life, local flora and fauna and property. The release of harmful gases into the atmosphere, during any wildfire degrades the quality of air. The quick control over forest fires requires the deployment of resources such as firefighting system at appropriate locations. Forest fires may be mapped based on their intensities or risk levels. The risk assessment helps estimate the likelihood of forest fire, its intensity, and effects. Autonomous unmanned aerial vehicles (UAVs), watchtowers, sensors, and base stations must be strategically located to ensure optimal visibility. The conventional methods of forest fire risk assessment face certain challenges as the behaviour of forest fires are nonlinear and complex. Modern techniques such as machine learning (ML) algorithms or models such as random forests, support vector machines, etc., may be used to overcome the challenges faced. The accuracy of these algorithms may be increased through their combinations or integrations with other ML algorithms to give hybrid and ensemble models. The data sets required for risk assessment may be obtained through Geographic information system (GIS) or aerial monitoring. Meteorology and topography are important factors in the risk assessment of forest fires. For information to be accurate, dependable, and timely, satellite observation is essential. Present author reviews the literature and presents a case study on prediction of forest fire risk for the region 'Dhanaulti Reserved Forest', Uttarakhand, India. The case study highlights the use of Microsoft Excel® in the analysis of weather data.

Keywords: Forest fires · Risk assessment · Management · Machine learning · Remote sensing · Satellite data · Geographic information system

1 Introduction

Globally, 1.3% of all forests are destroyed by the 200,000+ forest fires that occur each year [1]. A huge area of forest is affected by fires every year [2, 3]. The main reason behind the destruction of forests in India is a forest fire. It affects the structure of the ecosystem in the forest [4, 5]. In most cases, the nature of forest fire is found to be a ground fire. The fuel for such fire is a bioresidue, that is a dry fallen leaf of a tree. In

© The Author(s), under exclusive license to Springer Nature Singapore Pte Ltd. 2026
M. Kumar et al. (Eds.): HSFEA 2023, LNCE 899, pp. 10–21, 2026.
https://doi.org/10.1007/978-981-92-3200-0_2

India, particularly Uttarakhand state, forest fires occur during summers [6]. The major bioresidue responsible for such forest fires in the Himalayan region is pine needles. These fall from Chir pine trees [7]which are largely found in the Indian state of Uttarakhand [8, 9]. In addition, they are found in other Himalayan states of India [10]. These give rise to forest fires on account of human activity [7, 11]. In the Himalayan region, Chir pine is found at a height of 450 to 1800 m above sea level (masl). Sometimes it is found at a height up to 2300 masl. However, in eastern part of India, it is found at a height of 1000 masl [9, 10, 12]. A thick layer of pine needles gets formed on the floor of forest every year. This layer is highly inflammable [13]. Thus, huge amount of bioresidue gets collected on the forest surface [14], increasing the risk of forest fires. The main fire behaviour feature that represents the impact of a forest fire on connected resources during its spread is fire intensity. The moisture level of the fuel has a major impact on the characteristics of ignition and fire spread [15]. It is crucial to comprehend the origins, probability, and location of forest fires. Forest fires are primarily caused by factors related to topography and climate [16]. A reference foundation for managing forest fires can be established by estimating the likelihood of forest fires and creating risk maps for them. It is possible to build surveillance or monitoring systems in forest regions with a higher fire risk by mapping the likelihood of wildfires and potential fire dangers [17]. Numerous data types, such as hotspot, meteorological, vegetation, topographic and social and human data, are helpful in determining the variables influencing forest fires [18].

The fire management community and the organizations that support them can benefit greatly from the expansion of or development of tools [19].

Present article reviews the literature in assessment and management of forest fire risk. Moreover, the use of Microsoft Excel® in the statistical analysis of weather data from forest fire risk viewpoint, also presented and the results confirmed with press reports.

2 Literature Review

2.1 Prediction of Forest Fires

Risk of forest fires is the possibility of a fire occurring and the effects that could result from it [20]. A crucial component of the assessment of forest fire danger is the zoning map that indicates the risk level. Based on the likelihood of a forest fire occurring at a given threshold, it offers a useful resource allocation map for managing the danger of forest fires. To prevent and control forest fires, it is necessary to map the risk level zones [21, 22]. The water content of fuel and probability of forest fires is very much dependent on meteorology. Topographical variations can affect heat, water, and wind transport between locations [16]. Terrestrial systems have limited coverage but great accuracy and fast response times, according to the latest review studies. Ground sensors and aerial and satellite-based systems are alternatives to single-point sensor technology. These systems offer better coverage and have proven to be highly accurate and responsive. While early fire detection is possible with both terrestrial and aerial systems, tiny fires can be spotted in two to four hours after being observed by satellite-based imaging sensors like moderate resolution imaging spectroradiometer (MODIS) [4, 17].

Autonomous unmanned aerial vehicles (UAVs) have been used recently for early detection and fighting. It is possible due to the use of ML techniques [23]. Presently,

models for predicting the risk of forest fires have advanced from statistical analysis models to more intricate models as shown in Table 1. The weight of evidence, logistic regression, multiple linear regression, Poisson regression, and analytical hierarchy are examples of basic statistical and empirical techniques [24–27] that don't always produce satisfying outcomes due to complex and nonlinear nature of forest fires [28, 30]. The limitations of conventional techniques may be overcome by applying modern techniques. Examples are multilayer perceptron neural networks (MLP), random forests (RFs), and adaptive neuro-fuzzy inference systems (ANFISs), artificial neural networks (ANNs), support vector machines (SVMs) [29–32]. Tang and Fang [18] studied various models such as SVMs, RF, etc. and found RF model to be the best model with 91.96% precision and 91.68% accuracy. Furthermore, researchers have focused on hybrid and ensemble models as shown in Table 2, to achieve greater prediction accuracy [18].

Table 1. Conventional and modern techniques of forest fire prediction

Conventional (statistical and empirical)	Modern (machine learning)
Analytic hierarchy [33]	Random forests (RFs) [34]
Weight of evidence[25]	Support vector machines (SVMs)[35]
Multiple linear regression [26]	Multilayer perception neural networks (MLPNN)[24]
Poisson regression [27]	Artificial neural networks (ANNs) [36]
Logistic regression [37]	Adaptive neuro-fuzzy inference systems (ANFISs)[38]
	Hybrid and ensemble models [28, 39]

Table 2. Hybrid and ensemble models

Year	Author	Hybrid model	Improvement in prediction accuracy	Reference
2017	Bui et al	NF & PSO	Outperformed SVM & RF	[28]
2020	Jafari et al	ANFIS & GA	From 77.6 (ANFIS) to 88.1% (ANFIS & GA)	[40]
		ANFIS & FA	From 77.6 (ANFIS) to 90.8% (FA)	
2023	Moayedi et al	ANN & ACO	From 81.3 (ANN) to 84% (ANN & ACO)	[39]
		ANN & BBO	From 81.3 (ANN) to 83.9% (ANN & BBO)	

2.2 Data Sets for Risk Assessment

Geographic Information System (GIS) technology helps generate different datasets [41, 42]. Raster datasets with information on fuel, slope, aspect, elevation, canopy cover,

and fuel are also required to model the behaviour of fires. The canopy must also be characterized by stand-scale characteristics such base height, stand height, and crown bulk density [43].

Important additional elements include fuel moisture and meteorological data, as well as an ignition forecast raster. Certain types of information, such geography, and meteorological conditions, are readily available in public databases. Others, like fuels and canopy structure, however, necessitate the use of more sophisticated techniques, including statistical tools, remote sensing, spatial data processing, and ground observations from forest records, in order to produce highly accurate results [43].

Topography is described by height, slope, and aspect datasets. Elevation controls the adiabatic changes in temperature and humidity. In addition to aspect, the slope dataset is needed to convert spread velocities and directions, modify fuel moisture, and determine the direct effects on fire spread [17].

2.3 Mitigation of Forest Fires

Fighting fires requires the deployment of both people and material resources, which is one of the numerous rescue duties given to firemen. In direct firefighting, one of the most crucial pieces of equipment is the Forest Fire Fighting Vehicle (FFFV) [44]. Helicopters are used as the first line of defence against forest fires, particularly in remote places. Heliport placements are crucial in huge forest areas since helicopters are required to get to fire zones quickly. This may result in more precise forecasts and improved heliport allocation decision-making. Additionally, since nearby facilities can have a substantial impact on fire risk and control, enlarging the observation area can offer a more thorough understanding of the issue [45].

3 Case Study

A case study on analysis of weather data is presented here. Data analysis tool of Microsoft Excel is used to conduct analysis of variance (ANOVA). The case study predicts the risk of forest fire at Dhanaulti-Reserved Forest area of Uttarakhand, India. It studies the weather during the months of February and June 2023. Also, it studies the weather during first and second half of February 2023, from forest fires probability viewpoint.

3.1 Data

The data for case study was obtained from an internet source, www.timeanddate.com as presented in Figs. 1 and 2 and Table 3. The data was collected for two months, February 2023 and June 2023. The parameters considered were maximum temperature, wind speed and %humidity.

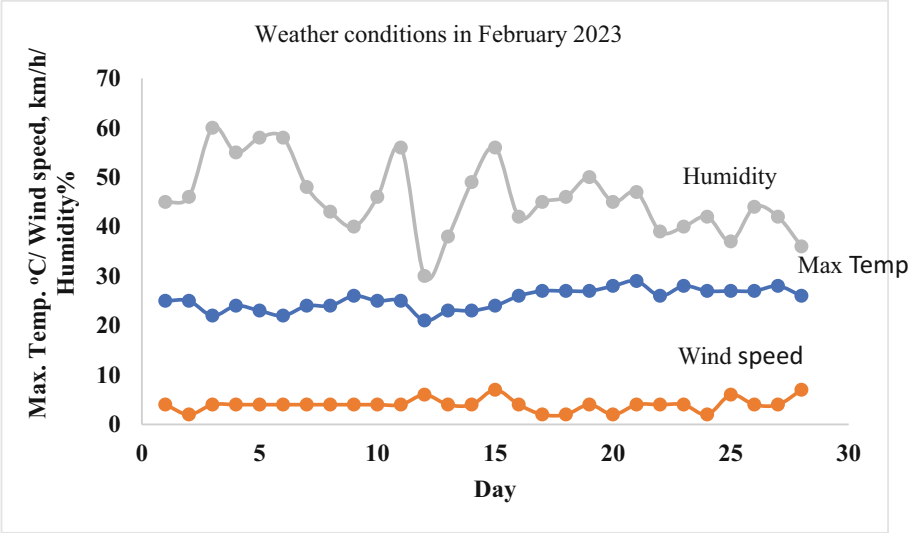


Fig. 1. Day wise variation of temperature, wind speed and humidity during February 2023 at Dhanaulti Reserved Forest, Uttarakhand, India [46].

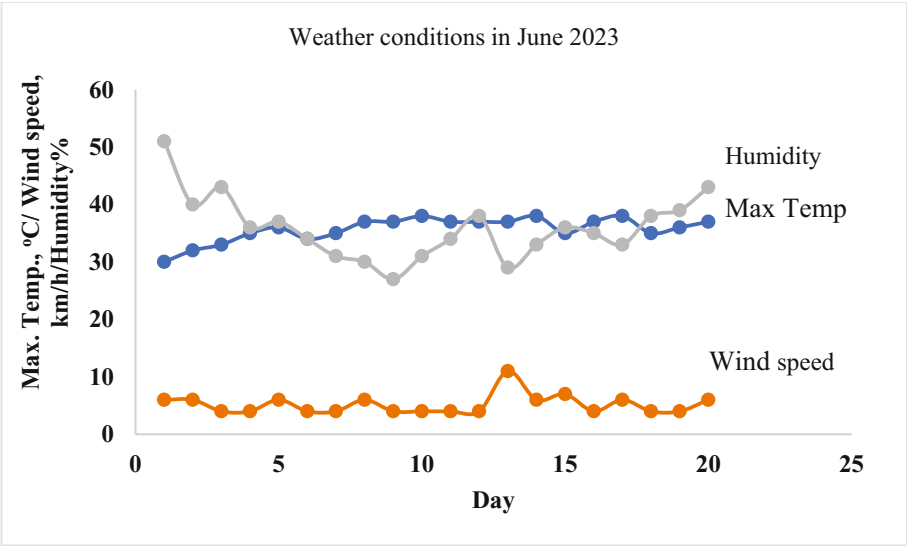


Fig. 2. Day wise variations of temperature, wind speed and humidity during June 2023 at Dhanaulti Reserved Forest, Uttarakhand [46].

Table 3. Weather data for of February 2023 [46]

Half	Day	Max Temp ^{o}C	Wind speed, km/h	Humidity %
First	1	25	4	45
	2	25	2	46
	3	22	4	60
	4	24	4	55
	5	23	4	58
	6	22	4	58
	7	24	4	48
	8	24	4	43
	9	26	4	40
	10	25	4	46
	11	25	4	56
	12	21	6	30
	13	23	4	38
	14	23	4	49
Second	15	24	7	56
	16	26	4	42
	17	27	2	45
	18	27	2	46
	19	27	4	50
	20	28	2	45
	21	29	4	47
	22	26	4	39
	23	28	4	40
	24	27	2	42
	25	27	6	37
	26	27	4	44
	27	28	4	42
	28	26	7	36

3.2 Data Analysis

A 'Two-factor ANOVA with replication tool' of Microsoft Excel was used to analyse the data. An alpha value (level of significance) of 0.05 was used for the analysis as shown in Table 4.

3.3 Results and Discussion

As shown in Table 3, the average maximum temperature during first half of February was 23.71 °C, while it was 26.93 °C during second half. Thus, the average temperature was higher by 3.22 °C during second half of February. An average % humidity during first half was 48, while it was 43.64 during second half. Thus, % humidity was lower by 4.36 during second half of February. The average wind speed in first and second half was same i.e. 4 km/h. High temperature and low humidity favour wildfires. Hence, the risk of forest fires is more in second half of February than that in first half. Additionally, as per Table 5, the interaction between first and second half of February indicate that, there exists a significant difference between the two. That is the weather conditions in the second half are significantly different than those in the first half, indicating the more probability of catching forest fires after mid-February. This inference from case study gets confirmed by the press releases on forest fires [47]. There were around 1,156 forest fire reports from India between February 13 and February 20, 2023 [48].

The average maximum temperature and average %humidity, recorded in February, were 25.3 °C and 45.8 °C, respectively. While the average maximum temperature and %humidity, recorded in June were 35.7 °C and 35.9 respectively (Figs. 1 and 2). Thus, the probability of catching forest fires is more in June than that in February. The average wind speed although nearly same during both the months, plays a vital role in creating friction between the branches of the trees. The temperatures keep increasing constantly from February till June. Thus, the probability of wildfire incidents is extremely high in June. The total number of incidents reported in Uttarakhand in 2023 till 7 March 2023 was 67 with corresponding affected area of 107.25 hectares [49]. However, more than 171 incidents of forest fires were reported only during 6 days' time of June 2023 i.e. 8 June 2023 to 13 June 2023, with a corresponding affected area of 98 hectares, in Uttarakhand, India [50]. Thus, the inference regarding the probability of forest fire incidents, drawn based on temperature and % humidity data, has been confirmed by the press reports on forest fires as mentioned above.

Table 4. ANOVA: Two-factor with replication for data in Table 3

Summary	Max Temp, °C	Wind speed, km/h	Humidity, %	Total
First half				
Count	14	14	14	42
Sum	332	56	672	1060
Average	23.71	4	48	25.24
Variance	2.06	0.61	76	356.67
Second half				
Count	14	14	14	42
Sum	377	56	611	1044
Average	26.93	4	43.64	24.86
Variance	1.46	2.92	27.63	280.66

(*continued*)

Table 4. (*continued*)

Summary	Max Temp, °C	Wind speed, km/h	Humidity, %	Total
Total				
Count	28	28	28	
Sum	709	112	1283	
Average	25.32	4	45.82	
Variance	4.37	1.7	54.82	

* Level of significance is 0.05

Table 5. Results of ANOVA for the data in Table 3

ANOVA						
Source of Variation	*SS*	*df*	*MS*	*F*	*P-value*	*F crit*
Sample	3.05	1	3.05	0.16	0.68	3.96
Columns	24489.59	2	12244.8	663.72	0	3.11
Interaction	202.17	2	101.08	5.48	0.01	3.11
Within	1439	78	18.45			
Total	26133.81	83				

4 Current Status and Future Prospects

The advances in data analytics and technology has improved the knowledge of the variables that contribute to wildfire incidents. With the use of machine learning, remote sensing, and GIS, scientists are now able to analyse and anticipate fire behaviour more accurately. Furthermore, incorporating climate change estimates into these models offers a more thorough evaluation of the risks associated with future fires. With an app, one can now send timely alerts concerning forest fires. The Indian Institute of Remote Sensing (IIRS) and the Uttarakhand Forest Department collaborated to produce this app.

In partnership with the Nepal Department of Forests, International Centre for Integrated Mountain Development (ICIMOD) assisted in the design of a system that employs satellite data to track and evaluate the extent of forest fire damage. The system then automatically sends emails and SMS messages to district forest officers and rangers, enabling them to better monitor the spread and direction of fires and notify local populations when an evacuation may be necessary. The data produced by the system is also being used by the Nepal Department of Forests to examine trends in forest fire behaviour and enhance readiness for upcoming fire seasons. The impacts of forest fires in the sensitive areas need to be understood. Based on remote sensing data, the testing and validation of risk maps is possible.

5 Conclusion

Even while data analytics and technological developments have made it easier to anticipate and comprehend fire behaviour, more interdisciplinary cooperation and the improvement of prediction models are still desperately needed. Developing comprehensive management plans requires integrating socio-economic aspects and climate change estimates into risk assessments. Going forward, it will be critical to give priority to preventive measures like planned burns, community involvement, and land-use planning to lessen the destructive effects of forest fires on ecosystems and human populations. Innovative machine learning techniques such as hybrid and ensemble models may be adopted to predict the risk of forest fires. Preliminary analysis of weather data using Microsoft Excel can be helpful in the assessment of risk.

Nomenclature

NF	Neuro-fuzzy inference system
PSO	Particle swarm optimization
ACO	Ant colony optimization
ANFISs	Adaptive neuro-fuzzy inference systems
ANOVA	Analysis of variance
FA	Firefly algorithms
GA	Genetic algorithm
BBO	Biogeography-based optimization

References

1. He, F., Ge, Q., Dai, J., Rao, Y.: Forest change of China in recent 300 years. J. Geogr. Sci. **18**, 59–72 (2008). https://doi.org/10.1007/s11442-008-0059-8
2. Hussain, A., Negi, A.K., Todaria, N.P.: History of forest fire around Globe, India and Uttarakhand—a brief scenario. J. Agric. Technol. **5**, 7–14 (2018)
3. Casal-Guisande, M., Bouza-Rodríguez, J.-B., Cerqueiro-Pequeño, J., Comesaña-Campos, A.: Design and conceptual development of a novel hybrid intelligent decision support system applied towards the prevention and early detection of forest fires. Forests **14**, 172 (2023)
4. Barmpoutis, P., Papaioannou, P., Dimitropoulos, K., Grammalidis, N.: A review on early forest fire detection systems using optical remote sensing. Sensors **20**, 6442 (2020)
5. Ahmad, L., Saran, S.: Anthropogenic evidences as precursors to forest fire trigger in Western Himalayan Region. Environ. Dev. Sustain. **26**, 16827–16846 (2024). https://doi.org/10.1007/s10668-023-03312-y
6. Singh, R.D., Gumber, S., Sundriyal, R.C., et al.: Chir pine forest and pre-monsoon drought determine spatial, and temporal patterns of forest fires in Uttarakhand Himalaya. Trop. Ecol. **65**, 32–42 (2024). https://doi.org/10.1007/s42965-023-00306-9
7. Sannigrahi, S., Pilla, F., Basu, B., et al.: Examining the effects of forest fire on terrestrial carbon emission and ecosystem production in India using remote sensing approaches. Sci. Total. Environ. **725**, 138331 (2020). https://doi.org/10.1016/j.scitotenv.2020.138331
8. Forest Survey of India, Ministry of Environment Forest and Climate Change, Dehradun, Uttarakhand, India(2019). https://fsi.nic.in/forest-report-2019?pgID=forest-report-2019. Accessed 8 May 2022

9. Singh, J.S., Singh, S.P.: Forests of the Himalaya, Structure Functioning and Impact of Man (1992). Gyanodaya Prakashan, Nainital
10. Fulé, P.Z., Garkoti, S.C., Semwal, R.L.: Frequent burning in chir pine forests, Uttarakhand, India. Fire Ecol. **17**, 20 (2021). https://doi.org/10.1186/s42408-021-00106-3
11. Singh, R.D., Gumber, S., Pankaj, T., Singh, S.P.: Nature of forest fires in Uttarakhand: frequency , size and seasonal patterns in relation to pre-monsoonal environment. Curr. Sci. **111**, 398–403 (2016). https://doi.org/10.18520/cs/v111/i2/398-403l
12. Troup, R.: The Silviculture of Indian Trees, vol. I-III. Clarendon Press, Oxford (1921)
13. Joshi, K., Sharma, V., Mittal, S.: Social entrepreneurship through forest bioresidue briquetting: An approach to mitigate forest fires in Pine areas of Western. Renew. Sustain. Energy Rev. **51**, 1338–1344 (2015). https://doi.org/10.1016/j.rser.2015.07.057
14. Uttarakhand Forest Department Order, Pine Needles for Biobriquetting, PCCF Letter no 1323/24–1(8) dated 18–02–2010 (2010)
15. Matthews, S., Sullivan, A.L., Watson, P., Williams, R.J.: Climate change, fuel and fire behaviour in a eucalypt forest. Glob. Chang. Biol. **18**, 3212–3223 (2012). https://doi.org/10.1111/j.1365-2486.2012.02768.x
16. Wu, Z., Li, M., Wang, B., et al.: Using artificial intelligence to estimate the probability of forest fires in heilongjiang, Northeast China. Remote Sens **13**, 1813 (2021). https://doi.org/10.3390/rs13091813
17. Barmpoutis, P., Kastridis, A., Stathaki, T., et al.: Suburban forest fire risk assessment and forest surveillance using 360-degree cameras and a multiscale deformable transformer. Remote Sens **15**, 1995 (2023). https://doi.org/10.3390/rs15081995
18. Tan, C., Feng, Z.: Mapping Forest Fire Risk Zones Using Machine Learning Algorithms in Hunan Province, China. Sustainability **15**, 6292 (2023). https://doi.org/10.3390/su15076292
19. Dunn, C.J., Thompson, M.P., Calkin, D.E.: A framework for developing safe and effective large-fire response in a new fire management paradigm. For. Ecol. Manage. **404**, 184–196 (2017). https://doi.org/10.1016/j.foreco.2017.08.039
20. Milanović, S., Milanović, S.D., Marković, N., et al.: Forest fire probability mapping in Eastern Serbia: logistic regression versus random forest method. Forests **12**, 5 (2021). https://doi.org/10.3390/f12010005
21. Naderpour, M., Rizeei, H.M., Khakzad, N., Pradhan, B.: Forest fire induced Natech risk assessment: a survey of geospatial technologies. Reliab. Eng. Syst. Saf. **191**, 106558 (2019). https://doi.org/10.1016/j.ress.2019.106558
22. Mohajane, M., Costache, R., Karimi, F., et al.: Application of remote sensing and machine learning algorithms for forest fire mapping in a Mediterranean area. Ecol. Indic. **129**, 107869 (2021). https://doi.org/10.1016/j.ecolind.2021.107869
23. Bouguettaya, A., Zarzour, H., Taberkit, A.M., Kechida, A.: A review on early wildfire detection from unmanned aerial vehicles using deep learning-based computer vision algorithms. Signal Process. **190**, 108309 (2022). https://doi.org/10.1016/j.sigpro.2021.108309
24. Ngoc Thach, N., Bao-Toan Ngo, D., Xuan-Canh, P., et al.: Spatial pattern assessment of tropical forest fire danger at Thuan Chau area (Vietnam) using GIS-based advanced machine learning algorithms: a comparative study. Ecol. Inform. **46**, 74–85 (2018). https://doi.org/10.1016/j.ecoinf.2018.05.009
25. Amatulli, G., Peréz-Cabello, F., de la Riva, J.: Mapping lightning/human-caused wildfires occurrence under ignition point location uncertainty. Ecol. Modell. **200**, 321–333 (2007). https://doi.org/10.1016/j.ecolmodel.2006.08.001
26. Oliveira, S., Oehler, F., San-Miguel-Ayanz, J., et al.: Modeling spatial patterns of fire occurrence in Mediterranean Europe using multiple regression and random forest. For. Ecol. Manage. **275**, 117–129 (2012). https://doi.org/10.1016/j.foreco.2012.03.003

27. Wotton, B.M., Martell, D.L., Logan, K.A.: Climate change and people-caused forest fire occurrence in Ontario. Clim. Change **60**, 275–295 (2003). https://doi.org/10.1023/A:1026075919710
28. Tien Bui, D., Bui, Q.-T., Nguyen, Q.-P., et al.: A hybrid artificial intelligence approach using GIS-based neural-fuzzy inference system and particle swarm optimization for forest fire susceptibility modeling at a tropical area. Agric. For. Meteorol. 233:32–44 (2017). https://doi.org/10.1016/j.agrformet.2016.11.002
29. Ma, W., Feng, Z., Cheng, Z., et al.: Identifying forest fire driving factors and related impacts in china using random forest algorithm. Forests **11**, 507 (2020). https://doi.org/10.3390/f11050507
30. Hong, H., Tsangaratos, P., Ilia, I., et al.: Applying genetic algorithms to set the optimal combination of forest fire related variables and model forest fire susceptibility based on data mining models. The case of Dayu County, China. Sci. Total Environ. **630**, 1044–1056(2018). https://doi.org/10.1016/j.scitotenv.2018.02.278
31. Satir, O., Berberoglu, S., Donmez, C.: Mapping regional forest fire probability using artificial neural network model in a Mediterranean forest ecosystem. Geomatics, Nat Hazards Risk **7**, 1645–1658 (2016). https://doi.org/10.1080/19475705.2015.1084541
32. Razavi-Termeh, S.V., Sadeghi-Niaraki, A., Choi, S.-M.: Ubiquitous GIS-Based forest fire susceptibility mapping using artificial intelligence methods. Remote Sens. **12**, 1689 (2020). https://doi.org/10.3390/rs12101689
33. Akay, A.E., Şahin, H.: Forest fire risk mapping by using GIS techniques and AHP method: a case study in Bodrum (Turkey). Eur. J. For. Eng. **5**, 25–35 (2019). https://doi.org/10.33904/ejfe.579075
34. Ma, W., Feng, Z.K., Cheng, Z.X., Wang, F.G.: Study on driving factors and distribution pattern of forest fires in Shanxi province. J. Cent. South Univ. For. Technol. **40**, 57–69 (2020)
35. Li, Y., Feng, Z., Chen, S., et al.: Application of the artificial neural network and support vector machines in forest fire prediction in the Guangxi autonomous region. China. Discret. Dyn. Nat. Soc. **2020**, 5612650 (2020). https://doi.org/10.1155/2020/5612650
36. Bisquert, M., Caselles, E., Sánchez, J.M., Caselles, V.: Application of artificial neural networks and logistic regression to the prediction of forest fire danger in Galicia using MODIS data. Int. J. Wildl. Fire **21**, 1025–1029 (2012)
37. Pan, J., Wang, W., Li, J.: Building probabilistic models of fire occurrence and fire risk zoning using logistic regression in Shanxi Province, China. Nat. Hazards **81**, 1879–1899 (2016). https://doi.org/10.1007/s11069-016-2160-0
38. Mabdeh, A.N., Al-Fugara, A., Khedher, K.M., et al.: Forest fire susceptibility assessment and mapping using support vector regression and adaptive neuro-fuzzy inference system-based evolutionary algorithms. Sustainability **14**, 9446 (2022). https://doi.org/10.3390/su14159446
39. Moayedi, H., Khasmakhi, M.A.S.A.: Wildfire susceptibility mapping using two empowered machine learning algorithms. Stoch. Environ. Res. Risk Assess **37**, 49–72 (2023). https://doi.org/10.1007/s00477-022-02273-4
40. Jaafari, A., Razavi Termeh, S.V., Bui, D.T.: Genetic and firefly metaheuristic algorithms for an optimized neuro-fuzzy prediction modeling of wildfire probability. J. Environ. Manage. **243**, 358–369 (2019). https://doi.org/10.1016/j.jenvman.2019.04.117
41. Barmpoutis, P., Stathaki, T., Kamperidou, V.: Monitoring of trees' health condition using a UAV equipped with low-cost digital camera. In: ICASSP 2019—2019 IEEE International Conference on Acoustics, Speech and Signal Processing (ICASSP), pp. 8291–8295 (2019). https://doi.org/10.1109/ICASSP.2019.8683128
42. Nuthammachot, N., Stratoulias, D.: Multi-criteria decision analysis for forest fire risk assessment by coupling AHP and GIS: method and case study. Environ. Dev. Sustain. **23**, 17443–17458 (2021). https://doi.org/10.1007/s10668-021-01394-0

43. Myroniuk, V., Kutia, M., Sarkissian, A., et al.: Regional-Scale forest mapping over fragmented landscapes using global forest products and landsat time series classification. Remote Sens. **12**, 187 (2020). https://doi.org/10.3390/rs12010187
44. Silva, F., Raposo, J., Farinha, J.T., et al.: Study of the condition of forest fire fighting vehicles. Fire **6**, 274 (2023). https://doi.org/10.3390/fire6070274
45. Maraş, E.E., Dönmez, K., Emecen, Y.: GIS-Based determination of the optimal heliport and water source locations for forest fire suppression using multi-objective programming. Aerospace **10**, 305 (2023). https://doi.org/10.3390/aerospace10030305
46. Weather in Dhanaulti Reserved Forest, Uttarakhand, India,. https://www.timeanddate.com. Accessed 29 Jun 2023
47. The forest fires in Uttarakhand, HT Editorial, Hindustan Times (2021). www.hindustantimes.com. Accessed 7 Jul 2023
48. Sharma, A., Das, P.J.: The Alarming rise in Forest Fires in India this February: Causes and Concerns, 6 March 2023. https://climatefactchecks.org/. Accessed 10 Mar 2024
49. 107 hectares of forest cover hit by wildfires in Uttarakhand, India Today, 7 March 2023. https://www.indiatoday.in/india/story/107-hectares-of-forest-cover-hit-by-wildfires-in-uttarakhand-2343481-2023-03-07. Accessed 16 Jul 2023
50. Mercury up in Uttarakhand: Over 170 forest fire incidents reported in a week, The New Indian Express, 14 June 2023. https://www.newindianexpress.com/nation/2023/jun/14/mercury-up-in-uttarakhand-over-170-forest-fire-incidents-reported-in-a-week-2584867.html. Accessed 16 Jul 2023
51. Bui, D.T., Le, K.T.T., Nguyen, V.C., et al.: Tropical forest fire susceptibility mapping at the Cat Ba National Park area, Hai Phong City, Vietnam, using GIS-based Kernel logistic regression. Remote Sens **8**, 1–15 (2016). https://doi.org/10.3390/rs8040347

Sustainable Techniques for Improvement of Black Cotton Soils

Guruprasad Ajay Chavan[1,2] and Purnanand Savoikar[1(✉)]

[1] Department of Civil Engineering, Goa College of Engineering, Farmagudi, Goa, India
psavoikar@gmail.com
[2] KIT'S College of Engineering, Kolhapur, Maharashtra, India

Abstract. Soil is the most significant natural building material. It is a complex phenomenon consisting of soil solids, water, air, and organisms in different proportions. Soil is not only a critical resource that nourishes and preserves life on earth, but it also acts as a foundation for all civil engineering structures. The strength and stability of these structures depend on the capacity of the soil to withstand loads and offer a stable foundation. Understanding the characteristics of soil and its behaviour is therefore essential to confirming the sustainability and safety of any building project. Soil property significantly impacts construction costs and safety. Black cotton (BC) soils, a type of expansive clay with undesirable properties that fluctuate in volume due to water content changes, are also crucial in the construction industry. Black cotton soil areas, which have a dark brown colour and are suited for the cultivation of cotton, are mostly found in India's Deccan Trap. They lack nitrogen, phosphoric acid, and organic matter but are high in calcium, potassium, and magnesium. They are unsuitable for building or engineering structures. It contains montmorrilonite, illite, kaolinite, iron oxide, calcium carbonate, and organic matter, with swelling and shrinkage primarily due to aluminum and magnesium silicates. Black cotton soils pose challenges for engineers globally, particularly in tropical countries like India, due to temperature and moisture variations. They are of a high expansive nature**,** highly compressible, have poor drainage capabilities, and have low load-bearing capacity, causing consolidation settlements, swelling, and shrinkage. These issues can cause structures to lift up and crack during dry seasons and cause settlement and shrinkage cracks. Many studies investigated different techniques and materials for improving black cotton soil, which were also tested in laboratories. The primary goal of this study is to investigate potential sustainable materials and techniques for enhancing black cotton soil so that black cotton soil zones could potentially be used for building and infrastructure development while maintaining stability and safety. Xanthan gum, a natural adhesive, and terrazyme, a natural liquid enzyme, were also used to enhance soil. The characterization of black cotton soil in Kolhapur, Maharashtra, India, has been done. Soil from 4.0 m below ground level was mixed with xanthan gum and terrazyme after being sampled up to a depth of 4.75 m in four separate layers. The potential of xanthan gum and terrazyme for enhancing black cotton soil with a high proportion of silt and clay was investigated. Xanthan gum was combined with various percentages of soil, and terrazyme doses were given per 100 ml of water. The results revealed that both additions increased the unconfined compression strength. These two compounds are non-toxic and may be used to effectively enhance black cotton soil.

© The Author(s), under exclusive license to Springer Nature Singapore Pte Ltd. 2026
M. Kumar et al. (Eds.): HSFEA 2023, LNCE 899, pp. 22–31, 2026.
https://doi.org/10.1007/978-981-92-3200-0_3

Keywords: Black cotton soil · Improvement · Stabilization · Sustainability

1 Introduction

Sustainable development is a method of growing a country's economy that is not detrimental to the quality of the environment for future generations. Land degradation, erosion of soil, pollution of the environment, destruction of forests, and other adverse environmental effects are paid for in the name of economic growth. This damage might offset the advantages of higher-quality goods and services. To foster environmentally friendly growth and to meet the needs of the current generation while preserving environmental quality for future generations. Various elements, such as material, procedure, people, and machinery, are critical in the construction industry. The environment is our primary source of building materials. Nowadays, we use many artificial materials for construction, but we also use a variety of natural resources for multiple purposes. Soil is one of the most crucial natural building resources, without which no structure can be built. Every construction project necessitates a robust foundation, which necessitates strong, adequate bearing capacity strata, i.e., soil strata. The carrying capacity of the soil stratum is measured in the construction industry using field testing, laboratory tests, and some correlations discovered by prior investigations. Bearing capacity is commonly used in the context of design and construction. Although other soil characteristics like density, plasticity, settlement, compatibility, swelling, and permeability are equally crucial when evaluating the soil.

Basically, soil is a complex phenomenon that consists of soil solids, and the void space between the solid particles may be filled with water, air, and organisms in different proportions. The state, consistency, and behaviour of soil largely depend on these constituents and their proportions. Particle size, plasticity, and mineralogy are used to classify soils. In practice, certain soils are deemed good for construction, while others are considered critical. In general, such soil requires treatment and improvement before it can be used as a building material. Expensive soils are often inappropriate for building and cause issues both during and after the construction activity. Black cotton soil is one of the most challenging soils for building across the world. Because of seasonal variations, this problem is especially acute in nations such as India.

1.1 Problems Associated with Black Cotton Soil

Clay minerals including Montmorrilonite, Illite, and Kaolinite, as well as compounds like iron oxide and calcium carbonate, make up the highly compressible black cotton soil. These minerals, which are hydrous silicates of aluminium and magnesium, cause soil swelling and shrinkage. The minerals attract and hold water molecules, causing the soil to swell. When water content decreases, the minerals lose their water storage capacity, causing the soil to shrink. This can cause uneven settling and structural damage in construction projects (Gidigasu and Gawu 2013), (Mishra 2014). Black cotton soils in tropical countries like India pose significant engineering challenges due to their compressibility, causing consolidation settlements and differential displacement during wet

seasons, leading to structures' rise and collapse, causing cracks (Mishra 2014). Black cotton soil poses significant challenges for geotechnical engineers during construction due to its volumetric shift and extensive deformations, causing significant damage to roads, canals, buildings, and lifelines. It also shrinks and inflates, causing fissures up to 15 cm in diameter and 3 m deep (Shukla et al. 2015). Engineers in tropical countries like India must carefully consider expansive soils when planning and constructing structures due to temperature changes and soil moisture content variations. Special foundation procedures like deep piling or soil stabilisation measures may be necessary to counteract soil expansion and contraction impacts. Regular monitoring and maintenance of structures built on expansive soils are crucial for recognising and correcting potential problems before they become major issues. Understanding these properties is essential for project stability and lifespan. Black cotton soil is crucial for construction, and researchers have studied and improved it using various stabilization techniques. Lime stabilization enhances soil's strength and plasticity, cement stabilizes compressive strength and expansiveness, and chemical stabilizes changes soil properties for building. These techniques help reduce problems caused by black cotton soil and ensure the stability and durability of structures erected on it. Lime stabilization involves adding lime to soil to boost strength and decrease plasticity, cement stabilizes by combining cement with soil to increase compressive strength and decrease expansiveness, and chemical stabilizes by applying different chemicals to change soil properties.

The main objective of this research is to explore sustainable materials for improving the expansive black cotton soil. The objective of this research is to find sustainable ways to improve the characteristics of black cotton soil. The project intends to identify a cost-effective and environmentally friendly way to alleviate the soil's swelling and shrinking properties by studying sustainable materials. The ultimate goal is to present engineers and construction professionals with realistic solutions for developing black cotton soil regions without negatively impacting the ecosystem.

2 Literature

Expansive soil was treated with various additives in different percentages and forms. As expansive soil is most critical in nature, behavior was analyzed with different test setups by previous researchers. Tri-axial shear tests, swelling tests, and consolidation tests were conducted to analyze soil taken from the Davangare area of Karnataka and evaluate the enhancement of strength, swelling, and compressibility properties of black cotton soil supplemented with coir fibres. The results showed that using coir as a random reinforcing material with expansive black cotton soil can improve engineering behavior. It was found that deviator stress at failure increases with fibre content, confining pressure, fibre diameter, and major principal stress at failure. Cohesion also increases with fibre content, and friction angle also increases. Coir fibres reduced the swell potential of black cotton soil and reduced the compression index due to fibre inclusion. The study also provided regression equations for predicting major principal stress at failure, shear strength parameters, and the compression index of black cotton soil at any fibre content (Babu et al. 2008). The performance of Nigerian black cotton soil designated as A–7–6 or CL in the AASHTO and Unified Soil Classification System (USCS) was investigated. For the West

African Standard Compactive effort (WA), the soil was treated with groundnut shell ash (GSA), resulting in a peak 7-day unconfined compression strength value of 455 kN/sq.m at 4% GSA content and 526 kN/sq.m at 6% GSA content. This value, however, is less than the 1710 kN/sq.m recommended by regulations for base material stabilisation using ordinary Portland cement (OPC). Peak soaking California bearing ratio (CBR) values of 4% at standard Proctor and 4% at WA were obtained at 6% (GSA) and 0% (GSA), respectively, failing to fulfill the Nigerian General Specifications (1997) specification (Oriola and Moses 2010). Clayey soil specimens reinforced with discrete coir fibres were evaluated, and triaxial compression tests on fibre-reinforced clay specimens were numerically simulated. The stress vs. strain curves for plain and fiber-reinforced soils indicated the usefulness of the proposed analytical model in forecasting the stress-strain response of fibre-reinforced soils. It has also been found that fibre reinforcement enhances the stress-strain response of clayey soils (Babu and Chouksey 2010). Addition of 30–50% shredded tyre waste to expansive black cotton soil reduced its volume change potential and shear strength, according to Atterberg's limit tests. This suggests that shredded tyre waste should be used as backfill material in mixing walls to reduce backfill pressure. Additionally, it helps reduce swelling and shrinkage characteristics. The addition of 5% shredded tyre waste in black cotton soil results in a lighter-weight mix with marginally improved shear strength. This suggests that coarser-sized shredded tyre waste can be used for lighter embankments over soft or weak foundations. Additionally, shredded tyre waste increases consolidation properties due to increased permeability values. The addition of shredded tyre waste increases the compressibility properties of the mix (Srivastava et al. 2014). Expansive soil from the Banda district in Uttar Pradesh, India, was analyzed and stabilized it with steel slag, rice husk ash, and quick lime. The optimum mix of these elements was found to be expansive soil, steel slag, rice husk ash, and quick lime at 65, 20, 5, and 10%, respectively. The soil plasticity decreased to 66.2%, while its strength increased to 96%. This mix was found to be as durable as the subgrade material, and its dynamic properties increased soil stiffness to 58–78% (Ashango and Patra 2016). The use of precipitated silica (PS) from rice husk to enhance the geotechnical engineering properties of black cotton soil was analyzed. The soil was collected from Tiruppur district in Tamil Nadu. The application of PS significantly improved the soil's properties, including reduced plasticity, increased permeability, and consolidation rate. This could reduce construction costs associated with excavation and transportation of unsuitable soil. The optimal PS content of 50% is recommended for improving the subgrade characteristics of the soil for pavement layer use (Gobinath et al. 2016). Agricultural and industrial waste to stabilize black cotton soil using a combination of bagasse ash, ground granulated blast furnace slag (GGBS), and wood powder was utilized. Wood powder provided better consistency and reduced plasticity compared to bagasse ash and GGBS. Wood powder effectively controlled swelling in the soil, up to 58%. Bagasse ash and GGBS improved the strength of the soil sample, with GGBS and bagasse ash contributing more to strength and wood powder for swelling control (Dalal et al. 2017). The Stabilization of black cotton soil with up to 8% lime admixed with up to 10% iron ore tailing (IOT) in Gombe State, Nigeria was evaluated. The soil was classified as CH or A-7–6 in the Unified Soil Classification System (USCS) and AASHTO classification

systems. The soil's compaction characteristics increased with higher lime and IOT contents. The peak 7-day UCS value of 1074.54 kN/sq.m met the 1034.25 kN/sq.m criterion for adequate lime stabilization. The peak CBR value of 50% for 8% lime and 8% IOT treatment met the minimum 40% requirement for sub base material in lightly trafficked road construction. The study also evaluated the leaching potential of iron from the soil-lime-IOT mixtures, revealing its suitability as a sub base material on lightly trafficked roads (Etim et al. 2017).

Kaolinite clay with gypsum and lime exhibits high expansion when cured, but adding ground granulated blast furnace slag (GGBS) reduces this expansion and increases compressive strength. Adjusting the lime-GGBS ratio can modify both properties. The reduction in expansion is due to a balance between competing hydration reactions, which inhibits ettringite nucleation. Further research is needed to confirm this hypothesis using a wider range of compositions and micro-analytical methods (Wild et al. 1996). The behaviour of Rajkot region BC soil was improved by using three additives, with cement dust providing substantial and durable benefits as a stabilizing agent. It was observed that, unconfined compressive strength was improved and plasticity reduced with different dosage of cement dust, cement dust and lime and also with lime alone(Oza and Gundaliya 2013). The effects of GGBS mixed with lime on the hydraulic conductivity of expansive clay minerals like kaolinite, montmorillonite, and illite clay was evaluated. A study revealed that adding lime and GGBS reduces kaolinite's permeability, increasing hydraulic conductivity as time elapses. However, kaolinite's conductivity decreases due to GGBS and lime, possibly due to calcium silicate hydrate gel formation or decreased inter-aggregate pore size (Das and Soni 2014). The impact of sugarcane bagasse ash (BA) on cement-stabilised black cotton soil (BCS) in Nigeria was investigated. The soil was treated with both cement and BA, resulting in a 73% soaked California bearing ratio value. The BCS blend with 8% cement and 5% BA did not meet the Nigerian Federal Ministry of Works, base course requirement, suggesting 5% BA and 8% cement as the optimal blend for BCS stabilization in flexible pavement (Batariet al. 2017).

Xanthan gum, a polysaccharide used as a food additive and rheology modifier, can significantly increase soil compressive strength when used with fine-grained soil. The strength of xanthan gum-coarse soil mixtures depends on the strength of xanthan gum gels, primarily due to hydrogen bonding between xanthan monomers and fine soil particles. Direct interaction between fine particles and xanthan gum strands occurs due to electrically charged clay particles. Xanthan gum bridges between distant particles, enhancing particle alignment and strength improvement. The most economical and efficient concentration for soil treatment is approximately 1–1.5%. Xanthan gum is recommended for soil improvement, especially for dry soil, with minimal adverse effects (Chang et al. 2015). The impact of xanthan gum on soil engineering properties using three mechanical tests as unconfined compression, unconsolidated undrained triaxial, and direct shear was investigated. Results showed that xanthan gum improved the strength of all soil types, with the highest strength achieved for silty sand The study also found that xanthan gum increased cohesion in cohesionless soils but not friction angles. The study suggests using xanthan gum for soil stabilization at the ground surface or deeper ground, with in-situ research needed to support its potential (Soldo and Miletic 2019). Terrazyme, a universally available bioenzyme, for soil augmentation and stabilization. Laboratory tests

showed that terrazyme reduces clay content, increases coarser particles, decreases liquid and plastic limits, and increases maximum dry density. It also reduces the compressive index and coefficient of compressibility, making it a cost effective solution for expansive soil intensification (Begum et al. 2020).

3 Geotechnical Properties of Kolhapur Black Cotton Soils

Sampling was done at twenty eight different locations in Kolhapur, Maharashtra, India. Samples were collected from different depths below ground level. Various tests were conducted on samples collected and results were analyzed, soil characteristics are listed in Table 1 (Chavan and Savoikar 2023). Classification of soil was done on the basis of plasticity chart with the help of soil test results.

Table 1. Characteristics of black cotton soil in study area

Sr. No	Soil property	Range of values
1	*Mechanical analysis*	
	Sand	15–30%
	Silt and Clay	60–95%
2	*Consistency limits*	
	Liquid limit (LL)	38.46–65.40%
	Plastic limit (PL)	22.–51.71%
	Plasticity index(PI)	11.89–30%
	Shrinkage limit (SL)	9.15–16%
3	Soil classification	CH-MH-CI
4	Specific gravity(G)	2.08–2.73
5	Field density	13.8–19.8 kN/m^3
6	Dry density	10.45–14.80 kN/m^3
7	Proctor density	13.5–17.2 kN/m^3
8	Optimum moisture content (OMC)	13.50–20.90%
9	Free swell index	10–70%
10	California bearing ratio (CBR un-soaked)	2.4–4.60%
11	Cohesion (c)	19.61–37.27 kN/m^2
12	Angle of internal friction (ϕ)	8.75–24.32°
13	Unconfined compression strength	62.22–68.95 kN/m^2
14	Compression index (Cc)	0.454–0.499
15	Recompression index (Cr)	0.030–0.033

4 Improvement Using Bio-Enzymes-Terrazyme

Terrazyme is a natural, non-toxic liquid boi-enzyme combination that alters the physical and chemical characteristics of soil. This enzymatic process improves soil engineering qualities by allowing for greater compaction densities and increasing soil stability via particle bonding (Farooq and Singh 2020). Terrazyme is a soil stabilizing agent that improves soil particle wetting and bonding, resulting in a compacted, wetter structure. It aids in chemical bonding, making it resistant to weathering, abrasion, and water penetration, available in two formulations. The study analyzed black cotton soil with bio-enzyme and terrazyme as an admixture using various laboratory tests. The soil was collected from a bore hole near Rankala, Phulewadi Road, Kolhapur, and treated with terrazyme. The soil was sampled up to a depth of 4.75 m in four layers, and treated with different dosages i.e., 0.25 ml per 100 ml of water, 0.50 ml per 100 ml of water, 0.75 ml per 100 ml of water, and 1 ml per 100 ml of water. The unconfined compression strength is analysed with curing period.

4.1 Unconfined Compression Strength (UCS) of Black Cotton Soil with Terrazyme

The effect of terrazyme on the unconfined compression strength value was investigated, and the findings are shown in Table 2. Figure 1 also depicts the fluctuation of unconfined compression strength with different terrazyme dosages. It increases soil strength; this impact is most pronounced after curing.

Table 2. Effect of terrazyme on unconfined compression strength on curing

Sr. No	Dosage(ml)/ 100 ml of water	UCS (kN/m^2)	
Curing period (days)		0	07
1	Untreated	64.45	71.12
2	0.25	74.20	80.41
3	0.5	82.30	86.30
4	0.75	85.41	89.14
5	1.0	86.20	90.71

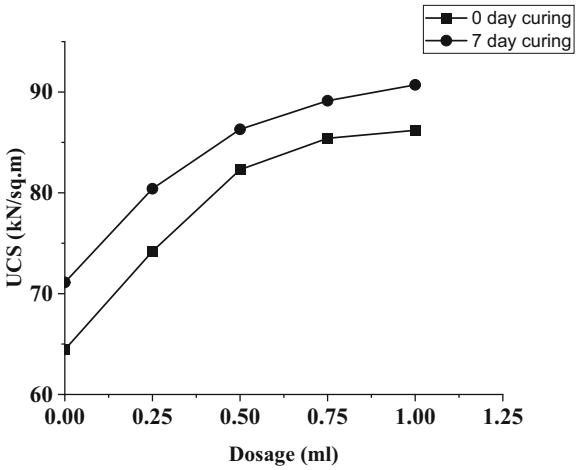


Fig. 1. Unconfined compression strength with terrazyme

5 Improvement Using Natural Adhesives

Xanthan gum, a polysaccharide produced by the xanthomonas campestris bacterium, is used in food, the oil industry, and concrete for its pseudo-plasticity, stability, and ability to thicken drilling mud (Chang et. al. 2015). Xanthan gum, is a common suspending and stabilizing agent in oral and topical medicinal formulations, cosmetics, and food products. Its anionic nature makes it an alternative to traditional alkaline activators like KOH, NaOH, and CaOH. (Kundeti et al. 2023). Unconfined compression strength tests were performed on black cotton soil taken from a bore hole by manual auger boring at a place specified behind Rankala, Phulewadi Road, Kolhapur, and treated with xanthan gum as an admixture. Xanthan gum was combined with soil from 4.0m below ground level. For this test, soil was treated with various concentrations of 0.2%, 0.4%, 0.6%, and 1.0% of soil. The effect of xanthan gum on the unconfined compression strength value was investigated, and the findings are shown in Table 3. Also shown in Fig. 2 is the fluctuation of unconfined compression strength with different dosages of xanthan gum, which enhances soil strength and is more pronounced with curing.

Table 3. Effect of xanthan gum on cured unconfined compression strength

Sr. No	Dosage of Xanthan in percentage of soil	UCS (kN/m^2)	
Curing period (days)		0	07
1	Untreated	64.45	71.12
2	0.2	78.55	90.42
3	0.4	90.50	98.52
4	0.6	98.30	120.40
5	1.0	110.00	177.30

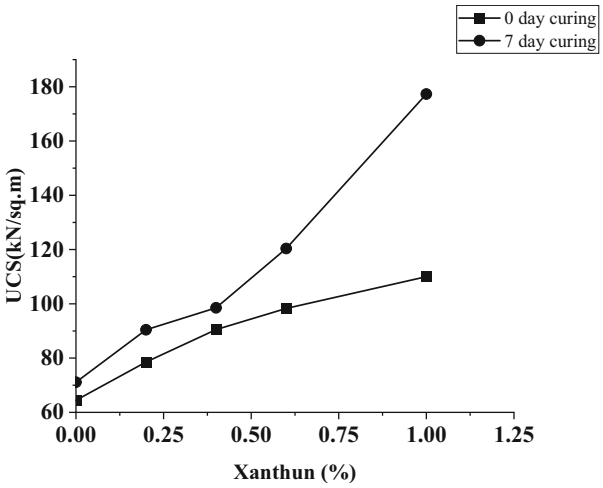


Fig. 2. Unconfined compression strength with Xanthan gum

6 Conclusion

This research reviews previous studies on improving black cotton soil using fibres and agricultural by-products. It aims to identify sustainable materials and improve mechanisation. The study used the natural adhesives xanthan gum and bio-enzyme terrazyme to enhance soil quality in Kolhapur, Maharashtra, India. The curing period was also considered. It was observed that the compounds increased unconfined compression strength. Terrazyme enhanced unconfined compressive strength by 33% without curing and 41% with a 7-day curing time at a dosage of 1 mL per 100 mL of water. Xanthan gum enhanced unconfined compressive strength by 71% without curing and 175% after 7 days of curing at a dosage of 1.0% soil. This study gives insights into soil improvement mechanisms, which can influence future research and the development of effective approaches.

References

Gidigasu, S.S.R., Gawu, S.K.Y.: The mode of formation, nature and geotechnical characteristics of black cotton soils-a review. Sci Res Essays **1**, 377–390 (2013)

Mishra, B.: A Study on Engineering Behavior of Black Cotton Soil and its Stabilization by Use of Lime. Int. J. Sci. Res. (IJSR) **4**(11), 290–294 (2014)

Shukla R.P., Parihar, N., Yadav, P., Mankotia N.: Problems and treatment of black cotton soil. In: 50th Indian Geotechnical Conference 17th–19th December 2015, Pune, Maharashtra, India (2015)

Babu, S., G.L., Vasudevan, A.K., Sayida, M.K.: Use of coir fibers for improving the engineering properties of expansive soils. J. Nat. Fibers **5**(1), 61–75 (2008). https://doi.org/10.1080/15440470801901522

Oriola, F., Moses, G.: Groundnut shell ash stabilization of black cotton soil. Electron. J. Geothechnical Eng. **15** (2010)

Babu, G.L.S., Chouksey, S.K.: Model for analysis of fiber-reinforced clayey soil. Geomech. Geoeng. **5**(4), 277 285 (2010). https://doi.org/10.1080/17486021003706804

Srivastava, A., Pandey, S., Rana, J.: Use of shredded tyre waste in improving the geotechnical properties of expansive black cotton soil. Geomech. Geoeng. **9**(4), 303–311 (2014). https://doi.org/10.1080/17486025.2014.902121

Ashango, A.A., Patra, N.R.: Behavior of expansive soil treated with steel slag, rice husk ash, and lime. J. Mater. Civ. Eng. **28**(7), 06016008 (2016). https://doi.org/10.1061/(asce)mt.1943-5533.0001547

Gobinath, R., Ganapathy, G.P., Akinwumi, I.I., Kovendiran, S., Hema, S., Thangaraj, M.: Plasticity, strength, permeability and compressibility characteristics of black cotton soil stabilized with precipitated silica. J. Central South University **23**(10), 2688–2694 (2016). https://doi.org/10.1007/s11771-016-3330-7

Dalal, S., Patel, R., Dalal, P.: Effect on engineering properties of black cotton soil treated with agricultural and industrial waste. Mater. Today: Proc. **4**, 9640–9644 (2017). https://doi.org/10.1016/j.matpr.2017.06.240

Etim, R.K., Eberemu, A.O., Osinubi, K.J.: Stabilization of black cotton soil with lime and iron ore tailings admixture. Transp. Geotech. **10**, 85–95 (2017). https://doi.org/10.1016/j.trgeo.2017.01.002

Wild, S., Kinuthia, J.M., Robinson, R.B., Humphreys, I.: Effects of ground granulated blast furnace slag (GGBS) on the strength and swelling properties of lime-stabilized kaolinite in the presence of sulphates. Clay Miner. **31**(03), 423–433 (1996). https://doi.org/10.1180/claymin.1996.031.3.12

Oza, J.B., Gundaliya, P.J.: Study of black cotton soil characteristics with cement waste dust and lime. Procedia Eng. **51**, 110–118 (2013). https://doi.org/10.1016/j.proeng.2013.01.017

Das, A., Soni, D.K.: Effect of the ground granulated blast furnace slag (GGBS) and lime mix on the hydraulic conductivity of expansive clay. In: International Conference on Recent Trends and Challenges in Civil Engineering December 12–14, MNNIT Allahabad, India (2014)

Batari, A., Chinade, A., Saeed, M., Ikara, I., Kabir, N., Mamuda, A.: Effect of bagasse ash on the properties of cement stabilized black cotton soil. Int. J. Transp. Eng. Technol. **3**(4), 67–73 (2017)

Chang, I., Im, J., Prasidhi, A.K., Cho, G.-C.: Effects of Xanthan gum biopolymer on soil strengthening. Constr. Build. Mater. **74**, 65–72 (2015). https://doi.org/10.1016/j.conbuildmat.2014.1

Soldo, A., Miletić, M.: Study on shear strength of xanthan gum-amended soil. Sustainability **11**(21), 6142 (2019). https://doi.org/10.3390/su11216142

Begum, A.S., Prasada Raju, G.V.R., Prasad, D.S.V., Anjan Kumar, M.: Influence of TerraZyme on compaction and consolidation properties of expansive soil. In: Problematic Soils and Geoenvironmental Concerns: Proceedings of IGC 2018, pp. 525–535. Springer Singapore, Singapore (2020)

Chavan, G.A., Savoikar, P.: Characterization of black cotton soil in Kolhapur Region. Indian Geotech. J. (2023). https://doi.org/10.1007/s40098-023-00766-9

Farooq, T., Singh, S.: Stabilization of Black Cotton Soil by Using Bio-Enzymes for Pavement Construction (2020). https://doi.org/10.13140/Rg.2.2.19819.36649

Kundeti, G., Karri, C.: Experimental study on black cotton soil treated with xanthan gum and palm oil fuel ash. E3S Web of Conferences. 391 (2023). https://doi.org/10.1051/e3sconf/202339101017

Efficient Removal of Acid Orange 7 Dye Using Acid-Activated Biochar Derived from *Averrhoa Carambola*: A Sustainable Approach for Wastewater Treatment

Anushree Srivastava[1(✉)], Atul Srivastava[2], and Vandana Saxena[3]

[1] Department of Applied Science and Humanities, ABES Engineering College, Ghaziabad, India
anushree.srivastava12@gmail.com

[2] Centre of Environmental Science, Institute of Interdisciplinary Studies, University of Allahabad, Prayagraj, Uttar Pradesh, India

[3] Department of Applied Science and Humanities, IIMT College of Engineering, Greater Noida, India

Abstract. The aggregative release of harmful azo dyes into the environment has become a major concern due to their adverse impacts on ecosystems and human health. Among these dyes, Acid Orange-7 (AO7) has been identified as a persistent and toxic pollutant, necessitating effective treatment strategies for its removal from wastewater. In this study, an innovative and environment friendly method is introduced for the removal of AO7 dye utilizing acid-activated biochar (AAB) derived from the dried stem of *Averrhoa carambola*. The biochar is subjected to surface activation by acetic acid to enhance its surface area and porosity, optimizing its adsorption capacity. A comparative study through batch adsorption experiments was established to understand the removal potential of acid-activated biochar in removing AO7 dye. The effects of various parameters such as initial dye concentration, contact time, pH, and dosage of the biochar are studied to understand their influence on the adsorption process. Additionally, adsorption isotherms and kinetics models are employed to interpret the adsorption mechanism and rate. The results demonstrate that the AAB derived from *Averrhoa carambola* exhibits a higher adsorption capacity for AO7 dye, with removal efficiency of 98.5% with monolayer adsorption capacity of 39.7 mgg^{-1}. The pH of the solution is found to significantly impact the adsorption process, with neutral conditions favoring better dye uptake. In addition, Langmuir model with better correlation coefficient in both the cases (unmodified and AAB) was found to be fitted better than Freundlich model suggesting monolayer adsorption. Moreover, the adsorption kinetics closely follow the pseudo-second-order model, suggesting chemisorption as the predominant mechanism. The AAB shows enhanced result than unmodified biochar due to its increased surface area, chemical modification, electrostatic attraction, pore filling, and chemisorption. Therefore, it holds a great potential for the removal of AO7 dye from wastewater, opening avenues for further research and practical implementation in water treatment technologies.

Keywords: Acid Orange 7 · Adsorption · Biochar · *Averrhoa carambola* · Wastewater treatment

© The Author(s), under exclusive license to Springer Nature Singapore Pte Ltd. 2026
M. Kumar et al. (Eds.): HSFEA 2023, LNCE 899, pp. 32–48, 2026.
https://doi.org/10.1007/978-981-92-3200-0_4

1 Introduction

Acid Orange 7 (AO7) is a prominent synthetic organic dye widely employed in various industrial sectors, including textiles, paper manufacturing, and leather processing, primarily for its striking orange-red coloration [1]. However, the extensive use of AO7 in these industries raises environmental concerns that necessitate a closer examination of its fate in the environment. AO7 is characterized by its resistance to biodegradation, which can result in its persistence in the environment, especially in aquatic ecosystems [2]. Furthermore, AO7 can adsorb strongly to sediments and soils in water bodies, which reduces its mobility and bioavailability, potentially impacting the concentration of AO7 in aquatic environments. While AO7 itself is generally considered to have low toxicity, the concern lies in the potential toxicity of its breakdown products or metabolites formed during chemical or biological transformations [3]. These metabolites may exhibit different toxicity profiles, posing risks to aquatic organisms and ecosystems. Consequently, ongoing research is crucial to comprehensively assess the ecological impacts of AO7 and its potential derivatives [4]. To address these environmental issues, numerous countries have enacted regulations governing the discharge of dyes like AO7 into wastewater, serving as a crucial safeguard to prevent the release of such dyes into natural water bodies and minimize their environmental impact [5]. Responsible use, proper wastewater management practices, and adherence to environmental regulations collectively play a pivotal role in ensuring the sustainable and eco-friendly utilization of AO7 across diverse industrial applications [6]. Meanwhile, the removal of the dye from aqueous environment has become a trending topic in the field of research. There are numerous methods like precipitation, photocatalysis, chemical reduction and adsorption developed so far in order to decontaminate water bodies from AO7 [7–9]. The adsorptive removal of dye from water is a highly favored method among wastewater treatment techniques due to its remarkable efficiency and versatility [10]. It excels in eliminating a wide range of synthetic dyes commonly found in industrial effluents, including those from textile, paper, and food processing industries [11]. One of its key advantages lies in selectivity, as adsorption can selectively target specific dyes without adversely affecting other components in the water, making it particularly valuable for treating complex wastewater streams [12]. Furthermore, adsorption processes are cost-effective, often employing readily available and affordable adsorbent materials like activated carbon, clay minerals, zeolites, or biochar [13]. They also incur lower operational and maintenance costs compared to alternatives such as membrane filtration or chemical precipitation [14, 15]. The method is easy to operate, scalable to various sizes and settings, generates minimal sludge, and is environmentally friendly, involving no chemical additions or harmful byproduct production [16]. Some of the earlier studied adsorbent like, pistachio shell powder [17], de-oiled soya [18], Kenya tea pulps [19], and pea pods [20] and *cucumis sativus* peels [21] have been reported with good potential to decontaminate water from acid orange 7. The acid activation of biochar holds immense significance in the realm of environmental remediation and water treatment. This process elevates the effectiveness of biochar as an adsorbent by substantially increasing its surface area, thereby creating more active sites for adsorption reactions [22]. By introducing and modifying surface functional groups through acid treatment, biochar gains enhanced chemical reactivity, making it proficient at selectively capturing specific contaminants like heavy

metals, organic pollutants, and dyes [23]. Similarly, AAB introduces additional functional groups, including carboxylic and hydroxyl groups, which enhance the chemical reactivity and ability of the biochar to form strong bonds with specific contaminants. This level of customization makes organic acid-activated biochar particularly effective in selectively removing target pollutants from water or soil, such as heavy metals and organic compounds. In the present study lactic acid was utilized in order to fabricate biochar for effective decontamination of AO7 from aqueous solutions. The potential of the developed biochar would be optimized at various experimental condition that helps to explain the working mechanism of the proposed adsorbent.

2 Materials and Methods

2.1 Preparation of Bio-Adsorbent

Ripe star fruit stems (*Averrhoa carambola* L.) were carefully collected, cleaned to remove impurities, and subsequently cut into small pieces. The carbonization process was conducted in a controlled environment, with the stem pieces being heated in a low-oxygen pyrolysis reactor at a temperature of 650 °C, employing a slow heating rate of approximately 10 °C/min and holding this temperature for 2 h to ensure complete carbonization. The resulting biochar was collected and allowed to cool to room temperature. Subsequently, activation with lactic acid commenced, involving the preparation of a 10% (v/v) lactic acid solution using 100 mL of lactic acid and 900 mL of distilled water. The carbonized biochar was submerged in this solution for 12 h at 25 °C with intermittent stirring for uniform contact. Post-activation, the biochar underwent thorough rinsing with distilled water until reaching neutral pH, followed by drying at 105 °C for 24 h.

2.2 Characterization of the Bio-Adsorbent

Fourier-Transform Infrared (ATR-FTIR) spectrometry, utilizing the Nicolet 6700 model from Thermo Scientific, was employed to investigate the vibrational modes of molecules in biochar and lactic acid modified biochar. A thorough FTIR analysis was conducted in the mid-infrared range (400–4000 cm^{-1}), comparing spectra of the control and modified biochar. The obtained data were processed to identify functional groups and assess physiochemical changes induced by lactic acid modification. Additionally, the Point of Zero Charge (PZC) determination for biochar and lactic acid modified biochar employed the mass titration method following Srivastava et al. [24]. 0.1 M NaCl solutions (25 ml) were adjusted to pH values from 3.00 to 11.00 using 0.1 M HCl or NaOH. 0.1 g of each adsorbent was added, stirred for 24 h at room temperature, and the final pH was measured. ΔpH (final–initial pH) against the initial pH was plotted to ascertain the PZC values. Understanding the PZC is vital in optimizing conditions for adsorption processes, predicting adsorbent behaviour, and enhancing the efficiency of pollutant removal from aqueous solutions.

2.3 Batch Adsorption Experiments

Batch adsorption setup was established for various experimental condition such as initial concentration, biomass dosage, pH and contact time. The remaining dye ion concentration in the solution was determined through UV-Visible Spectrophotometer. A calibration curve was established using three distinct dye concentrations: 2.5, 5, and 10 mg/L The biosorption capacity (q_e) of the acid AAB and the percentage dye removal were calculated from the following equations Eq. (1) and (2) respectively.

$$q_e\left(\frac{mg}{g}\right) = \frac{(C_i - C_e)V}{M} \tag{1}$$

$$\%\ \text{Removal} = \frac{C_i - C_f}{C_i} \times 100 \tag{2}$$

where, C_i and C_e (mg/l) are the initial and equilibrium concentration of the adsorbate respectively, V is the volume (L) of the solution and M denotes to the mass of adsorbent (g) used.

3 Result and Discussion

3.1 Characterization via FTIR and pHpzc

The FTIR analysis of biochar and acid-activated biochar revealed distinctive spectra, indicating changes in functional groups (Fig. 1). In the biochar spectrum, a prominent peak at around 3400 cm^{-1} signifies hydroxyl (OH) groups, indicative of moisture absorption [25]. A prominent peak at 2345 cm^{-1} signifies the stretching of alkene group while peaks around 1600 cm^{-1} and 2920 cm^{-1} correspond to C = O and C–H stretching, respectively [26]. In addition, a vibration peak in a fingerprint region at 1108 cm^{-1} indicates the stretching of C–O group of cellulose [27]. Further, the IR spectra of the AAB displayed enhanced peaks at 3422 cm^{-1} corresponds to OH group, suggesting modifications in hydrogen bonding or surface functionalities while peak shift around 1600 cm^{-1} suggests the presence of carboxylic acid groups [28].

The results of the Point of Zero Charge (PZC) analysis reveal distinct characteristics between unmodified biochar and AAB, with PZC values of 7.2 and 5.4, respectively as shown in Fig. 2. The AAB possesses a higher surface charge density compared to its unmodified counterpart. Such a variation is of paramount significance in the context of AO7 dye removal, as it directly influences the electrostatic interactions between the adsorbent and the dye molecules. AAB, with its lower PZC, offers enhanced electrostatic attraction towards acidic dye molecules like acid orange, thereby facilitating more efficient adsorption. Additionally, the higher surface charge density of AAB promotes greater surface reactivity, allowing for increased sites available for dye adsorption [29].

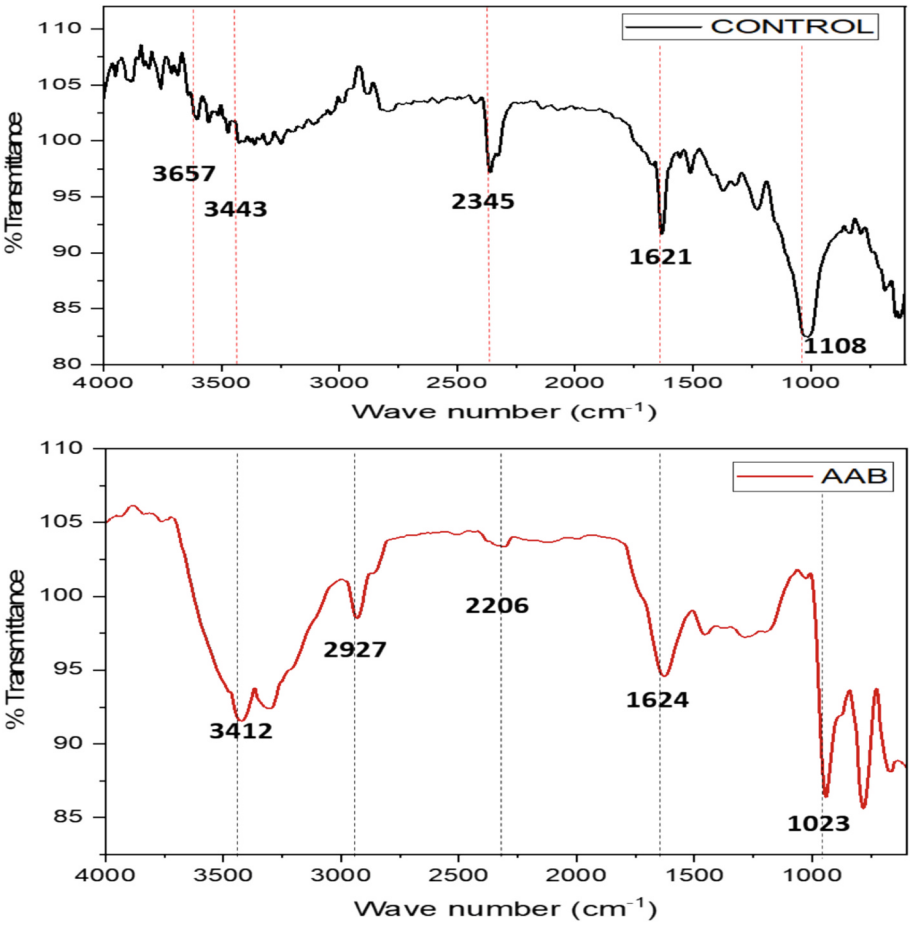


Fig. 1. FTIR spectra of unmodified biochar and AAB derived from *Averrhoa carambola L.*

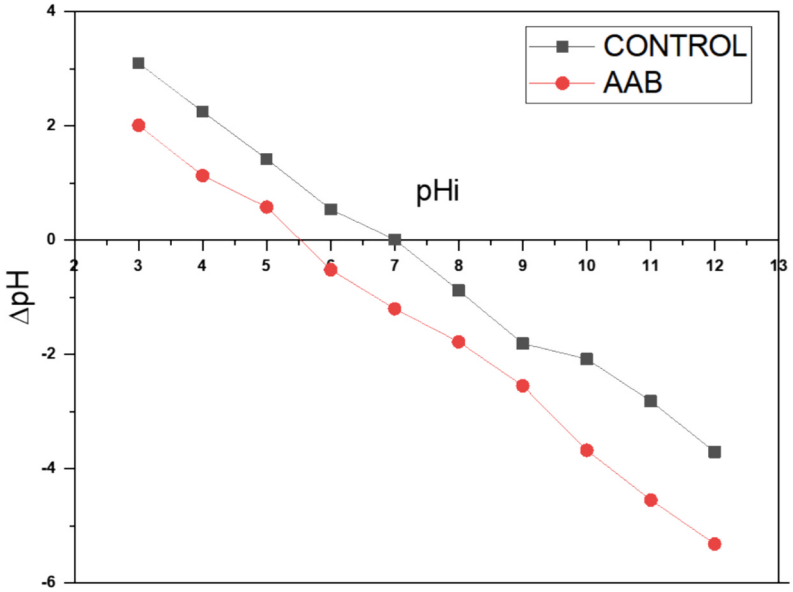


Fig. 2. A comparative graph (pHi verses ΔpH) to evaluate for Pzpc between Unmodified biochar as control and AAB

3.2 Effect of pH and Initial Concentration on AO7 Dye Removal

The study investigating the optimum pH for maximum adsorption of A07, utilizing both AAB and unmodified biochar, yielded insightful results. Notably, the maximum efficiency for A07 adsorption was observed around neutral pH in both cases (Fig. 3a). However, a significant difference in efficiency was evident between the AAB and the unmodified biochar, with the former exhibiting a remarkable efficiency of 98.5%, while the latter only achieved 62.5%. This discrepancy can be elucidated through fundamental chemical principles. Lactic acid activation of biochar involves treatment of biochar that resulted in the creation of a greater number of surface functional groups and increased surface area. These functional groups, such as carboxylic and hydroxyl groups, facilitate stronger interactions with A07 molecules through mechanisms such as electrostatic attraction and hydrogen bonding [30]. Consequently, the AAB possesses enhanced adsorption capacity compared to its unmodified counterpart. Moreover, the higher efficiency observed at a neutral pH suggests that electrostatic interactions, likely between protonated amine groups on A07 and the functional groups on the biochar surface, play a crucial role in the adsorption process. Adsorption of anionic dye at neutral pH using biochar is advantageous due to the favourable electrostatic interactions between the negatively charged dye molecules and the positively charged functional groups present on the biochar surface [31]. In contrast, several studies have reported an acidic condition for the removal of AO7 from aqueous environment [32, 33]. However, the limitation of anionic dye removal at acidic pH primarily stems from the reduced surface charge of the adsorbent material, typically a result of protonation. At low pH levels, the surface of the adsorbent becomes positively charged, diminishing its affinity for anionic species.

Consequently, the electrostatic repulsion between the positively charged adsorbent surface and the negatively charged anionic dye molecules hinders their adsorption, leading to decreased removal efficiency [34, 35]. At neutral pH, biochar maintains its optimal surface charge, enhancing its affinity for anionic dye molecules. Additionally, competing reactions such as protonation or deprotonation, which could hinder adsorption, are minimized [36].

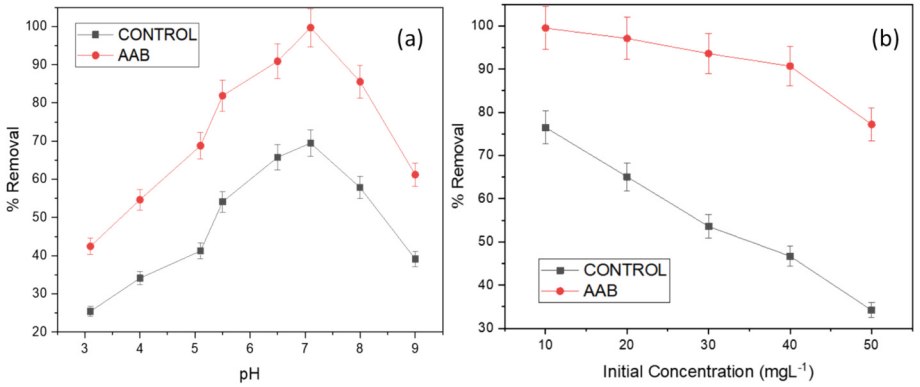


Fig. 3. Effect of pH (**a**) and Initial concentration (**b**) on removal efficiency of AO7 using unmodified (control) and acid activated (AAB) biochar.

The effect of the initial concentration (10 to 50 mg/L) on the removal efficiency of the AO7 dye with control and AAB (2 g/L) is shown in Fig. 3b. The AAB exhibits a remarkable removal efficiency of 98.8%, outperforming unmodified biochar by a significant margin, which achieves only 75.5% removal. Remarkably, as the initial concentration of AO7 increased from 10 mg/L to 50 mg/L, both acid-activated and unmodified biochar showed a decline in adsorption efficiency. This diminishing trend suggests that the capacity of the biochar to adsorb AO7 becomes saturated as the initial concentration of the pollutant rises. However, it is noteworthy that even at 50 mg/L, acid-activated biochar maintained a relatively high removal efficiency of 75.4%, whereas unmodified biochar exhibited a lower efficiency of 32.55%. The decrease in adsorption efficiency with increasing initial concentration may be attributed to the saturation of available adsorption sites on the biochar surface. At higher initial concentrations, the number of pollutant molecules exceeds the capacity of the biochar to adsorb them, resulting in reduced efficiency [9]. The superior performance of acid-activated biochar can be attributed to its enhanced surface properties resulting from the acid activation process. Acid activation introduces functional groups and increases surface area, thereby augmenting the availability of active sites for AO7 adsorption. Conversely, unmodified biochar lacks these surface modifications, leading to lower adsorption efficiency. Moreover, the process of acid activation results in an increase in surface area and pore volume, facilitating greater accessibility of active sites and thereby improving adsorption kinetics [37]. Additionally, the enhanced surface reactivity of acid-activated biochar promotes stronger interactions with AO7 molecules, reducing the likelihood of desorption [38].

3.3 Effect of Biomass Dosage and Contact Time on AO7 Dye Removal

In Fig. 4a, the effect of varying biomass dosage (ranging from 0.5 g/L to 3 g/L) on the removal efficiency of AO7 employing unmodified and acid-activated biochar was examined. AAB demonstrated maximal AO7 removal efficiency of 98.7% at a biomass dosage of 2.5 g/L, contrasting with the 67.2% removal efficiency exhibited by unmodified biochar at the same dosage. The observed increase in adsorption efficiency up to a dosage of 2 g/L can be attributed to an increase in the number of available adsorption sites on the biochar surface. At lower dosages, the concentration of active sites may be insufficient to fully capture the available pollutant molecules. However, as the dosage is increased within this range, more active sites become available, leading to enhanced adsorption efficiency [39]. Beyond a dosage of 2 g/L, no further improvement is observed, indicating saturation of available adsorption sites. The superior performance of AAB compared to unmodified biochar can be attributed to the enhanced surface area and surface chemistry of AAB resulting from the acid activation process. This augmentation leads to a higher density of functional groups and active sites, facilitating stronger interactions with AO7 molecules and thereby enhancing adsorption efficiency [40].

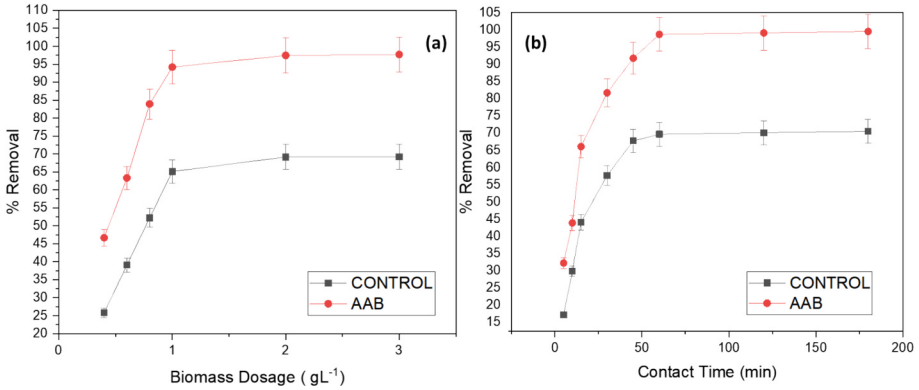


Fig. 4. Effect of biomass dosage (**a**) and contact time (**b**) on removal efficiency of AO7 using unmodified (control) and acid activated (AAB) biochar.

Further, the effect of contact time on the removal of AO7 using acid-activated and unmodified biochar was investigated and presented in Fig. 4b. Both adsorbents reached equilibrium conditions at 60 min of contact time. AAB achieved a maximum removal efficiency of 98.7%, while unmodified biochar exhibited a lower efficiency of 68.3% at the same contact time. With increasing contact time beyond 60 min, both acid-activated and unmodified biochar demonstrated an enhancement in adsorption efficiency. However, no further improvement was observed beyond 120 min. Notably, AAB exhibited an efficiency of 78% within 30 min, while unmodified biochar showed a lower efficiency of 56.5% that supports high rate of reaction at initial contact time [41]. The observed increase in adsorption efficiency with prolonged contact time can be attributed to the increased opportunity for AO7 molecules to interact with the adsorbent surface and be captured by active sites [42]. At shorter contact times, the adsorption process may not

have sufficient time to reach equilibrium, resulting in lower efficiency. However, as the contact time is extended, more AO7 molecules can be adsorbed onto the biochar surface until equilibrium is reached. Beyond the point of equilibrium, no further increase in adsorption efficiency is observed as all available adsorption sites become occupied [43].

3.4 Isotherm Modelling

In the present study, two isotherms namely, Langmuir and Freundlich are applied to understand the adsorption mechanism of AO7 onto AAB and unmodified biochar. The Langmuir and Freundlich isotherms are widely used models to describe the adsorption behaviour of solutes onto solid surfaces in solution. The Langmuir isotherm assumes a monolayer adsorption process on a homogeneous surface, where adsorption sites are equivalent and no interactions occur between adsorbed molecules [44]. It suggests that adsorption reaches saturation at a certain point, forming a monolayer, and follows a reversible process [45]. Langmuir equation can be expressed as follows:

$$q_e = q_m K_L \frac{C_e}{1 + K_L C_e} \tag{3}$$

where, q_e is the amount of solute adsorbed per unit mass of adsorbent (adsorption uptake), C_e is the equilibrium concentration of solute in the solution, q_m is the maximum adsorption capacity of the adsorbent and K_L is the Langmuir constant, related to the affinity of the adsorbate for the adsorbent. Additionally, The Langmuir isotherm model employs the dimensionless separation factor (R_L) to classify the shape of the isotherm, offering insights into the favourability and feasibility of adsorption processes. R_L values indicate whether adsorption is favourable ($0 < R_L < 1$), irreversible ($R_L = 0$), linear ($R_L = 1$), or unfavourable ($R_L > 1$) [46]. The R_L factor is calculated using the following equation:

$$R_L = \frac{1}{1 + K_L C_i} \tag{4}$$

In contrast, the Freundlich isotherm describes multilayer adsorption on heterogeneous surfaces, considering non-uniform distribution of adsorption energies and surface sites. It suggests that adsorption increases continuously with concentration and does not necessarily reach saturation. The non-linear expression of isotherm is given as follows.

$$q_e = K_f C_e^{1/n} \tag{5}$$

q_e is the amount of solute adsorbed per unit mass of adsorbent, K_f is the Freundlich constant related to adsorption capacity, C_e is the concentration of solute in the solution and n is the Freundlich exponent, indicating the intensity of adsorption. The Langmuir and Freundlich isotherm models were applied to analyse the adsorption behaviour of AO7 by unmodified and AAB. By plotting nonlinear graphs of equilibrium adsorption capacity (qe) against equilibrium concentration (ce), key parameters were determined for each model as shown in Fig. 5. For the Langmuir model, the maximum adsorption capacity (qm) was calculated as 39.73 mg/g for AAB and 28.63 mg/g for unmodified biochar. The

Langmuir constant (K_L) was found to be 1.8 for AAB and 0.16 for unmodified biochar, with R_2 values of 0.99 and 0.95 respectively, indicating a high degree of correlation between the experimental and model-predicted data. Additionally, the R_L values, used to assess the favourability of adsorption processes, were determined as 0.05 for AAB and 0.38 for unmodified biochar.

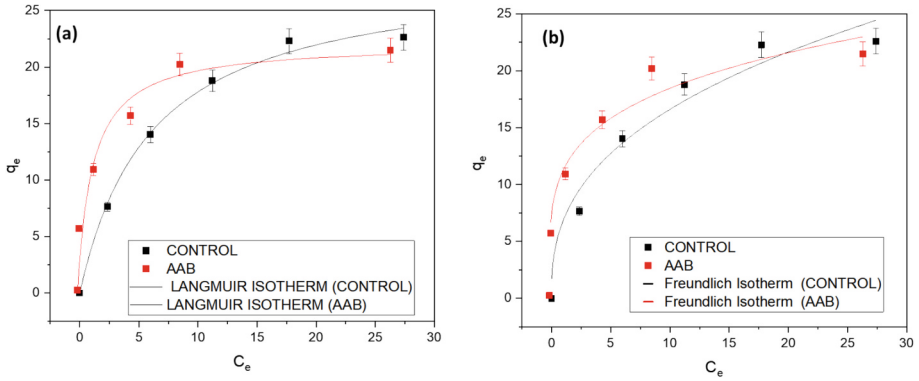


Fig. 5. Langmuir (**a**) and Freundlich (**b**) isotherm for adsorptive removal of AO7 using unmodified (CONTROL) and AAB.

On the other hand, the Freundlich model provided insights into the heterogeneous adsorption behaviour and varying adsorption energies of the biochar surfaces [47]. The parameter 1/n, indicative of adsorption intensity, was determined to be 4.34 for AAB and 2.63 for unmodified biochar. A value of 1/n signifies the intensity of adsorption. When $n > 1$, it suggests that adsorption is favourable on heterogeneous surfaces [48]. The Freundlich constant (K_f) values were 6.87 for AAB and 2.35 for unmodified biochar, with R_2 values of 0.94 and 0.92 respectively, signifying a good fit of the experimental data to the model. Table 1 shows comparison in the obtained parameters by both the isothermal modelling.

Table 1. Comparative values of the parameters calculated for the removal AO7 using unmodified biochar and AAB by equilibrium models

Langmuir isotherm			Freundlich isotherm		
Parameters	Control	AAB	Parameters	Control	AAB
Q_m (mg/g)	28.63	39.73	K_f (L/mg)	2.35	6.87
R^2 value	0.952	0.997	R^2 Value	0.92	0.94
K_L (L/mg)	0.16	1.8	1/n Value	4.34	2.63

Comparative analysis reveals that the Langmuir model better fits the experimental data, as evidenced by higher R_2 values and lower R_L values, indicating a favourable adsorption process. The higher q_m and K_L values obtained for AAB suggest a greater adsorption capacity and affinity compared to unmodified biochar. This underscores the

effectiveness of acid activation in enhancing the adsorption performance of biochar. The Freundlich model, on the other hand, suggests a heterogeneous adsorption process and varying adsorption energies across the biochar surfaces [49]. The higher K_f values for unmodified biochar indicate stronger adsorption interactions, possibly due to its inherent surface characteristics. The modification of biochar with acid has been also supported by several reported studies where acid treatment enhanced the adsorption capacity up to several folds [50]. Mohamed et al. (2020) were reported a study where both unmodified and modified biochar derived from pea peels (Pisum sativum) were assessed for the removal of Acid Orange 7 (AO7) dye. The modification process, which introduced functional groups like Pea-BO-NH and Pea-BO-TETA, resulted in enhanced adsorption efficiency. While specific adsorption capacities were not provided, the study demonstrated improved dye removal efficacy following the modification of the biochar [51]. Another study reported by Santos et al. (2020) where two bentonite samples, underwent modification with ethylene sulphide and ethylenediamine to produce organofunctionalized clay solids. These modified clays were employed for removing anionic azo dye from aqueous solutions, demonstrating increased adsorption capacities of around 40 mg/g [52]. Sterenzon et al. (2021) reported an adsorption capacity of 6 mg/g for AO7, utilizing a pine tree-derived low-cost biochar at pH 5. In contrast, our study demonstrated significantly enhanced adsorption capacities for these acid dyes under neutral pH conditions [53].

3.5 Kinetic Modelling

The adsorption mechanisms of AO7 onto unmodified biochar and AAB derived from star fruit stem are explored using pseudo-first order and pseudo-second order models. The pseudo-first order model posits that the rate of adsorption is directly proportional to the difference between the equilibrium adsorption capacity and the amount of solute adsorbed at any given time [54]. Meanwhile, the pseudo-second order model assumes that the rate of adsorption is directly proportional to the square of this difference [46].

The mathematical representation for the nonlinear pseudo first and pseudo second order model is given in Eqs. (6) and (7).

$$q_t = q_e\left(1 - e^{-kt}\right) \tag{6}$$

$$q_t = \frac{k_2 q_e^2 t}{1 + k_2 q_e t} \tag{7}$$

where qt is the amount of adsorbate adsorbed at time t, qe is the amount of adsorbate adsorbed at equilibrium, k_1 is the rate constant of pseudo-first order kinetics while k_2 is the rate constant of pseudo-second order kinetics [55]. A nonlinear graph for both the models were plotted between qe versus ce and presented in Fig. 6. In case of pseudo-first order model, it is observed that the equilibrium adsorption capacities (qe) for AAB (30.22 mg/g) found to be higher than those of unmodified biochar (21.34 mg/g). Similarly, the rate constant (k_1) for AAB (0.22) is also higher compared to unmodified biochar (0.11).

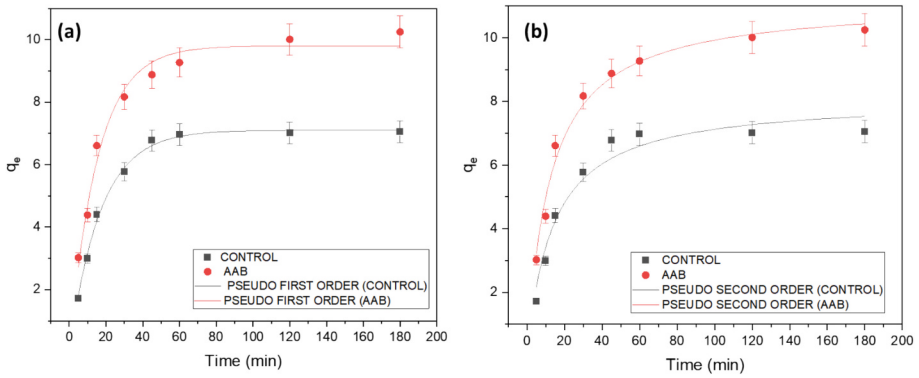


Fig. 6. Adsorption kinetic models for AO7 uptake **a** pseudo-first-order model-, **b** pseudo-second-order model using unmodified (control) and AAB.

These findings suggest that acid activation enhances both the adsorption capacity and rate of AO7 onto biochar. Nonetheless, the R-squared (R^2) values for both substrates show a moderate alignment with the pseudo-first order kinetics. it is evident that acid-activated biochar exhibits higher equilibrium adsorption capacities (q_e) and rate constants (k_2) compared to unmodified biochar. The R^2 values for both types of biochar are notably high, indicating a strong fit of the experimental data to the pseudo-second order model. By examining pseudo-second order model, it is evident that AAB exhibits higher q_e and rate constants (k_2) compared to unmodified biochar. The R^2 values for both types of biochar are notably high, indicating a strong fit of the experimental data to the pseudo-second order model. A comparative data for both the kinetic model is presented in Table 2. Therefore, the adsorption of AO7 onto biochar follows pseudo-second order kinetics more closely than pseudo-first order kinetics. The higher R_2 values and the better fit of experimental data to the pseudo-second order model imply that chemisorption, involving valence forces through sharing or exchange of electrons, likely governs the adsorption process [56]. This is supported by the observation that acid activation increases the surface area and functional groups of biochar, facilitating stronger interactions with AO7 molecules, leading to enhanced adsorption capacity and kinetics.

Table 2. Kinetic parameter obtained for adsorption of AO7 onto unmodified (CONTROL) and AAB

Pseudo first order			Pseudo second order		
Parameters	Control	AAB	Parameters	Control	AAB
K_1 (min^{-1})	0.05	0.06	K_2(g $mg^{-1}min^{-1}$)	0.090	0.07
R^2 value	0.954	0.982	R^2 value	0.959	0.986
q_e (mg/g)	5.1	7.89	q_e mg/g)	8.11	12.15

4 Conclusion

In conclusion, the utilization of lactic AAB derived from the dried stem of star fruit presents a promising avenue for sustainable and eco-friendly water treatment solutions. Through comparative analysis, it is evident that modification via lactic acid activation significantly enhances the adsorption capacity of biochar. This enhancement underscores the potential of biochar as an effective adsorbent for remediation of polluted water sources. The optimization study elucidated key parameters for maximizing adsorption efficiency, with pH 7, a contact time of 60 min, an initial concentration of 10 mg/L, and a biomass dosage of 2 g/L identified as optimal conditions. Isothermal and kinetic studies revealed the monolayer adsorption capacity of 39.73 mg/g for AAB, surpassing the capacity of unmodified biochar (28.63 mg/g). The Langmuir model fitting, supported by high R^2 values, further substantiates monolayer adsorption behaviour. Moreover, the superiority of the pseudo-second order model in fitting experimental data underscores its suitability for describing adsorption kinetics in both cases. This comprehensive investigation not only enhances our understanding of biochar-based water treatment processes but also highlights the potential of AAB as a sustainable and efficient adsorbent for addressing water pollution challenges.

References

1. Eskandari Azar, B., Ramazani, A., Taghavi Fardood, S., Morsali, A.: Green synthesis and characterization of $ZnAl_2O_4$@ZnO nanocomposite and its environmental applications in rapid dye degradation. Optik (Stuttg) **208**, 164129 (2020). https://doi.org/10.1016/j.ijleo.2019.164129
2. Sun, Z., Li, S., Ding, H., Zhu, Y., Wang, X., Liu, H., Zhang, Q., Zhao, C.: Electrochemical/Fe^{3+}/peroxymonosulfate system for the degradation of Acid Orange 7 adsorbed on activated carbon fiber cathode. Chemosphere **241**, 125125 (2020). https://doi.org/10.1016/j.chemosphere.2019.125125
3. Guo, G., Li, X., Tian, F., Liu, T., Yang, F., Ding, K., Liu, C., Chen, J., Wang, C.: Azo dye decolorization by a halotolerant consortium under microaerophilic conditions. Chemosphere **244**, 125510 (2020). https://doi.org/10.1016/j.chemosphere.2019.125510
4. Liu, X., Yuan, B., Zou, J., Wu, L., Dai, L., Ma, H., Li, K., Ma, J.: Cu(II)-enhanced degradation of acid orange 7 by Fe(II)-activated persulfate with hydroxylamine over a wide pH range. Chemosphere **238**, 124533 (2020). https://doi.org/10.1016/j.chemosphere.2019.124533
5. Hamidian, K., Najafidoust, A., Miri, A., Sarani, M.: Photocatalytic performance on degradation of Acid Orange 7 dye using biosynthesized un-doped and Co doped CeO_2 nanoparticles. Mater. Res. Bull. **138**, 111206 (2021). https://doi.org/10.1016/j.materresbull.2021.111206
6. Zeng, H., Xu, J., Li, J., Chen, Y., Zou, J., Liu, N., Wang, Y., Hao, R., Li, D., Zhang, J.: Activation of peroxymonosulfate by sludge-derived magnetic biochar for pollutant removal: performance, applicability, and synergetic mechanism of iron species and carboxylated biochar. Chem. Eng. J. 149744 (2024). https://doi.org/10.1016/j.cej.2024.149744
7. Tamer, T.M., Abbas, R., Sadik, W.A., Omer, A.M., Abd-Ellatif, M.M., Mohy-Eldin, M.S.: Development of novel amino-ethyl chitosan hydrogel for the removal of methyl orange azo dye model. Sci. Rep. **14**, 1284 (2024). https://doi.org/10.1038/s41598-024-51538-1
8. Zhang, Y., Chen, J., Wang, Y., Dou, H., Lin, Z., Gao, X., Chen, X., Guo, M.: Cu_2O/Ag-coated wood-based biochar composites for efficient adsorption/photocatalysis synergistic degradation of high-concentration azo dyes. Appl. Surf. Sci. **647**, 158985 (2024). https://doi.org/10.1016/j.apsusc.2023.158985

9. Keerthana, S.P., Yuvakkumar, R., Ravi, G., Arunmetha, S., Thambidurai, M., Velauthapillai, D.: Magnetically separable rare earth metal incorporated $CdFe_2O_4$ photocatalyst for degradation of cationic and azo dyes. J. Mol. Struct. **1302**, 137479 (2024). https://doi.org/10.1016/j.molstruc.2024.137479
10. Liu, X., Wang, J.: Decolorization and degradation of various dyes and dye-containing wastewater treatment by electron beam radiation technology: an overview. Chemosphere **351**, 141255 (2024). https://doi.org/10.1016/j.chemosphere.2024.141255
11. Shi, C., Wang, Y., Zhang, K., Lichtfouse, E., Li, C., Zhang, Y.: Fe-biochar as a safe and efficient catalyst to activate peracetic acid for the removal of the acid orange dye from water. Chemosphere **307**, 135686 (2022). https://doi.org/10.1016/j.chemosphere.2022.135686
12. Perera, H.J.: Removal of Acid Orange 7 Dye from Wastewater: Review. In: 2020 Advances in Science and Engineering Technology International Conferences (ASET), pp. 1–6 (2020)
13. Alsawy, T., Rashad, E., El-Qelish, M., Mohammed, R.H.: A comprehensive review on the chemical regeneration of biochar adsorbent for sustainable wastewater treatment. NPJ Clean Water **5**, 29 (2022). https://doi.org/10.1038/s41545-022-00172-3
14. Biswal, B.K., Balasubramanian, R.: Use of biochar as a low-cost adsorbent for removal of heavy metals from water and wastewater: a review. J. Environ. Chem. Eng. **11**, 110986 (2023). https://doi.org/10.1016/j.jece.2023.110986
15. Aguilar, M.I., Lloréns, M., Ortuño, J.F., Meseguer, V.F., Pérez-Marín, A.B., Cases, A.: Use of the Box–Behnken experimental design for the optimization of orange II (acid orange 7) adsorption on aloe vera. Sustainability **15** (2023)
16. Fdez-Sanromán, A., Pazos, M., Rosales, E., Sanromán, M.A.: Unravelling the environmental application of biochar as low-cost biosorbent: a review. Appl. Sci. **10** (2020)
17. Kaya, A., Şahin, S.A.: Acid Orange 7 adsorption onto quaternized pistachio shell powder from aqueous solutions. Biomass Convers Biorefinery **12**, 6015–6032 (2022). https://doi.org/10.1007/s13399-022-02414-3
18. Gupta, V.K., Mittal, A., Gajbe, V., Mittal, J.: Removal and recovery of the hazardous azo dye acid orange 7 through adsorption over waste materials: bottom ash and de-oiled soya. Ind. Eng. Chem. Res. **45**, 1446–1453 (2006). https://doi.org/10.1021/ie051111f
19. Naraghi, B., Zabihi, F., Narooie, M.R., Saeidi, M., Biglari, H.: Removal of Acid Orange 7 dye from aqueous solutions by adsorption onto Kenya tea pulps; granulated shape. Electron Physician **9**, 4312–4321 (2017). https://doi.org/10.19082/4312
20. El-Nemr, M.A., El Nemr, A., Hassaan, M.A., Ragab, S., Tedone, L., De Mastro, G., Pantaleo, A.: Microporous activated carbon from Pisum Sativum pods using various activation methods and tested for adsorption of acid orange 7 dye from water. Molecules 27 (2022)
21. Kapoor, R.T., Sivamani, S.: Biosorption behavior of acid orange 7 dye onto Cucumis sativus peel biochar and its effect on growth of Triticum aestivum. Environ. Prog. Sustain. Energy **42**, e14106 (2023). https://doi.org/10.1002/ep.14106
22. Murtaza, G., et al.: Recent trends and economic significance of modified/functionalized biochars for remediation of environmental pollutants. Sci. Rep. **14**, 217 (2024). https://doi.org/10.1038/s41598-023-50623-1
23. Aslam, A., et al.: Metal oxide-impregnated biochar for azo dye remediation as revealed through kinetics, thermodynamics, and response surface methodology. ACS Omega **9**, 4300–4316 (2024). https://doi.org/10.1021/acsomega.3c05321
24. Srivastava, A., Kumar, S., Kavita, A., Bablu, S., Madhu, P., Nandan, K.: Arsenite and arsenate ions adsorption onto a biogenic nano - iron entrapped dual network Fe @ alginate—κ—carrageenan hydrogel beads. Nanotechnol. Environ. Eng. (2022). https://doi.org/10.1007/s41204-022-00280-y
25. Adeniyi, A.G., Ighalo, J.O., Onifade, D.V.: Biochar from the thermochemical conversion of orange (citrus sinensis) peel and albedo: product quality and potential applications. Chem. Africa **3**, 439–448 (2020). https://doi.org/10.1007/s42250-020-00119-6

26. Premarathna, K.S.D., Rajapaksha, A.U., Adassoriya, N., Sarkar, B., Sirimuthu, N,M.S, Cooray, A., Ok, Y.S., Vithanage, M.: Clay-biochar composites for sorptive removal of tetracycline antibiotic in aqueous media. J. Environ. Manage. **238**, 315–322 (2019). https://doi.org/10.1016/j.jenvman.2019.02.069
27. Ma, Q., Song, W., Wang, R., Zou, J., Yang, R., Zhang, S.: Physicochemical properties of biochar derived from anaerobically digested dairy manure. Waste Manag. **79**, 729–734 (2018). https://doi.org/10.1016/j.wasman.2018.08.023
28. Bagheri, A., Abu-Danso, E., Iqbal, J., Bhatnagar, A.: Modified biochar from Moringa seed powder for the removal of diclofenac from aqueous solution. Environ. Sci. Pollut. Res. **27**, 7318–7327 (2020). https://doi.org/10.1007/s11356-019-06844-x
29. De Smedt, J., Heynderickx, P.M., Arauzo, P.J., Ronsse, F.: Adsorption mechanism of different dyes on chemical activated carbon as quantitative assessment for wastewater treatment: comparative study between $ZnCl_2$ and its eutectic. Sep. Purif. Technol. **334**, 126002 (2024). https://doi.org/10.1016/j.seppur.2023.126002
30. Keshta, B.E., Yu, H., Wang, L., Gemeay, A.H.: Cutting-edge in the green synthesis of MIL-101(Cr) MOF based on organic and inorganic waste recycling with extraordinary removal for anionic dye. Sep. Purif. Technol. **332**, 125744 (2024). https://doi.org/10.1016/j.seppur.2023.125744
31. Tajat, N., et al.: Simultaneous removal of anionic and cationic dyes from aqueous solutions using nickel–iron layered double hydroxide nanosheets. Int. J. Environ. Sci. Technol. **21**, 2843–2862 (2024). https://doi.org/10.1007/s13762-023-05155-6
32. Sillanpää, M., Mahvi, A.H., Balarak, D., Khatibi, A.D.: Adsorption of Acid orange 7 dyes from aqueous solution using polypyrrole/nanosilica composite: experimental and modelling. Int. J. Environ. Anal. Chem. **103**, 212–229 (2023). https://doi.org/10.1080/03067319.2020.1855338
33. Zaheer, Z., AbuBaker Bawazir, W., Al-Bukhari, S.M., Basaleh, A.S.: Adsorption, equilibrium isotherm, and thermodynamic studies to the removal of acid orange 7. Mater. Chem. Phys. **232**, 109–120 (2019). https://doi.org/10.1016/j.matchemphys.2019.04.064
34. Badawi, A.K., Abd Elkodous, M., Ali, G.A.M.: Recent advances in dye and metal ion removal using efficient adsorbents and novel nano-based materials: an overview. RSC Adv. **11**, 36528–36553 (2021). https://doi.org/10.1039/D1RA06892J
35. Yagub, M.T., Sen, T.K., Afroze, S., Ang, H.M.: Dye and its removal from aqueous solution by adsorption: a review. Adv. Colloid Int. Sci. **209**, 172–184 (2014). https://doi.org/10.1016/j.cis.2014.04.002
36. Moradihamedani, P.: Recent advances in dye removal from wastewater by membrane technology: a review. Polym. Bull. **79**, 2603–2631 (2022). https://doi.org/10.1007/s00289-021-03603-2
37. Gonçalves, J.O., Crispim, M.M., Rios, E.C., Silva, L.F., de Farias, B.S., Sant'Anna Cadaval Junior, T.R., de Almeida Pinto, L.A., Nawaz, A., Manoharadas, S., Dotto, G.L.: New and effective cassava bagasse–modified biochar to adsorb Food Red 17 and Acid Blue 9 dyes in a binary mixture. Environ. Sci. Pollut. Res. **31**, 5209–5220 (2024). https://doi.org/10.1007/s11356-023-31489-2
38. Eleryan, A., et al.: Kinetic and isotherm studies of Acid Orange 7 dye absorption using sulphonated mandarin biochar treated with TETA. Biomass Convers Biorefinery (2023). https://doi.org/10.1007/s13399-023-04089-w
39. Srivastava, A., Dave, H., Prasad, B., Maurya, D.M., Kumari, M., Sillanpää, M., Prasad, K.S.: Low cost iron modified syzygium cumini l. Wood biochar for adsorptive removal of ciprofloxacin and doxycycline antibiotics from aqueous solution. Inorg. Chem. Commun. **144**, 109895 (2022). https://doi.org/10.1016/j.inoche.2022.109895

40. Srivastava, A., et al.: Iron Modification of biochar developed from Tectona Grandis Linn. F. for adsorptive removal of tetracycline from aqueous solution. Anal. Chem. Lett. **11**, 360–375 (2021). https://doi.org/10.1080/22297928.2021.1934113
41. Srivastava, A., Dave, H., Prasad, B., Kumar, A., Maurya, D.M., Kumari, M., Prasad, K.S.: Adsorptive behavior of L-Arginine-silica micro-particles against arsenic and fluoride in aqueous solution. Environ. Nanotechnol. Monit. Manag. **17**, 100636 (2022). https://doi.org/10.1016/j.enmm.2021.100636
42. Das, S., Barui, A., Adak, A.: Montmorillonite impregnated electrospun cellulose acetate nanofiber sorptive membrane for ciprofloxacin removal from wastewater. J. Water Process Eng. **37**, 101497 (2020). https://doi.org/10.1016/j.jwpe.2020.101497
43. Zhang, M., Lin, K., Zhong, Y., Zhang, D., Ahmad, M., Yu, J., Fu, H., Xu, L., Wu, S., Huang, L.: Functionalizing biochar by Co-pyrolysis shaddock peel with red mud for removing acid orange 7 from water. Environ. Pollut. **299**, 118893 (2022). https://doi.org/10.1016/j.envpol.2022.118893
44. Al Ajmi, A.S.S., Bosu, S., Rajamohan, N.: Biomass—metal oxide nano composite for the decontamination of phenol from polluted environment—parametric, kinetics and isotherm studies. Environ. Res. **240**, 117467 (2024). https://doi.org/10.1016/j.envres.2023.117467
45. Dad, F.P., Khan, W.-D., Sharif, F., Nizami, A.S.: Adsorption of trace heavy metals through organic compounds enriched biochar using isotherm adsorption and kinetic models. Environ. Res. **241**, 117702 (2024). https://doi.org/10.1016/j.envres.2023.117702
46. Srivastava, A., Kumari, M., Prasad, K.S.: Biogenic nanozirconium in hydrogel beads for fluoride removal: equilibrium, thermodynamic and kinetic studies. Indian J. Chem. Technol. **27**, 248–253 (2020)
47. Pillai, P., Dharaskar, S., Shah, M., Sultania, R.: Determination of fluoride removal using silica nano adsorbent modified by rice husk from water. Groundw. Sustain. Dev. **11**, 100423 (2020). https://doi.org/10.1016/j.gsd.2020.100423
48. Mosavi, S.S., Zare, E.N., Behniafar, H., Tajbakhsh, M.: Removal of amoxicillin antibiotic from polluted water by a magnetic bionanocomposite based on carboxymethyl tragacanth gum-grafted-polyaniline. Water 15 (2023)
49. Jiang, H., Li, X., Bai, J., Pan, W., Luo, Z., Dai, Y.: Removal of ciprofloxacin lactate by phosphoric acid activated biochar: urgent consideration of new antibiotics for human health. Chem. Eng. Sci. **283**, 119403 (2024). https://doi.org/10.1016/j.ces.2023.119403
50. Azad, D., Pateriya, R.N., Sharma, R.K.: Chemical activation of pine needle and coconut shell biochar: production, characterization and process optimization. Int. J. Environ. Sci. Technol. **21**, 757–772 (2024). https://doi.org/10.1007/s13762-023-04913-w
51. El-Nemr, M.A., Abdelmonem, N.M., Ismail, I.M.A., Ragab, S., El, N.A.: The efficient removal of the hazardous azo dye acid orange 7 from water using modified biochar from pea-peels. Desalin. Water Treat. **203**, 327–355 (2020). https://doi.org/10.5004/dwt.2020.26190
52. Santos, S.S.G., França, D.B., Castellano, L.R.C., Trigueiro, P., Silva Filho, E.C., Santos, I.M.G., Fonseca, M.G.: Novel modified bentonites applied to the removal of an anionic azo-dye from aqueous solution. Colloids Surfaces A Physicochem. Eng. Asp. **585**, 124152 (2020). https://doi.org/10.1016/j.colsurfa.2019.124152
53. Sterenzon, E., Vadivel, V.K., Gerchman, Y., Luxbacher, T., Narayanan, R., Mamane, H.: Effective removal of acid dye in synthetic and silk dyeing effluent: isotherm and kinetic studies. ACS Omega **7**, 118–128 (2022). https://doi.org/10.1021/acsomega.1c04111
54. Masoudi, F., Naghizadeh, A.: Silica nanoparticles for the removal of fluoride from aqueous solution: equilibrium, isotherms, kinetics, and thermodynamics. Desalin. Water Treat. **137**, 23182 (2019). https://doi.org/10.5004/dwt.201
55. Srivastava, A., Azad, S.K., Singh, K., Prasad, B., Kumari, M., Srivastava, N., Dave, H., Maurya, D.M., Singh, D., Prasad, K.S.: Dual network nano-Zr@chitosan-κ-carrageenan hydrogel

beads as an adsorbent for fluoride removal from aqueous solution: equilibrium, kinetic and thermodynamic studies. Inorg. Nano-Metal. Chem. 1–10. https://doi.org/10.1080/24701556.2023.2271443

56. Thirunavukkarasu, A., Nithya, R.: Adsorption of acid orange 7 using green synthesized CaO/CeO_2 composite: an insight into kinetics, equilibrium, thermodynamics, mass transfer and statistical models. J. Taiwan Inst. Chem. Eng. **111**, 44–62 (2020). https://doi.org/10.1016/j.jtice.2020.04.007

The Sacred Art of Crafting Japamala: A Fusion of Tradition and Sustainable Innovation Though Fashion and Engineering

Achuthy Kottangal(✉)

Faculty Department of Fashion Designing, Amity University Dubai, Dubai, UAE
akottangal@amityuniversity.ae

Abstract. The purpose of this research is to examine the changing functions and important significance of japamala, or rosary beads, in Hinduism. It focuses on the Tulsi Japamala beads created at Amity University Dubai, highlighting their significance as precious spiritual treasures and examining how they evolved from being revered artifacts to trendy decorations. This study combines engineering and design perspectives through a multidisciplinary approach that includes project analysis, interviews, and qualitative research. The intricate production method, historical context, and cultural significance of Tulsi Japamala beads are examined. The study shows how Tulsi Japamala beads transformed from holy artifacts to modern symbols of spirituality and creativity. It makes clear Amity University Dubai's complex creation process and skillful fusion of innovation and tradition. These beads support mantra chanting and prayer as they symbolize a vital link to heritage and elegance. This study offers fresh insights into the intersection of tradition and innovation in the context of religious objects of worship by examining the usage of Tulsi Japamala beads as a bridge between traditional spirituality and contemporary design. The study provides knowledge to manufacturers, designers, and artisans on the creation and cultural significance of Tulsi Japamala beads, which may provide inspiration for the creation of genuine sacred objects. This study encourages a greater understanding of the spiritual and cultural value of japamala beads and highlights the need of preserving and interpreting religious traditions in modern culture. The Amity University tulsi Japamala beads pay tribute to contemporary spiritual practices and the smooth blending of tradition and innovation via the application of both old wisdom and revolutionary craftsmanship.

Keywords: Tulsi plant · Prayer beads · Tulsi beads · Rosary · Holy basil · Ayurvedic medicines

1 Introduction

Holy basil, also known as tulsi or tulasi, is a plant with the scientific name Ocimum tenuiflorum that is well-known for its fragrant qualities. Southeast Asia is where it is presently farmed, but its origins are in India. Ayurvedic medications frequently include holy basil, which is revered in Hinduism. Due to its strong flavor, which has a strengthening effect on the body, it is often used as a culinary herb. India's remarkable biodiversity

© The Author(s), under exclusive license to Springer Nature Singapore Pte Ltd. 2026
M. Kumar et al. (Eds.): HSFEA 2023, LNCE 899, pp. 49–63, 2026.
https://doi.org/10.1007/978-981-92-3200-0_5

provides a variety of medicinal and culinary plants that are employed in Ayurveda that no other medical system can match. However, none of the herbs used in Ayurveda have the same status as tulsi or holy basil (Ocimum sanctum). Ayurveda is the oldest medical system in the world and a science of life. It takes a holistic approach to health and illness, emphasizing the promotion and maintenance of good health as well as the prevention of disease via healthy lifestyle choices. Fresh, minimally processed food consumption, the use of Ramayana's (formulas) that reverse the effects of aging and disease, advanced detoxification techniques, and regular use of adaptogenic herbs—which improve the body's ability to maintain balance in the face of a range of stressors—are some of these practices. A small shrub, holy basil grows to a maximum height of 3.3 feet and has a lifespan of up to a year. The twigs of the plant have sharp edges that run parallel to the stem and are coated with hairs. The plant's fragrant leaves come in a variety of colors of green and purple. There are two different kinds of tulsi plants, Ram and Shyam, with Ram having elliptical, vivid green leaves [4]. It is frequently utilized for spiritual rituals and meditation, boosting self-esteem and bringing optimism into one's life. Ram Tulsi malas can be helpful for those with disturbed thoughts and unpredictable behavior since they aid to foster focus and tranquility. Tulsi is a fragrant shrub that grows natively in tropical regions of the eastern continent. It belongs to the Lamiaceae family of basil plants (tribe ocimene). It is believed to have originated in north central India [1]. Tulsi is regarded as an elixir of life that is unmatched for its therapeutic and spiritual qualities in Ayurveda. It is referred to as The Incomparable One, Mother Medicine of Nature, and The Queen of Herbs [12].

Tulsi has been included into Indian spiritual ceremonies and lifestyle practices that offer a wide range of health advantages that are just now being verified by contemporary science. According to new research on tulsi, which supports traditional Ayurvedic knowledge, the herb is a tonic for the body, mind, and spirit that can help with a variety of ailments. Shyam Tulsi, also called Krishna Tulsi, has pointed, purple-green leaves in contrast. The beads created from Shyam Tulsi are thought to boost the body's supply of good energy and aid in reducing stress. People who wear Shyam beads are claimed to be guided on their spiritual path and to experience material and financial riches.

Holy basil (Ocimum sanctum) and sweet basil (Ocimum basilicum) are two plants with a long history of medicinal usage. Particularly holy basil has been utilized for a number of things, including assisting in the treatment of heart disease and cancer as well as enhancing skin health. The word "tulsi" means "incomparable herb" and refers to the venerated plant tulsi, also known as holy basil. Most traditional Indian houses and temples include at least one tulsi plant, indicating its importance to the Hindu religion. For experimental study, here as per the (Fig. 1), Amity University Dubai provided holy basil (Ocimum sanctum). As part of a study initiative, its botanical qualities and its medical uses are being evaluated with the goal of examining its varied biological characteristics and therapeutic potentialities is revered and is used in prayers to support good health, spiritual clarity, and harmonious relationships among families narrated by Kulkarni and Adavirao [10] Tulsi is categorized as a Rasayana in Ayurvedic medicine, a botanical treatment said to support a person's path to maximum wellness and increased consciousness, ultimately resulting in a long and happy life.

The traditional applications of holy basil have been supported by extensive scientific study, which has also shown the herb's wide range of advantageous characteristics. Holy basil provides a variety of health benefits, including hepatoprotective, antiseptic in nature antidiabetic, apoptogenic, anti-inflammatory properties, radioprotective, anticarcinogenic, immunomodulatory, neuroprotective, and cardioprotective qualities, according to studies by Prakash and Gupta [14].

Holy basil, commonly referred to as Ocimum sanctum or Tulsi, has long been used in traditional medicine to treat a wide range of medical issues. Bronchitis, diarrhea, headaches, inflammation, digestive troubles, arthritis, heart problems, eye diseases, skin conditions, poisonings, malaria, and the relief of pain from insect stings are among these afflictions. The leaves, seeds, stalks, stem cells, buds, roots, and entire plant are just a few of the elements of the plant that are employed therapeutically for their medicinal characteristics [16]. Holy basil can be used to flavor traditional meals or taken internally as herbal tea, dried powder, or fresh leaves. Additionally, it can be used externally as a skin-contact bead.



Fig. 1. Holy basil (Ocimum sanctum) is grown at the Amity University Dubai Farm (*Credit* Author)

1.1 Holy Basil According to Hinduism

Hinduism reveres holy basil, also known as ocimum sanctum, as a sacred plant and as a representation of the goddess Lakshmi, the wife of the god Vishnu Growing a holy basil plant is believed to bring prosperity and luck to the home, according to Hindu tradition. The plant's leaves are used in a variety of religious ceremony and presented to the deities

[12]. A tulsi plant may purify the air in your home and ward off evil spirits, according to legend. In the spiritual and cultural rituals of Hinduism, holy basil, sometimes referred to as Tulsi, is highly revered and carries great significance. Respected and worshipped as a symbol of devotion, purity, and spiritual protection, tulsi is highly valued.

In Hindu mythology, Tulsi has a connection with the goddess Tulsi, who is revered as a symbol of purity and devotion. One of the main gods of Hinduism, Lord Vishnu, is thought to have her as his consort in Hinduism. Legend has it that she was a dedicated and unwavering follower of Vishnu, and that's why she was transformed into the aromatic plant known as Tulsi. The plant is known to be an effective meditation aid, and the scent of the leaves is said to promote spiritual and mental well-being. Because of its well-known anti-inflammatory and antioxidant qualities, holy basil is also utilized in Ayurvedic medicine to treat a range of illnesses [7].

Growing in many homes and temples, tulsi is considered a manifestation of the heavenly presence. Having a Tulsi plant in the house is supposed to draw blessings, purify the air, and ward off evil spirits.

Tulsi leaves are offered to the gods and are seen as an essential part of prayers and religious rites in Hindu festivals and festivities. For safety and spiritual purposes, Hindus also frequently wear Tulsi beads as a necklace, or Tulsi mala. Worshiping sacred basil is traditional in Hinduism, and it usually happens in the morning or evening. During these rituals, the plant is usually decorated with flowers, incense, and water from the holy Ganga River. Female family members are often in charge of watering and caring for the plants [8]. Holy basil is not only cultivated and worshipped in temples, but it is also used to make the hardwood stems required for creating rosaries and Japamala prayer beads. Since these prayer beads are used to repeat mantras, they are an indispensable tool for spiritual practice and focus.



Fig. 2. The Handmade Beads Produced at the Amity University Farm in Dubai (*Credit* Author)

1.2 Rosary Beads for Prayer

Prayer beads, often called rosaries, are used by people of many different religions to recite mantras, chants, or other kinds of prayer. Depicted in (Fig. 3). These handcrafted beads can be made from precious stones, wood, or metal, among other materials. Praying with the beads is made easier, as it is possible to recite mantras and prayers that are repeated while reflecting on the joyous, dazzling, sorrowful, and beautiful secrets of the religion. A useful tool for keeping track of prayers and strengthening spiritual ties during meditation is the rosary. It encourages followers of the Lord to reflect on the qualities, existence, and teachings of God by acting as a tool for prayer and meditation. Although the word rosary is frequently linked with the Catholic faith, Muslims, Hindus, and Buddhists also use similar prayer beads. These prayer beads are known as japa in Sanskrit. According to Miller [11] some people think that wearing rosaries or prayer beads might improve concentration, meditation, and spiritual development. People from many different cultures and religions use prayer beads, which are often made of wood or other appropriate materials, to enhance their spiritual activities and connect with the spiritual world.

In Hinduism, prayer beads are referred to as "japa mala." Variations are numerous, but these malas often include 108 beads and are crafted from sandalwood, tulsi wood, or other sacred materials. In order to track the number of times a devotee repeats a mantra or the name of a god, they are employed during meditation and mantra recitation. Mantras are said to help with dedication, attention, and spiritual focus as they are repeated while going through the beads.

Islam: Prayer beads are referred to as "misbaha" or "tasbih" in Islamic language. Muslims use them to keep note of the repetition of certain words or qualities of Allah, such as 'Subhan Allah' (glories to Allah), 'Alhamdulillah' (giving thanks to Allah), and 'Allahu Akbar' (God is the Greatest). Typically, they are composed of 99 or 33 beads. They are used for dhikr, or remembering Allah, and for seeking spiritual intimacy during private devotions, which frequently take place after daily prayers.

Christianity: A rosary is the term used to refer to prayer beads in Christianity. The rosary is made up of a circlet of beads with five decades, or groups of 10 beads each, spaced apart by bigger beads. Rosary beads are used by Christians as a guide for some prayers, such as the Hail Mary and Our Father prayers, which are repeated while reflecting on the person, teachings, and mysteries of Jesus Christ. Catholics and members of some other Christian religions use the rosary as a tool for devotion and meditation.



Fig. 3. Rosary all throughout the world (*Credit* Author)

According to [20] study findings, beads have been used as meditative and mystical instruments throughout a wide range of spiritual and supernatural traditions. The use of prayer beads in Catholic tradition, notably during the recitation of the rosary, is a notable illustration of their spiritual value. Similar to how japamala's are used in other traditions for meditation and prayer, each bead in this practice represents a distinct prayer and is numbered in a precise order. Prayer beads are a long-standing practice in some branches of Judaism, with each bead or knot standing in for one of the Psalms. In various spiritual pursuits, such as the Islamic custom of using misbaha beads to recite Allah's 99 names, beads are further used [11].

1.3 Exploring Hinduism's Rich Traditions: A Cultural Insights

Hinduism places a lot of emphasis on the use of the Japamala, often known as a rosary, which is a useful instrument for keeping track of the mantras chanted during prayers. These rosaries generally consist of 108 wooden beads that have been carefully strung together in a circle to represent the Hindu philosophy's faith in the endless cycle of birth and rebirth [11]. Among these beads, one stands out for its size and frequently serves as a starting or stopping point for the spiritual exercise. The mantra and God that a practitioner chooses might differ greatly throughout the several Hindu faiths. For instance, members of the Hare Krishna group prefer tulsi beads, which they use to sing the holy names of Lord Krishna. Other Hindu communities, on the other hand, can choose to use these beads to pronounce the names of their own deities. Some people think that depending the beads may take on different energies according on the mantras spoken. Because of this, a lot of individuals own a variety of rosaries, each designed for a certain kind of meditation. Beyond the confines of Hinduism, prayer beads are widely used in Buddhism, Islam, and Christianity, among other religions.

Prayer beads serve as useful instructions, helping followers in maintaining a consistent concentration and attention on their meditation and prayer practices. Buddhist malas which, depending on the sect, might contain 108 or 27 beads allow wearers to

keep track of their prayers and mantra repetitions and promote a deeper engagement with their spiritual activities. The misbahah, or prayer beads, are similar in that they are used in Islam for both repeating the 99 names of Allah and for dhikr, or remembering God. Christians have also used prayer beads for a very long time, most famously in the form of the rosary. A rosary, which has a particular bead arrangement and promotes focus and devotion, can be used to recite the prayer for the Lord and other sacred prayers. Beads of prayer serve as a connecting thread throughout these diverse spiritual practices, facilitating a deep connection with God and serving as a grounding force to keep followers in the here and now. Bead counting and the intonation of religious words create a rhythmic process that unites people from many spiritual traditions in their desire for inner calm, spiritual development, and greater attentiveness in their daily lives.

1.4 In Exploring Bhuddhism Rich Traditions: A Cultural Insights

A tradition known as japamala's, which involves using prayer beads, has endured throughout the history of Buddhism and is a priceless assistance to meditation and spiritual devotion. Although it is particularly common among Tibetan Buddhists, this tradition has Hindu roots but has been modified to fit Buddhist norms. A standard mala is made up of 108 beads, which stand in for all of humanity's many earthly aspirations. These malas frequently include a tassel or amulet at the end, which increases their value. These beads' main use is to make counting mantras easier during worship or meditation periods [5]. Each bead signifies the recitation of a mantra, aiding practitioners in maintaining focus and devotion throughout their spiritual practice. Making a japamala requires careful consideration of the materials, colors, and meditational goal.

Metals, seeds, shells, Bodhi wood, and a variety of other items may all be utilized to make malas. They come in a variety of hues. The choice of reading material depends on the practitioner's personal meditation goals and focus. The Bodhi tree, for instance, is of enormous significance and is regularly used in the manufacturing of these prayer beads. The Buddha is said to have gained enlightenment therein. Tulsi plant beads are extremely revered as they are crafted from the sacred tulsi plant, which is recognized as the holiest plant in many Buddhist traditions. In general, Japamala's are an intricate web of Buddhist spiritual practice that blends mindfulness, dedication, and symbolism to provide searchers with a useful tool for achieving enlightenment and inner peace.

1.5 In Exploring Christianity's Rich Traditions: A Cultural Insights

Eastern Christian monks were the first to employ prayer beads in Christianity, which began in the third century. Within the Christian religion, rosary styles have changed over time. The rosary has become a widely used tool for both individual and public devotion in Catholicism. One of the most popular rosaries in Christianity is the Holy Virgin Rosary, which is dedicated to Mary. During Christian prayer, a chaplet or rosary—made of beads strung together in rows known as many years is used. Each decade is made up of 10 tiny beads that are separated by a larger bead. The two ends of the chaplet are joined by a thread that is decorated with a cross consisting of two big and three little beads. The rosary is highly valued in Christianity as a potent tool for spiritual development and meditation [21]. By reciting prayers, reflecting on crucial moments in Christ's life, and

thinking about the mysteries of faith, Christians utilize the rosary as a tool to deepen their relationship with God and foster spiritual growth. Christians may worship and think in a flexible and enduring manner thanks to this practice. It entails both public rosary recitation at gatherings and solitary devotions [21].

1.6 In Exploring Islamic Rich Traditions: A Cultural Insights

Muslims may use rosary beads, a practice called in Islam as tasbih, to keep track of the recitation of specific phrases and prayers, particularly the 99 names of Allah. The classic Islamic rosary consists of 99 beads, each of which stands for a name of Allah, plus an extra, larger bead called the alif, which depicts God's completeness. Muslims usually carry these rosaries with them, using them for various spiritual activities such prayer, meditation, and Quran recitation [9]. A subha or misbaha is a smaller version of the Islamic rosary. This version, with its thirty-three beads, is suitable for shorter prayer sessions or moments of contemplation. Hajjis, or pilgrims traveling to Mecca, also have a habit of purchasing rosaries as precious gifts to give to others throughout their holy journey. Some Sufi organizations integrate the practice of dhikr, which comprises the repeating invocation of God's name, into their spiritual practices in addition to the traditional usage of rosary beads for prayer [16]. Making use of rosaries helps to increase mental clarity and develops a close relationship with God. As a result, the rosary plays an important and cherished part in Islamic tradition, serving as a concrete link between the practitioner and their inner and spiritual path of devotion.

2 A Step-By-Step Guide: Followed by the Procedure

There was no need to pay for any raw materials because the Tulsi stems used in the procedure came from the Amity farm. The stems were chopped into comparable sizes using a power hacksaw cutting machine, which generated clean cuts, to guarantee size consistency. Before being employed for the real operation, the machines underwent testing with tiny samples to guarantee the cutting process' precision [17]. The stems were ground prior to cutting using an industrial-grade Ford Bench Grinder, which effectively grinds utilizing grinding stones. The stems were uniform in size and shape thanks to the machine, which also assisted in preparing them for cutting. The tulsi stems were cut with a power hacksaw (Fig. 6) to the correct size and polished before being let too dry in the sun for two hours. This process was necessary to get rid of any moisture from the stems that would have impacted the final product's quality. A cheap and environmentally friendly way to make sure the stems were totally dried before further processing was to sun-dry them. The stems were prepared for the following step of manufacturing when the drying process was finished.

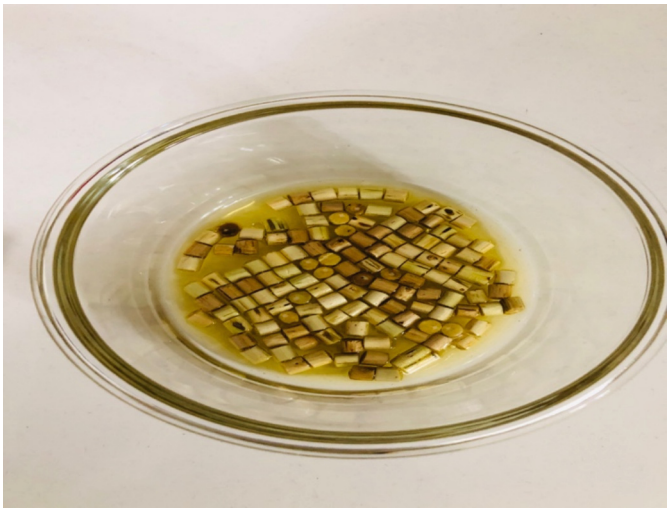


Fig. 4. Sesame oil being applied on beads (*Credit* Author)

After the stem parts were chopped and polished, they underwent a number of steps to become minimal beads, including two hours of sun drying, 24 h of soaking in sesame oil shown in (Fig. 4) to improve their durability and brightness, and one day of additional sun drying to let the beads to absorb the oil. Twenty milliliters of sesame oil were used for each mala. The prepared beads were then strung together with a 109th bead called Sumeru within a sturdy rope or natural thread. A mala typically has 108 beads, and the 109th and 109th beads serve as its starting and stopping points [19].

The tulsi stem parts were normally beaded together using only pure cotton threads, and the mala was then finished by adding tassels to the end of the thread shown in (Fig. 2) after the last bead was strung on. Overall, to produce a lovely and useful mala, this method needed a lot of perseverance, expertise, and attention to detail.



Fig. 5. Using an electronic scale to be weighing the crafted japa mala (*Credit* Author)

As per the (Chart 1) Each japamala had a cost sheet created for it that included the price of labor, raw materials, and overhead costs. Since the tulsi stems came straight from the Amity farm, the cost of them as raw materials were nothing whatsoever. Based on current labor rates, the cost of cutting, polishing, and beading the tulsi stems into a japa mala was calculated. Additionally taken into account were overhead expenditures like power and maintenance fees for the equipment. so even for the total expenses for one japamala the labor and machinery is mentioned in percentage 50%, tulsi 8% sesame oil 30% thread 12% so the information that follows down is the expected itemization of costs in United Arab Emirates Dirham (AED) for one japamala: Labor and machinery: 50%, Tulsi (raw material): 8%, Sesame oil: 30%, Thread: 12% The breakdown would be as follows, assuming that the entire cost of making one japamala is 25AED then the Labor and machinery (50% of 25 AED): 12.5 AED, Tulsi (8% of 25 AED): 2 AED, Sesame oil (30% of 25 AED): 7.5AED, Thread (12% of 25AED): 3 AED. Based on these percentages, the approximate total cost for one japamala would be AED 25, with each expense being assigned as mentioned.

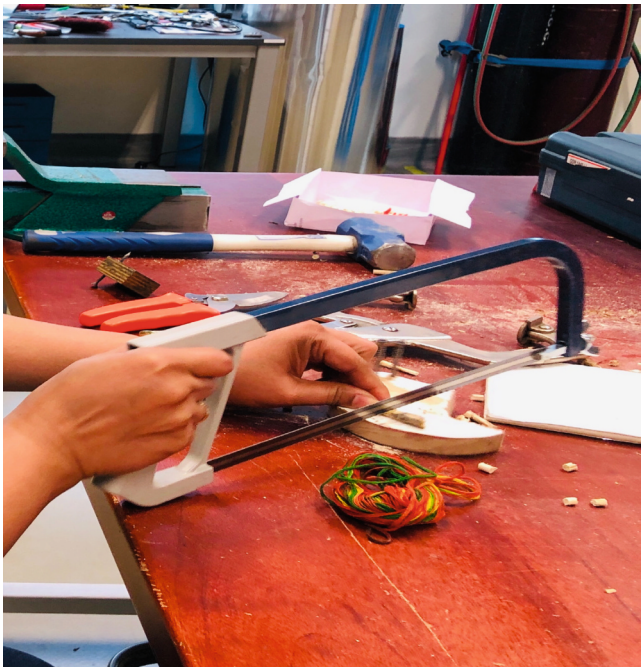


Fig. 6. Cutting and the processing with the tools (*Credit* Author)

The price of making one japa mala was established after considering every expenditure involved. When figuring out the price, the size of each bead was taken into consideration. The length of the japa mala is 38 cm, and the dimensions of each bead are 0.5 cm in length and 0.5 cm in breadth. When weighed using an electronic weighing machine (Fig. 5) one japamala weighed around 7.8 gms in total. Depending on the color of the Tulsi plant used, distinct japa malas were priced accordingly. Tulsi malas were offered in black, brown, and sandalwood hues, with prices ranging somewhat for each. The cost sheet was created to make sure the japa malas could be manufactured effectively and supplied for a fair price without sacrificing the quality of the final product.

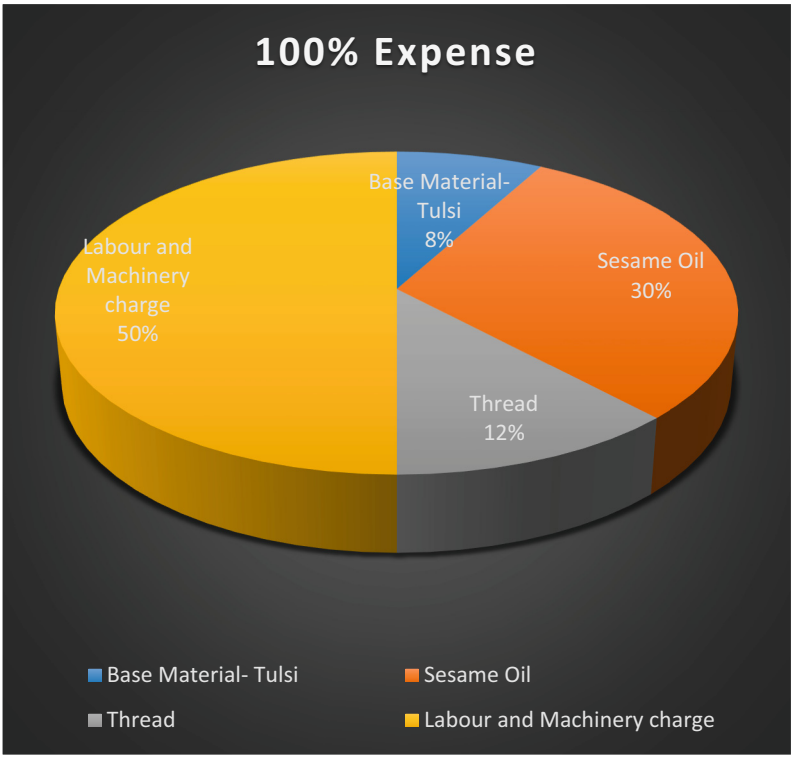


Chart 1 The expense list of this project.

3 The Importance of Wearing a Tulsi Mala as a Necklace and the Health Benefits

In Indian culture and religion, tulsi holds a unique position and is revered as a sacred herb. The presence of tulsi in a home is said to bring benefits and cleanliness. The herb has applications in Ayurveda and is also said to possess therapeutic qualities. Crafted from Tulsi wood or seeds, the Tulsi Mala is a powerful tool for spiritual development that is used for chanting prayers and mantras. It is said that chanting with a Tulsi mala may help one become more spiritually connected and cleanse their body and mind. Tulsi malas are highly valued and used often in Hinduism and other Indian faiths. In addition, tulsi malas are said to have remarkable healing properties both mentally and physically, to help focus the mind during prayer, and to encourage spiritual awakening. The Tulsi plant has been used in Ayurvedic medicine since ancient times because it is believed to have several medicinal effects. The intoxicating scent of the plant is supposed to soothe the mind, and saying while grasping Tulsi Mala beads is supposed to cleanse the soul. Thus, the Tulsi Mala is not just a religious object but also a symbol of spiritual health and healing.

A spiritual item fashioned of Tulsi wood; the Tulsi Mala normally has 108 beads tied together on a strong thread. A bigger Tulsi bead or the Sumeru bead, the 109th bead, is

also included. These beads can be made of the same or different materials, such metal or gemstones. One counts the beads on the Tulsi Mala by beginning at the bead next to the Sumeru bead and going all the way around. To prevent crossing the Sumeru bead during prayers, the Tulsi Mala must be counted in the opposite direction before doing another circuit [14]. The Tulsi Mala is a crucial piece of equipment for religious chanting and is revered as a holy item with exceptional abilities for both spiritual and physical healing. Hindu Vedas claim that as a person crosses the Sumeru bead, the energy contained in the mantras that have been held in the mala is released. Therefore, it is advised while wearing the Japa mala for prayer to avoid overlapping the Sumeru bead. Additionally, it is suggested against touching the mala with the forefinger since that finger is said to represent the ego and against setting the mala on the ground because doing so may sap its energy. Depending on the kind of Tulsi plant used, the Tulsi Mala can be found in black, sandalwood, or brown hues and forms. In general, Hinduism holds that the Tulsi Mala possesses great spiritual and curative abilities.

Wearing a Tulsi mala is said to give protection from negative energy, help avoid accidents, bad nightmares, tragedies, and even harm to one's body. According to Hindu legend, wearing a Tulsi mala at the moment of death might stop the soul from traveling to an undesirable place after death [13]. The Tulsi mala's power is thought to provide spiritual advantages as well, including enhancing general wellbeing and sharpening meditation focus in addition to physical protection. Tulsi is said to have Ayurvedic medicinal characteristics that may guard against a variety of illnesses, especially those that affect the throat, such allergies. It could also help to improve brain function and memory. You may promote spiritual purity, feel more at ease and protected from negative influences by wearing a Tulsi mala. Ayurveda considers it very beneficial for treating throat infections. In addition to its benefits for mental and emotional wellness, the Tulsi mala offers several advantages for physical health. It is widely known to improve the function of the kidneys, reduce stress, and cleanse the body. Tulsi beads help regulate illnesses like diabetes and high blood pressure by eliminating harmful substances from our bodies when they come into contact with them. It also effectively treats throat infections and decreases blood cholesterol. It is believed that those who wear Tulsi malas will be directed toward a greater understanding of spirituality and life.

4 Conclusion

These days, tulsi is considered an adaptogenic herb, one that helps the body overcome a range of difficulties while reinforcing the immune system. Traditional Chinese and Ayurvedic medicine has employed a family of herbs called adaptogens for thousands of years to promote overall health and reduce the negative effects of stress and anxiety. Tulsi is a well-known remedy in modern medicine for helping the body cope with a range of physical and mental diseases, including boosting immune function and reducing inflammation, because of its adaptogenic properties. Tulsi is frequently considered a heavenly plant in Hinduism with both medicinal and mystical uses. It is regarded as the queen of plants and is worshipped as an idol in India. The 108 Tulsi beads and one extra, bigger bead called the Sumeru bead make up the Tulsi Mala, a spiritual instrument. It is said to have amazing spiritual and therapeutic qualities as well as aid with prayer focus.

The Tulsi Mala is traditionally created with a great deal of care and devotion, and Indian culture is deeply linked with its use. The Sumeru bead, sometimes called the Bindu, is the center bead of the Tulsi Mala and has a larger diameter than the other beads.

Tulsi beads are made from the stem of the tulsi plant. The wood, branches, and roots are then let to cure in the sun. After curing, the pieces are hand-cut into smooth, spherical forms. Before the beads are strung onto the thread, they are punctured with a needle. A Tulsi Mala is made with great care and attention to every last detail. A stunning and long-lasting mala is made by stringing together pierced beads with natural threads. To improve the mala's visual attractiveness, elaborate patterns can be added. It is thought that wearing a Tulsi Mala will bring the person luck and wealth. It is also well recognized to possess therapeutic qualities that help treat throat infections, fevers, and coughs. One might benefit not just spiritually but also physiologically from wearing a Tulsi mala. Tulsi is said to cleanse the energy field that surrounds a person, and its pleasant perfume is thought to stimulate feelings of divine presence. To demonstrate the great healing power of Tulsi for the mind and spirit, which is known to offer many health advantages, our designs use genuine and sacred Tulsi stems that are collected from the Amity University Dubai farm.

5 Opertunities for Future Work

It could be important to examine the conservation of religious customs while utilizing revolutionary design and production methods further. Examine how other sacred items or rituals are changed in modern contexts without losing their spiritual meaning, based on the principles of cultural innovation and preservation. In order to increase knowledge, interdisciplinary research covering areas like anthropology, religion, design, and engineering should be promoted, according to Multidisciplinary Research. This can entail working together to investigate the more general implications of these changes in religious items.

While examining customer attitudes and behaviors about the use of historically religious goods for modern fashion or everyday usage, market analysis and consumer behavior are essential. Surveys and anthropological research may be used to learn how people see and appreciate these altered sacred objects. Evaluate Ethical and Sustainable Manufacturing Practices. Make sure that sustainable and ethical production practices are used while preserving the spiritual essence of the items. This can involve looking at the sources of materials, the manufacturing methods used, and the impact they had on the environment and customs of prehistoric communities.

Emphasize community involvement and educational initiatives that seek to educate both consumers and artists about the significance of these altered products on a spiritual and cultural level. It is possible to develop books, seminars, or workshops to increase understanding and appreciation. Consider how traditional things' spiritual meaning may be preserved or enhanced via the use of technology. Consider how modern tools or techniques may improve traditional handicrafts without sacrificing their integrity. Examine how comparable religious objects have changed throughout time in many global cultural contexts. This comparative approach might provide more thorough insights into the global patterns of combining modernity and tradition in sacred items. We might be

able to learn more about how sacred things are evolving in contemporary culture and cultivate a deeper awareness of their significance in terms of spirituality, culture, and design by looking into these avenues.

References

1. Bast, F., Rani, P., & Meena, D.: Chloroplast DNA phytogeography of holy basil (Ocimum tenuiflorum) in Indian subcontinent. The Scientific World J. (2014)
2. Beads and exploring their materiality alongside a Khaksari Sufi Murshid. Material Religion **14**(3), 368–388
3. Saha, S.K.: A device for making Tulsi Mala Beads (2013)
4. Cohen, M.M.: Tulsi-Ocimum sanctum: a herb for all reasons. J. Ayurveda Integrative Med. **5**(4), 251 (2014)
5. Ehrhard, F.K.: A rosary of rubies: the chronicle of the gur-rigs mdo-chen tradition from south-western Tibet (vol. 2). Indus Verlag (2008)
6. Gupta, R., Sharma, M., Singh, D. P., Suthar, B., Saha, S.K.: Women empowerment by technology supported manufacturing of beads from Holy Basil. Curr. Sci. 1660–1664 (2015)
7. Gupta, S.K., Prakash, J., Srivastava, S.: Validation of traditional claim of Tulsi, Ocimum sanctum Linn. as a medicinal plant (2002)
8. Keshavadas, S.: Japa-Yoga. In: Gayatri, pp. 15–26. Routledge (2022)
9. Kitat, S.E.S., Hassan, Z.H.: Praying beads and praying ropes in coptic art in the context of coptic heritage. J. Assoc. Arab Univers. Tour. Hospit. **19**(1), 25–64 (2020)
10. Kulkarni, K.V., Adavirao, B.V.: A review on: Indian traditional shrub Tulsi (Ocimum sanctum): the unique medicinal plant. J. Med. Plants Stud. **6**(2), 106–110 (2018)
11. Miller, J.D.: Beads and Prayers: The Rosary in History and Devotion. Bloomsbury Publishing (2002)
12. Mondal, S., Mirdha, B.R., Mahapatra, S.C.: The science behind sacredness of Tulsi (Ocimum sanctum Linn.). Indian J. Physiol. Pharmacol. **53**(4):291–306 (2009)
13. Prakash, P.A.G.N., Gupta, N.: Therapeutic uses of Ocimum sanctum Linn (Tulsi) with a note on eugenol and its pharmacological actions: a short review. Indian J. Physiol. Pharmacol. **49**(2), 125 (2005)
14. Parikh, M., Motiramani, N.K., Rastogi, N.K., Sharma, B.: Agro-morphological characterization and assessment of variability in aromatic rice germplasm. Bangladesh J. Agric. Res. **37**(1), 1–8 (2012)
15. Rathod, G.P., Kotecha, B.M., Sharma, R., Amin, H., Prajapati, P.K.: In vitro Antibacterial study of two commonly used medicinal plants in Ayurveda: Neem (Azadirachta indica L.) and Tulsi (Ocimum sanctum L.). Drugs, **9**, 10 (2010)
16. Saramifar, Y.: Objects, object-ness, and shadows of meanings: carving prayer beads and exploring their materiality alongside a Khaksari Sufi Murshid. Mater. Relig. **14**(3), 368–388 (2018)
17. Shannon, M.: Crafting Calm: Projects and Practices for Creativity and Contemplation. Cleis Press (2013)
18. Singh, N., Hoette, Y., Miller, D.R.: Tulsi: The mother medicine of nature. Int. Inst. Herbal Med. (2002)
19. Wiley, E., Shannon, M.O.: A string and a prayer: How to make and use prayer beads. Red Wheel (2002)
20. Wernik, U.: The use of prayer beads in psychotherapy. Ment. Health Relig. Cult. **12**(4), 359–368 (2009)
21. Winston, K.: Bead One, Pray Too: A Guide to Making and Using Prayer Beads. Church Publishing, Inc. (2008).



Optimizing Healthcare System Performance with Smart Device Usage in Cloud-Fog Systems

Sumit Bansal[1](✉) and Sunil Kumar[2]

[1] Thapar Institute of Engineering and Technology, Patiala 147004, Punjab, India
sumit.bansal@thapar.edu

[2] Department of Mechanical Engineering, Gurukula Kangri (DU), Haridwar, Uttarakhand, India

Abstract. As society has undergone a transformation in lifestyle, and IoT-based devices has become increasingly integrated into the healthcare system, a multitude of applications has surfaced in modern healthcare facilities, revolutionizing medical data processing. The market is now flooded with smart devices such as smartwatches, smart bands, smartphones, and various wearable sensors designed for continuous health monitoring which has led to a substantial increase in data generation. Thereby, amplifying the data processing load on data centers, which, in turn, presents a significant challenge for researchers. Additionally, there are several cooperative and network-related challenges which includes but are not limited to network utilization, power consumption, latency, and data traffic within healthcare systems. The present paper proposes two key strategies: (1) an efficient policy for prioritizing essential tasks and (2) executing the tasks on cloud, fog only, and a hybrid of cloud-fog nodes. These strategies aim to enhance the Quality of Service (QoS), time, network, and energy consumption. The performance of the system was evaluated in terms of cloud, fog, and hybrid cloud-fog systems. The results were verified using various datasets of sensors and cloud, fog devices. The simulation tool WorkflowSim was employed for this study.

Keywords: HealthCare · Cloud · Fog · Sensor · Actuator

1 Introduction

The adoption of IoT devices in our daily routine has witnessed substantial growth and continues to expand in the contemporary era [1, 2]. Presently, individuals are incorporating wearable technology to monitor an array of health metrics, such as daily step count, blood pressure, heart rate, and calories expended [3, 4]. In the current landscape of smart healthcare systems, wearable sensors play a pivotal role in monitoring patients' health status. These devices have led to a reduction in the physical presence of doctors while also enabling the prediction of potential health issues and disease detection. Furthermore, these devices contribute to the development of smart hospitals, aid in drug-related research, and enhance safety measures [5].

In traditional smart healthcare systems, a considerable volume of data is processed at the cloud servers, leading to the issue of overload on cloud servers and excessive

© The Author(s), under exclusive license to Springer Nature Singapore Pte Ltd. 2026
M. Kumar et al. (Eds.): HSFEA 2023, LNCE 899, pp. 64–76, 2026.
https://doi.org/10.1007/978-981-92-3200-0_6

energy consumption, often resulting in important tasks being neglected [6]. Additionally, the problem of redundant data in the cloud servers poses challenges, as sensors may repeatedly capture data when there is no change in the measured parameters. This is where fog computing comes into play, facilitating the development of efficient smart healthcare systems. Fog computing [7] enables the elimination of redundant data, thus expediting the analysis process and conserving valuable resources. Occasionally, biosensors may capture faulty data, compromising the accuracy of physiological monitoring and health assessments [8]. The diagnostic process relies on variations in sensor readings, with validation involving a comparison to previously sensed data readings.

The traditional healthcare systems were using two layered architecture in which the initial layer, biological sensors were utilized to gauge the patient's temperature, blood pressure, oxygen saturation, and pulse rate, assessing their overall well-being. The second layer employed cloud servers for real-time data processing, reducing the time required for healthcare decisions. However, there was a need to prioritize critical tasks and expedite decision-making. To address these issues, a three-tier architecture was proposed incorporating a fog layer in between to reduce delays and process data in real-time.

1.1 Inspiration and Motivation

This research was prompted by prevalent challenges within the healthcare system, which encompass issues such as delayed medical reports and medication, a shortage of personnel or caregivers, latency in addressing emergency health conditions, congestion in cloud networks, and the occurrence of duplicate or erroneous reports following data analysis. Table 1 outlines and delves into some of the research challenges within the healthcare system.

All these research works served as inspiration for us to innovate a state-of-the-art approach for managing data in intelligent healthcare systems. We have established specific objectives for this innovation, which are discussed below:

- Designing a smart healthcare system for hospitals using wearable sensors to monitor patients.
- Prioritizing the very critical tasks and processing them on the cloud-fog hybrid system.
- Analyzing the results on cloud, fog only, and hybrid cloud-fog architectures.

2 Architecture

The proposed design consisted of three distinct layers: sensor layer, fog layer, and cloud layer. The seamless transfer of data between these layers was achieved through wired or wireless networks, facilitating data transformation. Data processing initiated at the lower layer and propagated to both the upper tiers and vice versa.

The first layer incorporated a variety of sensors, including body temperature sensors, sphygmomanometer sensors, amperometry glucose sensor, infrared pulse oximeter sensor etc. which were used to monitor temperature, blood pressure, blood glucose, pulse rate and oxygen levels respectively. Patient data collected by these wearable sensors was

Table 1: Comparing existing and proposed approaches in healthcare systems

References	Year	Task scheduling	Priority	Time	Network utilization	Energy consumption	Scheduling environment			Comparison with other environment (s)
							Fog only	Cloud only	Cloud-fog	
Arya and Dave [9]	2017	Yes	Yes	No	No	No	No	Yes	No	No
Aladwani [10]	2019	Yes	Yes	No	No	No	No	Yes	No	Yes
Hassan et al. [11]	2020	Yes	Yes	Yes	No	Yes	Yes	Yes	No	No
Haque et al. [12]	2021	Yes	Yes	Yes	No	Yes	No	Yes	No	Yes
Ijaz et al. [13]	2021	Yes	No	No	No	Yes	No	Yes	No	No
Madhura et al. [14]	2021	Yes	Yes	No	No	No	Yes	No	No	No
Xu et al. [15]	2021	Yes	Yes	No	No	Yes	Yes	No	No	No
Abdel et al. [16]	2021	Yes	No	Yes	No	No	Yes	No	No	Yes
Liu et al. [17]	2022	Yes	No	No	No	Yes	No	Yes	No	No
Bansal and Aggarwal [18]	2022	Yes	Yes	Yes	Yes	Yes	No	Yes	No	Yes
Chen et al. [19]	2023	Yes	Yes	No	No	Yes	No	Yes	No	Yes
Our work	2023	Yes	Yes	Yes	Yes	Yes	Yes	Yes	Yes	Yes

expressed in specific units, such as oxygen percentage (%), glucose level (mg/dL), blood pressure (mm Hg), and body temperature (°F).

The middle layer of the proposed architecture accommodated numerous fog devices, including fog nodes, fog modules, and various interconnected hardware components. The top layer of the architecture was dedicated to database and cloud storage services. Beyond offering storage solutions, the cloud layer also provided computational resources for data-intensive processing tasks. Figure 1 (above) illustrates the distinct layers of the architecture, data flow connections, and associated devices.

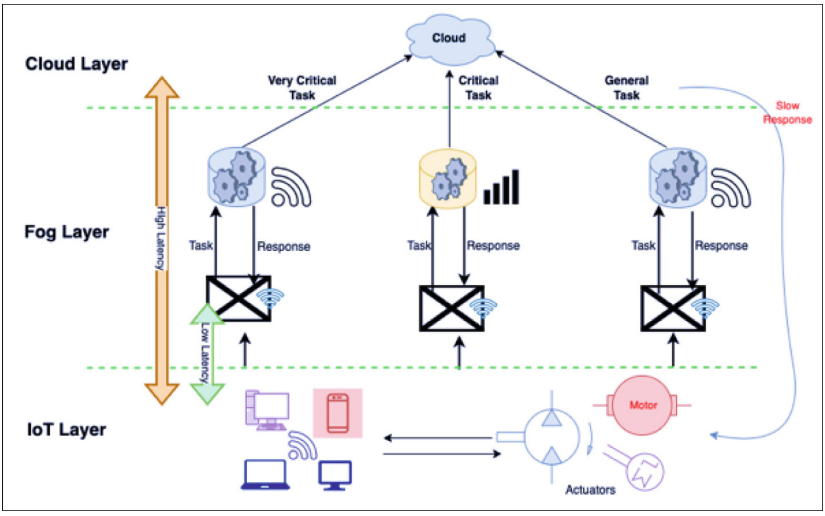


Fig. 1. The flow of data between all the layers of the architecture

3 Use Cases of Work in Healthcare Sector

This section illustrates various cases of applicability of cloud-fog systems, with several examples discussed in the following section.

3.1 Case: 1

In the simulation scenario, we integrated varying numbers of sensors deployed across multiple hospital wards to detect a range of signals generated by these sensors. These signal values were regularly transmitted to the fog layer for processing. The master fog layer conducted the analysis, and the corresponding fog modules examined the incoming values, determining if any action was needed, and generating an appropriate response.

The quantity of sensors across all priority levels could be adjusted as needed based on the task volume. To distinguish individual patients, we employed specific index numbers and their associated data, as illustrated in Fig. 2. The calculated value was transmitted to both the master fog device and the linked cloud. The actuator node, connected to the sensor, received the action value from the master fog device. Furthermore, the outcome value was stored in the cloud for future use.

3.2 Case: 2

In another case, you may access the patient's oxygen range with the use of smart sensors. For example, sensors detect the patient's oxygen levels and transmit this information to the upper tier. No action is necessary if the sensed value falls within the safe range, specifically between 94 and 100%. However, if the oxygen level is detected to be in a dangerous range (below 94%), the tier-3 fog module will activate and send an action

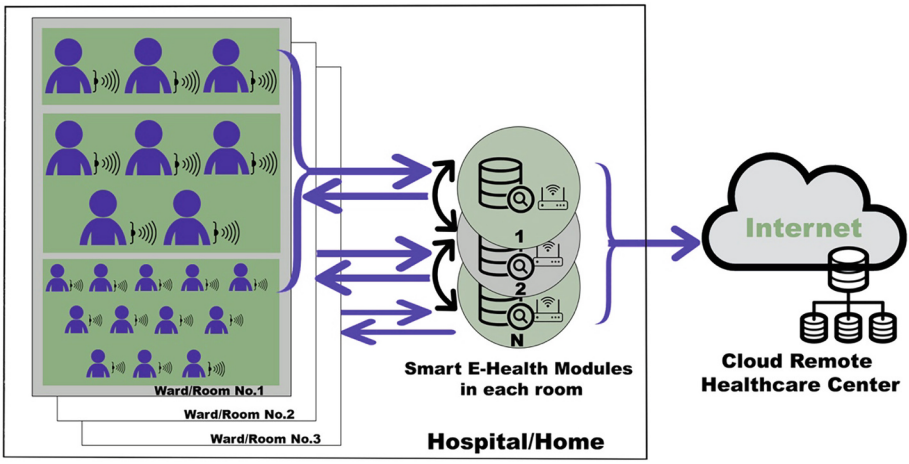


Fig. 2. An innovative smart hospital management solution in development

request to the associated actuator device. Actuators, which perform mechanical tasks in proximity to the patient or user, essentially consist of mechanical motors. In this specific case, an actuator can be employed to open the valve on an oxygen (O_2) cylinder. Such applications can be utilized by a smart healthcare system to potentially save patients' lives.

4 Simulation Work

The WorkflowSim simulation toolkit, an extension of the CloudSim toolkit designed for cloud-fog-based systems, was utilized to implement the proposed system. The complete package, including all the necessary tools and libraries, was installed on the laptop to streamline the creation of cloud-fog-based smart healthcare systems. Table 2 provides a comprehensive list of the hardware and software tools used in this setup.

Table 2. Overview of software tools used

Software	Description
IDE	Eclipse 2021–06
Simulation tool	Workflowsim
Simulator version	3.0.3
Programming language	Java
Development kit	JDK 1.8
Operating system	Big Sur 11.5.1
RAM	8 GB

In the simulation, variables representing sensors, wards, cloud, and fog devices were established. In our case, three distinct wards were designated, each connected to a single fog node. Initially, all three sensors collected data and transmitted the sensed values to the master fog device, which subsequently relayed data to the corresponding fog modules. The policies used to create the simulation environment are described in the article [20]. These policies included simulating different scenarios to assess network utilization, energy consumption, expenses, and variations in the number of sensor nodes per fog device. Algorithm 1 delineates the steps involved in implementing the cloud-fog computing-based architecture. Three separate lists were initiated for very critical, critical, and normal tasks, each connected to the master fog module and the cloud servers.

Algorithm 1: Fog Based sensor-actuator decision system with **First Come First Server** (FCFS) scheduling

1. Build fog broker
2. Create Application
3. Create Cloud, Fog devices, Actuator, Proxy server
4. int $i=5$
5. for $i=0$ to $No.\ of\ FogDevice_{max}$ do
6. Create *fog devices*
7. *for* $i=0$ to $No.ofSensors_{total}$ *do*
8. *Create Sensors*
   end
9. **end**
10. Add Modules (*CloudOnly, FogOnly, HybridCF*)
11. Defining data dependencies by creating edges between the application modules:
    Ward → *Master Module/Fog Module* → *Master Module/Cloud Module* → *Actuator*
12. Module mapping
13. Tuple mapping
14. Submit application
15. Start *WorkflowSim*

All the operations conducted within the WorkflowSim toolkit were referred to as ‘tuples.’ These tuples were generated by connected sensors and processed by Virtual Machines (VMs) situated at the Fog nodes. Each VM was configured to process a specific type of tuple. The Fog devices supplied the necessary computational resource for the application modules to perform their tasks. In our proposed architecture, a First Come First Serve (FCFS) scheduling strategy was employed to allocate tasks to the application modules.

As the number of sensors per Fog node increased, there was a corresponding escalation in the processing load on that particular fog node. The resources of each fog node were heavily utilized for task detection for an expanded number of patients, leading to heightened network utilization and increased power consumption for that specific fog node. To evaluate performance and alleviate the computational burden on the fog nodes, a hybrid cloud-fog architecture with a critical task's priority algorithm was introduced.

The parameter settings for the sensors, master fog, fog nodes, proxy server, and cloud—all of which are used in simulation—are shown in Table 3. As described in more detail below, these settings covered a variety of factors, including levels, RAM, million instructions per second (MIPS), upstream and downstream bandwidth, CPU length, idle power, busy power, and more.

Table3: Parameter settings for cloud and fog-based implementations

Parameters	Sensor	Master node	Fog node	Proxy server	Cloud
Level	3	2	2	1	0
Ram	1000	4000	4000	4000	40,000
CPU length (MIPS)	500	2800	2800	2800	44,800
Rate per MIPS	0	0	0	0	0.01
Idle power	82.44	83.43	83.4333	83.4333	16 * 83.25
Downlink bandwidth	–	10,000	10,000	10,000	10,000
Uplink bandwidth	10,000	10,000	10,000	10,000	1000
Busy power (in Watts)	87.53	107.339	107.339	107.339	16 * 103

5 Simulation Result and Discussion

In order to corroborate the outcomes of the suggested cloud, fog, and cloud-fog hybrid architectures, a comparative analysis was conducted between the cloud, fog-only, and hybrid cloud-fog systems with critical task priority. This examination focused on assessing parameters related to network consumption and energy utilization. Various simulations were executed to scrutinize performance of the proposed system, comparing the results achieved by cloud, fog-only, and hybrid cloud-fog systems. We employed an equal number of cloud and fog devices, totalling five. The results of the architecture with varying numbers of sensors and different flow scenarios, including cloud, fog-only, and cloud-fog, are presented in Table 4 below.

Table 4: Results of cloud, fog and hybrid cloud-fog system at different number of sensors

Number of sensors	Cloud only			Fog only			Cloud-fog		
	Time	Network	Energy	Time	Network	Energy	Time	Network	Energy
3	2591.82	813.66	105.44	–	–	–	–	–	–
5	1494.03	1361.04	101.67	–	–	–	–	–	–
10	734.04	2121.03	77.85	–	–	–	–	–	–
15	286.66	3218.82	46.14	–	–	–	–	–	–
3	–	–	–	3174.62	733.709	116.46	–	–	–
5	–	–	–	1596.91	1174.86	93.81	–	–	–
10	–	–	–	622.13	2241.89	69.74	–	–	–
15	–	–	–	227.44	3927.62	44.66	–	–	–
3	–	–	–	–	–	–	1922.15	515.79	59.49
5	–	–	–	–	–	–	1030.31	845.30	52.26
10	–	–	–	–	–	–	452.06	1454.31	39.45
15	–	–	–	–	–	–	171.37	2382.15	24.49

5.1 Comparative Results at Cloud Only

To assess the performance of the cloud, simulations were conducted across various numbers of sensors and cloud servers. The number of sensors is represented on the x-axis, while time, network data utilization, and energy in the cloud are depicted on the y-axis. Energy results are presented in Decijoule (10–1 J) units for better visibility in the bar graph.

Figure 3 illustrates that with 3, 5, 10, and 15 sensors, the values of network, energy, and time at the cloud server. Network data utilization at 10 and 15 sensors is 5.70% and 22.02% better when compared to fog servers, but at 3 and 5 sensors, the results showed a 9.83% and 13.68% decrease compared to fog servers. Similarly, when employing 3 sensors, energy utilization is 10.45% better than with fog nodes, while for 5, 10, and 15 sensors, the results decreased by 7.74%, 10.42%, and 3.19%, respectively.

Finally, in the case of 3 and 5 sensors with the cloud server, it resulted in a 22.49% and 6.89% improvement in energy comparison, but the results decreased for 10 and 15 sensors.

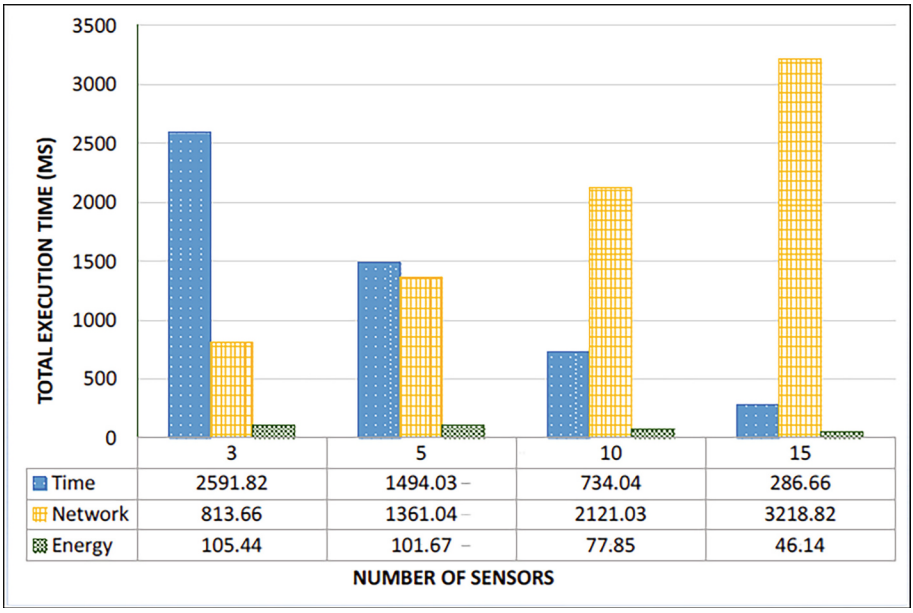


Fig. 3. Time, energy and network consumption in cloud servers only

5.2 Comparative Results at Fog Only

To evaluate cloud performance, simulations were conducted across a range of sensor configurations at the fog server. The number of sensors is plotted on the x-axis, while network data utilization, energy, and time in the fog are displayed on the y-axis. Energy results are presented in Decijoule (10–1 J) units to enhance their visibility in the bar graph.

Figure 4 reveals that, with 3, 5, 10, and 15 sensors, data values for network, energy, and time are observed at the fog-only server. Network data utilization with 10 and 15 sensors outperformed fog servers by 5.39 and 18.05%, whereas with 3 and 5 sensors, there is a 10.90 and 15.85% reduction compared to cloud servers. Due to the limited computational power of fog nodes, the results are degraded initially. Similarly, when using 5, 10, and 15 sensors, energy utilization is 8.38, 11.63, and 3.29% more efficient than with cloud servers, while for 3 sensors, the results declined by 9.46%.

In the case of 10 and 15 sensors with the fog nodes, there is a 17.99 and 26.04% improvement in time, but the results deteriorated for 3 and 5 sensors.

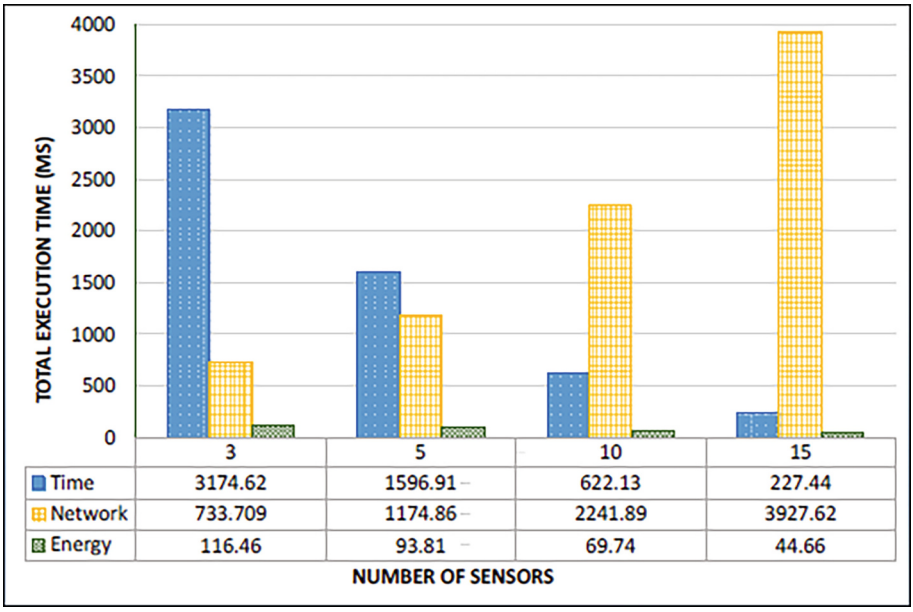


Fig. 4. Time, energy and network consumption in fog servers only

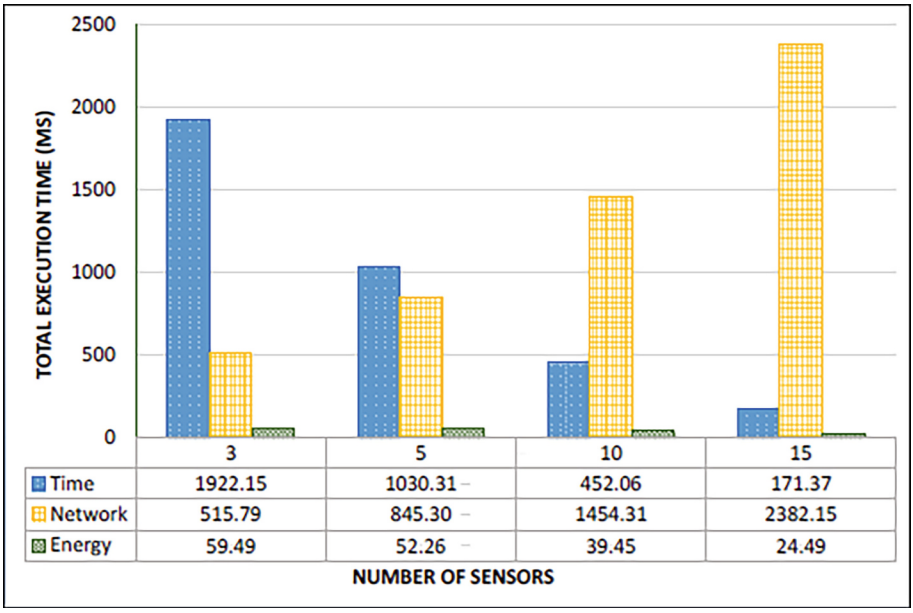
The results indicate that certain parameter values show higher utilization in cloud-only systems, while others are more prominent in fog-based systems.

5.3 Comparative Results at Cloud-Fog

To assess cloud-fog performance, simulations were executed using various sensor configurations with cloud-fog systems. The number of sensors is depicted on the x-axis, while network data utilization, energy consumption, and time within the fog are represented on the y-axis. The energy results are quantified in Decijoule (10–1 J) units to enhance visibility in the bar graph.

Figure 5 demonstrates that, with 3, 5, 10, and 15 sensors, data values for network, energy, and time are observed in the cloud-fog hybrid system. Network data utilization is superior with 3, 5, 10, and 15 sensors, surpassing fog servers by 29.70, 28.05, 35.13, and 39.35%, while for 3, 5, 10, and 15 sensors, the results increased by 36.61, 37.89, 31.43, and 25.99% compared to cloud servers.

Similarly, when employing 3, 5, 10, and 15 sensors, energy utilization is 48.92, 44.29, 43.44, and 45.16% more efficient than fog servers, whereas for 3, 5, 10, and 15 sensors, the results increased by 43.59, 48.60, 49.33, and 46.91% for cloud. In the case of 3, 5, 10, and 15 sensors with the fog nodes, there was a 39.45, 35.48, 27.34, and 24.65% improvement in time. The results for 3, 5, 10, and 15 sensors were 25.84, 31.04, 38.42, and 40.22% better in cloud only.



	3	5	10	15
Time	1922.15	1030.31	452.06	171.37
Network	515.79	845.30	1454.31	2382.15
Energy	59.49	52.26	39.45	24.49

Fig. 5. Time, energy and network consumption in cloud-fog system

6 Conclusion and Future Works

We implemented an architecture that combined cloud, fog-only, and a hybrid of cloud-fog systems to collect data from sensors, giving priority to highly critical tasks within the cloud-fog hybrid system. Following data processing, appropriate feedback was dispatched to actuators, enabling swift responses to any patient issues. Our approach revealed a prioritization of very critical tasks over critical and normal ones.

The simulation results demonstrates that the hybrid cloud-fog system outperforms both the cloud-only and fog-only systems in terms of time, energy efficiency, and network utilization. Specifically, with 3, 5, 10, and 15 sensors, the hybrid cloud-fog system exhibited time improvements of 39.45%, 35.48%, 27.34%, and 24.65%, respectively. In terms of energy utilization, the hybrid system is 48.92%, 44.29%, 43.44%, and 45.16% more efficient than the fog-only system for the same sensor quantities. Similarly, for 3, 5, 10, and 15 sensors, energy efficiency increased by 43.59%, 48.60%, 49.33%, and 46.91% when compared to the cloud-only system.

Moreover, the results indicate that the cloud-fog system outperforms fog-only systems by 29.70, 28.05, 35.13, and 39.35% for the respective sensor quantities, while surpassing cloud-only systems by 36.61, 37.89, 31.43, and 25.99%. In conclusion, our findings highlight the superior performance of the hybrid cloud-fog system compared to cloud and fog-only systems.

For future work, we aim to incorporate additional quality-of-service parameters, such as latency, sensor lifetime, and scheduling algorithms, into the architecture.

References

1. Miraz, M.H., Ali, M., Excell, P.S., Picking, R.: Internet of nano-things, things and everything: future growth trends. Futur. Internet **10**(8) (2018). https://doi.org/10.3390/fi10080068
2. Bansal, S., Aggarwal, M., Aggarwal, H.: Advancements and applications in fog computing. In: Security Designs for the Cloud, IoT, and Social Networking, pp. 207–240 (2019)
3. George, A.S.H., Shahul, A., George, A.S.: Wearable sensors: a new way to track health and wellness. Partners Univers. Int. Innov. J. **01**(August), 15–34 (2023). https://doi.org/10.5281/zenodo.8260879
4. Olshansky et al.: The future of smart health. Computer (Long. Beach. Calif) **49**(11), 14–21 (2016). https://doi.org/10.1109/MC.2016.336
5. Haleem, A., Javaid, M., Singh, R.P., Suman, R.: Telemedicine for healthcare: capabilities, features, barriers, and applications. Sens. Int. **2** (2021). https://doi.org/10.1016/j.sintl.2021.100117
6. Bohr, A., Memarzadeh, K.: The rise of artificial intelligence in healthcare applications (2020)
7. Bansal, S., Aggarwal, H., Aggarwal, M.: A systematic review of task scheduling approaches in fog computing. Trans. Emerg. Telecommun. Technol. **33**(9), 4523 (2022). https://doi.org/10.1002/ett.4523
8. Merrill, N., Eskandarian, A.: Modified autoencoder training and scoring for robust unsupervised anomaly detection in deep learning. IEEE Access **8**, 101824–101833 (2020). https://doi.org/10.1109/ACCESS.2020.2997327
9. Arya, D., Dave, M.: Priority based service broker policy for fog computing environment. Commun. Comput. Inf. Sci. **712**, 84–93 (2017). https://doi.org/10.1007/978-981-10-5780-9_8
10. Aladwani, T.: Scheduling iot healthcare tasks in fog computing based on their importance. Procedia Comput. Sci. **163**, 560–569 (2019). https://doi.org/10.1016/j.procs.2019.12.138
11. Hassan, H.O., Azizi, S., Shojafar, M.: Priority, network and energy-aware placement of IoT-based application services in fog-cloud environments. IET Commun. **14**(13), 2117–2129 (2020). https://doi.org/10.1049/iet-com.2020.0007
12. Haque, M., Islam, R., Rubayeth Kabir, M., Narin Nur, F., Nessa Moon, N.: A Priority-Based Process Scheduling Algorithm in Cloud Computing, vol. 755. Springer, Singapore (2019)
13. Ijaz, S., Munir, E.U., Ahmad, S.G., Rafique, M.M., Rana, O.F.: Energy-makespan optimization of workflow scheduling in fog–cloud computing. Computing **103**(9), 2033–2059 (2021). https://doi.org/10.1007/s00607-021-00930-0
14. Madhura, R., Elizabeth, B.L., Uthariaraj, V.R.: An Improved List-Based Task Scheduling Algorithm for Fog Computing Environment, vol. 103, no. 7. Springer, Vienna (2021)
15. Xu, F., Yin, Z., Gu, A., Li, Y., Yu, H., Zhang, F.: Adaptive scheduling strategy of fog computing tasks with different priority for intelligent production lines. Procedia Comput. Sci. **183**, 311–317 (2021). https://doi.org/10.1016/j.procs.2021.02.064
16. Abdel-Basset, M., Moustafa, N., Mohamed, R., Elkomy, O.M., Abouhawwash, M.: Multi-objective task scheduling approach for fog computing. IEEE Access **9**, 126988–127009 (2021). https://doi.org/10.1109/ACCESS.2021.3111130
17. Liu, Y., Du, C., Chen, J., Du, X.: Scheduling energy-conscious tasks in distributed heterogeneous computing systems. Concurr. Comput. Pract. Exp. **34**(1), 1–18 (2022). https://doi.org/10.1002/cpe.6520
18. Bansal, S., Aggarwal, H.: Priority-based cloud-fog architecture for smart healthcare systems. In: 2022 IEEE International Conference on Current Development in Engineering and Technology (CCET), pp. 1–7 (2022). https://doi.org/10.1109/CCET56606.2022.10080672
19. Chen, J., Han, P., Zhang, Y., You, T., Zheng, P.: Scheduling energy consumption-constrained workflows in heterogeneous multi-processor embedded systems. J. Syst. Archit. **142**(July), 102938 (2023). https://doi.org/10.1016/j.sysarc.2023.102938

20. Awaisi, K.S., Abbas, A., Khan, S.U., Mahmud, R., Buyya, R.: Simulating fog computing applications using iFogSim toolkit. In: Mobile Edge Computing, pp. 565–590. Springer International Publishing, Cham (2021)

Evaluation of Engineering Properties of Sandy Soil Stabilized with RBI Grade-81 Stabilizer

Neero Gumsar Sorum(✉) and Jinata Sanasam

Department of Civil Engineering, North Eastern Regional Institute of Science and Technology (NERIST), Nirjuli, Arunachal Pradesh, India
neerogsorum@gmail.com

Abstract. The present study aimed to examine the effects of Road Building International (RBI) Grade-81 stabilizer, a revolutionary inorganic and eco-friendly additive, on the engineering properties of sandy soil. For this, various performance evaluation experiments such as Compaction, Unconfined Compression Strength (UCS), Permeability, and California Bearing Ratio (CBR) were carried out. The different dosages of RBI grade-81 used in the present study were 2, 4, 6, and 8%. In the test result of compaction characteristics, it was found that the RBI Grade-81 stabilizer decreased maximum dry density and increased the optimum moisture content of the soil samples. The maximum reduction in permeability value was found to be 71% at 6% RBI Grade-81. The UCS value of the soil at 6% RBI Grade-81 was two times higher with respect to the untreated soil at curing period of 14 days. Further, the UCS values increased proportionally to the curing periods. The CBR value of the stabilized soil under unsoaking and soaking states increased significantly with the stabilizer. The maximum increase in CBR values at 6% RBI Grade-81 were 48.22% and 58.65% respectively for soaking and unsoaking conditions. In concluding remark, RBI Grade-81 can be optimized up to 6% as a promising stabilizer, especially for heavy rainfall areas like Arunachal Pradesh state region and sandy subgrade.

Keywords: RBI Grade-81 · Compaction · Unconfined compressive strength · Permeability

1 Introduction

Construction of pavements is done by passing through different locations having different soil types and different weather conditions. For such kind of road construction, stabilization of weak soils is required to improve its strength, durability, and load-bearing capacity. Soil stabilization is a practical process to upgrade the engineering properties of the soils by blending and mixing other materials. Several researchers have explored various soil stabilization techniques using different stabilizers (e.g., lime, bitumen, fiber, cement, pozzolana, fly ash, tire, glass, fiber, zeolite) for many years to investigate geotechnical properties of soils [1–9].

Al-Swaidani et al. [2] found that the addition of pozzolona on lime-treated clay enhanced significantly the CBR value by up to 90%. The test results of micrographs

© The Author(s), under exclusive license to Springer Nature Singapore Pte Ltd. 2026
M. Kumar et al. (Eds.): HSFEA 2023, LNCE 899, pp. 77–87, 2026.
https://doi.org/10.1007/978-981-92-3200-0_7

also showed the existence of C-S-H and C-A-S-H in treated soils, due to which the workability, strength compaction, and shrinkage properties of the treated soil improved. Choobbasti and Kutanaei [7] conducted a similar kind of study on cemented-stabilized sandy soil with nano-silica stabilizer. They found that the UCS value increased till 8% of nano-silica content and then dropped down with the rise in the stabilizer content from 8 to 12%. It was also found that the soil samples with longer curing periods exhibited higher UCS values for all nano-silica contents. Further, The X-ray diffraction results showed the appearance of micro-cracks in the soil samples. Brahmachary and Rokonuzzaman [5] stabilized organic soil with various percentages of bamboo fiber. With the increase in length, diameter, and dosage of the fiber, the CBR value, under soaking and unsoaking conditions, was increased [5]. Singh and Mittal [9] conducted an experimental examination of the stabilization of silty soil using different contents of plastic waste. They found that increase of plastic waste dosage to the soil samples showed drastically increment in UCS and OMC values (by 3–13%), and marginal effect on MDD (0.06–0.23%). Aryal and Kolay [3] experimented durability property of silty soil which was stabilized with two stabilizers i.e., Cement and polypropylene fiber. The best combination in terms of economical and durability was 5% cement + 0.5% fibre mixture. Beena and Santhosh [4] evaluated the impact of lime and Jarofix additives on various mechanical properties of the red soil. They concluded that the soil may be stabilised using 40–50% Jaofix and 7.5% lime without compromising the UCS and CBR criteria or polluting the ecosystem.

However, all the above-mentioned soil stabilization techniques have some limitations which are well documented in the review article by Firoozi et al. [10]. In such cases, the soil stabilization technique using RBI Grade-81 stabilizer is considered to be an alternative because the stabilizer has a broad scale of response spectrum [11]. The RBI Grade-81, considered one of the promising stabilizers in the recent past, is an environmental-friendly and natural soil additive that can alter characteristics of the soils to improve the performance of pavement subgrade [12]. This stabilizer functions effectively via hydration process [13]. It is a good material for reducing the costs of flexible pavement constructions [14].

Some studies have reported RBI Grade-81 usage as a stabilizer in stabilizing clayey subgrade soil [11–13, 15–19]. Gunturi et.al. [15] conducted a micro-level investigation of expansive Soil stabilised with RBI Grade-81. Reduced soil pores were seen in Scanning Electron Microscope (SEM) micrographs, and this structural alteration at the micro level indicated an increase in the UCS values. Similar findings were seen in Taib et al. [18] study. The UCS value improved as proportion of the stabiliser and curing time increased [15]. Taib et al. [18] evaluated the strength characteristics of Serian soil stabilized with RBI Grade-81 stabilizer. They found that the UCS attained at 8% of RBI Grade-81 after a 14-day curing period was 6.0 times more than that of the untreated soil. Kodicherla and Nandyala [12] found that the CBR value increased with increase in percentages of the stabiliser. The UCS value of the clayey soil stabilized at 8% of RBI Grade-81 was 3–3.5 times more than that of the untreated. A similar study was conducted by Kumar and Solanki [16], wherein it was concluded that RBI Grade-81 with a maximum of 5% might optimise mechanical properties of the clayey soil, which could then be employed as the subgrade. Jala and Sharma [11] studied the impact of RBI Grade-81stabilizer

along with Cement Kiln Dust (CKD) on mechanical properties of plastic clay. Plasticity of the clayey soil was reduced, and UCS and CBR values increased when the soil was stabilized with CKD and RBI Grade-81. They also recommended using up to 4% RBI Grade-81 and 15% CKD in subgrade soil for roads in rural areas [11]. RBI Grade-81 and fly ash stabilisers were used to stabilise clay, and it was observed that the addition of these stabilizers enhanced OMC value and lowered MDD value of the soil [13]. Further, they proposed that the optimal ratio for building a sub-base course for roads was 5:20:75 (RBI Grade-81:Fly ash: Soil). Mallick and Verma [17] conducted a thorough laboratory experiment to see the performance of coal mine overburden stabilised with RBI Grade-81 stabilizer. They found that addition of the stabilizer enhanced UCS, CBR and dynamic Young's modulus values of all composites. Further, it was observed that the composite (94%Murrum + 6%RBI) exhibited a satisfactory performance in term of strength gain. The impacts of RBI Grade-81 stabilizer on the expanding soil strength parameters were investigated by Venugopal et al. [19]. According to their findings, the maximum increase in CBR value were 9.8% for a soaked condition and 24.02% for an unsoaked condition.

Based on the above literature, it is observed that all researches were concentrated on expansive soil (i.e., clayey soil) only. This motivated the authors to examine the effects of Road Building International (RBI) Grade-81 stabilizer on the geotechnical properties of locally available sandy soil.

2 Materials and Method

2.1 Soil

The soil was gathered from an open excavation that was about 1.0 m below the level of the road near Joram—Palin—Sangram—Koloraing Road, Arunachal Pradesh state, India. The soil was dried by air, ground, and then stored in airtight containers in the lab. The Indian Standard Code of conduct (IS:2720) was followed in conducting the fundamental tests and the results are presented in Table 1.

Table 1. Physical properties of the soil

Properties	Values
Grain size distribution	
Gravel	2%
Sand	93%
Silt	4%
Clay	1%
Specific gravity	2.64
Classification of soil	SP
Maximum dry density (g/cm^3)	1.78
Optimum moisture content (%)	15.47

(*continued*)

Table 1. (*continued*)

Properties	Values
Unconfined compressive strength (kPa)	127
Permeability (cm/s)	8.2×10^{-3}
California bearing ratio (%)	
Soaked	7.14
Unsoaked	8.61

2.2 RBI Grade-81

This stabilizer, recognized across worldwide including India, was used for the present work which was obtained from M/S Alchemist Touchnology Limited, Delhi, India. The properties of RBI Grade-81 are reported in Table 2 [20, 21].

Table 2. Properties of RBI Grade-81 [20, 21]

Properties	Values
Odor	Odorless
Storage	Dry
PH	12.5
Specific gravity	2.5
Bulk density	700 kg/m^3
Flammability	Inflammable
Solubility	0.2 pts/100 pts (in water)
Freezing point	None
Self-life	12 months

2.3 Method

Different laboratory experiments were performed on the sandy soil samples with and without RBI Grade-8 for the determination of particle size distribution (IS: 2720, Part 4-1985), compaction characteristics (IS: 2720, Part 8-1983), permeability (IS: 2720, Part-17-1986), UCS (IS: 2720, Part 10-1986), and CBR (IS: 2720, Part 16-1987). The 2, 4, 6, and 8% of RBI Grade-81 were used in the present study.

3 Results and Discussion

3.1 Compaction Characteristics

The results of compaction characteristics (MDD and OMC) are tabulated in Table 3, and presented in Figs. 1 and 2. The MDD and OMC are the key parameters of compaction characteristic of the subgrade soil and so these values must be maintained in quality control process to attain stable pavement subgrade. It is illustrated, from the Fig. 1, that the MDD values decreased with increasing RBI Grade-81 content. The development of a flocculated structure due to cementitious bonding between sand grains and the stabilizer, which makes compaction more difficult, may be the cause of decrease in MDD values. RBI Grade-81 particles' lower specific gravity than the parent soil was cited as another explanation for this decline in MDD value. The OMC values increased with increasing percentage of the stabilizer (Fig. 2). This is because a flocculated structure has formed, which contains more water and needs lubrication to compress.

Table 3. OMC and MDD values

Mixture proportion (%)	OMC (%)	MDD (g/cm^3)
Soil + RBI (100: 0)	15.47	1.78
Soil + RBI (98: 2)	15.60	1.70
Soil + RBI (96: 4)	15.90	1.66
Soil + RBI (94: 6)	16.20	1.61
Soil + RBI (92: 8)	16.38	1.57

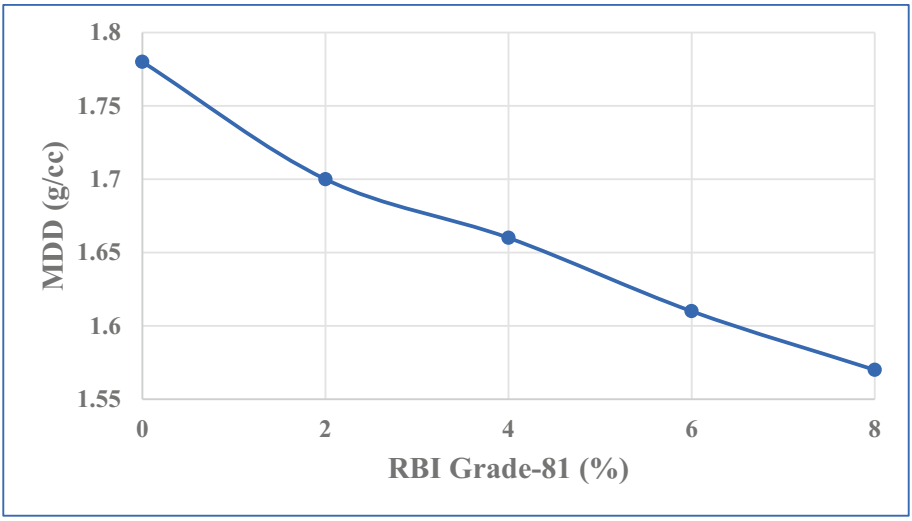


Fig. 1. MDD with RBI Grade-81

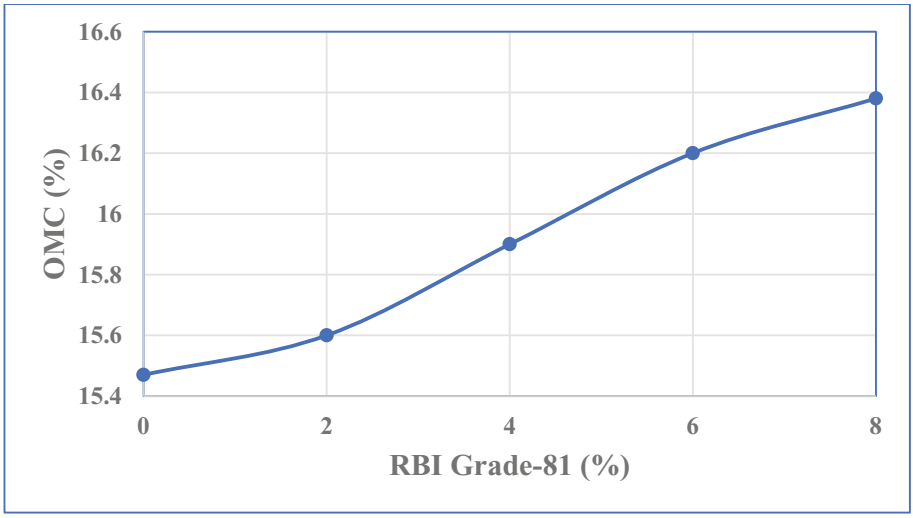


Fig. 2. OMC with RBI Grade-81

3.2 Permeability

Permeability values of Falling-Head Permeability Test are tabulated in Table 4 and presented in Fig. 3. The test results show that with increasing stabilizer dosage, a significant reduction in permeability value was observed, but marginal reduction was observed after 6% RBI Grade-81. The permeability values of the untreated and 6% RBI Grade-81treated soils were 8.2×10^{-3} cm/s and 2.4×10^{-3} cm/s respectively, and reduction amount in permeability value was calculated to be 71% at the corresponding stabilizer dosage. This may be interpreted as an indication of pore spaces filled with the stabilizer. The stabilizer bounds particles to each other which, in turn, leads to the strength enhancement as well as permeability reduction of the treated soil.

Table 4. Reduction in permeability value of the treated soil.

Mixture proportion (%)	Permeability value ($\times 10^{-3}$) (cm/s)	Reduction in permeability value (%)
Soil + RBI (100: 0)	8.2	–
Soil + RBI (98: 2)	6.5	21
Soil + RBI (96: 4)	3.9	52
Soil + RBI (94: 6)	2.4	71
Soil + RBI (92: 8)	2.3	72

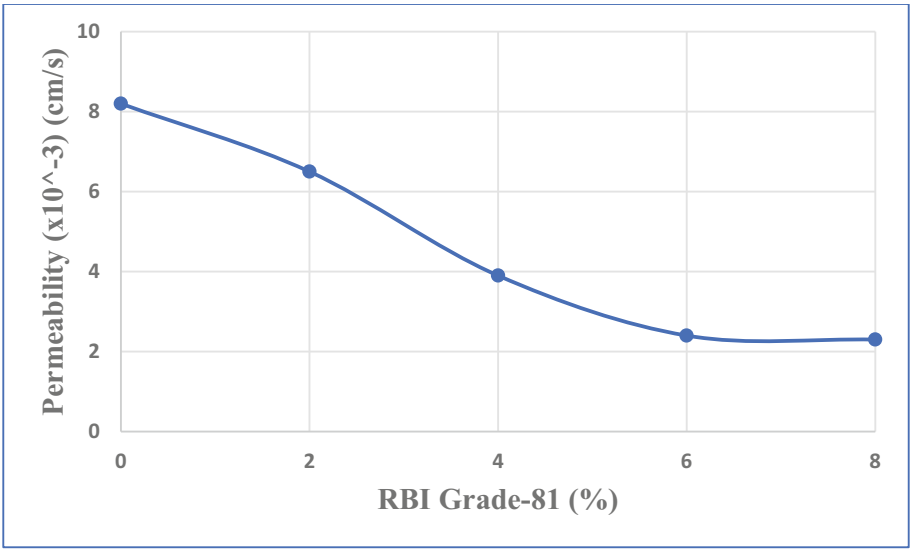


Fig. 3. Permeability variation with different dosage of RBI Grade-81

3.3 Unconfined Compressive Strength (UCS)

The UCS values of the samples for different curing time are reported in Table 5 and presented graphically in Fig. 4. The obtained results show that an increased dosage of RBI Grade-81 stabilizer induced a significant increment in UCS values. However, this increase was only seen up to 6% of RBI Grade-81; after that, there was no significant change. The reason for this condition may be the excess amount of stabilizer and a lack of water to react with the extra RBI Grade-81. When compared to untreated soil at 14 days of curing, the UCS value was twice as high at 6% of RBI Grade-81. Additionally, it has been shown that the UCS values increased proportionately to the curing time, and this tendency became more pronounced as stabilizer amounts increased.

Table 5. UCS values of the soil at different curing period.

Mixture proportion (%)	Unconfined compressive strength (kPa)			
	Curing period (days)			
	0	7	14	28
Soil + RBI (100: 0)	127	127	127	127
Soil + RBI (98: 2)	133	170	187	235
Soil + RBI (96: 4)	147	201	261	297
Soil + RBI (94: 6)	152	267	312	322
Soil + RBI (92: 8)	154	269	314	320

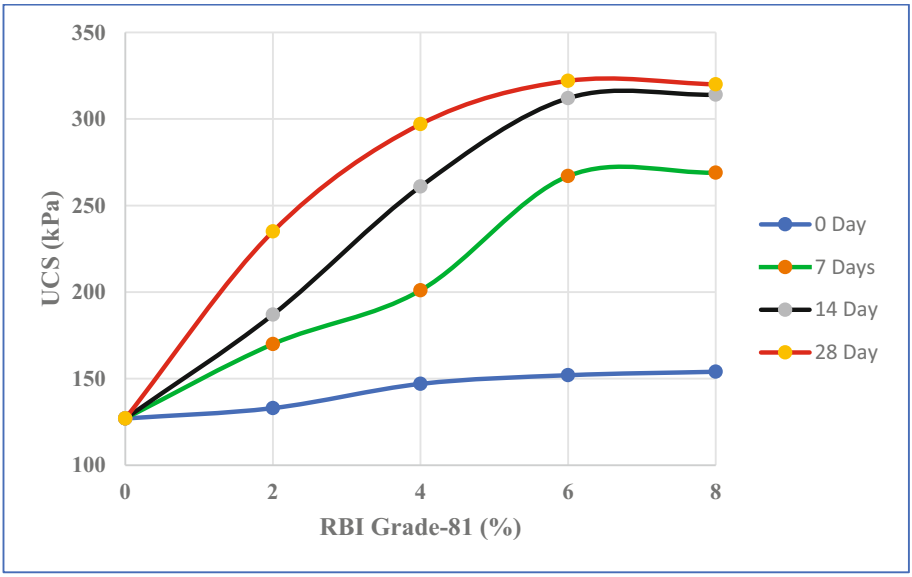


Fig. 4. UCS variation with curing period and RBI Grade-81

3.4 California Bearing Ratio (CBR)

The laboratory results of CBR test for the stabilized soil under soaking and unsoaking state are tabulated in Table 6 and presented in Fig. 5. The figure illustrates that CBR value, under both soaking and unsoaking conditions, increased with the increasing the RBI Grade-81 content. Further, the CBR values of the soaking condition were lesser than that of the unsoaking condition in all dosages of the stabilizer. The percentage increases in CBR values under soaking and non-soaking conditions were 49.29% and 59.23%, respectively. Also, there was marginal increase in the CBR value which was stabilized at 8% RBI Grade-81 as compared to that at 6% stabilizer addition.

Table 6. Unsoaked and soaked CBR values

Mixture proportion (%)	CBR (%)	
	Unsoaked	Soaked
Soil + RBI (100: 0)	8.61	7.14
Soil + RBI (98: 2)	12.43	9.82
Soil + RBI (96: 4)	16.32	11.65
Soil + RBI (94: 6)	20.82	13.79
Soil + RBI (92: 8)	21.12	14.08

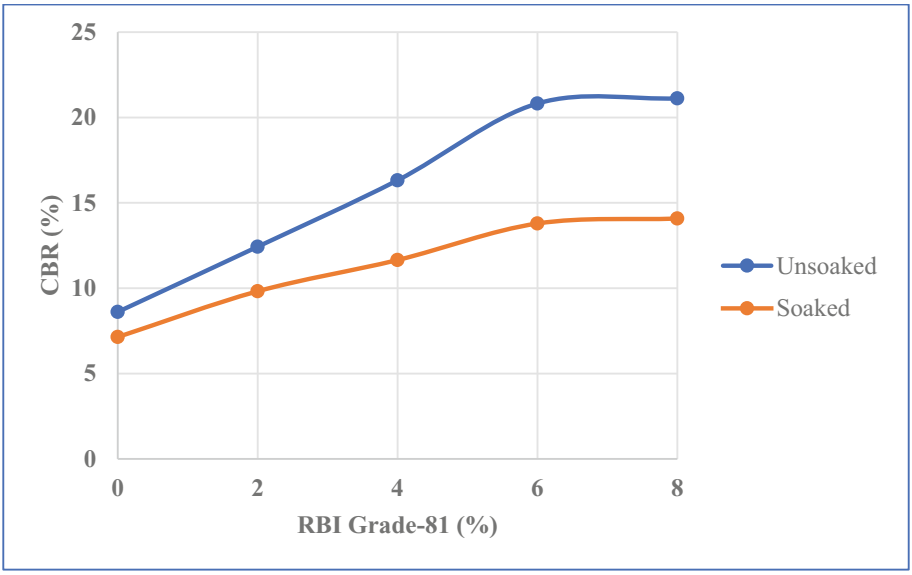


Fig. 5. Soaked and unsoaked CBR values variation with RBI Grade-81

4 Conclusions

Some of the key findings of this paper are outlined below:

- The MDD value decreased with increasing percentage of RBI Grade-81 stabilizer, whereas the OMC value was increased.
- The permeability value was decreased with increasing dosage of the stabilizer. The maximum reduction in permeability value was found to be 71% at 6% RBI Grade-81.
- The UCS of the soil improved with increasing RBI Grade-81 dose and curing time. When compared to untreated soil at 14 days of curing, the UCS value was twice as high at 6% of RBI Grade-81.
- The CBR value, under both soaking and unsoaking conditions, marked considerable increased with the increasing dosages of the stabilizer in the soil mixture. This increase was evident up to 6% of the stabilizer, beyond which no significant increase was noticed.

Overall, it is concluded based on above findings that the RBI Grade-81 can be suggested as a promising additive at 6% dose with curing period of 14 days, especially for heavy rainfall areas like Arunachal Pradesh state region and sandy subgrade.

References

1. Al-Bared, M.A.M., Marto, A., Latifi, N.: Utilization of recycled tiles and tyres in stabilization of soils and production of construction materials—a state-of-the-art review. KSCE J. Civ. Eng. **22**, 3860–3874 (2018). https://doi.org/10.1007/s12205-018-1532-2

2. Al-Swaidani, A., Hammoud, I., Meziab, A.: Effect of adding natural pozzolana on geotechnical properties of lime-stabilized clayey soil. J. Rock Mech. Geotech. Eng. **8**, 714–725 (2016). https://doi.org/10.1016/j.jrmge.2016.04.002
3. Aryal, S., Kolay, P.K.: Long-term durability of ordinary Portland cement and polypropylene fibre stabilized kaolin soil using wetting–drying and freezing–thawing test. Int. J. Geosynth. Gr. Eng. **6** (2020). https://doi.org/10.1007/s40891-020-0191-9
4. Beena, K.S., Santhosh, G.: Transport geotechnical properties of lateritic soil stabilized with Jarofix and lime. Environ. Dev. Sustain. **23**, 1601–1622 (2021). https://doi.org/10.1007/s10668-020-00641-0
5. Brahmachary, T.K., Rokonuzzaman, M.: Investigation of random inclusion of bamboo fiber on ordinary soil and its effect CBR value. Int. J. Geo-Eng. **9** (2018). https://doi.org/10.1186/s40703-018-0079-x
6. Diaz Caselles, L., Hot, J., Roosz, C., Cyr, M.: Stabilization of soils containing sulfates by using alternative hydraulic binders. Appl. Geochem. **113** (2020). https://doi.org/10.1016/j.apgeochem.2019.104494
7. Choobbasti, A.J., Kutanaei, S.S.: Microstructure characteristics of cement-stabilized sandy soil using nanosilica. J. Rock Mech. Geotech. Eng. **9**, 981–988 (2017). https://doi.org/10.1016/j.jrmge.2017.03.015
8. Rios, S., Da Fonseca, A.V., Bangaru, S.S.: Silty sand stabilized with different binders. Procedia Eng **143**, 187–195 (2016). https://doi.org/10.1016/j.proeng.2016.06.024
9. Singh, K., Mittal, A.: Soil Stabilisation Using Plastic Waste, vol. 32. Springer, Singapore (2019). https://doi.org/10.1007/978-981-13-7017-5_10
10. Firoozi, A.A., Guney Olgun, C., Firoozi, A.A., Baghini, M.S.: Fundamentals of soil stabilization. Int. J. Geo-Eng. **8** (2017). https://doi.org/10.1186/s40703-017-0064-9
11. Jala, S.K., Sharma, P.: Effect of Cement Kiln Dust and RBI Grade 81 on Engineering Properties of Plastic Clay, vol. 32. Springer, Singapore (2019). https://doi.org/10.1007/978-981-13-7017-5_5
12. Kodicherla, S.P.K., Nandyala, D.K.: Effect of RBI Grade 81 on strength characteristics of clayey subgrade. Int. J. Geo-Eng. **8** (2017). https://doi.org/10.1186/s40703-017-0061-z
13. Verma, V., Abhishek.: Stabilization of clayey soils using fly ash and RBI grade 81. In: Lecture Notes in Civil Engineering; 21 LNCE:95–102 (2019). https://doi.org/10.1007/978-3-030-02707-0_13
14. Patil, V., Joshi, P., Kale, S., Pingle, T.: Design of Flexible Pavement on Black Cotton Soil Stabilized with RBI Grade 81, vol. 31. Springer, Singapore (2019). https://doi.org/10.1007/978-981-13-7010-6_18
15. Gunturi, M., Ravichandran, P.T., Divya Krishnan, K., Annadurai, R., Kannan Rajkumar, P.R.: Micro level analysis of RBI 81 stabilized expansive soil. Int. J. ChemTech Res. **7**, 666–672 (2015)
16. Kumar, K., Solanki, A.J.: Evaluation of RBI Grade 81 for stabilization of expansive soil as sub-grade material. Mater. Today Proc. **4**, 9737–9741 (2017). https://doi.org/10.1016/j.matpr.2017.06.258
17. Mallick, S.R., Verma, A.K.: Performance of RBI"' stabilized coal mine overburden material for haul road pavement. Arab. J. Geosci. **13** (2020). https://doi.org/10.1007/s12517-020-05649-4
18. Taib, S.N.L., Striprabu, S., Ahmad, F., Charmaine, H.J., Patricia, N.E.: Investigation on strength development in RBI Grade 81 stabilized serian soil with microstructural considerations. IOP Conf. Ser. Mater Sci. Eng. **136** (2016). https://doi.org/10.1088/1757-899X/136/1/012016
19. Venugopal, G., Naagesh, S., Gangadhara, S.: Impact of RBI Grade-81 on expansive soil strength characteristics. Mater. Today Proc. **46**, 5171–5175 (2019). https://doi.org/10.1016/j.matpr.2021.01.716

20. Gupta, G., Sood, H., Gupta, P.K.: Geotechnical and geo-environmental properties of discrete polyester fibre-reinforced and RBI Grade-81-stabilized clay and sand. IOP Conf. Ser. Earth Environ. Sci. 219 (2019). https://doi.org/10.1088/1755-1315/219/1/012019
21. Munaga, T., Kumar, K.: Comparative studies of black cotton soil with RBI Grade 81 and ground granulated blast furnace slag (2015)

Biodiesel Production with Algae Oil Blend with ANFIS, ANN and RSM Technique

Sunil Kumar[1](✉), Siddharth Jain[2], and Harmesh Kumar[3]

[1] Department of Mechanical Engineering, Gurukula Kangri (DU), Haridwar, India
Sunil508@rediffmail.com
[2] Department of Mechanical Engineering, University of Petroleum and Energy Studies, Dehradun, India
[3] Department of Mechanical Engineering, Panjab University, Chandigarh, India

Abstract. Artificial neural network, Adaptive neuro-fuzzy inference system and Response surface methodology are accessed on transesterification of Algae-Jatropha oil with methanol along with KOH with microwave power. This was investigated considering mole ratio (6–12), catalyst amount (0–2 wt%), Temperature (35–55 °C) and time (60–180 min.) by Box Behnken Design. Statistical performance showed ANFIS ($R^2 = 0.9998$, Root mean square error = 0.225 and adj $R^2 = 0.997$) and ANN ($R^2 = 0.9976$, Root mean square error = 1.8628 and adj $R^2 = 0.9797$) models depict process have great precision parallel to RSM ($R^2 = 0.9867$, Root mean square error = 2.121 and adj $R^2 = 121.54$).

Keywords: Jatropha-Algae oil · Box–Behnken design · ANFIS · ANN

1 Introduction

In last studies, clean oil has been selected by researchers in case of biodiesel development, as oils has less processing time & not suggested pre-treatment transesterification [1]. Inedible oils from tobacco, rubber, castor, jatropha and another for biodiesel extraction. Biodiesel is favourable alternate for diesel due to likeness between physiochemistry of diesel and biodiesel [2]. Karanja oil fatten in large amount on Indian regions, is promising raw feed for biodiesel generation [3]. RSM is tool used for design of experiment, modelling, and optimization. It is modelling tool that relates more than one response to independent variables. It gives numerical on individual model and interactions between them [4]. Biodiesel generation from different oils using RSM [5, 6]. It is not as effective as ANFIS and ANN during estimation capability [7, 8].

ANN is tool, which work like neurology of mankind brain. It was described as excellent tool in simulation and modelling of complex systems by its ability of learning and identify correlation between output and input [9]. Neural Network is best evolutionary method in few years. ANN contain capacity to resolve complex situations and control of nonlinear, non-parametric regression, data classification and grouping, or as behavioural simulations by accumulation of neurons. Number of topologies have been

© The Author(s), under exclusive license to Springer Nature Singapore Pte Ltd. 2026
M. Kumar et al. (Eds.): HSFEA 2023, LNCE 899, pp. 88–101, 2026.
https://doi.org/10.1007/978-981-92-3200-0_8

created to optimize biodiesel production, along with to improve property, engine efficiency and emission effect [10–12]. ANFIS is joint of neuro and fuzzy. It contains both in one capsule which delivered it potential to get advantages of tools [13]. Contribution toward setting benefit of selection of modelling and optimization of process and to further behaviour of 3 techniques. Present investigation is concentrated on modelling transesterification for of Algae oil into biodiesel by three tools. Efficiency of techniques are observed statistically using R^2, adjusted R^2, MSE and Root Mean Square Error.

2 Experimental Methodology

Biodiesel Preparation

Figure 1 depicts process of conversion Jatropha-Algae oil into biofuel with household used microwave with, ANFIS, RSM and ANN. In biodiesel generation process, transesterification implemented. Make this possible, catalyst is poured to reaction [14] the general sequence of 3 steps, In 1st point, triglycerides to diglycerides are created, then diglycerides to monoglycerides it is generated in 2nd point and in final step, esters and glycerine created [15, 16]. Stoichiometric ratio between oil and alcohol is 1:3. To conduct transesterification reaction, reactor having stirrer and thermometer was utilized. Reactor is primarily poured with required oil, and after that put on hot plate. After getting oil at required temp., catalyst and alcohol were put to vessel. Transesterification reaction, calculated quantity of molar ratio (6–12), KOH (0–2%), time (60–180 min) and temperature (35–55 °C). Mixture is put to funnel, permitted glycerol to distinguish for one day. After removing glycerol, methyl ester is washed 3 times, with hot distilled water to dived catalyst and glycerol.

$$\text{Yield} = \frac{\textit{Weight of methyl ester produced}}{\textit{Weight of Oil used}} \times 100 \tag{1}$$

Experimental design and model development by RSM

RSM is mixture of statistical and mathematical technique depend on fit of equation, which depict response of data with aim of creating data measurement. It could be implemented during response influenced by variables. RSM is created by Box and others in 50s [17, 18]. Implementation of RSM for analytical technique is consolidated principally due to its benefits to classical optimization technique, such as creation of huge quantity of data by little number of practices and possibility of estimating interaction [19].

A 4-factor-3-level BBD is implemented on process. Table 1 depicts level and range of independent variables. Table 2 depict table with 29 numbers of run testing are performed. Experimental outcomes by matrix are identified by RSM in Design Expert.

Development of the ANFIS model

ANFIS is system employed in structure of network. Neuro-fuzzy integrate neural network and fuzzy to generate great expert decision [20]. It was both neural and fuzzy principles, capacity to get advantages of both in one. So, ANFIS is consider universal estimator [21]. 2 types of fuzzy generally used are Mamdani method and Sugeno method [22]. 29 data numbers are split into 60%, 20%, and 20% sets for training, testing, and

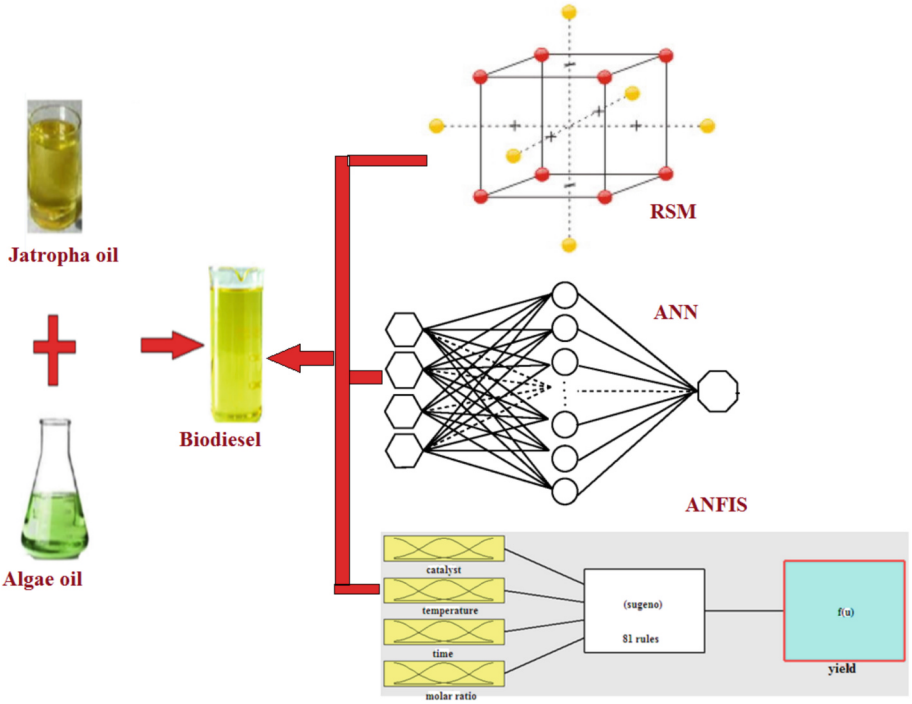


Fig. 1. Conversion of Jatropha-Algae oil into biodiesel

Table 1. Variable range

Parameters	Unit	Range
Catalyst amount	%	0–2
Temperature	°C	35–55
Reaction time	Minutes	60–180
Methanol/oil ratio	%	6–12

validating respectively. Epochs value is 100 and error tolerance is 0. Node was 12 and Error found is 0.2073. Figure 2 depicts ANFIS model for oil blend. First layer considers as inputs which were displayed with black colour nodes on left part. Catalyst quantities, temperature, reaction duration, and molar ratio are all inputs into the proposed model. There were 12 nodes with appropriate membership functions in the second layer, three for each input. This layer is subjected to a fuzzification procedure using Gaussian functions. 3rd layer display fuzzy set's rules, which amount 81 in total. Output membership functions for different rules were dealt with in fourth layer, and fifth layer is an average of fourth-layer outputs. Last layer displays the defuzzified result. Figure 3 depicts experimental and estimated result with run, confirming model's precision.

Table 2. Responses results

S. No.	X_1: catalyst amount	X_2: temperature	X_3: reaction time	X_4: methanol/oil ratio	Biodiesel yield (Y) Experimental	ANFIS	Biodiesel yield ANN	Biodiesel yield RSM
1	2	45	120	12	54.82	54.82	60.24	55.85
2	1	55	180	9	94.12	94.12	89.51	91.31
3	1	55	120	12	92.21	92.21	92.50	90.35
4	0	45	120	6	91.57	91.57	91.65	88.31
5	1	35	120	12	77.11	77.11	77.33	78.44
6	1	55	60	9	77.76	77.76	77.91	75.85
7	1	45	120	9	76.57	76.09	76.43	76.06
8	0	45	60	9	87.57	87.57	87.73	86.98
9	1	35	60	9	80.4	80.4	80.85	81.43
10	1	55	120	6	75.28	75.28	75.39	74.32
11	1	45	180	12	93.26	93.26	93.70	93.31
12	1	45	120	9	76.62	76.09	76.43	76.09
13	1	45	120	9	75.82	76.09	76.43	76.09
14	2	45	180	9	62.39	62.39	62.54	63.08
15	1	35	120	6	90.16	90.16	90.01	92.41
16	2	35	120	9	72.32	72.32	73.21	68.49
17	2	45	120	6	56.37	56.37	56.44	57.38
18	1	45	60	12	65.36	65.36	66.20	66.67
19	2	55	120	9	53.84	53.84	54.72	54.98
20	1	45	120	9	75.28	76.09	76.43	76.09
21	0	45	120	12	96.98	96.98	97.05	93.61
22	0	35	120	9	92.4	92.02	92.59	91.74
23	0	55	120	9	98.92	98.92	94.81	105.89
24	1	45	120	9	76.17	76.09	76.43	76.09
25	1	45	60	6	77.83	77.83	72.00	78.86
26	1	35	180	9	91.14	91.14	93.33	91.80
27	1	45	180	6	76.93	76.93	77.08	76.46
28	2	45	60	9	53.12	53.12	54.02	52.39
29	0	45	180	9	96.29	96.29	96.17	98.03

Development of ANN model

One of the most powerful mathematical modelling techniques is the ANN. Build the right model with ANN, many more experiments will be required. However, if data in input and output are numerically viable, Design of experiments [23], ANN can operate effectively even with very minimal data. It is made up of neurons, which are fundamental computing units that are coupled in a parallel framework. In order to forecast the process under consideration, a neuro-evolutive approach was used (reading of yield depend on

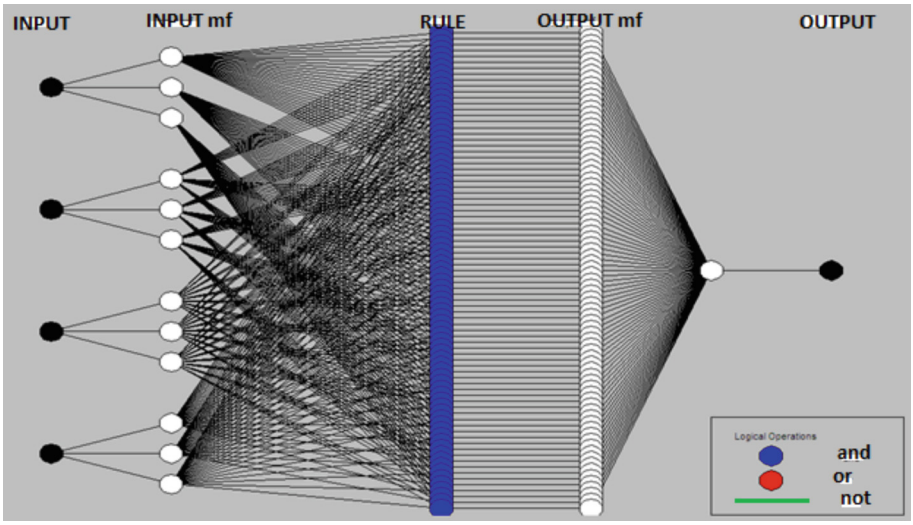


Fig. 2. ANFIS structure

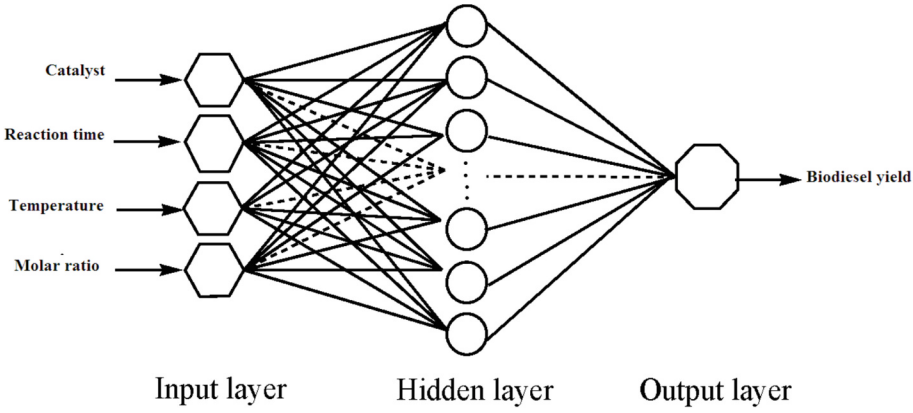


Fig. 3. Architecture of ANN

catalyst, time, m-ratio and temperature). Three-layered neural network is employed in this investigation, using tansig at input and hidden layers, and purelin at output layer. Equation 3 shows tangent sigmoid function:

$$f(x) = [2/(1 + e^{-2x})] - 1 \tag{3}$$

And linear transfer function depict in Eq. 4:

$$f(x) = \mathrm{x} \tag{4}$$

Input, output layer & hidden layer contain 10 neurons made up ANN architecture. Figure 3 depicts the architect structure of ANN. It functions as "black box", needing no

particular knowledge system and no explicit statement of equations that control system under investigation. Biodiesel yield was utilised as benchmark. Fundamental aim is to understand link between previously recorded input and output data [24].

3 Results and Discussion

Interactive effect of parameters using RSM model

Depend on research reading as written in Table 2, regression equation generated which describe empirical link between output variable and parameters. Polynomial model has been developed as shown in Eq. 5.

$$\begin{aligned}\mathrm{Ln(Yield)} = {} & +7.78758 + 0.33308 \times X_1 - 0.10125 \times X_2 \\ & - 6.27034 \times 10^{-3} \times X_3 - 0.19875 \times X_4 \\ & - 9.08171 \times 10^{-3} \times X_1 \times X_2 + 2.74690 \times 10^{-4} \times X_1 \times X_3 \\ & - 7.10692 \times 10^{-3} \times X_1 \times X_4 + 2.73170 \times 10^{-5} \times X_2 \times X_3 \\ & + 2.99339 \times 10^{3} \times X_2 \times X_4 + 5.09878 \times 10^{-4} \times X_3 \times X_4 \\ & - 0.065152 \times X_1^2 + 8.68911 \times 10^{-4} \times X_2^2 \\ & + 6.04019\mathrm{E} \times 10^{-6} \times X_3^2 + 6.98471 \times 10^{4} \times X_4^2 \end{aligned} \quad (5)$$

where X_1 represents catalyst concentration, X_2 represents temperature, X_3 represents reaction duration, and X_4 represents the m-ratio. Suggested results is examined to check whether any problems in normalcy consideration. Influence of factors on output is described by regression eqn. Each point positive notation describes a synergetic effect, although negative notation describes an antagonistic effect [27].

Table 3 depicts the ANOVA of experimental work for the jatropha-algae biodiesel project. Model was important. By the noise, only 0.01 percent probability that F reading must be high. R^2 and R^2 adj, which shows model dependability, are measured to be 0.98 and 0.97

Table 3. ANOVA result

S. N.	Parameters	Process
1	Model	Significant
2	Lack of fit	Not significant

The three-dimensional plot is shown in Fig. 4a–f. Direct link between two independent factors and impacts on yield is shown in Fig. 4a–f. Effect of temp. and catalyst on manufacturing output of methyl ester is shown in Fig. 4a. The biodiesel production improves dramatically when the catalyst is used in small amounts and at low temperatures. Furthermore, with a large amount of catalyst and a high reaction temperature, the yield drops dramatically. This is because the triglyceride saponification reaction is aided

by a bigger amount of catalyst at a high temperature. Figure 4b shows response graph of interaction impact between time and catalyst quantity. After increasing the conversion performance of biodiesel to ideal level, it is determined that there was no substantial improvement in efficiency. A longer period of time not indicate significant change in transformation performance. While maintaining other variables constant, Fig. 4c depicts effect of catalyst quantity and m-ratio on conversion. The graphical depiction shows that increasing quantity of KOH has no meaningful effect on output.

In 35–55 °C, raising temperature has influence on biodiesel performance, as shown by Fig. 4d, when all other factors, such as molar ratio, KOH concentration, and temperature, are maintained constant. Increases in time have favourable effect on yield, with the duration range being 60–180 min and all other factors being held constant. Facts listed above correspond to the graphs in Figs. 4e–f methanol was used in transesterification, yield initially rises as molar ratio rises. Temperature effect is less on greater time because longer time allow reaction to depict better output at low temperature.

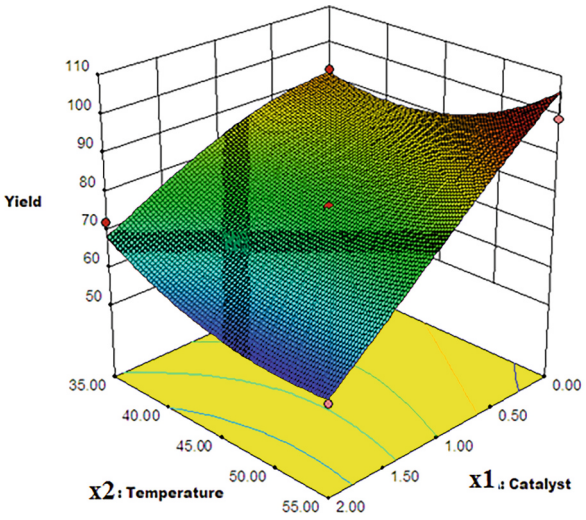
Optimization of Biodiesel

Design Expert application was utilized to create an optimisation process for independent value and found great values for output target. Goal is to maximise yield output. Optimisation at (1:10) molar ratio, (0.3) percent KOH concentration, (53 °C) temperature, and (172) minute duration resulted in 100% yields. Practical validation tests predicted best conditions. Average output of biodiesel in experiment 96%.

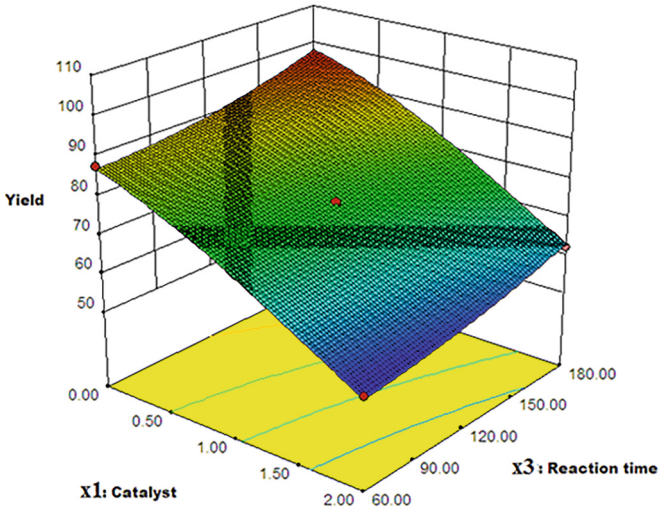
Performance test of predictive capability of models

Figure 5 shows experimented and predicted reading versus run, proving model's accuracy. R^2 and RMSE for ANFIS model are 0.999 and 0.225. High R^2 and low RMSE described that model's evaluation is excellent and that it may be used to produce biodiesel yields. When compared to other algorithms, Levenberg–Marquardt method having topology 4-10-1 produces the great results. TRAINLM with back propagation has superior convergence [25] along with great training element [26] out of 15 topologies and three training functions. For this ANN model, the maximum overall R, R^2 and topology values are 0.997 and 0.991 with 4-10-1. Figure 6 depicts scatter plot. R^2, modified R^2, RMSE, and sum of square error are used to evaluate performance of created RSM, ANFIS, and ANN in predicting yield value of Jatropha-Algae oil. Figure 7 shows the regression graphs of estimated and experimental values.

The three models all showed high R^2 values that were virtually unity, suggesting that they were well-fitting. According to statistical indices, best model was ANFIS, followed ANN, and finally RSM. Run numbers were shown against experimental and anticipated values from three models (Fig. 8). RSM model was less accurate, as shown by the graph. Prediction abilities, ANFIS appears to be more accurate than ANN. Both ANN and ANFIS are shown to be higher to RSM in prediction accuracy in this study. ANFIS was superior to ANN.

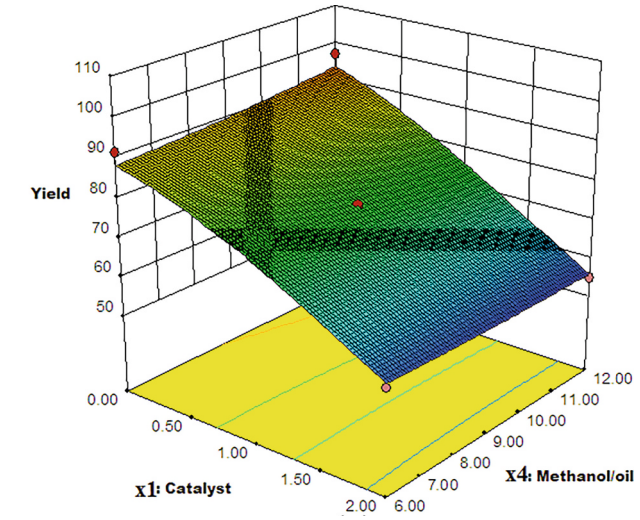


(a)

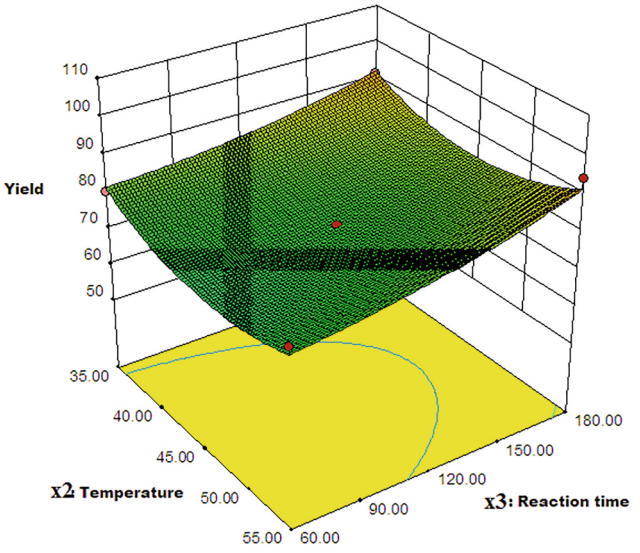


(b)

Fig. 4. **a** Yield versus catalyst amount & temperature. **b** Yield versus catalyst amount & time. **c** Yield versus catalyst amount & methanol to oil. **d** Yield versus temperature & time. **e** Yield versus temperature & methanol/oil. **f** Yield versus time & methanol/oil

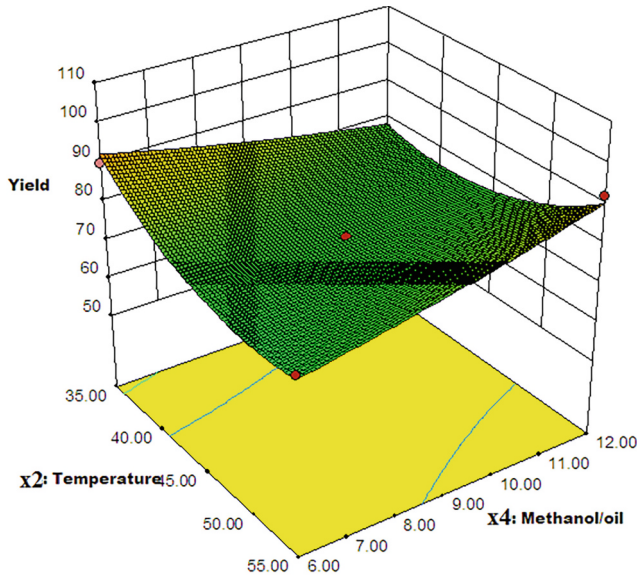


(c)

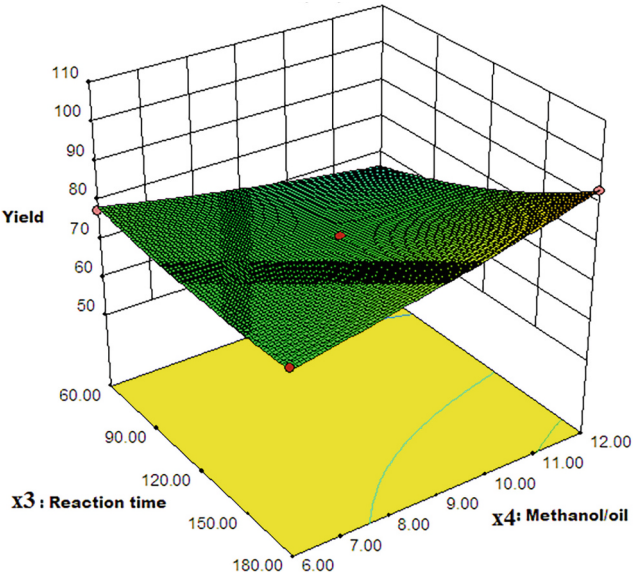


(d)

Fig. 4. (*continued*)



(e)



(f)

Fig. 4. (*continued*)

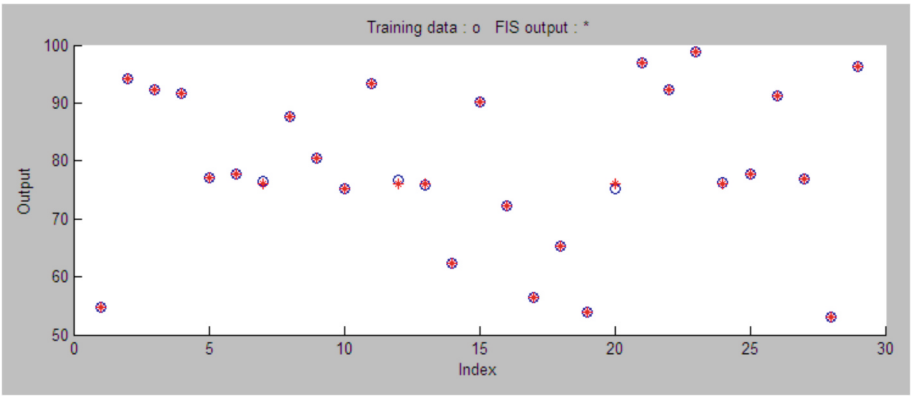


Fig. 5. FIS output

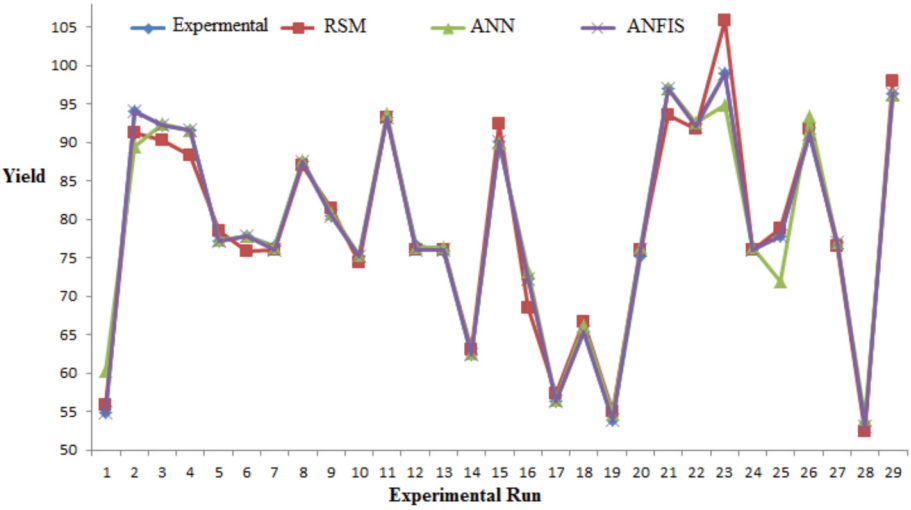


Fig. 8. Comparison of predicted and experimental value

4 Conclusion

In this article, choice of modelling and optimization in transformation of Jatropha-Alge oil to biodiesel by microwave assisted transesterification. Based on numerical evaluated, performance of model according to accuracy was in as ANFIS, ANN and RSM. Statistical data utilize in measuring capacity of generated models depict RSM model ($R^2 = 0.9867$, Root mean square error = 2.121 and adj R^2 = 121.54) was least efficient in accuracy and precision of estimated yield. ANFIS model (R^2 = 0.999, Root mean square error = 0.225 and adj R^2 = 0.997) was superior to ANN (R^2 = 0.9976, Root mean square error = 1.8628 and adj R^2 = 0.9797). Biodiesel blend yield with 96% is achieved by methanol/oil volume ratio (1/10) mixing KOH (potassium hydroxide) as catalyst (0.3%

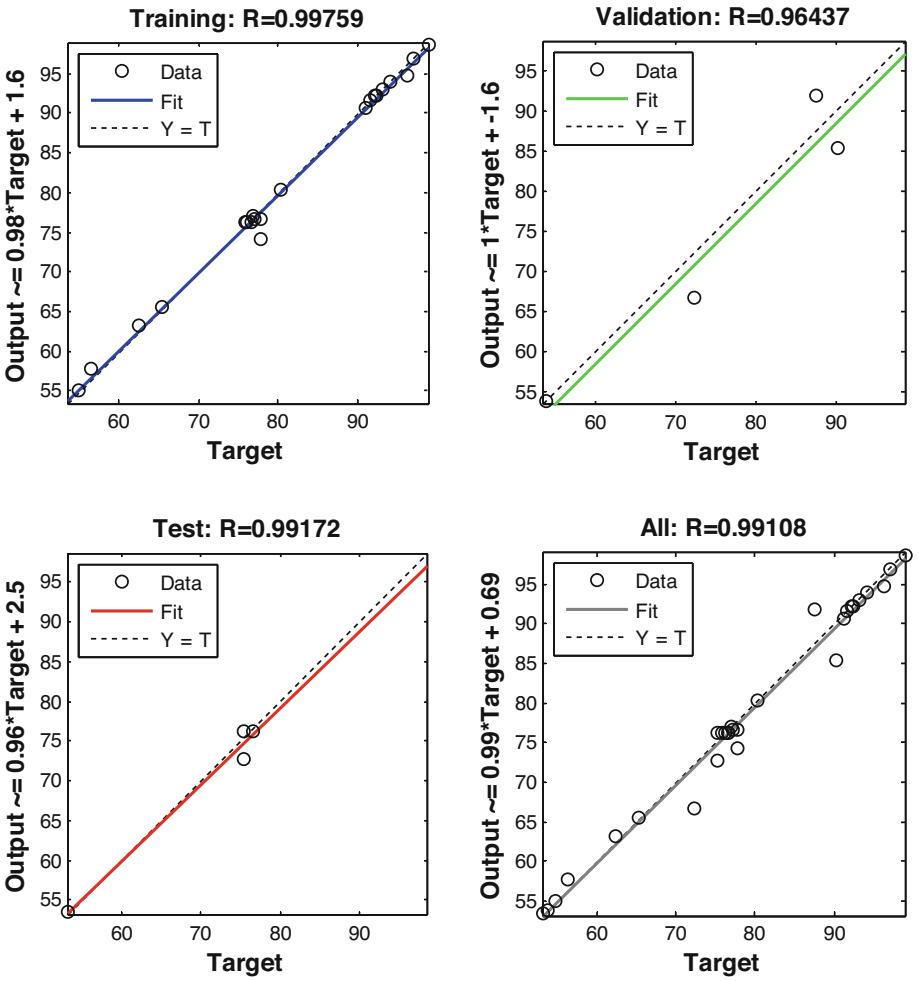


Fig. 6. Training, validation, test and overall scatter plot

w/w) in 172-min. time on 53 °C. Its physical and chemical properties are nearby to standard specifications (Table 4).

Table 4. Comparison between performance of ANFIS, ANN and RSM

S. No.	Methodology	R^2	ADJ-R^2	RMSE	SSE
1	ANFIS	0.9998	0.9997	0.225	1.378
2	ANN	0.9976	0.9797	1.8628	93.683
3	RSM	0.9867	0.9735	2.121	121.54

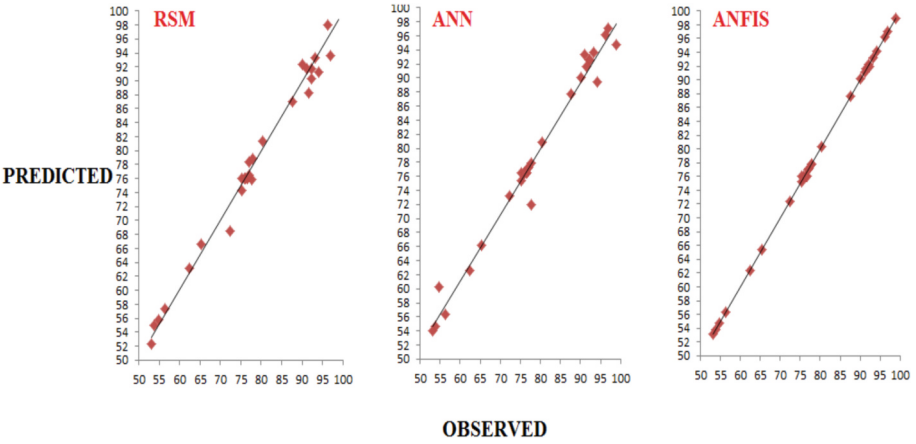


Fig. 7. Regression plot of predicted and experimental value

References

1. Giwa, S., Abdullah, L.C., Adam, N.M.: Investigating "Egusi" (*Citrullus Colocynthis* L.) seed oil as potential biodiesel feedstock. Energies **3**, 607–618 (2010). https://doi.org/10.3390/en3040607
2. Faried, M., Samer, M., Abdelsalam, E., Yousef, R.S., Attia, Y.A., Ali, A.S.: Biodiesel production from microalgae: processes, technologies and recent advancements. Renew. Sustain. Energy Rev. **79**, 893–913 (2017). https://doi.org/10.1016/j.rser.2017.05.199
3. Meher, L.C., Dharmagadda, V.S.S., Naik, S.N.: Optimization of alkali-catalyzed transesterification of Pongamia pinnata oil for production of biodiesel. Biores. Technol. **97**, 1392–1397 (2006). https://doi.org/10.1016/j.biortech.2005.07.003
4. Sarve, A., Sonawane, S.S., Varma, M.N.: Ultrasound assisted biodiesel production from sesame (*Sesamum indicum* L.) oil using barium hydroxide as a heterogeneous catalyst: comparative assessment of prediction abilities between response surface methodology (RSM) and artificial neural network (ANN). Ultrason. Sonochem. **26**, 218–228 (2015). https://doi.org/10.1016/j.ultsonch.2015.01.013
5. Kumar, S., Deswal, V.: Optimization at low temperature transesterification biodiesel production from soybean oil methanolysis via response surface methodology. Energy Sources, Part A 1–10 (2019).https://doi.org/10.1080/15567036.2019.1649331
6. Kumar, S., Jain, S., Kumar, H.: Performance evaluation of adaptive neuro-fuzzy inference system and response surface methodology in modeling biodiesel synthesis from jatropha–algae oil. Energy Sources, Part A **40**, 3000–3008 (2018). https://doi.org/10.1080/15567036.2018.1515277
7. Betiku, E., Odude, V.O., Ishola, N.B., Bamimore, A., Osunleke, A.S., Okeleye, A.A.: Predictive capability evaluation of RSM, ANFIS and ANN: a case of reduction of high free fatty acid of palm kernel oil via esterification process. Energy Convers. Manage. **124**, 219–230 (2016). https://doi.org/10.1016/j.enconman.2016.07.030
8. Betiku, E., Okunsolawo, S.S., Ajala, S.O., Odedele, O.S.: Performance evaluation of artificial neural network coupled with generic algorithm and response surface methodology in modeling and optimization of biodiesel production process parameters from shea tree (Vitellaria paradoxa) nut butter. Renewable Energy **76**, 408–417 (2015). https://doi.org/10.1016/j.renene.2014.11.049

9. Zobel, C.W., Cook, D.F.: Evaluation of neural network variable influence measures for process control. Eng. Appl. Artif. Intell. **24**, 803–812 (2011). https://doi.org/10.1016/j.engappai.2011.03.001
10. Kusumo, F., Silitonga, A.S., Masjuki, H.H., Ong, H.C., Siswantoro, J., Mahlia, T.M.I.: Optimization of transesterification process for Ceiba pentandra oil: a comparative study between kernel-based extreme learning machine and artificial neural networks. Energy **134**, 24–34 (2017). https://doi.org/10.1016/j.energy.2017.05.196
11. Dharma, S., Hassan, M.H., Ong, H.C., Sebayang, A.H., Silitonga, A.S., Kusumo, F., et al.: Experimental study and prediction of the performance and exhaust emissions of mixed Jatropha curcas-Ceiba pentandra biodiesel blends in diesel engine using artificial neural networks. J. Clean. Prod. **164**, 618–633 (2017). https://doi.org/10.1016/j.jclepro.2017.06.065
12. Kumar, S.: Comparison of linear regression and artificial neural network technique for prediction of a soybean biodiesel yield. Energy Sources, Part A **42**, 1425–1435 (2020). https://doi.org/10.1080/15567036.2019.1604858
13. Yaghoobi, A., Bakhshi-Jooybari, M., Gorji, A., Baseri, H.: Application of adaptive neuro fuzzy inference system and genetic algorithm for pressure path optimization in sheet hydroforming process. Int. J. Adv. Manuf. Technol. **86**, 2667–2677 (2016). https://doi.org/10.1007/s00170-016-8349-2
14. Ma, F., Hanna, M.A.: Biodiesel production: a review. Bioresour. Technol. **70**, 1–15 (1999). https://doi.org/10.1016/S0960-8524(99)00025-5
15. Hartman, L.: Methanolysis of triglycerides. J. Am. Oil Chem. Soc. **33**, 129 (1956). https://doi.org/10.1007/BF02632297
16. Junzo, O.: Transesterification. Chem. Rev. **93**, 1449–1470 (1993). https://doi.org/10.1021/cr00020a004
17. Gilmour, S.G.: Response surface designs for experiments in bioprocessing. Biometrics **62**, 323–331 (2006). https://doi.org/10.1111/j.1541-0420.2005.00444.x
18. Bruns, R.E., Scarminio, I.S., B de Neto, B.: Statistical Design—Chemometrics. Elsevier (2006)
19. Bezerra, M.A., Santelli, R.E., Oliveira, E.P., Villar, L.S., Escaleira, L.A.: Response surface methodology (RSM) as a tool for optimization in analytical chemistry. Talanta **76**, 965–977 (2008). https://doi.org/10.1016/j.talanta.2008.05.019
20. Avci, E.: Comparison of wavelet families for texture classification by using wavelet packet entropy adaptive network based fuzzy inference system. Appl. Soft Comput. **8**, 225–231 (2008). https://doi.org/10.1016/j.asoc.2007.01.003
21. Jang, J.S.R., Sun, C.T., Mizutani, E.: Neuro-fuzzy and soft computing-a computational approach to learning and machine intelligence [book review]. IEEE Trans. Autom. Control **42**, 1482–1484 (1997). https://doi.org/10.1109/TAC.1997.633847
22. Negnevitsky, M.: Artificial Intelligence: A Guide to Intelligent Systems, 2nd ed. Addison-Wesley, Harlow, England ; New York (2005)
23. Chakraborty, R., Sahu, H.: Intensification of biodiesel production from waste goat tallow using infrared radiation: process evaluation through response surface methodology and artificial neural network. Appl. Energy **114**, 827–836 (2014)
24. Kara Togun, N., Baysec, S.: Prediction of torque and specific fuel consumption of a gasoline engine by using artificial neural networks. Appl. Energy **87**, 349–355 (2010). https://doi.org/10.1016/j.apenergy.2009.08.016
25. Rezaei, J., Shahbakhti, M., Bahri, B., Aziz, A.A.: Performance prediction of HCCI engines with oxygenated fuels using artificial neural networks. Appl. Energy **138**, 460–473 (2015). https://doi.org/10.1016/j.apenergy.2014.10.088
26. Bhowmik, S., Panua, R., Debroy, D., Paul, A.: Artificial neural network prediction of diesel engine performance and emission Fueled with diesel–kerosene–ethanol blends: a fuzzy-based optimization. J. Energy Res. Technol. **139** (2017). https://doi.org/10.1115/1.4035886

Prediction of Biodiesel Production from Algae Oil by Different Algorithm in Machine Learning

Sunil Kumar[1(✉)], Siddharth Jain[2], and Harmesh Kumar[3]

[1] Department of Mechanical Engineering, Gurukula Kangri (DU), Haridwar, India
sunil508@rediffmail.com
[2] Department of Mechanical Engineering, University of Petroleum and Energy Studies-, Dehradun, India
[3] Department of Mechanical Engineering, Panjab University, Chandigarh, India

Abstract. Biodiesel emerged as a renewable and clean energy source with potential to decline earth warming. So, data-driven machine learning system for biodiesel prediction via regression is investigated in study. Support vector machines, Linear regression, regression trees, and Gaussian process regression with various functions are among the regression algorithms used. The developed models were evaluated using a variety of performance indicators (such as R^2, residual analysis, MAE, and RMSE), as well as 5-fold cross validation. GPR model with Matérn class best results with R^2 of 0.91 and 4.1134 RMSE. The built models demonstrate performance using various algorithms. As a result, proposed approach would certify fast calculation of biodiesel yield from algal oil, potentially reducing time-consuming, expensive, and labor-intensive laboratory testing.

Keywords: Algae oil · Machine learning · Regression · Biodiesel · GPR

1 Introduction

As a renewable fuel for various applications such as transportation, biodiesel had proven to be wonderful substitute to traditional diesel. It has the capability to be useful in the growing of green friendly energy sources. So, the production of biodiesel from numerous renewable sources is latest topic. Biodiesel can be made from a variety of bio-based sources, including, algae, palm oil, waste cooking, and so on [1]. Algal oil is nice source for biodiesel production. Produces more oil per square metre of fertile land than other related sources. Indeed, using algal oil as a source of mass for biodiesel synthesis can be both economically and environmentally advantageous. In this case, either homogeneous or heterogeneous catalysts can be used to make biodiesel, but heterogeneous catalysts are favoured since they are easier to separate and recover spent catalyst at the conclusion of the process. As a result, much effort has gone into the synthesis and development of innovative and effective catalysts for the manufacture of biodiesel from various sources. Chemical synthesis using various methodologies is essential for catalyst development to improve its activity. Processing variables such as reaction time, temperature, and others must be inclined in generation of biodiesel by algal oil to produce best yield financially

© The Author(s), under exclusive license to Springer Nature Singapore Pte Ltd. 2026
M. Kumar et al. (Eds.): HSFEA 2023, LNCE 899, pp. 102–116, 2026.
https://doi.org/10.1007/978-981-92-3200-0_9

viable. Machine learning models for fetching useful experimental data are significant breakthroughs that have impacted a wide range of industries. Most experimental sciences have been affected by this truth. Ensemble methods such as bagging, boosting, and stacking are among the most employed. The goal of Ensemble models is to join numerous less effective models to create robust model [2–5]. Using response surface methods, various research have recently been proposed for projecting microalgae-based biodiesel yield [6–8]. In recent years, data science technologies have been used to solve complex scientific challenges. Machine learning model has been demonstrated be a good for predicting process in complex reaction, such as biodiesel production processes [9–15]. As can be seen from the above, yield prediction is a major concern for various applications, with various methodologies being considered. The goal of current study is use measured working value inputs to machine learning model to forecast biodiesel yield. As a result, decisions in biodiesel manufacturing can be made more efficiently. Many of the current studies use a variety of approaches and datasets, as well as diverse data collecting devices, processing strategies, and data scaling methods. As a result of this discrepancy, it is impossible to say model is the most accurate for prediction. To close gap, goal of this research is use a high-quality operational dataset to train along with validate multiple traditional regression model to compare and examine their biodiesel production prediction efficiency. Regression trees, Linear Regression (LR) of various sizes, Ensembles trees used boosting and bagging techniques, Support Vector Machine and Gaussian Process Regression used various kernels and covariance among machine learning regression models investigated. These are often used algorithms, and are selected for their efficiency, robustness, accuracy, and power. Different numbers of reading chosen for validation are undertaken to test their effect on output of models. Computational and correlation experiments are also carried out to investigate and investigate relationship between biodiesel yield and parameters.

In this study, multiple supervised regression modelling methods for predicting biodiesel production were chosen, including Linear Regression, Tree, SVM, and Gaussian Process Regression models. Catalyst amount and molar ratio with time and temperature, were chosen as model's inputs, while biodiesel production yield was chosen as model's output. The acquired results were used to calculate the production of biodiesel.

2 Methodology

Dataset and approach for concentrating on algorithms that result in given models are detailed in this section.

2.1 Data Set and Computational

A combination of algae oil and jatropha oil was utilize to transform biodiesel via a transesterification reaction. Figure 1 shows a representation of biodiesel production. Table 1 shows the experimentally observed biodiesel output from 29 tests. Box Behnken Design, one of RSM, was used to acquire the experimental data. SVM, LR, GPR, and tree are utilised to model these data. All models were created using Matlab R2020a. The catalyst (KOH), blend oil to methanol, temperature (°C), and reaction duration are all

descriptors variables in suggested models. Four descriptors are fed into model as input data. These characteristics have a significant impact on biodiesel yield, which can be linked to the development of intelligence systems that are extremely capable of learning the relationship between inputs and responses (biodiesel yields). Figure 2 depicts a flow chart of machine learning processing using fivefold cross-validation.

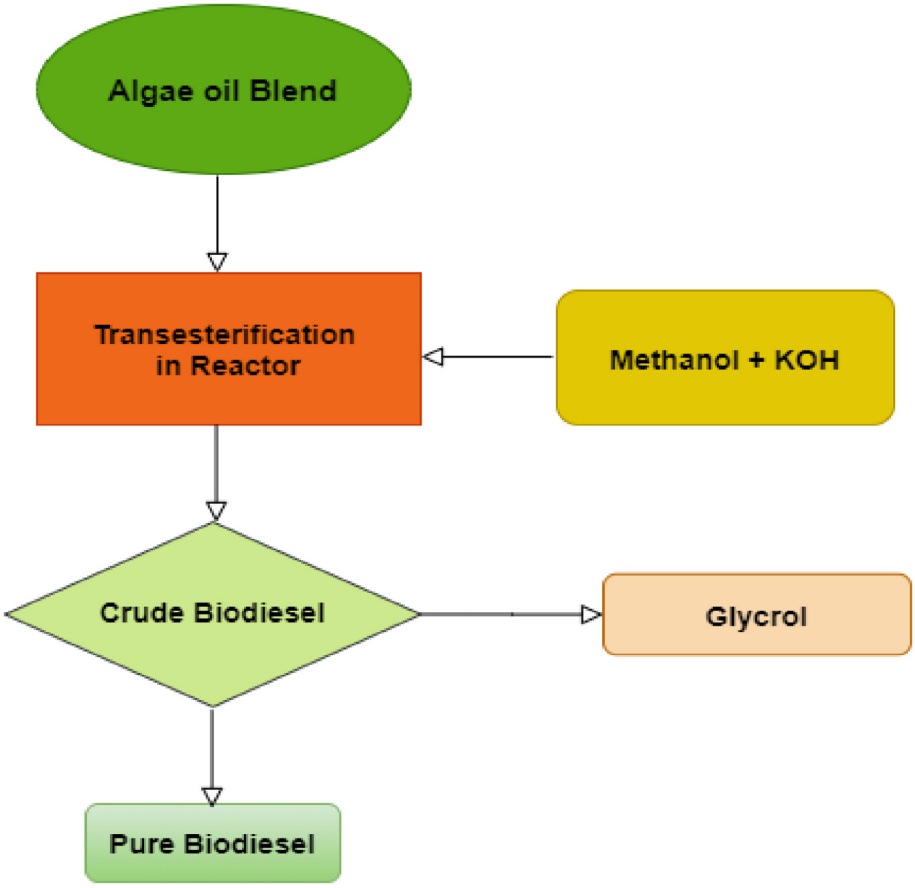


Fig. 1. Schematic diagram of biodiesel production

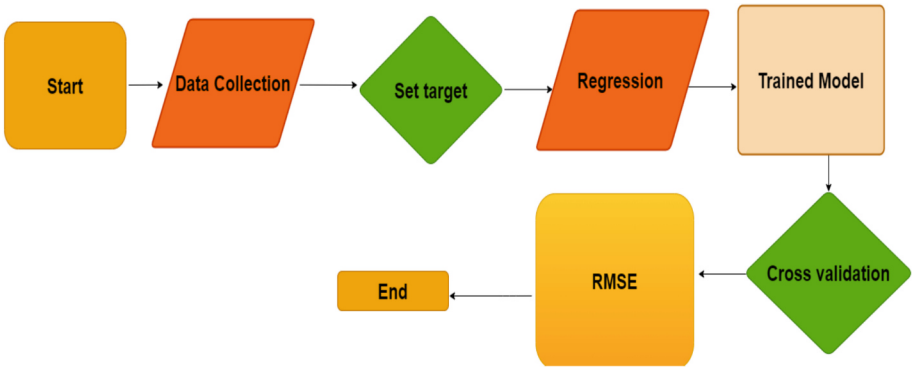


Fig. 2. Computational diagram machine learning

Table 1. Experimental values with parameters

Run	Catalyst amount	Temperature	Reaction time	Methanol/oil ratio	Blend biodiesel yield (%)	
					Experimental	Predicted
1	2	45	120	12	54.82	57.12
2	1	55	180	9	94.12	85.44
3	1	55	120	12	92.21	89.82
4	0	45	120	6	91.57	87.74
5	1	35	120	12	77.11	79.83
6	1	55	60	9	77.76	75.51
7	1	45	120	9	76.57	75.98
8	0	45	60	9	87.57	89.6
9	1	35	60	9	80.4	76.72
10	1	55	120	6	75.28	75.44
11	1	45	180	12	93.26	89.08
12	1	45	120	9	76.62	76.19
13	1	45	120	9	75.82	76.17
14	2	45	180	9	62.39	68.76
15	1	35	120	6	90.16	85.75
16	2	35	120	9	72.32	64.65
17	2	45	120	6	56.37	58.99
18	1	45	60	12	65.36	71.55
19	2	55	120	9	53.84	60.25
20	1	45	120	9	75.28	76.19
21	0	45	120	12	96.98	95.22
22	0	35	120	9	92.4	92.48

(*continued*)

Table 1. (*continued*)

Run	Catalyst amount	Temperature	Reaction time	Methanol/oil ratio	Blend biodiesel yield (%)	
					Experimental	Predicted
23	0	55	120	9	98.92	105.6
24	1	45	120	9	76.17	76.08
25	1	45	60	6	77.83	76.99
26	1	35	180	9	91.14	84.68
27	1	45	180	6	76.93	79.68
28	2	45	60	9	53.12	51.36
29	0	45	180	9	96.29	102.2

3 Prediction Models

Many factors influence biodiesel production, including operational conditions (such as alcohol, temperature, and catalyst), which are modelled. This study uses machine learning regression techniques predict yield as function of measured operational parameters. Variables are managed to train model to build mapping function with input to deduce output and then make predictions for data. Below sections explain variety of regression model with varying degrees of complexity and accuracy.

3.1 Linear Regression (LR)

Dependent variable (y) is predicted using linear regression by describing it, linear function of a predictor variable. y is monotonically connected to x in a single predictor variable regression issue, meaning that any variation in x will incline or decline (y). Scatter diagram of x and y displays basic trend, after which great line fit of form [16] is performed.

Formula for linear regression:

$$y = a + bx \tag{1}$$

a and b are the y-intercept and slope of linear regression, respectively. Equation becomes if best fit line pass by the origin.

$$y = bx \tag{2}$$

e is the error term in the generalised model for every output (y) and predictors (x, x,…, x). In this scenario, the biodiesel production process parameters are as follows:

$$y = \beta + \beta x + \beta x + \beta x + e \tag{3}$$

3.2 Regression Trees

The tree-based evaluation is an accurate and next level non-parametric model that works well with non-linear factors like ship operational records [17]. The first stage in creating a regression tree for prediction is to divide predictor variable into different non-overlapping regions (R_1 to R_j). Mean response values of training are then used to make predictions for each observations in distinct regions R(1…j) [18]. Meanwhile, the major objective is, locate regions that minimise Residual Sum of Square (RSS) as indicated.

$$\mathrm{RSS} = \sum_{j=1}^{n} (y_i - (\alpha + \beta x_i))^2 \tag{4}$$

Where,

α, β constant value
x, y set of values
n set value counts.

The size of the regression tree, as well as its accuracy, flexibility, and robustness, is determined by number of these leaves. While fine regression tree can yield accurate output, it also increases danger of overfitting. A coarse regression tree, on the other hand, has lesser training efficiency but is extra robust with reduced variance [18]. As a result, selecting the regression tree size is critical for striking a balance between complexity, accuracy.

3.3 Gaussian Process Regression

Has been widely recommended. GP-based regression models can also use a nonparametric technique to characterise uncertainty and non-linearity between parameters [19]. As a result, GPR models for biodiesel yield operational data analysis and prediction are proposed [20, 21].

A GPR is group of random variables for which joint Gaussian probability distribution describes any finite collection of them. In GPR, however, function of variables $f(x)$ is considered to be distributed like GP.

$$f(x) \sim GP(m(x), k(x, \dot{x})) \tag{5}$$

It should be highlighted, however, that considered SE smoothness should not be appropriate for modelling some systems. As a result, Matérn Gaussian process class is preferred since it offers parameter (v) that can regulate smoothness of the learned function [22].

3.4 Support Vector Machine

SVM is most effective supervised learning method proposed for numerous disciplines that may be utilised for modelling by its accuracy, resilience, power, and capacity [23, 24]. SVMs are used as regressors in regression issues, attempting to fit hyperplane that

estimate continuous target value within margin, or decision border based on training. The goal of changing margin was to reduce error during maintaining model complexity and resilience. SVM was next kernel-based technique that extended by utilising different kernel functions depending on the data classification. As a result, SVM could be either parametric or non-parametric model when utilising a linear kernel. The linear kernel, polynomial kernel, and Gaussian kernel are all popular kernel functions. To discover the best model configuration, this study investigates various polynomial degrees and kernel scales.

4 Model Performance

Prediction level indicators can be used to assess predicted accuracy and efficacy of the models in use. However, utilising same dataset to train and test prediction models can lead to overoptimistic findings [25]. As a result, validation method is used to divide dataset into 2 parts: training dataset for training prediction model and test dataset for validating their output after training. as indicated in the following subsections, a number of performance parameters can be employed to compare performance of models.

4.1 Cross Validation

Validation decreases danger of overfitting and assures that trained prediction models' generalisation capabilities and hyperparameter settings are robust. However, splitting available data into test and training datasets limits data accessible for model training and validation. Validation is utilised in form of K-folding to overcome this issue, which is frequently used and preferred in the literature [23, 26]. Dataset is parted into k subsets cross validation approach, with (K − 1) subsets pooled and utilize train models and remaining subset utilised for crosscheck. Process is looped K times, with one K folds serving as validation subset each time. Validation error of K runs is then measured. Most of data is used for training and validation, reducing bias and variation, providing good estimate of predictive accuracy of researched models.

4.2 Coefficient of Determination

Determination coefficient R^2 explains variability of measured output variable y_i function of trained model $\hat{y}_i$ response parameter prediction and response variable $\overline{y}_i$ average value as follows, where n is the sample size s. R^2 reading limit from 0 to 1, with greater value depict better match between the trained model and the data.

$$R^2 = 1 - \frac{\sum_{i=1}^{n} (y_i - \hat{y}_i)}{\sum_{i=1}^{n} (y_i - \overline{y}_i)} \tag{6}$$

4.3 Root Mean Square Error

Most easily and used interpreted data is root mean square error, which has same unit as researched variable and so better reflects prediction model's performance. Square root of the MSE is used to calculate it, as demonstrated in the equation below.

$$\text{RMSE} = \sqrt{\frac{1}{n}\sum_{i=1}^{n}(y_i - \hat{y}_i)^2} \tag{7}$$

4.4 Mean Absolute Error (MAE)

.The RMSE is like this criterion. In comparison to the MSE, it is great resilient and less attachment to data outliers. Average of all absolute errors is known as MAE, and it calculated as.

$$\text{MAE} = \frac{1}{n}\sum_{i=1}^{n}|y_i - \hat{y}_i| \tag{8}$$

4.5 Mean Squared Error (MSE)

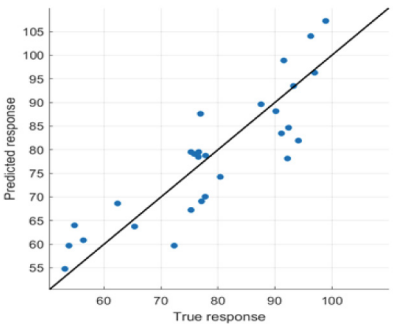
As stated in the equation below, index measures mean of square of errors between predicted and experimental of response variable.

$$\text{MSE} = \frac{1}{n}\sum_{i=1}^{n}(y_i - \hat{y}_i)^2 \tag{9}$$

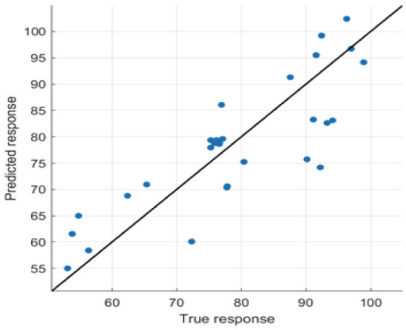
5 Results and Discussions

The predicted values for all machine learning algorithms are shown in Table 2. To find good forecasting model, performance of these strategies was tested and compared to one another. The expected R^2, mean absolute error (MAE), and RMSE are three essential performance measurement indicators used to compare the results (RMSE). The fact that the R^2 reveals how good model predicts for new observation is interesting. Because it is generated using observed values rather than model estimations, it helps to prevent overfitting. Using raw dataset, GPR model with Matérn class produced great results, with a R^2 of 0.91 and RMSE of 4.1134. This demonstrates that using the Matérn class to modify the smoothness behaviour of stochastic process realisations could be useful for modelling realistic physical work. With a R^2 of 0.85, GPR model with squared exponential kernel and rational exponential model produces correct response. The SVM model with coarse Gaussian kernel, on other hand, achieves worst estimation, with R^2 of 0.44. Result of the rapid variation in SVM response function, model overfits and fails to appropriately predict biodiesel yield. Figure 3 shows a scatter plot of various machine

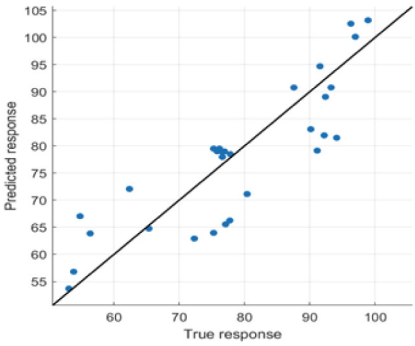
learning techniques. RMSE is produced for another regression models to examine their reactivity to dataset scale and compare performance suitably. Raw dataset is used to calculate the RMSE for several models. Figure 4 shows RMSE of various models compared to lowest RMSE baseline. The GPR-Matern model is utilised as a baseline since it has the lowest RMSE. Residual display of the predictive GPR-Matern for biodiesel yield is shown in Fig. 5. GPR-Matern residuals have randomly scattered around 0 lines. A residual is vertical distance between point and regression line. Generally described, it is difference predicted and real number. Residual data are on Y-axis, and independent data is on x-axis on residual plot.



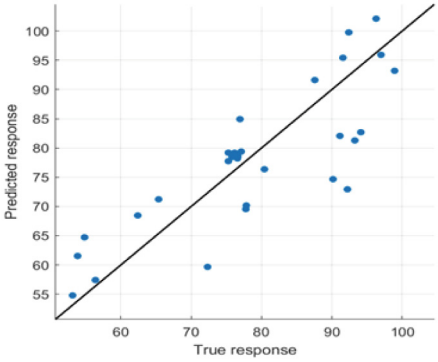
3.1 Stepwise Linear



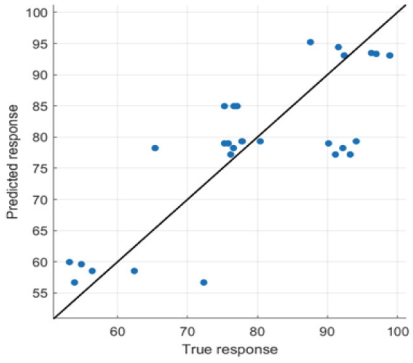
3.2 Linear



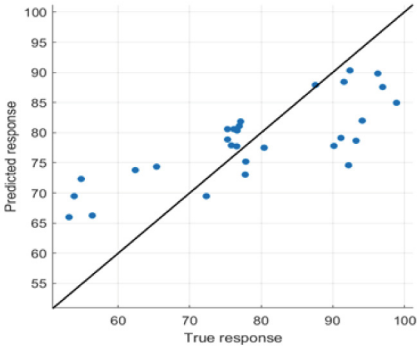
3.3 Interaction linear



3.4 Robust linear

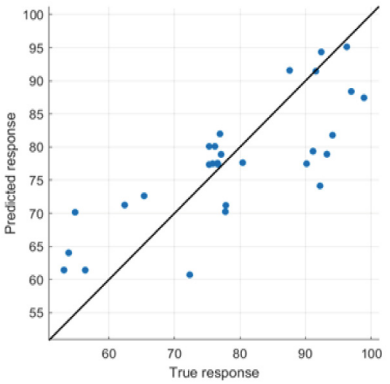


3.5 Fine Tree

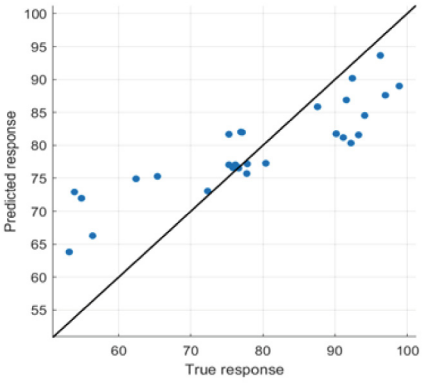


3.6 SVM Linear

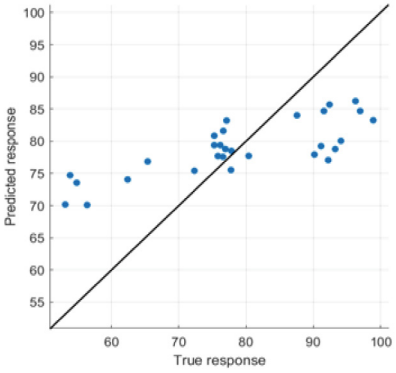
Fig. 3. Predicted versus actual measurements for different machine learning approaches using 5-fold cross validation



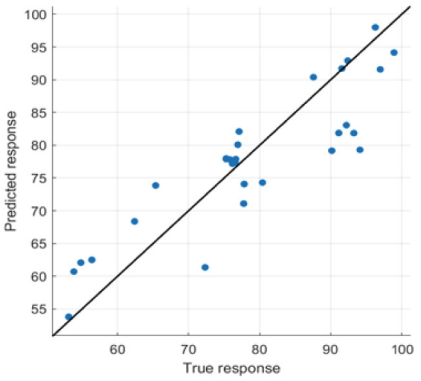
3.7 SVM-Quadratic



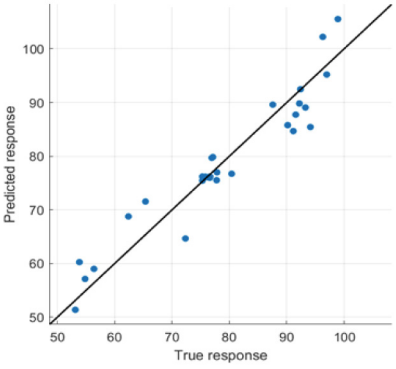
3.8 SVM- Medium Gaussian



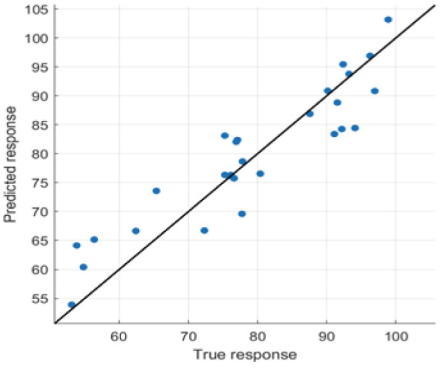
3.9 SVM- Coarse Gaussian



3.10 SVM-Cubic

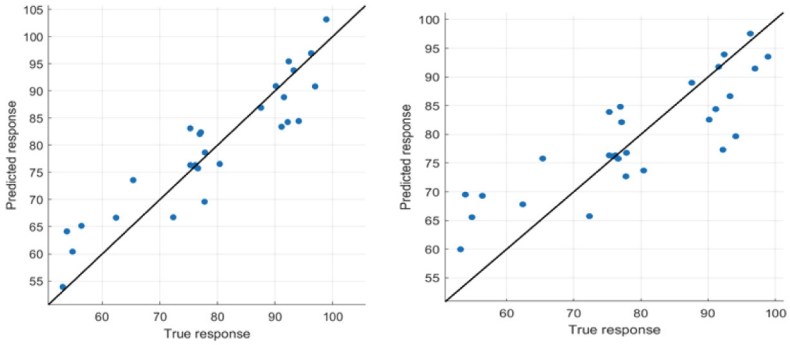


3.11 GPR- Matern



3.12 GPR-Rational Quadratic

Fig. 3. (*continued*)



3.13 GPR- Square Exponential 3.14 GPR- Exponential

Fig. 3. (*continued*)

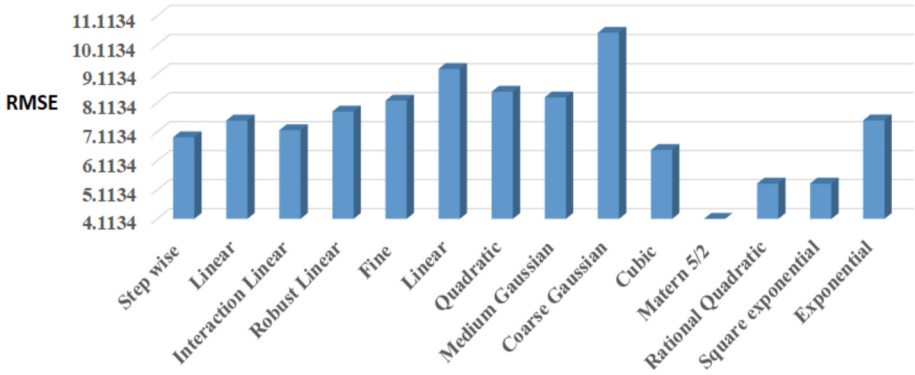


Fig. 4. RMSE of different machine learning approaches using the standardized data

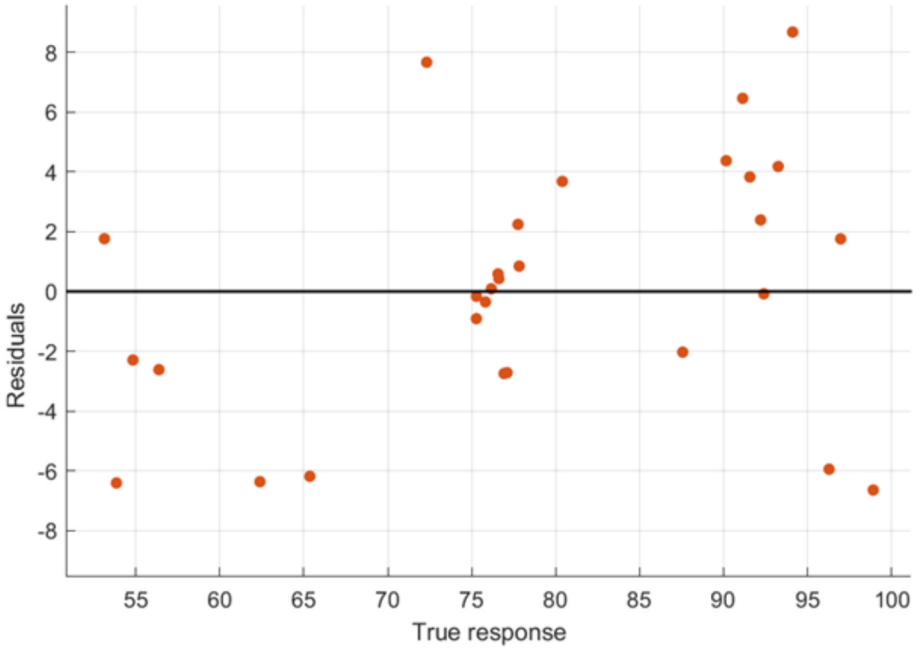


Fig. 5. The plot of residual versus number of the experiment for GPR-matern

Table 2. Performance measures for different machine learning approaches using 5-fold cross validation

Model type		R^2	RMSE	MSE	MAE
Linear regression	Step wise	0.75	6.9248	47.953	5.8109
	Linear	0.71	7.5024	56.285	6.278
	Interaction linear	0.74	7.1681	51.382	5.914
	Robust linear	0.69	7.8121	61.029	6.4064
Tree	Fine	0.65	8.1876	67.037	6.5538
Support vector machines	Linear	0.56	9.2814	86.145	7.6802
	Quadratic	0.63	8.4972	72.202	6.9344
	Medium Gaussian	0.65	8.2989	68.872	6.4775
	Coarse Gaussian	0.44	10.529	110.85	8.7547
	Cubic	0.78	6.4887	42.104	5.2549
Gaussian process regression	Matern 5/2	0.91	4.1134	16.92	3.2576
	Rational quadratic	0.85	5.3287	28.395	4.2077
	Square exponential	0.85	5.3287	28.395	4.2077
	Exponential	0.71	7.5089	56.383	5.9236

6 Conclusions

Algal oil has the potential to be a promising sustainable biodiesel source. Four critical variables were used predictors or input factors: catalyst dose (KOH), temperature, time, and oil to methanol ratio. Predicting and optimising biodiesel output for improved sustainability has been increasingly popular in recent years. Machine learning has acquired significant traction among different techniques to prediction, owing to increases in calculating power and more operating data. By extracting in between information from acquired datasets, data-driven model in machine learning could improve their response, analytical, and prediction capability with great accuracy. Several metrics, including as residual analysis, R^2, MAE, and RMSE, were used to evaluate efficiency of established smart models as well as current RSM model. This study presents comparing of most widely used machine learning estimation accuracy in actual-world operational situations using an operational dataset. Then, to avoid overfitting, cross validation was performed. This research also sheds light on the impact of alternative data scaling approaches on the regression models' prediction accuracy. Despite SVM with coarse Gaussian kernel, which has R^2 of 0.44, regression models evaluated can accurately estimate biodiesel yield.

References

1. Narula, V., Khan Mohd, F., Negi, A., Kalra, S., Thakur, A., Jain, S.: Low temperature optimization of biodiesel production from algal oil using CaO and CaO/Al_2O_3 as catalyst by the application of response surface methodology. Energy **140**, 879–884 (2017). https://doi.org/10.1016/j.energy.2017.09.028
2. Ferreira, A.J., Figueiredo, M.A.T.: Boosting algorithms: a review of methods, theory, and applications. In: Zhang, C., Ma, Y. (eds.) Ensemble Machine Learning: Methods and Applications. Springer US, Boston, MA, pp. 35–85 (2012). https://doi.org/10.1007/978-1-4419-9326-7_2
3. Dietterich, T.G.: Ensemble methods in machine learning. In: Multiple Classifier Systems, pp. 1–15. Springer, Berlin, Heidelberg (2000).https://doi.org/10.1007/3-540-45014-9_1
4. Zhou, Z.-H.: Ensemble Methods: Foundations and Algorithms, 1st ed. Chapman & Hall/CRC (2012)
5. Schapire, R.E.: The boosting approach to machine learning: an overview. In: Denison, D.D., Hansen, M.H., Holmes, C.C., Mallick, B., Yu, B. (eds.) Nonlinear Estimation and Classification. Springer, New York, NY, pp. 149–71 (2003). https://doi.org/10.1007/978-0-387-21579-2_9
6. Vinoth Arul Raj, J., Bharathiraja, B., Vijayakumar, B., Arokiyaraj, S., Iyyappan, J., Praveen Kumar, R.: Biodiesel production from microalgae Nannochloropsis oculata using heterogeneous Poly Ethylene Glycol (PEG) encapsulated $ZnOMn^{2+}$ nanocatalyst. Bioresour. Technol. **282**, 348–352 (2019). https://doi.org/10.1016/j.biortech.2019.03.030
7. Srivastava, G., Paul, A.K., Goud, V.V.: Optimization of non-catalytic transesterification of microalgae oil to biodiesel under supercritical methanol condition. Energy Convers. Manage. **156**, 269–278 (2018). https://doi.org/10.1016/j.enconman.2017.10.093
8. Kumar, M., Sharma, M.P.: Optimization of transesterification of *Chlorella protothecoides* oil to biodiesel using Box-Behnken design method. Waste Biomass Valor. **7**, 1105–1114 (2016). https://doi.org/10.1007/s12649-016-9485-5

9. Pelalak, R., Soltani, R., Heidari, Z., Malekshah, R.E., Aallaei, M., Marjani, A., et al.: Synthesis, molecular dynamics simulation and adsorption study of different pollutants on functionalized mesosilica. Sci. Rep. **11**, 1967 (2021). https://doi.org/10.1038/s41598-020-80566-w
10. Li, X., Wang, B., Hu, Q., Yapanto, L.M., Zekiy, A.O.: Application of artificial neural networks and fuzzy logics to estimate porosity for Asmari formation. Energy Rep. **7**, 3090–3098 (2021). https://doi.org/10.1016/j.egyr.2021.05.034
11. Chen, X., Yi, Z., Zhou, Y., Guo, P., Farkoush, S.G., Niroumandi, H.: Artificial neural network modeling and optimization of the Solid Oxide Fuel Cell parameters using grey wolf optimizer. Energy Rep. **7**, 3449–3459 (2021). https://doi.org/10.1016/j.egyr.2021.05.068
12. Heidari, Z., Alizadeh, R., Ebadi, A., Pelalak, R., Oturan, N., Oturan, M.A.: Degradation of furosemide using photocatalytic ozonation in the presence of ZnO/ICLT nanocomposite particles: experimental, modeling, optimization and mechanism evaluation. J. Mol. Liq. **319**, 114193 (2020). https://doi.org/10.1016/j.molliq.2020.114193
13. Pelalak, R., Nakhjiri, A.T., Marjani, A., Rezakazemi, M., Shirazian, S.: Influence of machine learning membership functions and degree of membership function on each input parameter for simulation of reactors. Sci. Rep. **11**, 1891 (2021). https://doi.org/10.1038/s41598-021-81514-y
14. Khoshmaram, A., Zabihi, S., Pelalak, R., Pishnamazi, M., Marjani, A., Shirazian, S.: Supercritical process for preparation of nanomedicine: Oxaprozin case study. Chem. Eng. Technol. **44**, 208–212 (2021). https://doi.org/10.1002/ceat.202000411
15. Cao, Y., Seyed Alizadeh, S.M., Fouladvand, M.T., Khan, A., Taghvaie Nakhjiri, A., Heidari, Z., et al.: Mathematical modeling and numerical simulation of CO_2 capture using MDEA-based nanofluids in nanostructure membranes. Process Saf. Environ. Prot. **148**, 1377–1385 (2021). https://doi.org/10.1016/j.psep.2021.03.007
16. Hazra, A., Gogtay, N.: Biostatistics series module 6: correlation and linear regression. Indian J. Dermatol. **61**, 593–601 (2016). https://doi.org/10.4103/0019-5154.193662
17. Soner, O., Akyuz, E., Celik, M.: Use of tree based methods in ship performance monitoring under operating conditions. Ocean Eng. **166**, 302–310 (2018). https://doi.org/10.1016/j.oceaneng.2018.07.061
18. James, G., Witten, D., Hastie, T., Tibshirani, R.: An Introduction to Statistical Learning: with Applications in R. 1st ed. 2013, Corr. 7th printing 2017 edition. Springer, New York (2017)
19. Rasmussen, C.E., Williams, C.K.I.: Gaussian Processes for Machine Learning. MIT Press, Cambridge, Mass (2006)
20. Yoo, B., Kim, J.: Probabilistic modeling of ship powering performance using full-scale operational data. Appl. Ocean Res. **82**, 1–9 (2019). https://doi.org/10.1016/j.apor.2018.10.013
21. Petersen, J.P., Jacobsen, D.J., Winther, O.: Statistical modelling for ship propulsion efficiency. J. Mar. Sci. Technol. **17**, 30–39 (2012). https://doi.org/10.1007/s00773-011-0151-0
22. Stein, M.L.: Interpolation of Spatial Data: Some Theory for Kriging. Springer Science & Business Media (2012)
23. Uyanık, T., Karatuğ, Ç., Arslanoğlu, Y.: Machine learning approach to ship fuel consumption: a case of container vessel. Transp. Res. Part D: Transp. Environ. **84**, 102389 (2020). https://doi.org/10.1016/j.trd.2020.102389
24. Awad, M., Khanna, R.: Efficient Learning Machines: Theories, Concepts, and Applications for Engineers and System Designers. Springer Nature (2015). https://doi.org/10.1007/978-1-4302-5990-9
25. Arlot, S., Celisse, A.: A survey of cross-validation procedures for model selection. Stat. Surv. **4**, 40–79 (2010). https://doi.org/10.1214/09-SS054
26. Gkerekos, C., Lazakis, I., Theotokatos, G.: Machine learning models for predicting ship main engine Fuel Oil Consumption: a comparative study. Ocean Eng. **188** (2019). https://doi.org/10.1016/j.oceaneng.2019.106282

Critical Parameters and Indicators for Assessing Soil Health

Srishti Sinha Ray, Dimple Bhadane, and Nishu Goyal(✉)

School of Health Sciences and Technology, UPES, Dehradun, Uttarakhand, India
nishu.goyal@ddn.upes.ac.in

Abstract. Soil quality refers to the overall health and suitability of plant growth and functioning of other ecosystem properly like all the animal's growth, improvement of human health and sustainability of environment. Chemical compounds from agrochemicals, industries waste and pharmaceutical are causing serious threat to ecosystem and human health as a whole. Emergence of these contaminants from various sources have increased the pollution leads to reduction of microbial diversity of soil which influenced soil health. In this context, continuous assessment of soil is necessary for evaluating soil quality transitions for detecting and mitigating pollution. Any minimal disturbance coming from contaminants in the soil cause changes in the physical, chemical, and biological variables. These variables may serve as symbols when evaluating the quality of the soil. A thorough physicochemical and biological analysis helps in evaluating soil quality and making quality decision about aspects of soil conditions, applications, and protection.

Keywords: Soil pollution · Physicochemical parameter · Biological parameters · Multiparameter analysis

1 Introduction

Soil is an essential constituent of the Earth's ecosystem and it has critical impact in encouraging and supporting life. It also serves as an important reservoir of water and essential nutrients and acts as a storage unit, ensuring the availability of these resources to plants and other organisms. In addition, soil acts as a key medium for the purification and decomposition of harmful waste materials, contributing to the overall balance and well-being of the environment. Another most crucial function of soil lies in its integral role in the carbon cycle, which is essential for supporting the earth's climate (Maurya et al. 2020). Soil helps to regulate the movement of carbon, a vital element for all living organisms, by storing it and releasing it into the atmosphere. This process is paramount to reducing the impacts on climate change and ensuring the stability of the global ecosystem (Vogel et al. 2019).

Moreover, soil is irreplaceable in agriculture, supplying the nutrients necessary for plant growth. Soil fertility and quality directly affect crop yields. Therefore, understanding and managing soil conditions is essential for sustainable agriculture. The distribution

© The Author(s), under exclusive license to Springer Nature Singapore Pte Ltd. 2026
M. Kumar et al. (Eds.): HSFEA 2023, LNCE 899, pp. 117–127, 2026.
https://doi.org/10.1007/978-981-92-3200-0_10

of essential plant nutrients for example nitrogen, potassium and phosphorus are eased by the soil so that plants have access to these vital elements. In addition to its role as a source of life for plants, soil also plays crucial role in degradation of the soil organic matter. The microbial community exist in the soil to break down dead plants, animals, and other organic matter, resulting the nutrients return into the ecosystem and contributing to the overall nutrient cycle (Hemkemeyer et al. 2021). Apart from its biological functions, soil also serves as a fundamental foundation for construction and infrastructure. The stability and composition of soil figure out the suitability of an area for development and are therefore a principal factor in urban planning and development (Rinot et al. 2019).

Soil physicochemical and biological properties are the key parameters in deciding its quality and typical characteristics. Physical properties of soil like porosity, texture, density and colour supply valuable insight into soil composition. These physical properties are influenced by several factors, including the presence of organic matter, microorganisms, and available nutrient of the soil. The chemical properties for example pH, macro and micronutrients and biological properties, such as the presence of microorganisms, fertilisers, and decomposition processes, also contribute to our comprehensive understanding of soil quality. These properties help evaluate soil fertility and health (Naga Raju et al. 2017).

Soil quality can be significantly affected by natural disasters such as heavy rains, wind erosion, and soil degradation, as well as by human activities such as construction and landfills. These activities can introduce harmful chemicals that can compromise the integrity of the soil and its ability to sustain life (Saco et al. 2021). Knowledge of our soil is critical to the improvement of our planet and the well-being of all living organisms. Soil is the foundation for every living organism, and understanding its properties can help name any deficiencies and guide efforts to support and improve its quality.

2 Key Parameters for Soil Health Study

The fundamental indicators for determining the degree of soil characteristics are physicochemical and biological variables of that soil. Understanding the biological and physicochemical characteristics of soil are necessary for getting insights into the soil dynamics, soil functioning and soil management for sustainable environment. The physicochemical variables of soil vary throughout the time and location because of variations in landscape, climate, physical weathering processes, plant diversity, microbiological activity, and various other biotic and abiotic factors. Variation in the chemical, physical and biological features of soil give rise to infertile or desolate soil, which is unable to sustain regular crop growth for a prolonged time (Tale and Ingole 2015).

Soil evaluation cannot be defined by only measuring individual soil characteristics, and also it is not possible to evaluate all soil characteristics together. So that minimum dataset (MDS) is necessary, that includes a fundamental set of properties such as chemical, physical and biological features of soil that assist in monitoring soil health status, fertility and health (Maurya et al. 2020). Conventionally, the primary indicators used to monitor the characteristic and standards of the soil health are biological, chemical and physical characteristics of soil. The most often used parameters to evaluate soil quality

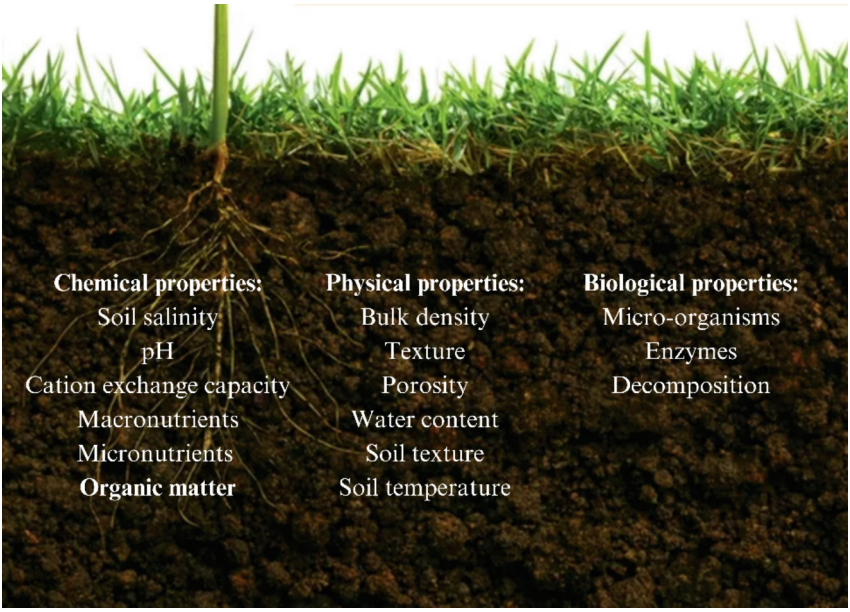


Fig. 1. Soil attributes as indicators of soil health

are chemical properties, for example pH, total N, and soil organic carbon, and the physical characteristics, which include bulk density, aggregate stability, water content, soil structure, and particle size distribution (Muñoz-Rojas 2018) (Fig. 1).

2.1 Physical Parameters

(i) Soil Texture

The three types of mineral particles that form soil texture are clay, silt, and sand. The proportion of different particle sizes in a soil determines its textural category, i.e., whether it is loamy, sandy loamy, or clay or any other type of soil. The coarse mineral part of soil, which is made with particles larger than 2 mm of diameter, is typically ignored when determining texture. But they might have an impact on the physicochemical characteristics of soil, including water retention (Naga Raju et al. 2017). Mineralogy and the texture of the soil have strong impact on carbon content and nutrients, native pH, aggregation, water holding capacity, and other factors.

For black soil, silty clay and loamy texture prevailed, while yellow soil had loamy clay texture. The nutrient composition of soil is also affected by the texture of soil. The sandy soil is light soil, that are rapidly permeable, have low cation exchange capacity, low moisture retention capacity, low nutrient concentration, and low buffer capacity. Maintaining the soil's ability to retain moisture and addressing nutrient deficiencies because presence of little organic matter are the primary issues can be faced in sandy-textured soil (Tale and Ingole 2015).

(ii) **Bulk Density**

The bulk density of soil is defined by the physical configuration of solid particles that produce the soil. Since bulk density does not represent an intrinsic characteristic of soil, this can be varied upon the number of variables including root growth, and rainfall (Casanova et al. 2016; Maurya et al. 2020). Bulk density is a fundamental soil property that is influenced from tillage, weather, soil properties, and agricultural practices. One of the primary indications of soil quality, bulk density is strongly correlated with generation of biomass and the state of the environment. It is influenced by natural phenomenon like the climate that affect the extent of soil cover, soil organic matter contents porosity, as well as land and crop management techniques (Makovníková et al. 2017; özdemir et al. 2022).

(iii) **Soil moisture content**

Moisture content of soil is important physical properties that defines soil health. The amount of water retained in the soil is called as its water content. The amount of water in soil has a significant impact on microbial diversity because it is essential for hydrolysis processes as well as acting as a transport medium for substrates (Maurya et al. 2020). The water content in the soil has a significant impact on root growth because availability of water directly affects root growth, affect photosynthesis, which increases the availability of carbohydrates, and affect the presence of oxygen in wet soil (Lynch et al. 2012). More soil water content leads to limited oxygen transport because oxygen diffusion in water is about 104 times lower than in air. Therefore, it will reduce the functioning and growth of aerobic microorganisms but may increase that of anaerobes (Yan et al. 2015).

2.2 Chemical Parameters

(i) **Soil pH and soil electrical conductivity**

Soil pH is the most important soil variable that regulates a wide range of physical, chemical and biological characteristics of soil which impact plant growth and production of biomass. The pH of soil is influenced by the many physiological and chemical processes such as humus formation from soil organic matter, leading to produce high-density carboxyl and phenolic groups, acid rain, nitrification, and nitrogen consumption by plants, and basic cations like Ca, Mg, K, and Na are deposited after leaching from eroded minerals, H^+ and Al^{3+} ions are left as predominant exchangeable cations (Neina 2019). The soil is a crucial factor that affects the microbial activity, nutrient availability, and soil physical characteristics. There are numerous nutrients that are only available within a specific pH range (Sharma 2022).

An essential indicator of soil health study is the electrical conductivity of soil, which indicates the presence of salts in soil i.e., measurement of the salinity of the soil (Sharma 2022). Soil EC has been used as an indirect indicator of salinity levels and the amount of nutrients available for plant uptake, but it has no direct effect on plant growth. Soil texture, salt concentration, organic matter content, cation-exchange capacity, soil depth,

nutrients (such as nitrate), water-holding capacity, and drainage conditions have all been measured by the knowledge of EC (USDA Natural Resource Conservation Service).

(ii) **Cation-anion exchange capacity**

Cation exchange capacity (CEC) serves as a critical indicator during assessing the soil's ability to hold nutrients, fertility, and long-term productivity. The capability of soil to accept cations and retain negative charge of soil is known as cation exchange capacity. Additionally, it offers buffering property towards soil pH variations (Graber et al. 2017; Maurya et al. 2020). Furthermore, CEC plays a crucial role in the adsorption of organic pollutants like antibiotics and heavy metals in soils (Yunan et al. 2018). The moisture content of soil particles affects the electrical conductivity of soils. It aids in the assessing of organic matter mineralization in soil. The electrical conductivity of normal soil is less than 1 dS/cm; 1–2 dS/cm electrical conductivity indicates critical for germination; Electrical conductivity of 2–3 dS/cm is crucial for the development of crops which are sensitive to salt, and electrical conductivity of more than 3 dS/cm indicates several crop injuries (Tale and Ingole 2015).

(iii) **Macronutrients**

According to their requirement in the soil, nutrients required by plants are categorized as either macronutrients or micronutrients. Macronutrients are the nutrients that the plants require in concentrations greater than 1–150 g/kg, or one part per million (ppm) of dry matter. (Pandey 2018). The macronutrients are hydrogen, carbon, oxygen, phosphorus, nitrogen, potassium, magnesium, calcium, and sulphur.

One of the nutrients that plants primarily need for vegetative growth is nitrogen. It is also necessary for the amino acid synthesis for the protein production, starch synthesis in plant leading to crop yield. Phosphorus are required for synthesizing enzymes, cellular membranes, and nucleic acids. Numerous cellular functions like photosynthesis, energy production, redox-homeostasis, and cell signalling, depend on phosphorus (Kumar et al. 2021). Potassium is very much important for performing many physiological and metabolic reactions in the plants and it is necessary in huge quantity for satisfactory plant development. Potassium functions as an osmoticum, retaining turgor pressure and cell growth, leaf growth, root elongation and stomatal guard cell regulation. Plants can only absorb K when it is dissolved in water (Torabian et al. 2021).

While aerial plant parts can absorb and use atmospheric sulfur as sulfur dioxide (SO_2), inorganic sulphate (SO_4^{2-}) is the primary source of S. It is absorbed by roots and metabolized into a number of important metabolites, including amino acids cysteine and methionine as well as different prosthetic groups. Sulfur has a more noticeable impact on the protein composition of cereal grains compared to nitrogen, which influences the protein content more broadly. Secondary metabolites that contain sulfur, such as glucosinolates and alliins, are essential defense compounds in cruciferous vegetables like onions, and garlic. These compounds provide their distinct flavour and aroma (de Bang et al. 2021).

There are also calcium and magnesium also help in plant cell formation, chlorophyll formation and growth of the plant. Plant uptakes calcium and magnesium from soil as Ca^{2+} and Mg^{2+} form.

(iv) **Micronutrients**

Micronutrients are those elements which are required less than 0.1–100 mg per kg or 1 ppm per kg of dry plant weight in concentrations. These elements are iron, copper, manganese, molybdenum, boron, zinc and chlorine. It has been found that this classification is conventional as these values vary amongst plant species and groups (Kumar et al. 2021).

Plants absorb zinc in its ionic form from soil for metabolic enzyme activation such as DNA replication, and for chlorophyll biosynthesis in some plants, and synthesis of cytochrome (Naeem et al. 2020). Chlorophyll synthesis and structure and functioning of chloroplast depend on iron. Although it is typically found in large concentrations in soil, but aerobic and neutral pH conditions reduce its bioavailability. The majority of iron in aerobic soils is found in the Fe^{3+} form, which has a very low solubility that does not satisfy the requirement of plants. Therefore, in many crop plants, fe-deficiency becomes a common disorder (Kumar et al. 2021). Apart from zinc and iron, molybdenum and boron are also essential for the growth of plants. Though requirement of these elements for plant is less, still plants absorb these nutrients from soil.

2.3 Biological Parameters

The intricate relationships that exist between physicochemical factors and biological communities within soil ecosystems determine the overall quality of soils. Regardless of this fact, the majority of soil monitoring programs, which are essential for sustainable land use practices, ignore the changes in bacterial communities (Hermans et al. 2020). Due to the sensitivity in abiotic stresses microorganisms show very little changes and their impact on plant productivity, structure, and composition, organisms in the soil and rhizosphere are thought to be biological indicators of soil quality (Tahat et al. 2020).

Rich microbial populations exist in soil and they influence plant growth, aid in essential nutrients cycling, and either act as pathogens or defend plant from other pathogens. Microorganisms also play a separate role in processes like decomposition which is dependent on the variability and abundance of the microorganisms (Hermans et al. 2020). Protozoa, fungi, bacteria, and archaea are examples of soil microorganisms. They help in soil's enzymatic activities and store nutrients and energy in their biomass. Protozoa and archaea only constitute about 2% and 1% of the soil microbial biomass, respectively (Buerkert et al. 2012).

Examples of beneficial microbes include symbiotic relationships between arbuscular mycorrhizal fungi and phosphate-solubilizing bacteria, nitrogen-fixing bacteria (rhizobium) and legume crops. The uptake of available nitrogen and phosphorus for the growth of the plants is increased by the interaction between phosphate-solubilizing bacteria and nitrogen-fixing bacteria with plant root. Phosphate solubilizer organism include the bacteria *Pseudomonas, Rhizobium, Bacillus, Azotobacter, Microbacterium, Erwinia,* etc. (Suman et al. 2022). Microbial populations influence the mobility and availability of heavy metals to plants through phosphate solubilization, redox changes, chelating agent release, and acidification. Microbes itself and sometimes with the help of plant can help in reduction of pesticide and the remaining organic contaminants of the soil (Alori et al. 2017). Clay soil indirectly surges the bacterial population by changing the soil chemical

constituents like pH, phosphorus content, and potassium content and also by changing the root growth (Tahat et al. 2020). Apart from these factors there are still some other factors which works as indicator of declining of soil health efficiently are described in Table1.

Table1. Key parameters act as indicator of soil health

Soil parameters as indicators	Type of indicators	Function	Reference
Soil temperature	Physical	Soil temperature has impact on root growth, branching, water uptake from soil etc.	Sabri et al. (2018)
Particle size distribution	Physical	It influences water retention capacity, and water-air interaction in soil	Sowiński et al. (2023)
Organic carbon	Chemical	Directly effects on abundance of microbiome in soil and also nutrient content of soil	Kumar et al. (2022)
Bacteria—*Pseudomonas, Bacillus, Burkholderia, Flavobacter*	Biological	Nutrient solubilization and uptake by root from soil	Hayat et al. (2010)
Fungi—*Fusarium, Ascomycota, Trichoderma*	Biological	Decomposition of biomass, reduce abiotic stress	Frąc et al. (2018)
Enzymes dehydrogenase	Biological	Stimulate microbial degradation of petroleum products in soil	Kaczyńska et al. (2015)
Cellulase	Biological	Helps in biodegradation of contaminant in soil and nutrient cycling	Neemisha and Sharma (2022)
Laccase	Biological	Humic substance and other organic pollutant degradation	Gangola et al. (2018)
Urease	Biological	Degradation of urea (chemical fertilizer)	Mekonnen et al. (2021)
β-glucosidase	Biological	Helps in defense mechanism, pigment formation in cell and fruit ripening	Strahsburger et al. (2017)

3 Current Approaches for Soil Health Study

The recent development of molecular technologies offers new possibilities to understand in better way the interactions and feedbacks between plants and soil system for ecosystem recovery. New spectroscopic methods such as remote sensing, portable X-ray fluorescence, near-infrared spectroscopy, and X-ray tomography, make it possible to quickly and affordably measure a variety of soil physicochemical and biological parameters (Muñoz-Rojas 2018). Recently another widely used technique is landscape function analysis (LFA) which helps for assessment and monitoring soil quality for restoration. This assay is a visual evaluation method depending on quantifiable parameters of soil which creates indices of soil function using markers of soil biogeochemical processes and characteristics (Muñoz-Rojas 2018).

Spatial sampling design must be followed for sampling points selection using advanced geostatistical techniques and remote sensing equipment. Also mapping of specific attributes like soil organic matter at high resolution, utilizing a typical soil sampling plan and analysis techniques and model constraints concerning the choice of indicators, algorithms, and presumptions will help to asses soil status preciously (Rinot et al. 2019).

Since soil can contain thousands or millions of distinct microbial species and functional genes, many of which are yet to be known. This high diversity of soil microbial community can help to investigate wide range of soil environmental aspects. Similarly satellite hyperspectral images allow for the identification of hundreds of different unique spectra for any given location on this planet, are more insightful than the simple images of the planet's surface (Fierer et al. 2021).

4 Conclusion

Conventional agriculture is heavily dependent on chemical compounds like chemical fertilizers, chemical pesticides for increasing food productivity. Due to uncontrolled use of chemical pesticides and fertilizers, soil health gets declined so that analysis of soil parameters is therefore crucial. There has been much discussion about the characteristics of the soil that define and measure successful restoration, as well as the tracking and evaluation of soil health status. Recently for achieving the Sustainable Development Goals (SDG) by 2030 encourages people to take serious steps for recovering soil health. Achieving several sustainable development goals such as SDG 1 (End Poverty), SDG 2 (Zero Hunger), SDG 6 (Clean Water and Sanitation) etc. soil health monitoring is required. Few are dependent on plant production, while others are dependent on soil processes. In order to meet international goals, it will be crucial to acknowledge the fundamental criteria such as employing a list of indicators, including chemical, physical and biological ones that play important role in soil ecosystem restoration. A recent approach towards understanding the relationships between plant soils and microbes may be promisingly evaluate soil ecosystem recovery easily.

It is not easier to evaluate the soil quality using only the physical, chemical, and biological variables listed above. Therefore, it is essential to develop a standard Minimum Data Set (MDS) based on the soil specific to the agro-ecological site. Then more accurate summary of soil assessment can be found for further analysis. Nowadays significant

progresses are observed to improve systems regarding the gathering information of soil and evaluation systems in terms of the regional, local and global quality parameters for soil ecosystem restoration techniques.

References

Alori, E.T., Dare, M.O., Babalola, O.O.: Microbial inoculants for soil quality and plant health. pp. 281–307 (2017). https://doi.org/10.1007/978-3-319-48006-0_9

Buerkert, A., Joergensen, R.G., Ludwig, B., Schlecht, E.: Nutrient and carbon fluxes in terrestrial agro-ecosystems. In Marschner's Mineral Nutrition of Higher Plants, pp. 473–482. Elsevier (2012). https://doi.org/10.1016/B978-0-12-384905-2.00018-2

Casanova, M., Tapia, E., Seguel, O., Salazar, O.: Direct measurement and prediction of bulk density on alluvial soils of central Chile. Chilean J. Agric. Res. **76**(1), 105–113 (2016). https://doi.org/10.4067/S0718-58392016000100015

de Bang, T.C., Husted, S., Laursen, K.H., Persson, D.P., Schjoerring, J.K.: The molecular–physiological functions of mineral macronutrients and their consequences for deficiency symptoms in plants. New Phytol. **229**(5), 2446–2469 (2021). https://doi.org/10.1111/nph.17074

Fierer, N., Wood, S.A., Bueno de Mesquita, C.P.: How microbes can, and cannot, be used to assess soil health. In Soil Biology and Biochemistry, vol. 153. Elsevier Ltd. https://doi.org/10.1016/j.soilbio.2020.108111

Frąc, M., Hannula, S.E., Bełka, M., Jędryczka, M.: Fungal biodiversity and their role in soil health. Front. Microbiol. **9** (2018).https://doi.org/10.3389/fmicb.2018.00707

Gangola, S., Sharma, A., Bhatt, P., Khati, P., Chaudhary, P.: Presence of esterase and laccase in Bacillus subtilis facilitates biodegradation and detoxification of cypermethrin. Sci. Rep. **8**(1), 12755 (2018). https://doi.org/10.1038/s41598-018-31082-5

Graber, E.R., Singh, B., Hanley, K., Lehmann, J.: Determination of cation exchange capacity in biochar. Biochar 74–84 (2017)

Hayat, R., Ali, S., Amara, U., Khalid, R., Ahmed, I.: Soil beneficial bacteria and their role in plant growth promotion: a review. Ann. Microbiol. **60**(4), 579–598 (2010). https://doi.org/10.1007/s13213-010-0117-1

Hemkemeyer, M., Schwalb, S.A., Heinze, S., Joergensen, R.G., Wichern, F.: Functions of elements in soil microorganisms. Microbiol. Res. **252**, 126832 (2021). https://doi.org/10.1016/j.micres.2021.126832

Hermans, S.M., Buckley, H.L., Case, B.S., Curran-Cournane, F., Taylor, M., Lear, G.: Using soil bacterial communities to predict physico-chemical variables and soil quality. Microbiome **8**(1), 79 (2020). https://doi.org/10.1186/s40168-020-00858-1

Kaczyńska, G., Borowik, A., Wyszkowska, J.: Soil dehydrogenases as an indicator of contamination of the environment with petroleum products. Water Air Soil Pollut. **226**(11), 372 (2015). https://doi.org/10.1007/s11270-015-2642-9

Kumar, S., Kumar, S., Mohapatra, T.: Interaction between macro- and micro-nutrients in plants. Front. Plant Sci. **12** (2021).https://doi.org/10.3389/fpls.2021.665583

Kumar, S., et al.: Remote sensing for agriculture and resource management. In: Natural Resources Conservation and Advances for Sustainability, pp. 91–135. Elsevier (2022). https://doi.org/10.1016/B978-0-12-822976-7.00012-0

Lynch, J., Marschner, P., Rengel, Z.: Effect of internal and external factors on root growth and development. In: Marschner's Mineral Nutrition of Higher Plants, pp. 331–346. Elsevier (2012). https://doi.org/10.1016/B978-0-12-384905-2.00013-3

Tahat, M.M., Alananbeh, K.M., Othman, Y.A., Leskovar, I.D.: Soil health and sustainable agriculture. Sustainability **12**(12), 4859 (2020). https://doi.org/10.3390/su12124859

Makovníková, J., Širáň, M., Houšková, B., Pálka, B., Jones, A.: Comparison of different models for predicting soil bulk density. Case study—Slovakian agricultural soils. Int. Agrophys. **31**(4), 491–498 (2017). https://doi.org/10.1515/intag-2016-0079

Maurya, S., Abraham, J.S., Somasundaram, S., Toteja, R., Gupta, R., Makhija, S.: Indicators for assessment of soil quality: a mini-review. In Environmental Monitoring and Assessment, vol. 192, Issue 9. Springer Science and Business Media Deutschland GmbH (2020). https://doi.org/10.1007/s10661-020-08556-z

Mekonnen, E., Kebede, A., Nigussie, A., Kebede, G., Tafesse, M.: Isolation and characterization of urease-producing soil bacteria. Int. J. Microbiol. **2021**, 1–11 (2021). https://doi.org/10.1155/2021/8888641

Muñoz-Rojas, M.: Soil quality indicators: critical tools in ecosystem restoration. In Current Opinion in Environmental Science and Health, vol. 5, pp. 47–52. Elsevier B.V. (2018). https://doi.org/10.1016/j.coesh.2018.04.007

Naeem, M., Ansari, A.A., Gill, S.S. (eds.). (2020). Contaminants in Agriculture. Springer International Publishing. https://doi.org/10.1007/978-3-030-41552-5

Naga Raju, M., Golla, N., Vengatampalli, R.: Soil Physicochemical Properties, pp. 5–10 (2017). https://doi.org/10.1007/978-3-319-42655-6_2

Neemisha, Sharma, S.: Soil enzymes and their role in nutrient cycling. In: Structure and Functions of Pedosphere, pp. 173–188. Springer Nature Singapore (2022). https://doi.org/10.1007/978-981-16-8770-9_8

Neina, D.: The role of soil pH in plant nutrition and soil remediation. Appl. Environ. Soil Sci. **2019**, 1–9 (2019). https://doi.org/10.1155/2019/5794869

Özdemir, N., Demir, Z., Bülbül, E.: Relationships between some soil properties and bulk density under different land use. Soil Stud. **11**(2), 43–50 (2022). https://doi.org/10.21657/soilst.1218353

Pandey, N.: Role of plant nutrients in plant growth and physiology. In Plant Nutrients and Abiotic Stress Tolerance, pp. 51–93. Springer, Singapore (2018). https://doi.org/10.1007/978-981-10-9044-8_2

Rinot, O., Levy, G.J., Steinberger, Y., Svoray, T., Eshel, G.: Soil health assessment: a critical review of current methodologies and a proposed new approach. Sci. Total Environ. **648**, 1484–1491 (2019). https://doi.org/10.1016/j.scitotenv.2018.08.259

Sabri, N.S.A., Zakaria, Z., Mohamad, S.E., Jaafar, A.B., Hara, H.: Importance of soil temperature for the growth of temperate crops under a tropical climate and functional role of soil microbial diversity. Microbes Environ. **33**(2), 144–150 (2018). https://doi.org/10.1264/jsme2.ME17181

Saco, P.M., McDonough, K.R., Rodriguez, J.F., Rivera-Zayas, J., Sandi, S.G.: The role of soils in the regulation of hazards and extreme events. Philos. Trans. R. Soc. B: Biol. Sci. **376**(1834) (2021). https://doi.org/10.1098/rstb.2020.0178

Sharma, S.B.: Trend setting impacts of organic matter on soil physico-chemical properties in traditional vis-a-vis chemical-based amendment practices. PLOS Sustain. Transform. **1**(3), e0000007 (2022). https://doi.org/10.1371/journal.pstr.0000007

Sowiński, P., Smólczyński, S., Orzechowski, M., Kalisz, B., Bieniek, A.: Effect of soil agricultural use on particle-size distribution in young glacial landscape slopes. Agriculture **13**(3), 584 (2023). https://doi.org/10.3390/agriculture13030584

Strahsburger, E., de Lacey, A.M.L., Marotti, I., DiGioia, D., Biavati, B., Dinelli, G.: In vivo assay to identify bacteria with β-glucosidase activity. Electron. J. Biotechnol. **30**, 83–87 (2017). https://doi.org/10.1016/j.ejbt.2017.08.010

Suman, J., Rakshit, A., Ogireddy, S.D., Singh, S., Gupta, C., Chandrakala, J.: Microbiome as a key player in sustainable agriculture and human health. Front. Soil Sci. **2** (2022).https://doi.org/10.3389/fsoil.2022.821589

Tale, S.K., Ingole, S.: A review on role of physico-chemical properties in soil quality. Chem. Sci. Rev. Lett. **4**(13), 57–66 (2015)

Torabian, S., et al.: Potassium: a vital macronutrient in potato production—a review. Agronomy **11**(3), 543 (2021). https://doi.org/10.3390/agronomy11030543

Vogel, H.-J., et al.: Quantitative evaluation of soil functions: potential and state. Front. Environ. Sci. **7** (2019).https://doi.org/10.3389/fenvs.2019.00164

Yan, N., Marschner, P., Cao, W., Zuo, C., Qin, W.: Influence of salinity and water content on soil microorganisms. Int. Soil Water Conserv. Res. **3**(4), 316–323 (2015). https://doi.org/10.1016/j.iswcr.2015.11.003

Yunan, D., Xianliang, Q., Xiaochen, W.: Study on cation exchange capacity of agricultural soils. IOP Conf. Ser.: Mater. Sci. Eng. **392**(4), 042039 (2018). https://doi.org/10.1088/1757-899X/392/4/042039



Comparative Analysis of Enhanced Power Yield Through Photovoltaic System Under Partial Shading Situations by Simulations and Experimental Setup

Divya Ahluwalia[1(✉)] and Shahroz Anjum[2]

[1] Department of Mathematics, Applied Science Cluster, UPES, Dehradun, Uttarakhand, India
dahluwalia@ddn.upes.ac.in
[2] GENCO Department, Alliant Energy, Cedar Rapids, Iowa, USA

Abstract. The solar photovoltaic technique to extract the solar energy is gaining importance day by day. The prime reason being the free and ubiquitous availability of the primary source of light which is 'Sun'. The power extracted from the photovoltaic arrays (PVAs) is depleted to a larger extent owing to several natural factors which is a serious issue. One of the most common causes is partial shading situation (PSS) which comes into picture primarily due to the dust which settles on the panels, moving clouds, bird droppings, etc. The geographical location and the topographical conditions also affect the power yield from the PVA systems. Thus, it is paramount to predict and fix the adverse effects of the environmental factors such as PSSs that may hinder the performance of the solar energy systems, in order to achieve the maximum output. A 4 × 4 Jigsaw SuDoKu (JSSDK) scheme is introduced in this article and the performance is studied by experiments through lab prototype under various PSS. The experimental results when compared to the theoretical ones proved that the JSSDK topology reduced the mismatch power losses and produced better performance with enhanced power output under different PSSs.

Keywords: Photovoltaic · Partial shadings · Power generation · Mismatch power loss · Power enhancement

1 Introduction

With the increased global concern for energy generation, the role of renewable energy is gaining more relevance these days. In order to produce clean electricity devoid of CO_2, sulphur oxides (Sox) and nitrogen oxides (NO_x) emissions, etc., the installation of solar photovoltaic (PV) power systems needs diligent planning and execution, as some of these emissions are a severe threat to cause global warming. Before constructing any significant PV power plant, it is also essential to investigate the performance analysis of photovoltaic array (PVA) models at a smaller scale and investigate the effects of different topologies of the PVA on the system's overall performance. One such mini project is installed, and studies carried out through an experimental setup to assess the effectiveness of prototype of the PVA power systems.

© The Author(s), under exclusive license to Springer Nature Singapore Pte Ltd. 2026
M. Kumar et al. (Eds.): HSFEA 2023, LNCE 899, pp. 128–137, 2026.
https://doi.org/10.1007/978-981-92-3200-0_11

The site selected for this study is New Jersey (USA) and the experiment was performed in the month of September 2022. As per records, the chosen location receives enough solar insolation over the majority of the year.

The project's location, the PVA system's construction details, working of the PVA unit, the solar PV module's (PVM) *P-V* and *I-V* characteristic curves, and the PVA's performance and maintenance aspects are some of the factors which are to be taken care of during the planning process for PVA solar plants.

Power generation with photovoltaic systems is faced with numerous difficulties and challenges. The parameters such as the surrounding temperature, the geometric position of the sun, its insolation levels, and the field variables, have a significant impact on the performance of the PVA. A PVA is a group of PV cells (PVC) linked in parallel and series. Thus, the behavior of each PVC affects the overall performance of the PVA. If the PVCs work under non-uniform situations, the electrical properties of the cells would vary considerably and thus the short circuit current of the PVC might alter for a number of technical and environmental reasons. The PVA's are adversely influenced by the PSS which may be caused due to several factors such as dirt and dust settling on the panels and shadows cast by nearby objects and these also ultimately affects the short circuit current.

Further, the electrical properties of the series-connected PVCs are not identical, in general and are therefore prone to mismatch losses (MPLs) under varying operating conditions. To prevent the PVCs from being affected by hot spots, PVM manufacturers couple the bypass diodes in antiparallel with the PVCs (Patel and Agarwal 2008) The *P-V* and *I-V* plots of a PVA exhibits several disruptions which results in misleading the MPP tracking algorithms through erroneous calculations for the peak values, under non-uniform conditions. Conventional global maximum power point (GMPP) tracking techniques have been developed (Subudhi and Pradhan 2012), however most of them still pose complications to track precisely the GMPP under varied irradiances.

Several GMPP tracking approaches for PVAs under the influence of PSSs are introduced by different researchers (Guo et al. 2018; Sen et al. 2018).

Partial shading situations (PSSs) results in power loss that is not proportional to the area of the shaded part but rather the extent of MPLs depend on the shading pattern, PVA configuration, and the position of the shaded PVM within the PVA. In literature, many PVA reconfiguration techniques have been suggested (Sai Krishna and Moger 2019). to minimize MPL in the PVA systems. Series-Parallel (SP), Total-Cross-Tied (TCT), and Bridge-Link (BL) configuration schemes are three suitable configurations that are compared in (Subudhi and Pradhan 2012) for MPL, maximum power, fill factor, and energy yield under PSSs and manufacturer's tolerances in PVC characteristics.

The TCT configuration, which has the most parallel ties in contrast to any other configurations available, is the most widely accepted configuration for enhanced energy due to its ability to diminish the MPL under PSSs. The incorporation of cross ties in TCT PVA augments its life period, according to a probability theory analysis (Picault et al. 2010; Kaushika and Gautam 2003) since the MPLs are significantly reduced.

In order to reduce MPL caused by PS which in turn improves efficiency, various techniques for reconfiguring the PVAs, both static and dynamic, have been devised and suggested in literature (Anjum and Mukherjee 2022). The connections between the

modules in the reconfigured PVA are altered dynamically in line with a switching matrix to maximize the current of the single string in the case of shading. Under severe PSSs, the power loss is decreased, but the dynamic method involves higher cost and increased complexity.

To increase power yield under PSSs, static reconfiguration techniques are widely used, and these follow the concept of physical relocation of the PVMs based on the mathematical logics such as the SuDoKu puzzle pattern and several of its reconfigurations in a TCT linked PVA (Sai Krishna and Moger 2019). In this technique, the physical position of the PVMs is changed keeping the electrical connections same. The reconfigured PVA's effectiveness is then investigated under various shading scenarios.

SS, SP, HC, BL, and TCT PVAs have been compared for the MPL along with other parameters (Wang and Hsu 2011). The drawbacks of these static reconfigured PVA topologies includes the presence of numerous peaks in the PVA characteristics as well as the inefficiency to disperse the shadings effectively to obtain better power output. A unique technique proposed by (Rani et al. 2013) could effectively dissipate the PS effects but it too had a limitation that the positions of the first column PVMs were kept fixed. To overcome these inadequacies, a new technique is proposed in this article and the theoretical results are validated through experimentation carried on a 4×4 PVA.

To achieve authenticated results, a lab prototype setup is examined for the performance of the PVA systems. The main focus of this study is to validate the power output and fix the reasons such as PSS, for the diminished output, if it exists. A reconfigured scheme Jigsaw SuDoKu (JSSDK) is introduced, and the simulations are performed using MATLAB/SIMULINK. The parameters are selected for examining the variations in the performance of JSSDK with that of TCT. These parameters are GMPP, power enhancement (PE) and MPL. The theoretical results are compared with those obtained through the experiment and the results are presented.

This manuscript is divided into four sections. In Sect. 1 a brief description of the PVA systems is given. Section 2 gives describes the basic solar cell, TCT and JSSDK PVA configurations. The hardware setup considered in this study along with the results are presented in Sect. 3. Finally, Sect. 4 concludes the present study with suggestions on the future scope.

2 System Description

The fundamental unit of a PVA is a PVC. The one-diode model is as represented in Fig. 1 and the output current value of a PVC is as given by Eq. (1) below

$$I_{out} = I_{pg} - I_{sat}\left\{\exp\left[q\frac{V_{out-}(R_{se})(I_{out})}{\eta k T_{act}}\right] - 1\right\} - \frac{V_{out-}(R_{se})(I_{out})}{R_{sh}} \tag{1}$$

where I_{out} represents the current and I_{pg} represents the photo current generated from the PVC, I_{sat} is the notation for the diode reverse saturation current, V_{out} represents the PVC output voltage, T_{act} stands for the actual temperature of the PVC, q is the electron charge, k denotes the Boltzmann constant, and η represents the ideality factor of a diode. Further, the resistance in series is denoted by R_{se} and resistance in parallel is denoted by R_{sh}.

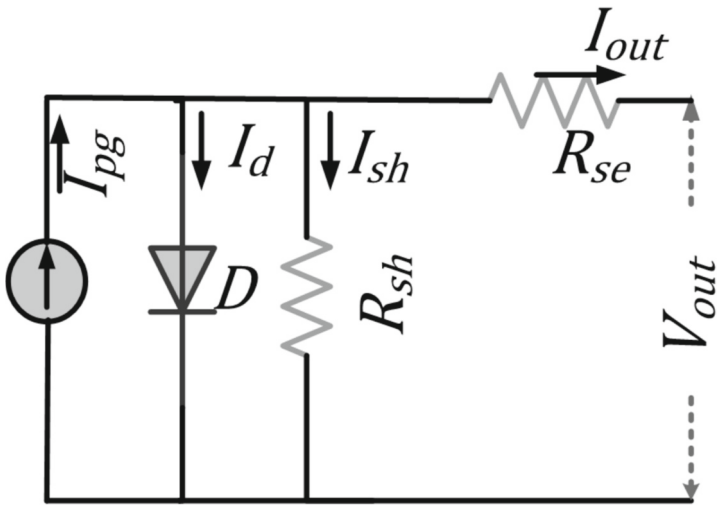


Fig. 1. Equivalent circuit of a PVC.

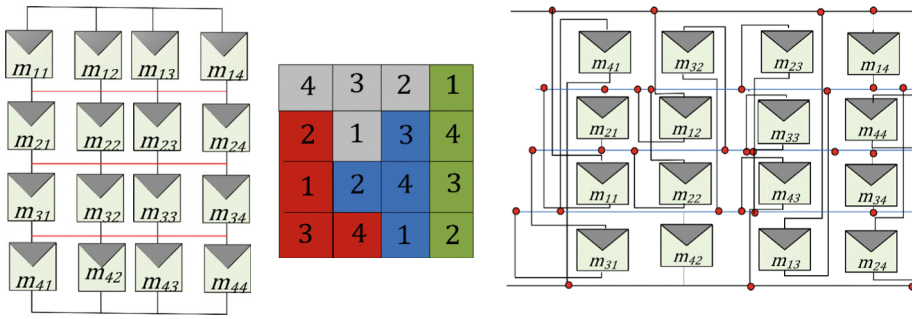
2.1 TCT

A 4 × 4 PVA with PVMs connected in TCT arrangement is as shown in Fig. 2(a). A simple series parallel PVA can be modelled as a TCT configuration by interconnecting every row using crossties. Further, the column PVMs are connected in series and the row PVMs are connected in parallel. The TCT PVA considered in this study consists of four rows and four columns with a total of 16 modules. In Fig. 2(a) each cell is denoted by m_{rc} where r and c denote the row and column numbers respectively.

2.2 JSSDK

The algorithm of the JSSDK scheme applied to a 4 × 4 PVA consists of the allocation of the numbers 1–4 such that (i). Each row and column consist of the numbers 1–4 only once (ii). Different groups of coloured cells are assigned unique numbers 1–4 only once. The 4 × 4 JSSDK puzzle pattern is as shown in Fig. 2(b) and its PVA arrangement is as depicted in Fig. 2(c).

The JSSDK topology can be applied to PVAs of any order. It is capable of structuring the PVMs efficiently, without changing the electrical interconnections, which in turn helps to disseminate the shadows casted upon the PVAs. It overcomes the limitations posed by earlier topologies which may be insufficiency to disperse the shadows falling on the first column of the PVA as well as limitation to uniquely allot the numbers to different sub arrays. The JSSDK scheme dissipates the shadings thereby decreasing the MPLs and increasing the power generation.



(a) (b) (c)

Fig. 2. A 4 × 4 pattern **a** TCT, **b** JSSDK puzzle, **c** JSSDK module arrangement.

3 Hardware Setup and Results

Different patterns (each numbered from 1 to 4) are merged to form a 4 × 4 JSSDK puzzle pattern and module arrangement as in Fig. 2. This is done for experimental purposes by setting up a lab prototype to validate the results under different PSSs for TCT and JSSDK configurations. The experimental hardware setup is made up by using 16 PVMs having the same rating (specification details are given in Table 1), a rheostat, two multi-meters for measuring the voltage and currents, a temperature gun for measuring the operating temperature for the PVMs, solar power meter for measuring the incident irradiance, connecting wires and different colored cellophane sheets to virtually create a partial shading scenario (Table 1). This setup for 4 × 4 PVA prototype is shown in Fig. 3.

The output power for the experimental setup is the product of the current (the multi-meter reading connected with the rheostat in series) and voltage (the multi-meter reading connected in parallel to the rheostat). These experiments are performed to benchmark the TCT and the proposed JSSDK reconfigured models at 12: 30 PM EST with irradiance level of 1355 W/m^2 at temperature 28 °C in New Jersey USA on the day of 1st September 2022. The output power for 4 × 4 PVA in normal operating conditions (at 1355 W/m^2 and 28 °C) is calculated to be 10.13 W. To achieve the real-time shading conditions, different solar irradiances of 720, 600, 430, 320 and 200 W/m^2, highlighted in yellow, orange, blue, green, and grey respectively, are created by using transparent coloured sheets spread over the PVA in the 2 × 2 sub-array form as shown in Fig. 4.

Table 1. Specifications of the PVM (for experimental purpose) at standard test conditions (STC).

Parameters	Values
Maximum power, $P_{\max}$ (W)	0.65
Open circuit voltage, V_{oc} (V)	1.7
Short circuit current, I_{sc} (A)	0.437
Current at maximum power point, I_{mp} (A)	0.423
Voltage at maximum power point, V_{mp} (V)	1.5

(*continued*)

Table 1. (*continued*)

Parameters	Values
Area (mm^2)	80 * 60
Wire used for panel connection	Polysilicon
Type of PVM	Polycrystalline

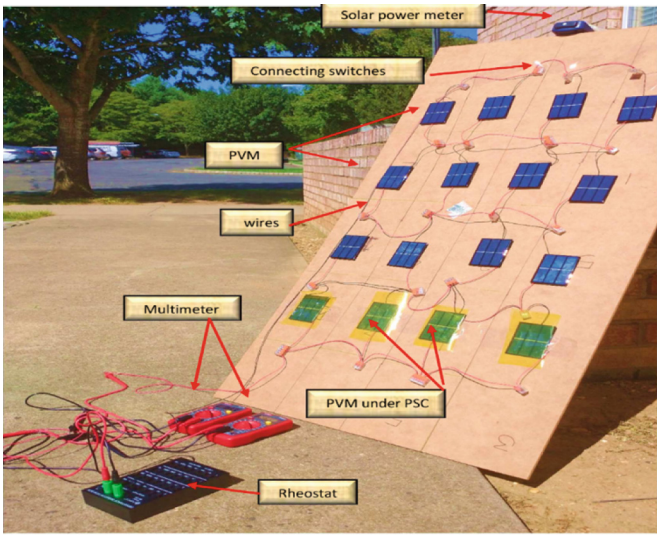


Fig. 3. Experimental setup

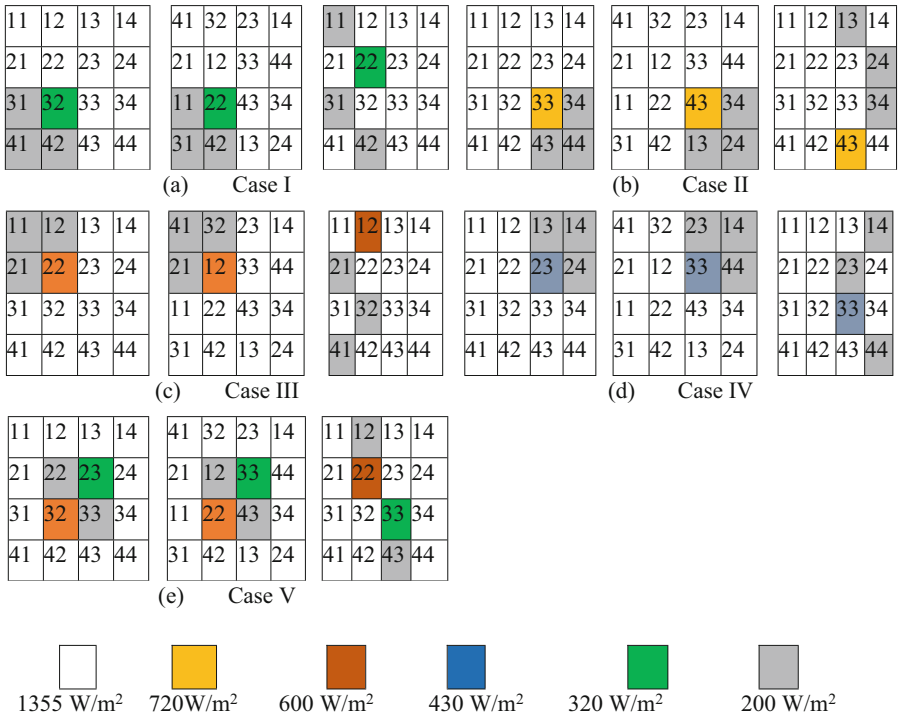


Fig. 4. Different shading patterns for TCT and JSSDK with its shade dispersion related to **a** pattern I, **b** pattern II, **c** pattern III, **d** pattern IV and **e** pattern V.

Table 2. Theoretical and experimental values of GMPP and % PE for TCT and JSSDK PVAs for patterns I–V under PSS

Shading pattern	TCT (P_{max}, W)		JSSDK (P_{max}, W)		PE (%)	
	Theoretical	Experimental	Theoretical	Experimental	Theoretical	Experimental
Pattern I	9.6 V_mI_m	6.54	12.8 V_mI_m	8.06	33.3	23.24
Pattern II	9.6 V_mI_m	6.66	12.8 V_mI_m	8.17	33.3	22.67
Pattern III	9.6 V_mI_m	6.63	12.8 V_mI_m	8.15	33.3	22.92
Pattern IV	9.6 V_mI_m	6.59	12.8 V_mI_m	8.10	33.3	22.91
Pattern V	10.08 V_mI_m	6.86	12.8 V_mI_m	8.21	26.98	19.67

Table 3. Theoretical and experimental value of MPL for TCT and JSSDK PVAs for patterns I–V under PSS

Shading groups	TCT		JSSDK	
	Theoretical (W)	Experimental (W)	Theoretical (W)	Experimental (W)
Pattern I	6.4 $V_m I_m$	3.59	3.2 $V_m I_m$	2.07
Pattern II	6.4 $V_m I_m$	3.47	3.2 $V_m I_m$	1.96
Pattern III	6.4 $V_m I_m$	3.5	3.2 $V_m I_m$	1.98
Pattern IV	6.4 $V_m I_m$	3.54	3.2 $V_m I_m$	2.03
Pattern V	5.92 $V_m I_m$	3.27	3.2 $V_m I_m$	1.92

3.1 Power at GMPP

The maximum theoretical and experimental output power in the lab prototype setup for all shading conditions is given in Table 2. For Pattern I, the GMPP for TCT is 6.54 and 8.06 W for reconfigured JSSDK PVA. The results indicate that the GMPP for the JSSDK method is higher, and the power enhancement achieved is 23.24%. In Pattern II shading condition, the TCT arrangement generates 6.66 W of power while JSSDK arrangement generates 8.17 W. It clearly indicates towards higher power generation in case of reconfigured arrangement and a percentage increment of 22.67% is observed. In case of Pattern III scenario, JSSDK configuration generates more power (i.e., 8.15 W) than TCT (6.63 W) by 22.92%. For Pattern IV, JSSDK reconfiguration method produces 8.10 W of power as compared to 6.59 W produced by TCT indicating higher power enhancement of 22.91% by JSSDK method. JSSDK configuration generates 8.21 W of power as compared to 6.86 W generated by the TCT in Pattern V shading conditions indicating 19.67% increment in power as compared to the TCT. In case of reconfiguration (JSSDK), the relocation of the PVMs provides a dispersing effect leading to higher power output for the shading scenarios. *P-V* and the *I-V* curves (Patterns I to V) based on experimental values are shown in Fig. 5.

3.2 *Mismatch Power Loss* (*MPL*)

It can be seen from Table 3 based on the experimental analysis, the power loss in JSSDK topology is reduced from 3.59 to 2.07 W for Pattern I, 3.47 to 1.96 W for Pattern II, 3.5 W to 1.98 W for Pattern III, 3.54 W to 2.03 W for Pattern IV and 3.27 W to 1.92 W for Pattern V scenario.

On the basis of above practical results, it is observed that the GMPP gets improved with the implementation of the proposed reconfiguration technique, the MPLs decreases resulting in augmented power yield.

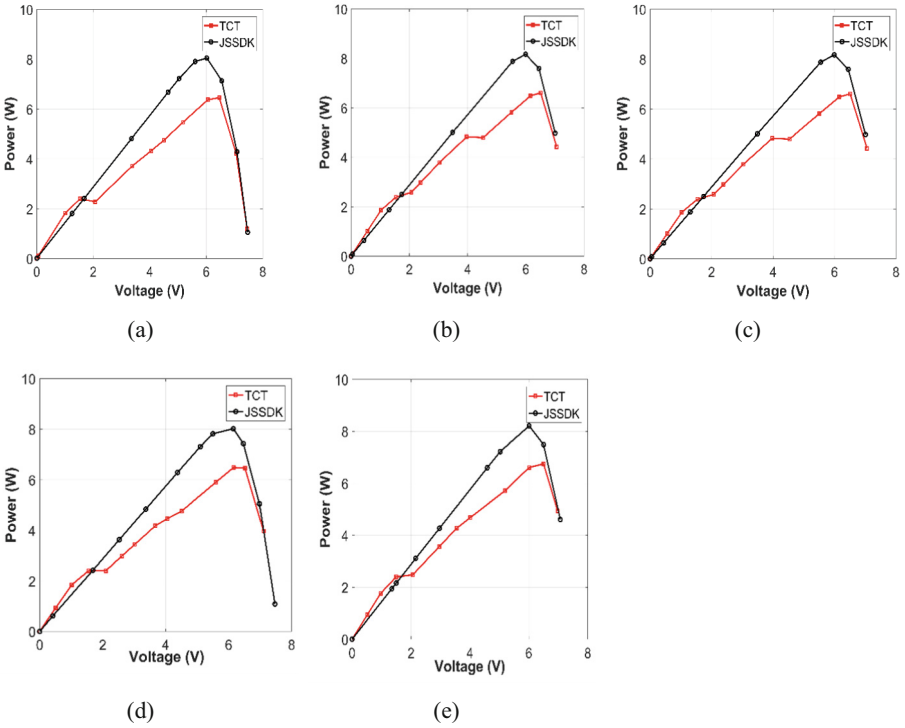


Fig. 5. Experimental *P-V* curves for JSSDK and TCT under partial shading condition for **a** pattern I, **b** pattern II, **c** pattern III, **d** pattern IV and **e** pattern V.

4 Conclusions and Scopes of Future Work

A new topology namely JSSDK is proposed in this article which takes into account the methodological rearrangement of PVMs. This is done exclusively by relocating the modules in a structured pattern within an array. The physical location of the modules is altered as per the shading pattern and the results are experimentally verified and compared with the conventional topology TCT. The efficiency of the proposed model JSSDK is augmented as compared to that of TCT which is justified through experimental setups and close observations. This is efficiently achieved due to uniform dispersal of shades across the PVA through the proposed scheme, thereby diminishing the adverse effects of the concentrated shadows. The JSSDK topology thus proves its ability to deliver better results in terms of GMPP, minimising the power losses and delivering enhanced power output under varied shading scenarios. Further, this reconfiguration technique can be applied to any squared PVA size.

References

1. Patel, H., Agarwal, V.: MATLAB-based modeling to study the effects of partial shading on PV array characteristics. IEEE Trans. Energy Convers. **23**(1), 302–310 (2008)

2. Subudhi, B., Pradhan, R.: A comparative study on maximum power point tracking techniques for photovoltaic power systems. IEEE Trans. Sustain. Energy **4**(1), 89–98 (2012)
3. Guo, L., Meng, Z., Sun, Y., Wang, L.: A modified cat swarm optimization based maximum power point tracking method for photovoltaic system under partially shaded condition. Energy **144**, 501–514 (2018)
4. Sen, T., Pragallapati, N., Agarwal, V., Kumar, R.: Global maximum power point tracking of PV arrays under partial shading conditions using a modified particle velocity-based PSO technique. IET Renew. Power Gener. **12**(5), 555–564 (2018)
5. Picault, D., Raison, B., Bacha, S., De La Casa, J., Aguilera, J.: Forecasting photovoltaic array power production subject to mismatch losses. Sol. Energy **84**(7), 1301–1309 (2010)
6. Kaushika, N.D., Gautam, N.K.: Energy yield simulations of interconnected solar PV arrays. IEEE Trans. Energy Convers. **18**(1), 127–134 (2003)
7. Krishna, G.S., Moger, T.: Reconfiguration strategies for reducing partial shading effects in photovoltaic arrays: state of the art. Sol. Energy **182**, 429–452 (2019)
8. Wang, Y.J., Hsu, P.C.: An investigation on partial shading of PV modules with different connection configurations of PV cells. Energy **36**(5), 3069–3078 (2011)
9. Rani, B.I., Ilango, G.S., Nagamani, C.: Enhanced power generation from PV array under partial shading conditions by shade dispersion using Su Do Ku configuration. IEEE Trans. Sustain. Energy **4**(3), 594–601 (2013)
10. Anjum, S., Mukherjee, V.: Static and dynamic reconfiguration strategies for reducing partial shading effects in photovoltaic array: a comprehensive review. Energ. Technol. **10**(7), 2200098 (2022)

Circular-Core PCF Employing Different Materials of Nano-rods for Sensing Enhancement

Simarpreet Kaur[1], Vikas Wasson[2(✉)], and Ruchi[1]

[1] ECE, Chandigarh University, Gharuan, Mohali, India
ruchi061179@gmail.com
[2] CSE, Chandigarh University, Gharuan, Mohali, India
vikaswasson.cse@gmail.com

Abstract. Photonic crystal optical fibers (PCOFs) are emerged as a peculiar and potential medium nowadays for sensing and receiving ample consideration due to their flexibility, multiple designs such as cladding holes and core variations, their respective positions, guiding mechanism and geometric versatility etc. The comprehensive literature revealed that most of the PCFs are investigated with the silica material in the background but nano-particles or rods integrated with the PCFs bear large potential in the development of ingenious optical devices. New applications, primarily in the field of sensing, are made possible by the union of PCFs with ideal nano-rods. In this research, a circular PCF (C-PCF) with silica backdrop and high index nano-rods imbibed has been presented. The interaction between the optical field and the analyte to be sensed is a crucial aspect of the sensing process. The attenuation coefficient (low) exhibited by the presented fiber is 10^{-6} dB/m and less than 0.0002 dB/m confinement loss. The value of most suitable effective area is found out to be 4.33 μm^2in comparison to the all other investigated materials. The presented nano-rods can gain distinctive sensing qualities for diverse applications such as optical-sensor systems, bio-medical optics and etc.

Keywords: CPCF · Nano-rods · Confinement losses · V-number · Effective area

1 Introduction

Photonic Crystal Fiber (PCF) is indeed a prominent and emerging technology in the field of photonics and optical communication. PCFs have gained significant attention and popularity due to their unique properties and versatile applications. The choice of material in nano-rods, especially in the context of PCFs, can indeed have a significant impact on several important optical properties and characteristics of the PCF. In PCFs designed with a periodic lattice structure, certain wavelengths or frequencies of light can be prohibited from propagating through the structure due to the presence of a photonic band gap. Similar to traditional optical fibers, PCFs can also guide light by exploiting the principle of total internal reflection (Birks et al. 1997). A variety of arrangements,

© The Author(s), under exclusive license to Springer Nature Singapore Pte Ltd. 2026
M. Kumar et al. (Eds.): HSFEA 2023, LNCE 899, pp. 138–148, 2026.
https://doi.org/10.1007/978-981-92-3200-0_12

including hexagonal, octagonal, square, and rectangular ones, are possible for the air holes. The properties of PCFs can be customized by carefully choosing the parameters of the microstructure, allowing for a extensive fields in different areas of optics and photonics. Their versatility and unique characteristics have made them an essential tool in many advanced optical and photonic systems (Gander et al. 1999; Knight et al. 1998), etc. The combination of these attributes has established PCFs as a versatile and valuable platform in the fields of optical sensing and photonics. They are used in various applications, including environmental monitoring, medical diagnostics, telecommunications, and scientific research. Researchers and engineers continue to explore new ways to leverage the unique properties of PCFs to develop innovative devices and sensors to meet the evolving demands of these fields. An ingenious use of fiber optic technology is PCF-oriented sensors. There are many different types of sensing applications, including mechanical sensors, temperature sensors, chemical sensors, and etc. (Liu And Salemink 2014). The nano-particles or rods integrated with the PCFs bear large potential in the development of ingenious optical devices. New applications, primarily in the field of sensing, are made possible by the union of PCFs with nano-rods. PCF exhibit numerous arrangements within their geometry like air holes, hole-to-hole distance and, by selecting an appropriate structure, the spectral as well as spatial characteristics of the light can be manipulated and engineered. Various application of guided light has been suggested such as the detection of gases, and liquids. An index guiding or a solid core PCF is considered as the best candidate for sensing applications. Due to their applications in several fields it has now become more important to enhance sensing of liquid and gas sensors. The liquid and gas-based PCF sensors offer outstanding sensing as the core simply participate or interact with material to be analyzed. When crystal fibers are combined with materials such as fluoride, tellurite, bismuth, and several chalcogenides glasses (higher-index materials, these fibers outperform silica based PCFs and provide applications in mid-IR transmissions and nonlinear optics (El-Amraoui et al. 2010; Liao et al. 2009; Liu et al. 2011). C-PCF was investigated to explore the dispersion and its dependence on diameter of air-hole, number of holes, and circular spacings (Maji And Roy Chaudhuri 2013). The low confinement loss of 7.64×10^{-3} dB/km was seen at 1550 nm wavelength with $d/\Lambda = 0.16$ air filling fraction over 1000 μm^2 mode area in CPCF (Medjouri et al. 2015). Confinement losses in square shaped PCF are lower than circular shaped in hexagonal arrangement as demonstrated in Sharma and Sharma (2016). Nanostructured composite materials improve PCF bandwidth, mode field diameter and reduce confinement losses (Johny et al. 2017). Senthil et al. (2019) investigated different solid core fillings such as ethanol ($n = 1.354$), glycerol ($n = 1.4722$), toluene ($n = 1.4968$) and it was perceived that glycerol show highest sensitivity of 65.16%.Further, hexagonal PCF structure having core surrounded by 4 circular air hole rings was investigated and numerical investigation of chromatic dispersion, birefringence and confinement losses was performed (Agbemabiese And Akowuah 2020). Cyclic olefin copolymer was used as the PCF material and results revealed that the material evenly gets distributed over THz window with consistent RI (1.53), decreased dispersion and attenuation, more tolerance to thermal effects, and low humidity sensitivity (Jibon et al. 2021). The opting of materials in core and nano-rods in a PCF is crucial for tailoring its optical properties.

By selecting appropriate materials and optimizing their properties, it's possible to control the effective area, confinement loss, and attenuation coefficient to meet the specific requirements of different applications, such as high-power laser delivery, supercontinuum generation, or sensing. Researchers often conduct detailed studies and simulations to find the right combination of materials and structural parameters for the desired optical performance.

In this paper, a four air holes based cladding in C-PCF has been proposed. The structure has higher index rods imbibed in its core area which are having different materials (indices) and it is observed that different characteristics of the fiber show variance with these materials and the influence of different semiconductor materials in these nano-rods on the parameters has been studied and the best one has been chosen. Attenuation coefficient of 10^{-6} and confinement loss 10^{-6} has been obtained with our proposed design using only four air holes rings. By carefully designing and engineering the nano−rods and materials, it is possible to achieve the desired V number and mode properties, making them suitable for specific applications where single−mode propagation is crucial for performance and signal quality. Therefore, it is studied for different nano−rods imbibed materials.

The presented paper is structured as: Sect. 2 discuss the theory of effective area, confinement loss, and V-number. Structural design is discussed in Sect. 3 and elaborated results are presented in Sect. 4. Section 5 encloses the conclusion.

2 Theory

(a) **Confinement Loss**

Confinement loss can significantly impact the efficiency and performance of optical fibers, especially in specialty fibers like PCFs, where the guidance of light is achieved through more complex mechanisms than traditional step-index fibers. Minimizing confinement loss is crucial to ensure that the majority of guided light remains within the core, enabling efficient transmission and signal quality in optical communication and other applications and is demoted by L. For keeping the L below 0.1 dB/km, twenty air holes are required in cladding as discussed by (Saitoh et al. 2003). In 2011, Xu et al. used five air hole rings to get 10^{-3} dB/km value of confinement loss. The imaginary portion refractive index can be used to compute it, *neff*, using Eq. (1) (Pourmahyabadi And Nejad 2009),

$$L(\mathrm{dB/m}) = \frac{40\pi}{\ln(10)\lambda}\mathrm{Im}\left[n_{eff}\right] = 8.686k_0\mathrm{Im}\left[n_{eff}\right] \tag{1}$$

where wavelength of light is λ, c is light speed in vacuum, and imaginary portion refractive index is $Im\,[n_{eff}]$. Minimum attenuation is observed near λ 1.55 μm in silica fiber around 0.2 dB/km. Additionally, losses are substantially larger at shorter wavelengths, as has been reported.

(b) **Effective Area**

This is a critical factor in determining nonlinear effects in optical fibers. Nonlinear effects are phenomena in which the properties of light, such as its intensity or frequency, change as it propagates through a medium like an optical fiber. These effects become more pronounced in fibers with smaller effective areas. To achieve and observe these nonlinear effects, high input power is often necessary in fibers with smaller effective areas. The increased intensity due to the smaller effective area results in a more pronounced nonlinear response. However, it's essential to strike a balance between high power and the potential for optical damage or unwanted nonlinear effects. Excessive power can lead to issues such as optical damage, increased attenuation, and the onset of detrimental nonlinear effects that can degrade the signal quality (Agrawal 2001). Researchers and engineers carefully select the appropriate fiber geometry and effective area to suit the specific needs of their applications, whether it's for signal transmission, optical amplification, or nonlinear effect generation. Effective area's numerical value can be calculated using the Eq. (2) (Jain et al. 2016),

$$A_{eff} = \frac{\left(\iint E^2 d_x d_y\right)^2}{\iint E^4 d_x d_y} \tag{2}$$

where electric field is depicted by E.

(c) **V-number**

The V-number allows a straightforward and efficient protocol to determine the mode structure of an optical fiber and is a fundamental parameter in optical fiber design and characterization. By controlling the core size, numerical aperture, and wavelength, engineers can tailor the V-number to meet specific requirements for different optical communication and sensing applications. Step index fiber has $V < 2.405$, as determined by the following equation (Keiser 2016):

$$V = k_0 a\left(n_1^2 - n_2^2\right)^{1/2} \tag{3}$$

where $k_0 = 2\pi/\lambda$, is radius of the core, n_1 and n_2 are refractive indexes of the core and cladding respectively.While both the types of PCF, i.e. solid and hollow core, have shown novel optical properties providing a basis for a medle-phenomena, showing prominent single mode behaviour, and PCFs with large-mode-area (Knight et al. 1998). The V number for a PCF's value was chosen somewhat arbitrarily and was first offered as (Mortensen et al. 2003):

$$V_{PCF} = \frac{2\pi\,\Lambda}{\lambda}\left[n_{c_}^2 n_{cl}^2\right]^{1/2} \tag{4}$$

where effective index and core index are n_{cl} and n_c respectively, lattice pitch is denoted by Λ (Birks et al. 1997).

3 Structural Design

Proposed design of PCF is realized with circular arrangement of four cladding air hole rings in silica backdrop. Figure 1 illustrates the pitch of PCF representing distance maintained neighboring air holes by removing central air holes. Distance is same between

the air holes in the lattice such as $d_1 = d_2 = d_3 = d_4$, (*dn*: diameter of air hole in nth ring; 'n' represents the no. of air hole rings). To eliminate back reflections at boundary, a perfectly matched layer (PML) is applied to cross section. Design has a number of high index rods—those with an index higher than silica—inserted on the inner most layer's edge of air hole ring. Diameter of these rods is indicated by the notation dnano. The oxides of niobium, titanium (in its anatase and rutile forms), glasses (chalcogenide glasses, AMTIR-1, arsenic sulphite), and aromatic conjugated polymer are the ingredients utilised to make these nano-rods. The materials differ in their refractive indices and vary from 2.3 to 2.9.The addition of these high index rods improves the light's confinement and increases its nonlinearity. The design exhibits changes in its confinement loss, attenuation profile, V number and effective refractive index by gradually raising the higher index rods' refractive index. The cross-section of PCF is depicted in Fig. 1 with a nanometer thickness of $dnano = 0.1$ micron meter and 0.7 air fill fraction, and $\Lambda = 1.88$ micron meter. The simulated Electric mode field distribution and height expression plot of the propagating mode at 1.55 μm are depicted in Figs. 2 and 3 respectively.

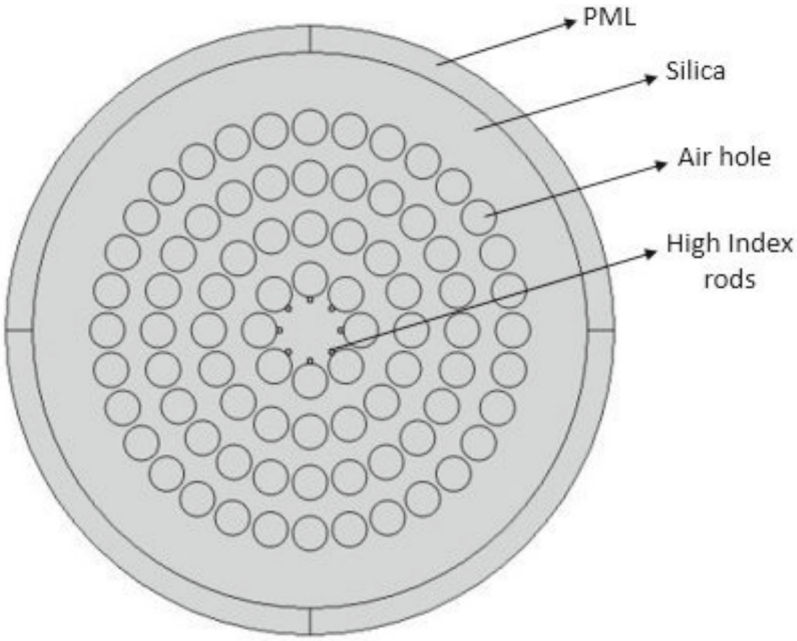


Fig. 1. Depiction of the C-PCF cross section

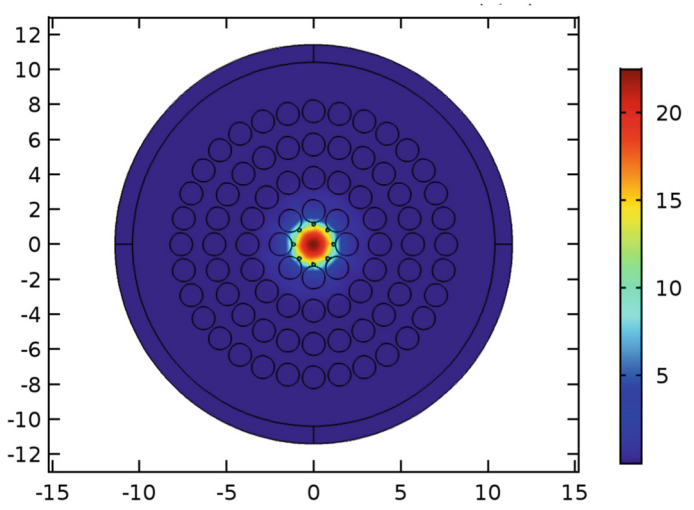


Fig. 2. Electric field norm

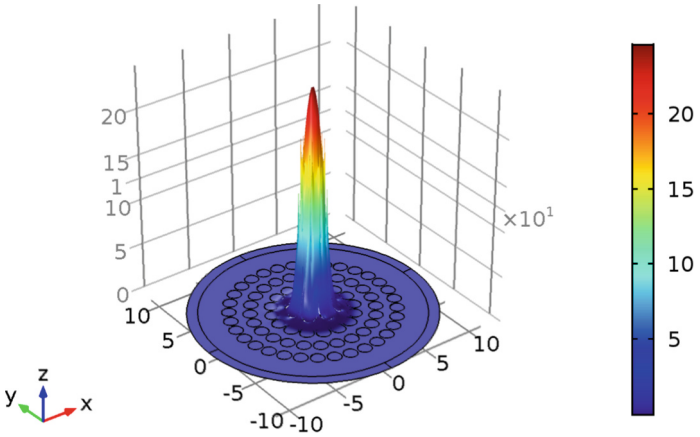


Fig. 3. Representation of height expression plot

4 Results and Discussion

For the accomplishment of proposed investigations, a widely employed simulation tool named COMSOL Multiphysics is considered. This simulation environment enables vectorial-based finite element method (FEM) programme. Sub-domains in the shapes of triangle are divided in cross-section of fiber and for FEM, C-PML boundary conditions are fixed and purpose is investigation of guiding qualities. There are 30552 triangular mesh elements in total, as well as 2434 edge mesh elements and 352 vertex mesh elements. XY plane shows the modal analysis and Z direction represents the light propagation. Effective refractive indices calculations in approximation, Saitoh et al. (2003) calculated Maxwell's vectorial equation.

Figures 4, 5, 6, 7 and 8 are representation of the effective refractive index, attenuation coefficient, V number and confinement loss in case of the PCF core imbedded different higher index roads. The simulations and findings were run over a wave-length range of 1.9–2.2 μm. The maximum and minimum values of the attenuation coefficient for the proposed fiber are achieved incorporating oxide of Niobium and employing the Aromatic polymer respectively, while the chalcogenide and AMTIR-1 glasses showed medium attenuation for the said range of wavelength. Figure 4 represents the best optimizied Aromatic polymer and the rutile form of oxide of titanium.

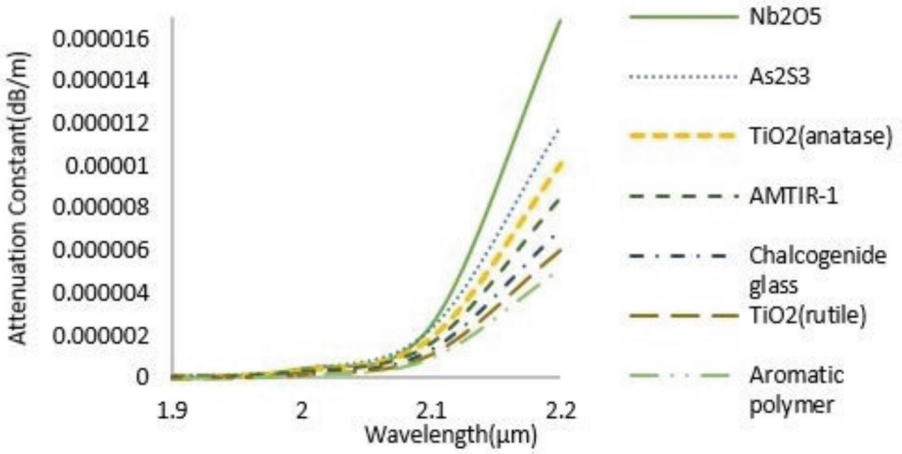


Fig. 4. Variation of the attenuation cofficient with respect to the different wavelengths

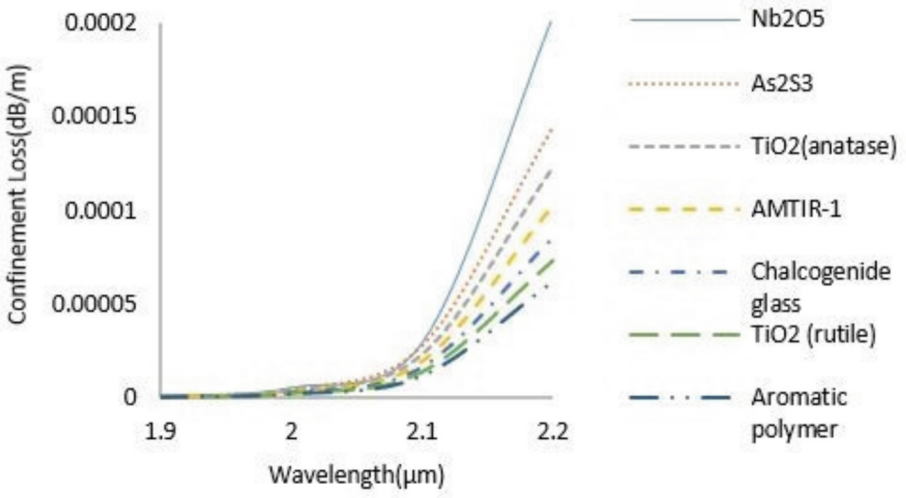


Fig. 5. Representation of wavelength effects on confinement loss

The minimum value of the attenuation coefficient achieved is 9.4×10^{-7} dB/m at 2.1 μm for the Aromatic polymer. The confinement losses achieved from the proposed structure are of the order 10^{-4} (Fig. 5) and are obtained minimum for the Aromatic polymer and the rutile form of TiO_2 while the maximum values are obtained for the oxide of Niobium (Nb_2O_5) and the Arsenic trisulphide (As_2S_3) while the glasses stand in the medium range of the achieved values in the said range of wavelength.

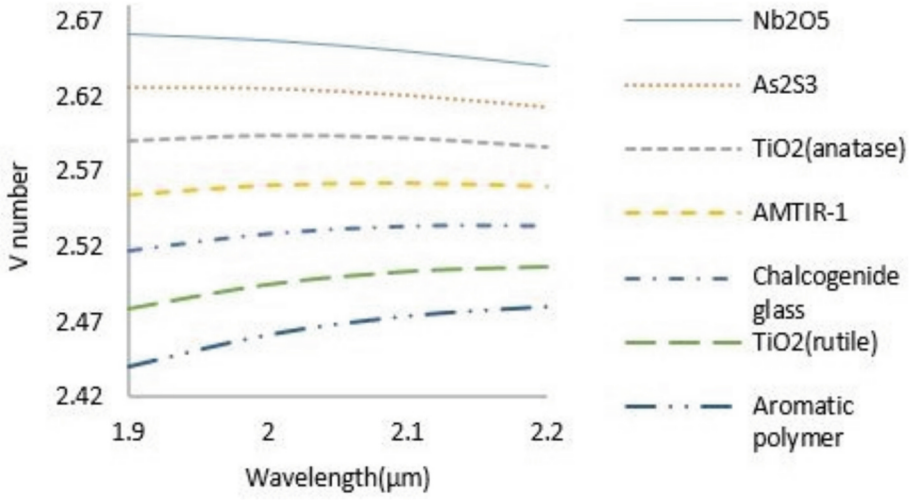


Fig. 6. V-number versus wavelength

As was already mentioned, the V number represents the number of fiber modes and determines whether or not the fiber will enable multimode or single mode propagation. For a typical step index fiber, this number must be $< 2.405$for the fiber to propagate in a single mode, however for a PCF, this value must be $< p$ or 3.14 (Mortensen et al. 2003; Anand et al. 2017). Investigation and analysis of nano-rods having different materials is performed in terms of V number as depicted in Fig. 6.

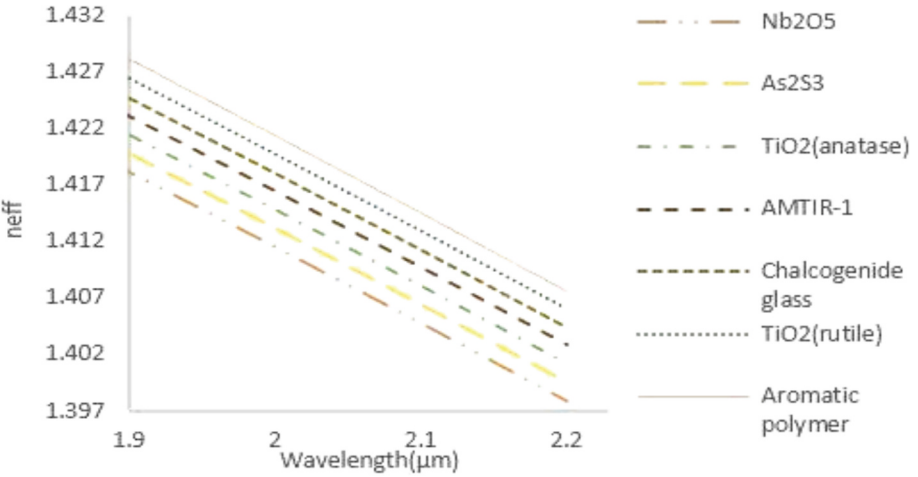


Fig. 7. Effective refractive index versus wavelength

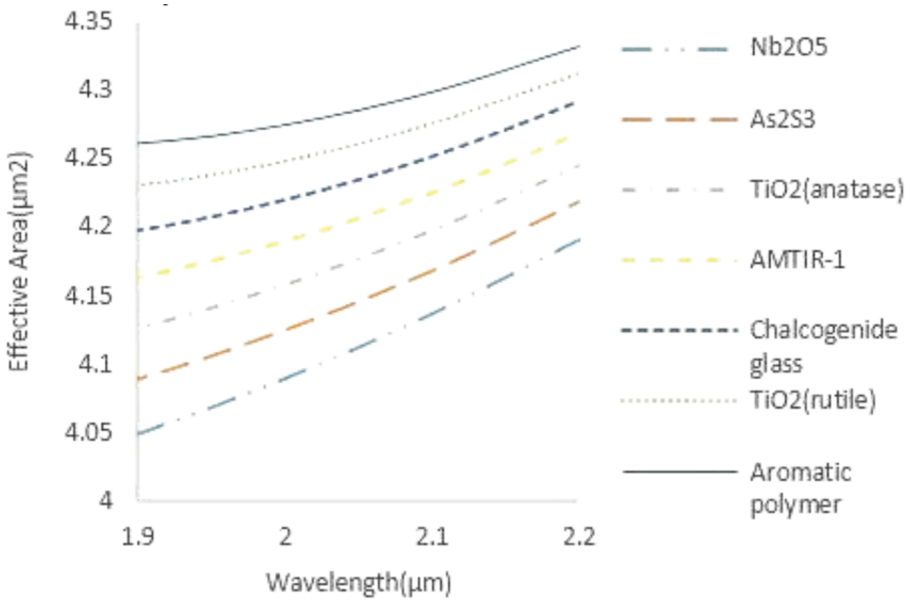


Fig. 8. Effective area versus wavelength

It is perceived that single mode is supported at considered wavelength array and these structures accomplished value $< p$. Further, different materials are investigated in Fig. 7 showing effective refractive index and results revealed that highest refractive index is obtained in case of As_2S_3 and lowest in case Nb_2O_5. Figure 8 represents the

different effective areas at varied wavelengths and it is clear from the results that Nb_2O_5 has least effective area and Aromatic material has highest value of effective area.

Titanium oxide (rutile form) (n = 2.8) and Aromatic polymer (n = 2.9) materials offered best performance as compared to other investigated materials in nano-rods. The two materials depict coefficient of attenuation 1.12×10^{-6} dB/m (TiO_2) and 9.45×10^{-7} dB/m (Aromatic polymer) at 2.1 mm, out of which the Aromatic polymer considered as an ultimate solution for sensing applications. Both the materials achieved confinement losses as low as 1.3×10^{-5} dB/m (TiO_2) and 1.16×10^{-5} dB/m (Aromatic polymer) at 2.1 mm. The effective areas are achieved as 4.27 μm^2 and 4.29 μm^2 for TiO_2 and the Aromatic polymer respectively. The TiO_2 and Aromatic polymer have effective refractive indices are 1.435 and 1.440 at 2.1 μm. The proposed structure with the above mentioned materials in its nano-rods has the value of V number as 2.50 (TiO_2) and 2.47 (Aromatic polymer) which catered single mode at given wavelengths with the $< pV$ number in a PCF. For different sensing applications, lower attenuation coefficient, lower confinement loss, are predominantly satisfactory indispensable parameters for designing PCF structure.

5 Conclusions

We have suggested a circular PCF with four air-hole rings and nanorods ingested in the centre, together with a high air-fill fraction. To maximise losses and attenuation, seven different materials are inserted into the nano-rods. To select the most suitable PCF candidate with minimal loss and attenuation, it's essential to perform a thorough evaluation of these characteristics and compare multiple options. Often, simulations and experimental measurements are used to validate the PCF's performance in real-world applications. Additionally, consultation with experts in the field or PCF manufacturers can provide valuable insights and guidance in the selection process. The developed PCF has a 10^{-6} dB/m attenuation coefficient and less than 0.0002 dB/m confinement loss. The design was successful in achieving an adequate effective area of 4.33 μm^2, which results in a more restricted space. Additionally, it provides single mode propagation for all materials placed into the nano-rods throughout the whole wavelength of interest. By adjusting the composition, size, and shape of the nanorods, researchers and engineers can optimize their sensitivity, selectivity, and responsiveness to external stimuli, making them versatile tools in a wide range of sensing and optical technologies.

References

Agbemabiese, P.A., Akowuah, E.K.: Numerical analysis of photonic crystal fiber of ultra-high birefringence and high nonlinearity. Sci. Rep. **10**, 21182 (2020)

Agrawal, G.: Fiber couplers in applications of nonlinear fiber optics, p. 60. Academic Press (2001)

Anand, G., Nippani, S.K., Kuchhal, P., Vasishth, A., Sarah, P.: Dielectric, ferroelectric and piezoelectric properties of $Ca_{0.5}Sr_{0.5}Bi_4Ti_4O_{15}$ prepared by solid state technique. Ferroelectrics, 516 (2017)

Birks, T.A., Knight, J.C., Russell, P.S.J.: Endlessly single-mode photonic crystal fiber. Opt. Lett. **22**(13), 961 (1997). https://doi.org/10.1364/ol.22.000961

El-Amraoui, G., et al.: Microstructured chalcogenide optical fibers from AS_2S_3 glass: towards new IR broadband sources. Opt. Express **18**(25), 26655 (2010). https://doi.org/10.1364/oe.18.026655

Gander, M.J., et al.: Experimental measurement of group velocity dispersion in photonic crystal fiber. Electron. Lett. **35**(1), 63 (1999). https://doi.org/10.1049/el:19990055

Jain, V., Sharma, S., Saini, T.S., Kumar, A., Sinha, R.K.: Design and analysis of single-mode tellurite photonic crystal fibers for stimulated Brillouin scattering based slow-light generation. Appl. Opt. **55**(25), 6791–6796 (2016)

Jibon, R.H., Bulbulo, A., Rahaman, M.E.: Numerical investigation of the optical properties for multiple PCF structures in the THz regime. Sens. Bio-Sens. Res. **32**, 100405 (2021)

Johny, J., Prabhu, R., Fung, W.: Numerical investigation of nanostructured silica PCFs for sensing applications. JOM **69**, 2286 (2017)

Keiser, G.: Optical fibers for bio-photonics applications in bio-photonics: concepts to applications springer. In: Peng, G.D. (ed.) Handbook of Optical Fibers, pp. 1069–1095. Springer, Singapore (2016)

Knight, J.C., et al.: Large mode area photonic crystal fiber. Electron. Lett. **34**(13), 1347 (1998). https://doi.org/10.1049/el:19980965

Liao, M., et al.: Tellurite microstructure fibers with small hexagonal core for supercontinuum generation. Opt. Express **17**(14), 12174 (2009). https://doi.org/10.1364/oe.17.012174

Liu, L., et al.: Numerical investigation of mid-infrared supercontinuum generation up to 5 μm in single mode fluoride fiber. Opt. Express **19**(11), 10041 (2011). https://doi.org/10.1364/oe.19.010041

Liu, Y., Salemink, H.W.: All-optical on-chip sensor for high refractive index sensing in photonic crystals. EPL (Europhysics Letters) **107**(3), 34008 (2014). https://doi.org/10.1209/0295-5075/107/34008

Maji, P.S., Roy Chaudhuri, P.: Circular photonic crystal fibers: numerical analysis of chromatic dispersion and losses. ISRN Optics **2013**, 1 (2013). https://doi.org/10.1155/2013/986924

Medjouri, A., et al.: Analysis of a new circular photonic crystal fiber with large mode area. Optik **126**(24), 5718 (2015). https://doi.org/10.1016/j.ijleo.2015.09.035

Mortensen, N.A., Folkenberg, J.R., Nielsen, M.D., Hansen, K.P.: Modal cut off and the V number in photonic crystal fibers. Opt. Letters **28**, 1879 (2003)

Pourmahyabadi, M., Nejad, S.M.: Numerical analysis of index-guiding photonic crystal fibers with low confinement loss and ultra-flattened dispersion by FDFD method. Iranian J. Electr. Electron. Eng. **5**, 170–179 (2009)

Saitoh, K., Koshiba, M., Hasegawa, T., Sasaoka, E.: Chromatic dispersion control in photonic crystal fibers: application to ultra-flattened dispersion. Opt. Express **11**(8), 843–852 (2003)

Saitoh, K., Koshiba, M.: Full-vectorial imaginary-distance beam propagation method based on a finite element scheme: application to photonic crystal fibers. IEEE J. Quantum Electron. **38**(7), 927 (2002)

Senthil, R., Soni, A., Bir, K., et al.: Circular-pattern photonic crystal fiber for different liquids with high effective area and sensitivity. Plasmonics **14**, 1783 (2019)

Sharma, S., Sharma, C.: Analysis of birefringence and V-parameter in PCF with modified air holes in cladding region. J. Engg. Tech. **2**(1), 33 (2016)

Xu, H., Wu, J., Xu, K., Dai, Y., Xu, C., Lin, J.: Ultra-flattened chromatic dispersion control for circular photonic crystal fibers. J. Opt. **13**(5), 055405 (2011)

Status of CCUS Project Viability for Mumbai Offshore and Cambay Basins, Western India

Rahul Kumar Singh and Atul Kumar Patidar(✉)

Department of Petroleum Engineering and Earth Sciences, Energy Cluster, UPES, Dehradun, Uttarakhand 248007, India
apatidar@ddn.upes.ac.in

Abstract. India, a country with a population of 1.4 billion, requires a massive amount of energy resources to sustain its expanding infrastructural needs. Since the country's energy sectors continue to be largely dependent on the generation of energy from fossil fuels, it is among the top emitters of CO_2 which was estimated to be around 2.5 Gt in the year 2024. Hence, India still faces significant difficulty in controlling its high greenhouse gas (GHG) emissions and adhering to the Paris Agreement's rules. However, the Government in India is focusing on green technology like the use of fuel cells and the hydrogen-based economy to minimize these challenges. Carbon capture, utilization, and storage (CCUS) is one such technique that can help in managing a nation's overall GHG emissions. CCUS is a three-step procedure that involves capturing carbon, its transportation, and storage for future usage. The third stage of the process, where captured or transported carbon is stored in geologically secure and economically feasible subsurface formation, is also known as carbon sequestration. According to a report by the Ministry of Petroleum and Natural Gas (MOPNG), India has 26 sedimentary basins that together have a geological storage capability of 500–1000Bt. According to MOPNG's proposed 2030 roadmap for CCUS, exploiting the nation's tremendous capacity for storing CO_2 can help it reach its net zero emissions objective and reduce anthropogenic carbon emissions in the environment.

The current study focuses on the possibilities for the geological CO_2 storage potential in highly producing category-1 hydrocarbon basins of western India, the Mumbai offshore and Cambay basins. Over the last four decades, these two basins have demonstrated their hydrocarbon potential, and their underlying stratigraphic records are well-studied and ideal for CCUS. According to studies carried out by MOPNG, the Mumbai offshore basin (a mature oil field), which is now in the brownfield development phase, is the best option for CO_2-based enhanced oil recovery (EOR) and has the potential for geological storage of about 9.25 Gt. Similar to this, national oil and gas (E&P) companies have estimated the Cambay basin's capacity to store CO_2 to be around 16.13 Gt. A current study covered a quick techno-economic assessment and risk analysis of CCUS in the two basins mentioned above.

Keywords: CO_2 storage · Geological sequestration · Decarbonisation · CCUS · Carbon mineralization

© The Author(s), under exclusive license to Springer Nature Singapore Pte Ltd. 2026
M. Kumar et al. (Eds.): HSFEA 2023, LNCE 899, pp. 149–159, 2026.
https://doi.org/10.1007/978-981-92-3200-0_13

1 Introduction

Carbon capture, utilization, and storage (CCUS) is an emerging technology that has gained international recognition as a substitute for lowering greenhouse gas (GHG) emissions in the environment (Singh et al. 2024). There are three steps to it, with the first and most important step being the capture of anthropogenic carbon. The second and third steps are its transportation and utilization as well as (iii) risk-free & economically feasible underground storage (Raza et al. 2019). Since this technology's major goal is to reduce atmospheric emissions, just capturing and using the carbon won't finish the cycle. To achieve this goal, environmentally friendly, long-term storage is crucial. Commonly, deep ocean basins, depleted reservoirs, and subsurface porous rock formations at sufficient depth can all store CO_2. Another unique process is known as carbon mineralization, in which CO_2 reacts with Ca and Mg-rich carbonate rocks to produce and store solid carbonate minerals Kumar Singh and Priyadarshini Nayak (2023a, b). Storage of industrial as well as anthropogenic emissions is being carried out at a large scale across multiple sites in Europe, the Americas, China, and other parts of the world since the early 2000s in deep saline formations and as CO_2-EOR in exhausted oil and gas fields (Zahasky nd Krevor 2020). After China and the United States, India ranks third in terms of emissions, although it is still lagging in the adoption of long-term deep decarbonization measures. Although the country has enormous storage capacity with both onshore and offshore storage options (Lau et al. 2021). India constitutes around 3.36 million km^2 of the basinal area with 1.63 million km^2 being on land and the rest offshore (Mitra and Kumar 2008). Additionally, the nation's ~ 7500 km long coastline, together with the presence of mega-refineries, fertilizer & chemical plants, and other industrial infrastructures, make it suited for carbon transportation and the adoption of CCUS on a small to mega-scale mainly in associated sedimentary basins (Patidar et al. 2023). Although the physiography and challenging topography of individual basins preclude the use of such expensive technologies, a well-planned study is required to identify a suitable location that is less risky and more economical (Ghiat and Al-Ansari 2021). An area of 3.14 million square kilometers is covered by 26 sedimentary basins in India, 7 of which are currently in the exploring stage. Around 15–20% of the country's hydrocarbon needs were met by these seven basins, which are categorized as category 1 basins (Sakthipriya et al. 2015). The current study is focused on the Mumbai offshore and Cambay basins, which are crucial for the sustainability of the CCUS project in the country (Fig. 1).

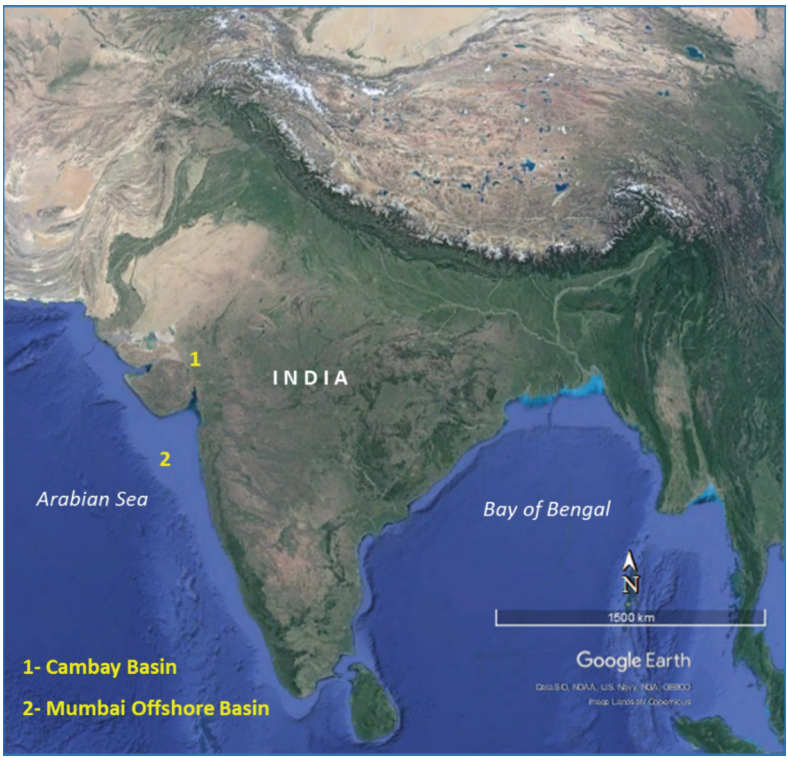


Fig. 1. Location of Mumbai offshore & Cambay basins

2 Generalised Geological Setup of the Study Area

The Mumbai offshore is situated near the western margin of the Indian continent, and a pericratonic rift basin continues deeper in the Arabian Sea while extending up to the Cambay basin towards the NNE direction on land (Fig. 1). The Saurashtra and Kerala-Konkan basins are located in the NNW and South, respectively, and encircle this basin. The Mumbai offshore and Cambay basins were chosen for the current study because they are located in the vicinity of Indian states, Gujarat and Maharashtra, which have the highest carbon emissions in the country and a good concentration of industries (Li et al. 2021). The combined emissions from the power and industrial sectors in these two states in 2021 were more than 280 Mtpa (Zimmermann et al. 2020).

The Mumbai offshore basin covers an area of ~ 116,000 km^2, with a sedimentary fill thickness ranging from 1 to 5 km, and is primarily composed of late Cretaceous to Holocene age sediments (Sahay, 1985). This is the country's most promising basin having the existence of commercially viable hydrocarbons at numerous pay zone intervals (Chakraborty et al. 2019). Recent data indicates that it produces between 55 and 70% of India's domestic crude oil and gas production, respectively. The Mumbai offshore basin is one of the finest candidates for CCUS demonstration, specifically, CO_2-EOR, as it experiences production decline over time and so qualifies as brownfield development. This basin's structurally mature sedimentary strata, which vary in depth from 800

to 1100 m (Tertiary age), may be perfect for geological carbon storage (Singh et al. 2023b).

On the other hand, the narrow and elongated Cambay Rift Basin (CRB), which spans an area of around 53,500 km^2, has an NNW-SSE trend and has demonstrated hydrocarbon prospectivity at multiple stratigraphic intervals. The sedimentary thickness in this basin varied from 4 to 6 km. The CRB extends from Surat to Sanchor region of Gujarat from South to North respectively and continues further north up to the Barmer basin of Rajasthan. CRB has been divided into five significant tectonically controlled segments by the oblique trending transverse fault systems. The Govt. of India has narrowed down this basin to make it the first mega-scale CCUS project prototype in the country. An MoU has been signed between the Oil and Natural Gas Corporation (ONGC) and Indian Oil Corporation Limited (IOCL) for implementing the CCUS project in the Cambay basin. The source from which CO_2 will be treated, compressed, and transported to the Gandhar field in the Cambay basin, which is ~ 110 km away from the IOCL Koyali refinery located in Vadodara city. Transportation through pipelines is part of the existing infrastructure and will be renewed for CO_2 transportation (Mishra et al. 2019). Figure 1 depicts the location of both Mumbai offshore and the Cambay basins.

3 Methodology Followed

This article presents a concise examination of the outlined structure for evaluating the cost of CCUS projects starting from capture through storage in onshore and offshore conditions for Mumbai offshore and Cambay basins based on various assumptions. This analysis divides the projects into onshore and offshore storage and takes into account road, rail, and marine (pipelines/ships) possibilities for conveyance, depending on physiographic conditions and distance from source and sink. This analysis is unique in that we have highlighted the likely scenarios with special attention to India based on existing literature on commissioned CCUS projects around the world. In the very first stage, we identified the source and sink locations in each basin with the shortest distance. Source and sink both refer to locations from which emissions will be gathered and stored. The routes for both locations were then selected after conducting a systematic literature review and consulting reports from various governmental organizations and MOPNG. The two essential elements for the cost analysis are the selection of the shortest route and the preferred mode of transportation. The cost was determined for each process step using the data provided in the literature and our assumptions. Although it is not possible to estimate the precise cost of a full-fledged CCUS project here due to the need for a complete techno-commerciality analysis, multidisciplinary data sets (engineering, geotechnical, mode of transportation, and supply chain), as well as information on specific governmental policies. Hence, the authors agreed on the limitations of their work and presented here some initial conclusions made using constrained data. The following sections show a flow chart (Fig. 2) and address the CCUS project's costs and basin-level details.

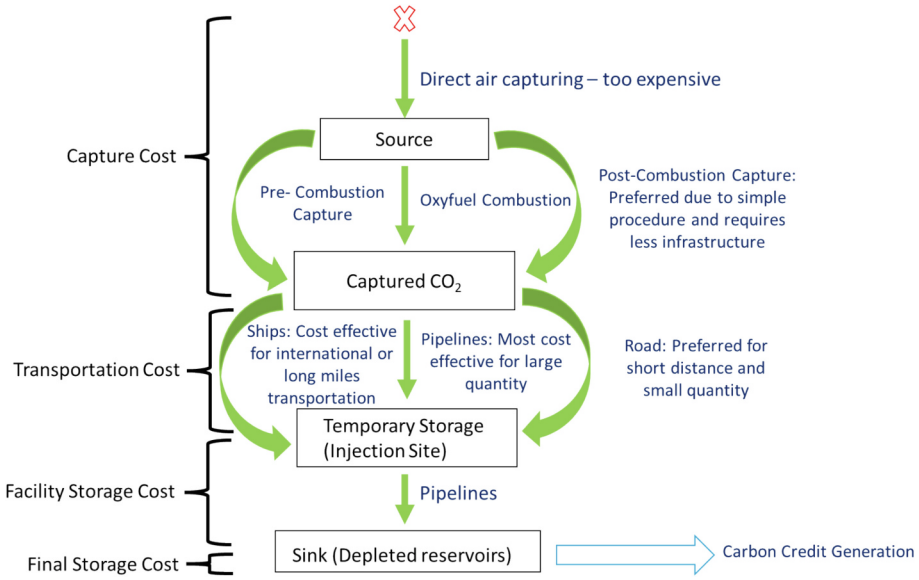


Fig. 2. Flow chart showing stepwise cost determination for the CCUS project in the Indian scenario

4 Indian Sedimentary Basins CCUS Potential and Probable Costs

India has 26 basins totaling 3,359,729 km^2 of the sedimentary basin area. Based on their potential for producing hydrocarbons, all these basins have been further categorized into categories 1 through 4. Such a big basinal region also provides a sizable area of porous formation, making it an appropriate choice for CO_2 sequestration (Chakraborty et al. 2019). Figure 3 (a) and (b) depict the total area of 7 individual category 1 Indian basins and their basin-wise probable geological carbon storage potential, respectively. These numbers unequivocally demonstrate the significant level of carbon storage capacity of Indian sedimentary basins mainly connected with the open coastline of the country (Zhang et al. 2022).

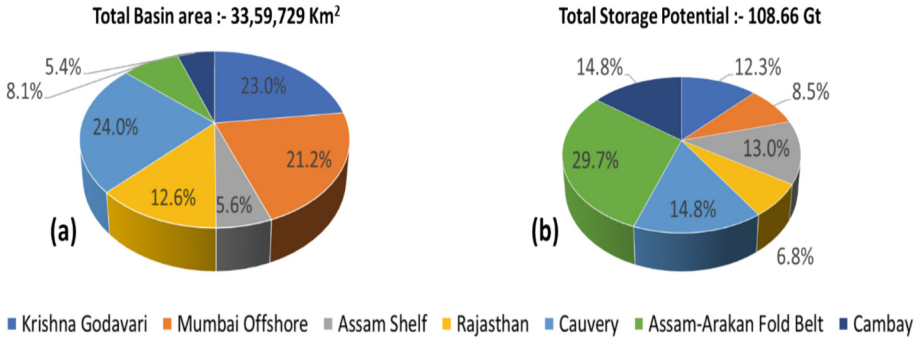


Fig. 3. Comparison between basinal area and storage potential of category 1 Indian sedimentary basins

The country's two main oil and gas producing basins, Mumbai offshore and Cambay basins, are now seeing a decline in their production rate. To balance supply and demand for energy, which is increasing along with population growth, new petroleum recovery techniques are desperately needed (Bokka et al. 2022). In such a situation, it is vital to analyze effective EOR techniques with a focus on the decarbonization process. By adopting carbon sequestration techniques, it may be possible to boost oil and gas output while also lowering atmospheric levels of anthropogenic carbon (Farajzadeh et al. 2020). CCUS has consistently made headlines throughout the world and has been demonstrated to be an essential and crucial option for lowering emissions in the environment. India, meanwhile, is still working on implementing this technology at a demonstration scale (Núñez-López and Moskal 2019). Lack of infrastructure and exorbitant costs may be the main causes of this backlog. Therefore, it becomes crucial to control project costs to speed up the implementation of this green technology (Loria and Bright 2021).

4.1 Cambay Basin

By breaking down the overall cost into multiple categories like capture cost, transportation cost, facility storage cost, ultimate storage cost, and additional charges, Vishal et al. 2021 have illustrated a scenario for cost computation. This segmentation was created to demonstrate the hazy fluctuations in cost over the entire procedure. The costs listed in Table 1 were gathered from a variety of company websites, including ONGC, HPCL, and IOCL, as well as project reports, case studies, and other materials related to the Mumbai offshore and Cambay basins. The scenario for the Cambay basin can be,

Source: Koyali Refineries (IOCL)

Sink: ONGC oilfield, Gandhar

Shortest on land Distance: ~ 110 km

Mode of transportation: Pipeline (Marine).

Table 1. Different types of costs associated with the CCUS project at the Cambay basin

Type of cost	Cost (INR)/t	Cost USD/t (1 INR = 0.013 USD)	Comments
Capturing cost	1760	22.22	This cost also covers the cost of emissions and infrastructure maintenance (associated with emissions that occurred during capturing)
Transportation cost	6200	78.29	This cost includes tanker maintenance as well as fuel charges
Facility storage cost	748	9.45	This cost is the price required to store CO_2 temporarily close to the storage site

(*continued*)

Table 1. (*continued*)

Type of cost	Cost (INR)/t	Cost USD/t (1 INR = 0.013 USD)	Comments
Final storage cost	1380	17.43	This covers the cost of using, maintaining, and injecting CO_2 using the already-existing infrastructure
Others	100	1.26	A reasonable figure for any added costs associated with the process
Total	10,188	128.64	Cost at the primary stage with broad parameters. It may alter as a result of adjustments made to the facilities for capturing and transporting as well as the need for new infrastructure

4.2 Mumbai Offshore Basin

A similar scenario for the Mumbai offshore basin is given below and the brief cost segmentation is shown in Table 2.

Source: HPCL Mumbai Refinery

Sink: Base in oilfield, Mumbai Offshore

Shortest Distance: ~ 29 km (onland) and ~ 156 km (offshore)

Mode of transportation: Road (Tanker) and pipelines.

Table 2. Different types of costs associated with the CCUS project at the Mumbai offshore basin

Type of cost	Cost (INR)/t	Cost USD/t (1 INR = 0.013 USD)	Comments
Capturing cost	1760	22.22	This cost also covers the cost of emissions and infrastructure maintenance (associated with emissions that occurred during capturing)
Onland terminal processing facility cost	748	9.45	This cost is the price required to store CO_2 temporarily close to the storage site

(*continued*)

Table 2. (*continued*)

Type of cost	Cost (INR)/t	Cost USD/t (1 INR = 0.013 USD)	Comments
Transportation cost	6500	82.08	This cost includes tanker maintenance as well as fuel charges. It also includes the pipeline and its maintenance charges
Final storage cost	1510	19.07	This covers the cost of using, maintaining, and injecting CO_2 using the already-existing infrastructure
Others	100	1.26	A reasonable figure for any added costs associated with the process
Total	10,618	134.08	Cost at the primary stage with broad parameters. It may alter as a result of adjustments made to the facilities for capturing and transporting as well as the need for new infrastructure

5 Discussion

The overall cost of the CCUS operation in the Mumbai offshore basin and Cambay basin was roughly estimated. The total cost was determined to be INR 10,188/t (USD 128.64/t) for the Cambay basin and about INR 10,618/t (USD 134.08/t) for the Mumbai offshore basin. Figure 4 shows the project's contribution to various sub-costs for these two basins. The following are the likely causes of the significant disparity in technological costs between these two basins:

(1) Storage Type: When offshore storage is used, transportation costs go up since both tanker and pipeline modes of transportation are used.
(2) Infrastructure: Special infrastructure facilities are needed in offshore basins to acclimate CO_2 for pipeline transit, which inevitably raises costs.
(3) Capturing Cost: In both circumstances, it is essentially the same. Given that the methods of capture are likewise similar.

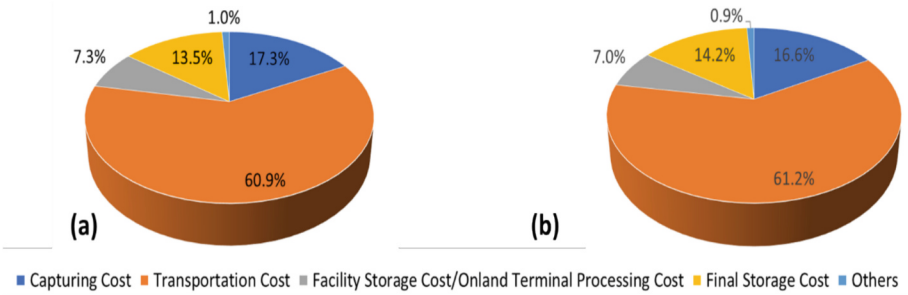


Fig. 4. (a) Shares of different cost types in the Cambay Basin and (b) Mumbai Offshore Basin. Details are shown in Tables 1 and 2

Figure 5 displays the CCUS cost/t for various nations (Budinis et al. 2018). The graph makes it very evident that India's cost/t charges are significantly greater than those in other parts of the world mostly in comparison to the developed nations. High population density, limited availability of existing infrastructure, lack of government subsidies, flaws in administrative planning and strategy, and other factors may all be contributing factors (Hepburn et al. 2019; Martin-Roberts et al. 2021).

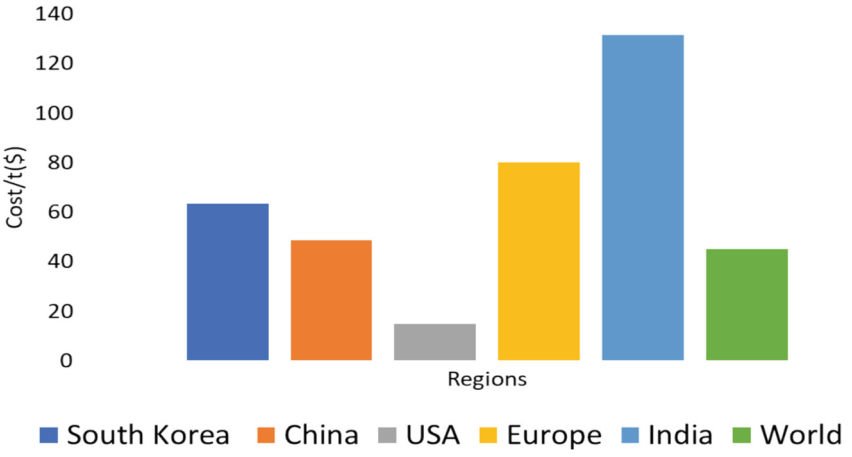


Fig. 5. Comparison of CCUS cost/ tonnes amongst different countries

6 Conclusion

- Due to its high population density and rising energy needs, India is one of the top GHG emitters and has a rapidly expanding economy. Sustainable green technology integration is still a work in progress in the nation, raising concerns about its carbon neutrality targets by adhering to the UN regulations for carbon neutrality.

- The government has given the green flag to the first CCUS project proposal that IOCL has planned to cut carbon emissions at its Koyali refinery. This project is now in the initial phase and will be launched after a thorough techno-economic analysis to show the effectiveness of CO_2-EOR by ONGC.
- The Mumbai offshore basin, which is currently in the brownfield development phase, is another excellent choice for CCUS's mega-scale model project in the nation. Although it is expensive to construct such projects in offshore regions, given the infrastructure already in place. When compared to other developed countries like the USA, UK, and China, India's cost/t of emission reduction is currently 40–50% higher.
- Due to the estimated 40 billion tonnes of GHG emissions worldwide each year, the 1.5 °C warming tipping point is getting closer. The government, decision-makers, and business leaders are all concerned and moving toward green/renewable technologies. In light of this situation, CCUS adoption is necessary for the world to reach its net zero emission goal.

References

Bokka, H.K., Zhang, K., Lau, H.C.: Carbon capture and storage opportunities in the west coast of India. Energy Rep. **8**, 3930–3947 (2022). https://doi.org/10.1016/J.EGYR.2022.03.012

Budinis, S., Krevor, S., Mac Dowell, N., Brandon, N., Hawkes, A.: An assessment of CCS costs, barriers and potential. Energy Strat. Rev. **22**, 61–81 (2018). ISSN: 2211–467X. https://doi.org/10.1016/j.esr.2018.08.003

Chakraborty, P.P., Tandon, S.K., Saha, S.: Development of Phanerozoic sedimentary basins of India. J. Asian Earth Sci. **184**, 103991 (2019). https://doi.org/10.1016/j.jseaes.2019.103991

Farajzadeh, R., Eftekhari, A.A., Dafnomilis, G., Lake, L.W., Bruining, J.: On the sustainability of CO_2 storage through CO_2—enhanced oil recovery. Appl. Energy **261** (2020). https://doi.org/10.1016/j.apenergy.2019.114467

Ghiat, I., Al-Ansari, T.: A review of carbon capture and utilisation as a CO_2 abatement opportunity within the EWF nexus. J. CO_2 Util. **45** (2021). https://doi.org/10.1016/j.jcou.2020.101432

Hepburn, C., et al.: The technological and economic prospects for CO_2 utilization and removal. Nature **575**(7781), 87–97 (2019). https://doi.org/10.1038/S41586-019-1681-6

Kumar Singh, R., & Priyadarshini Nayak, N.: Complications in drilling operations in basalt for CO_2 sequestration: an overview. Mater. Today: Proc. (2023a). https://doi.org/10.1016/j.matpr.2023.04.441

Kumar Singh, R., & Priyadarshini Nayak, N.: Opportunities and challenges of nanotechnology in enhanced oil recovery: An overview. Mater. Today: Proc. (2023b). https://doi.org/10.1016/j.matpr.2023.04.392

Lau, H.C., Ramakrishna, S., Zhang, K., Radhamani, A.V.: The role of carbon capture and storage in the energy transition. Energy Fuels **35**(9), 7364–7386 (2021). https://doi.org/10.1021/ACS.ENERGYFUELS.1C00032

Li, H., Lau, H. C., Wei, X., Liu, S.: CO_2 storage potential in major oil and gas reservoirs in the northern South China Sea. Int. J. Greenhouse Gas Control **108** (2021). https://doi.org/10.1016/j.ijggc.2021.103328

Loria, P., Bright, M.B.H.: Lessons captured from 50 years of CCS projects. Electricity J. **34**(7) (2021). https://doi.org/10.1016/j.tej.2021.106998

Martin-Roberts, E., Scott, V., Flude, S., Johnson, G., Haszeldine, R.S., Gilfillan, S.: Carbon capture and storage at the end of a lost decade. One Earth **4**(11), 1569–1584 (2021). https://doi.org/10.1016/J.ONEEAR.2021.10.002

Mishra, G.K., Meena, R.K., Mitra, S., Saha, K., Dhakate, V.P., Prakash, O., Singh, R.K.: Planning India's First CO2-EOR Project as Carbon Capture Utilization & Storage: A Step Towards Sustainable Growth. Day 2 Wed, April 10, 2019 (2019). https://doi.org/10.2118/194629-MS

Mitra, N.K., Kumar, A.: Managing mature Indian offshore fields—a case history. In: Society of Petroleum Engineers—13th Abu Dhabi International Petroleum Exhibition and Conference, ADIPEC 2008, 2, pp. 963–970 (2008). https://doi.org/10.2118/117950-MS

Núñez-López, V., Moskal, E.: Potential of CO_2-EOR for near-term decarbonization. Front. Climate **1** (2019). https://doi.org/10.3389/FCLIM.2019.00005

Patidar, A.K., Singh, R.K., Choudhury, T.: The prominence of carbon capture, utilization and storage technique, a special consideration on India. Gas Sci. Eng. **115**, 204999 (2023). https://doi.org/10.1016/j.jgsce.2023.204999

Raza, A., Gholami, R., Rezaee, R., Rasouli, V., Rabiei, M.: Significant aspects of carbon capture and storage – A review. Petroleum **5**(4), 335–340 (2019). ISSN: 2405–6561. https://doi.org/10.1016/j.petlm.2018.12.007

Sahay, B.: Geology and hydrocarbon potential of Bombay offshore Basin. In: Proceedings of the Annual Offshore Technology Conference, 1985-May, pp. 97–104 (1985). https://doi.org/10.4043/4908-MS

Sakthipriya, N., Doble, M., Sangwai, J.S.: Enhanced oil recovery techniques for Indian reservoirs. Springer Geol., 237–269 (2015). https://doi.org/10.1007/978-3-319-03119-4_11

Singh, R.K., Nayak, N.P., Kumar, S., Vishal, V.: A critical meta-analysis of CO_2-water-rock interaction in basalt for CO_2 storage: a review based on global and Indian perspective. Mar. Pet. Geol. **168**, 107002 (2024). https://doi.org/10.1016/j.marpetgeo.2024.107002

Zahasky, C., Krevor, S.: Global geologic carbon storage requirements of climate change mitigation scenarios. Energy Environ. Sci. **13**(6), 1561–1567 (2020). https://doi.org/10.1039/D0EE00674B

Zhang, K., Lau, H.C., Bokka, H.K., Hadia, N.J.: Decarbonizing the power and industry sectors in India by carbon capture and storage. Energy **249** (2022). https://doi.org/10.1016/J.ENERGY.2022.123751

Zimmermann, A.W., Wunderlich, J., Müller, L., Buchner, G.A., Marxen, A., Michailos, S., Armstrong, K., Naims, H., McCord, S., Styring, P., Sick, V., Schomäcker, R.: Techno-economic assessment guidelines for CO_2 utilization. Front. Energy Res. **8** (2020). https://doi.org/10.3389/FENRG.2020.00005

The Serious 2018 Summer Water Crisis in Shimla

Navjot Hothi(✉)

Department of Physics, University of Petroleum and Energy Studies, Dehradun 248007, India
nhothi@ddn.upes.ac.in

Abstract. Considered by many to be the "Queen of Hills," Shimla will go down in history as having experienced its darkest period during the summer of 2018. The severe water scarcity that the people of this well-liked hill station experienced caused it to descend into a state of unrest and general mayhem. The residents of the six natural water resources i.e. Ashwani Khadd, Nauti Khadd, Giri Khadd, Churat Nallah, Chair Nallah, and Dhalli Catchment were severely deprived of water due to water rationing, which resulted in extremely limited water supplies that were insufficient to meet even the necessities for other basic needs, let alone enough drinking water. The government authorities had to close the schools. The town's main industry, tourism, took a hit when hotels had to revoke reservations. This serious catastrophe was caused by a number of variables, the main one being climate change. Due to the significant changes in climate, Shimla saw very little snowfall in the winter and very little rainfall during the previous monsoon season, which caused the natural water resources to dry up. After analyzing the rain precipitation data from the preceding six years, it was discovered that 2017 saw a significant drop in rainfall. In order to ensure a better and more secure future for this lovely colonial town, the government and the locals must act quickly to address this worrying issue and restore the natural water eco-balance.

Keywords: Natural water resources · Rain precipitation · Water reservoirs · Acute water crisis · Rainwater harvesting

1 Introduction

Shimla is the state capital of Himachal Pradesh and is the primary hub of education, commerce, legislation, and culture. It was the summer capital of British India. The credit for the development of this town goes to the British who were attracted to its climate which resembled that of Britain. In the 18th century, most of the presently occupied city was a dense forest with a few scattered houses. The British found this place to be easily assessable from Delhi and it provided a serene refuge from the burning plains of India. They built the first wood cottage here in the year 1819 (Bhasin 1994). Within a few decades, the settlement grew very rapidly and buildings were styled in the colonial architecture. The British officers along with their families started spending their summer vacations in Shimla. Thus, Shimla soon turned into a center for socialization amongst the British elite where it hosted frequent balls, festivities, and celebrations.

© The Author(s), under exclusive license to Springer Nature Singapore Pte Ltd. 2026
M. Kumar et al. (Eds.): HSFEA 2023, LNCE 899, pp. 160–167, 2026.
https://doi.org/10.1007/978-981-92-3200-0_14

Consequently, Shimla witnessed widespread development and the population increased multifold. Residential schools were established for the children of influential families and an uptown mall area was developed. Theatre activities were frequently organized along with exhibitions.

In the year 1864, Shimla became the summer capital of the Indian government. In the subsequent years to follow, a new road named the Grand Hindustan-Tibet road was developed which stretched 94 km from Kalka to Shimla. The rail line to Shimla opened up in the year 1903 which was considered to be an engineering marvel and made this hill town extremely accessible. This route had around 806 bridges and a record 103 tunnels. In the year 2008, this track became a UNESCO world heritage site. On a prosaic scale, the city was designed to accommodate a population of 20,000. The British brought the first methodical potable water scheme in the year 1875 (Gilmour 2018). They realized that water in Shimla is a crucial renewable and limited resource. Water to the city was tapped by a catchment area developed in Dhalli which was sourced from a natural spring. The rainwater was completely harvested in this catchment area wherein the natural flora and fauna flourished in the form of a sanctuary. However, the Dhalli catchment water supply system was devised to cater to the needs of only 20,000 people (Bhasin 1994). Even now, the water supply system in Shimla completely relies on natural streams, tributaries, and springs. Eventually, several other water supply systems were augmented on these natural resources.

Shimla remained a place of high historic relevance even after independence from the British. As Himachal Pradesh became the eighteenth state of the Indian Union in the year 1971, Shimla became its state capital. Thereby, the hill town witnessed an upsurge in growth and development but at the cost of nature and the environment. This expansion, which is continuing is very chaotic and unplanned. The vision which the British had for Shimla seems to be long lost or has become somewhat shady. Today, this hill town is slowly reducing to a concrete jungle wherein mankind is destroying its natural beauty and shrinking it out of its natural resources. As a result of meddling extensively with nature, the repercussions are now witnessed as wrath amongst its residents in the form of the acute water crisis. Though Shimla has observed water shortage for several decades, the summer of 2018 became a full-blown water crisis leading to a Cape Town-like situation. Residents protested immensely over the taps running dry for weeks and government bodies were unable to provide any respite.

The current manuscript outlines the reasons leading to this water crisis and the possible solutions for the future to overcome this predicament. Section 2 outlines several water resources and reservoirs in and around Shimla city. In Sect. 3, the crisis is discussed in detail. It is followed by Sect. 4, wherein all the factors leading to this crisis are outlined. Section 5 deals with the future solutions to this problem and conclusions are edged in Sect. 6.

2 Natural Water Resources and Reservoirs

Water for Shimla city is tapped mainly from six natural water resources namely Ashwani Khadd, Dhalli Catchment, Nauti Khadd, Giri Khadd, Chair Nallah, and Churat Nallah. These sources have a capacity of 54.21 MLD (Town and Country Planning Department

2017). The cost of water supply is around Rs. 28 for every 1000 L of water. The population of this biggest city of Himachal Pradesh is around 1.42 lacs and adds to that about 3 lac tourists who visit the city each year.

The water reservoirs are uniformly distributed around the entire Municipal Area of Shimla. 11 primary reservoirs have a storage capacity of around 36.92 MLD. Apart from these primary reservoirs, there are around 28 reservoirs in different localities and societies which have a capacity of 5.8 MLD. Furthermore, 16 more primary reservoirs have been proposed to fulfill the demands of the residents. The details of the reservoirs are as follows (Town and Country Planning Department 2017) (Table 1):

Table 1. Capacity of water reservoirs in Shimla

S. No.	Reservoir	Capacity
1	Seog	10.9 MLD
2	Sanjauli	8.78 MLD
3	Ridge	4.63 MLD
4	Mansfield	3.63 MLD
5	Mashobra	3 MLD
6	Carignano	3 MLD
7	Kasumpti	2 MLD
8	Jakhu	0.32 MLD
9	Boileauganj	0.24 MLD
10	Vice Regal Lodge	0.23 MLD
11	Kasumpti	0.22 MLD

3 Acute Crisis in the Summer of 2018

The daily water requirement of Shimla city is about 44 MLD whereas the intake is limited to only 39.21 MLD by the different water supply sources. This intake was further reduced to around 12.38 MLD during the summer of 2018. Rationing of water was done in different parts of the city and as result, the residents received water for a few hours and that too once a week. In some localities, water was dispensed after a gap of 16 days. This relentless crisis forced the government to shut down schools in the area. There was huge outrage and outcry amongst the residents triggering city-wide protests. The linemen were forced to dispense water under the presence of police protection. Police forces were present at almost every nook and corner of the city to disperse the agitating crowd and avoid confrontations between the locals and government authorities. The demand for mineral water increased multifold as people had to buy it for cooking purposes. Water tankers of the Shimla municipal corporation went to several localities and large ques of people hovering around them were observed. People had to wait for hours just to get a bucket of water. However, this scenario is quite common every year in

Shimla during the summertime. But this year the situation was aggravated on a massive scale and triggered many fights and mishaps during water distribution from tankers due to extreme need and chaos amongst people.

The prestigious International Shimla Summer Festival, which is held every year in May or June was canceled for the year 2018 due to this acute water crisis. Shimla used to host this five-day-long festival continuously from the year 1960 which is considered to be one of the biggest cultural retreats in the state.

The town's main industry, tourism, took a hit when hotels had to cancel reservations and residents widely appealed on social media for visitors to avoid this state capital. The crisis became national news and a topic of widespread debate in the entire country. This Cape Town-like water crisis poses to be very alarming and requires immediate remedial steps to be undertaken or else Shimla will be doomed shortly.

4 Factors Leading to Acute Water Shortage

Shimla is witnessing very long dry spells and inconsistent heavy rainfalls and this in turn is disturbing the lives of residents for irrigation and consumption purposes. Acute and even erratic heavy rainfall causes many problems. Heavy rainfall also leads to water shortage as the rivulets and streams carry heavy slits, making them redundant due to the non-functioning of the pumps. Generally, the month of May is dry in Shimla. Also, in the year 2018, there was very little rain at the start of winter and therefore, the snowfall was also scanty. There was a 91% deficiency of water and snowfall in January. February was around 53% deficient and 70% deficiency was witnessed in March (Bhargava 2018; Chaturvedi 2018; Lohumi 2018; Saihgal 2018; Sreevatsan 2018; Sehgal 2018).

5 Materials and Methods

In order to analyze the reason for the acute water crisis, rainfall precipitation data from 2013 to 2018 has been analyzed. Figure 1 depicts the season-wise rain precipitation data along with the expected normal rainfall data for the past six years. Figure 1(a) shows the data for the winter season from December to February. Similarly, Fig. 1(b) depicts the data for the spring season from March to May. Figure 1(c) shows the data for the summer season (which also includes the monsoon months) from June to August. Finally, Fig. 1(d) portrays the data for the autumn season from September to November.

As per Fig. 1(a), it is observed that the rainfall/snowfall was negligible during the winter months in 2017–2018 leading to an acute water shortage in the summer of 2018. Figure 1(b) points out the fact that during the spring of 2018, the rainfall was very low as compared to normal. In the monsoon months as depicted in Fig. 1(c), the rainfall is erratic and is far above the normal. This heavy erratic rainfall leads to the deposition of silt in the reservoirs which in turn leads to water shortage. Figure 1(d) clearly points out the fact that a sharp decrease in rainfall is observed in the autumn months and precipitation is way lower than normal.

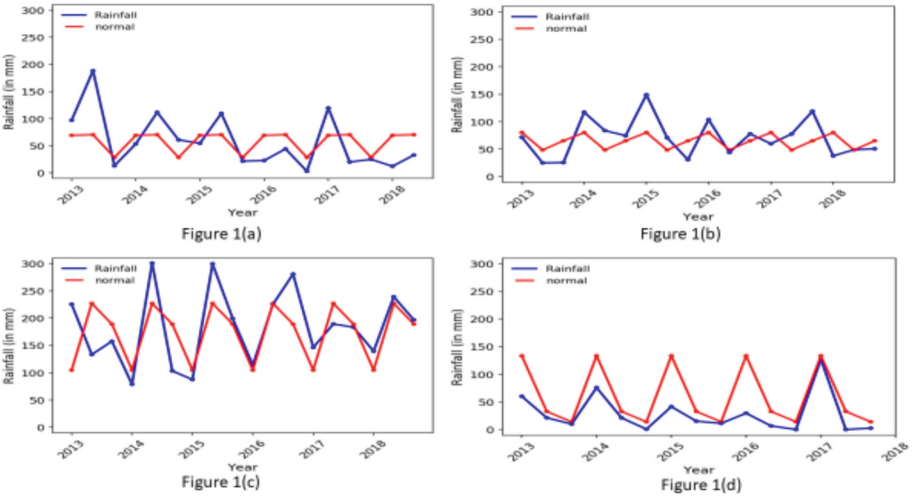


Fig. 1. Monthly rainfall and snowfall data from January 2013 to August 2018. The data for the winter, spring, summer, and fall seasons are shown in Figs. 1(a), 1(b), 1(c), and 1(d), respectively. The data on rain and precipitation is shown by the blue line, while the data on typical rainfall is shown by the red line Meteorological Centre (2019), Monzonís et al. (2015).

6 Future Solutions to Avoid Water Crisis

Taking into account the present crisis, immediate remedial steps should be undertaken to avoid any future disaster (Hothi and Hothi 2022). Both government and residents will need to walk hand in hand to curb this crisis and bring back the old glory and grace of the hill town. The government of Himachal Pradesh had proposed to get a loan from the World Bank to finance the lifting of 104 MLD of water from the Kol Dam in Mandi District which is located on the Sutlej river. Funding has been received from the World Bank for 50 MLD of water. This process needs to speed up on a high scale. Shimla city is located at a height of 7467 feet, which is far high than the nearest major rivers. However, lifting water on such heights is not at all cost-effective. Furthermore, this water mustn't get contaminated with water from the decentralized sewage treatment plants (Corominas et al. 2010).

Out of all the water supply systems, Giri seems to be a very practical solution to solve the water crisis in Shimla. It needs to be planned and reformed with an adequate storage system. The Ashwani Khadd supply system needs to be restored without contamination. It is also necessary to extend the green cover around all the catchment areas. Construction should be completely banned in and around these areas and natural vegetation should be allowed to spread. Cutting of trees for construction purposes, be it roads or buildings should be completely banned in Shimla. Saplings of coniferous trees should be planted at a massive scale to compensate for the losses which Shimla has witnessed due to modernization.

Furthermore, the wastewater from sewage treatment plants can be recycled for non-potable purposes such as gardening, construction, and flushing purposes. This endeavor would require separate reservoirs for storage and the laying down of separate pipelines

for supply. The present crisis is also due to a lack of knowledge amongst the residents as well as government reluctance to find a permanent cure to the situation. Indian Institute of Advanced Studies, which is a prominent historic building of the British era harvested rainwater for more than a century. Thereby, the locals should take up the initiative of rainwater harvesting and even the government should frame a policy for implementation of this process. Government should also provide special subsidies to those people who are opting for rainwater harvesting.

7 Results and Discussion

In May 2018 the Nauti Khadd stream almost dried up. Its water supply system was commissioned by the British in the year 1922. This is one of the key sources of water feeding in Shimla. By the end of May, the water discharge by the stream reduced to around 9.39 MLD which is far below the average of 19.75 MLD (Bhargava 2018; Chaturvedi 2018; Lohumi 2018; Saihgal 2018; Sreevatsan 2018; Sehgal 2018).

The Shimla Municipal Corporation had to adjourn the supply of water from Ashwani Khadd in the year 2016 as it was found to be highly contaminated and led to the outburst of jaundice in the city (Kanwar 2018). It was contaminated by the leakage from a nearby Sewage treatment plant in Malayana (Adimalla and Taloor 2020). The epidemic had spread in 4 different wards under the municipal corporation which was provided water from the Ashwani Khadd supply system. This water contamination nearly two years ago led to an acute water shortage in the city.

The Irrigation and Public Health Department had to shut down Chair and Churat reservoirs because of the poor quality of water which could not be used for drinking. The major water reservoirs not being in use led Shimla to face this acute crisis. The people are also installing a lot of tube wells in and around the catchment area. This process of mechanization is leading to an increase in the consumption of water and thereby is causing a decrease in the level of ground water. Additionally, with development of pukka roads and streets in the villages is leading to the disposal of debris down the hills, thus heading to the blockage of the natural course of the streams and rivulets. In the past few years, the green cover surrounding most of the water supply resources has reduced. Not only trees but also grass and shrubs have decreased in the catchment areas. Moreover, these catchment areas are in the rural segments wherein the villagers are adopting new farming techniques wherein water is being tapped tremendously leading to a decrease in supplies for the Shimla city. Previously during the dry spells, streams, and rivulets used to still have water as the adjacent trees, shrubs and grass absorbed rain water and used to steadily release it during the dry spells.

The four-lining work of the Shimla–Chandigarh highway is also one of the factors responsible for the deepening of this water crisis in Shimla as it is at the cost of axing around 34,000 green trees. The National Highway Authority of India (NHAI) has already axed over 12,000 green trees and the process is still undergoing. Around 66 hectares of forest land are being destructed under this project which is severely damaging the natural eco-system of Himachal Pradesh leading to widespread climate change. This is increasing the impact of global warming leading to rain deficit months and excess rainfall in very short spans.

8 Conclusions and Future Scope

Water has become the most treasurable resource for mankind and should be intelligently harvested for ourselves and future generations. Scarcity of water makes life difficult, and this was explicitly evident in the acute water crisis faced by Shimla in the summer of 2018. Tourists were urged not to visit this popular hill station during that time. Consequently, it affected the economy of the state which greatly relies upon tourism. Schools were shut down and protests and agitations were done by the residents throughout the city and this situation become nationwide news.

Thus, it can be concluded that disturbing nature will eventually have punitive repercussions which ultimately leads to distress amongst mankind. The six-year rainfall precipitation data points towards rain deficiency in Shimla city and there persists sudden abrupt increase in rainfall in some months. A drastic decrease in rainfall is observed in the summer of 2017 and also during the winter months of 2017–2018. This was a primary cause of the acute water crisis. Nature must be respected by humans in order for nature to return the favor. In the summer of 2018, Shimla experienced a severe water crisis that was preventable and caused by human action. The city's native aquatic ecology must be revived. The community and the government should work together to implement water harvesting systems and enhance the amount of greenery. Systems for supplying water need to be changed, and wastewater shouldn't pollute the water that comes from them. Shimla is turning into a concrete jungle, and in order to prevent the situation from getting worse, building should either be completely prohibited or severely restricted. The city's unplanned expansion needs to be entirely restrained, and water catchment regions need to be fully safeguarded and kept so that the native flora and fauna can thrive there.

References

Adimalla, N., Taloor, A.K.: Introductory editorial for 'Applied Water Science' special issue: "Groundwater contamination and risk assessment with an application of GIS." Appl Water Sci **10**, 216 (2020). https://doi.org/10.1007/s13201-020-01291-3

Bhargava, K.: Shimla crisis offers a terrifying glimpse of what most of our cities could be facing in future. The Economic Times (2018). https://economictimes.indiatimes.com/news/politics-and-nation/shimla-crisis-offers-a-terrifying-glimpse-of-what-most-of-our-cities-could-be-facing-in-future/articleshow/64733470.cms. Accessed 15 October 2023

Bhasin, R.: Simla: The Summer Capital of British India. Rupa Publications Private Limited, India (1994)

Chaturvedi, A.: Shimla out of water, may run out of tourists, too, this summer. The Economic Times (2018). https://economictimes.indiatimes.com/industry/services/travel/shimla-out-of-water-may-run-out-of-tourists-too-this-summer/articleshow/64486968.cms. Accessed 15 October 2023

Corominas, L., et al.: New framework for standardized notation in wastewater treatment modelling. Water Sci. Technol. **61**(4), 841–857 (2010)

Gilmour, D.: The British in India: Three Centuries of Ambition and Experience. Penguin Publishers, United Kingdom (2018)

Hothi, N., Hothi, G.: Water crisis of Shimla Town: past and present scenario. Mater. Today Proc. **64**, 1250–1254 (2022). https://doi.org/10.1016/j.matpr.2022.03.715

Kanwar, Y.: Shimla Corporation suspends water supply from Ashwani Khad. The Hindu (2018). https://www.thehindu.com/news/cities/Delhi/Shimla-Corporation-suspends-water-supply-from-Ashwani-Khad/article14023649.ece. Accessed 15 October 2023

Lohumi, B.P.: Shimla Summer Festival postponed indefinitely due to water scarcity. The Tribune (2018). https://www.tribuneindia.com/news/himachal/shimla-summer-festival-postponed-indefinitely-due-to-water-scarcity/596833.html. Accessed 15 October 2023

Meteorological Centre.: Shimla (2019). http://weathershimla.nic.in/. Accessed 15 October 2023

Monzonís, M.P., et al.: A review of water scarcity and drought indexes in water resources planning and management. J. Hydrol. **527**, 482–493 (2015). https://doi.org/10.1016/j.jhydrol.2015.05.003

Saihgal, T.: 3 reasons why Shimla is facing an acute water crisis, and how locals are reacting. India Today (2018). https://www.indiatoday.in/education-today/gk-current-affairs/story/3-reasons-shimla-water-crisis-locals-reaction-1246720-2018-05-31. Accessed 15 October 2020

Sreevatsan, A.: What other cities can learn from the Shimla water crisis. Livemint (2018). https://www.livemint.com/Politics/PULfnEfotEtFp4PCyMqvbI/What-other-cities-can-learn-from-the-Shimla-water-crisis.html. Accessed 15 October 2023

Sehgal, R.: Shimla water crisis: Residents brace themselves for a dry spell and tepid tourism season. Firstpost (2018). https://www.firstpost.com/india/shimla-water-crisis-residents-brace-themselves-for-a-dry-spell-and-tepid-tourism-season-4497639.html. Accessed 15 October 2023

Town and Country Planning Department.: Draft Development Plan for Shimla Planning Area (2017). http://tcp.hp.gov.in/Application/uploadDocuments/news/News20170811_125200.pdf. Accessed 15 October 2023

Reviving Tradition: Exploring the Craft of "Chindi Dari" of Uttarakhand for Sustainable Textile Upcycling and Wearable Innovations

Priyanka Sharma[1(✉)] and Nilakshi Yein[2]

[1] Chitkara Design School, Chitkara University, Rajpura, Punjab, India
priyankasharma142000@gmail.com
[2] IIT Delhi, New Delhi, India

Abstract. Textile crafts, such as quilting, patchwork, and kantha, play a crucial role in repurposing textile waste. These techniques actively prevent the disposal of fabrics, garments, and other textile waste into landfills, contributing to the creation of new products and significantly extending the lifespan of garments. In the village of "Timli" in Uttarakhand, the artistry of crafting "Chindi Dari," or recycled fabric rugs, is practiced, deeply rooted in the native language. Discarded materials like old t-shirts, denim, saris, bedsheets, and fabric undergo meticulous cutting into 1.5-inch strips. These strips are expertly interwoven to create eco-friendly and resilient rugs. This study delves into the production of fabric using the process of "Chindi Dari" weaving, and access its wearability and broader implications. Secondary data was gathered using keywords recycled rugs, fabric rugs, circular fashion, textile recycling, and upcycling textiles. A prototype textile was meticulously crafted on a loom, and garments were constructed for trial purposes. The user experience was further scrutinized, providing valuable insights into the wearability and aesthetic appeal of the recycled fabric. The Friedman's two-way ANOVA was applied followed by Wilcoxon Signed Rank test and a Bonferroni adjusted α of 0.017 indicated that comfort (Mean Rank = 1.77) was perceived as significantly more than durability (Mean Rank = 2.31), T = 27, $z = -2.995$ (corrected for ties), N-Ties = 32, $p = 0.003$. ($r(30) = 0.79$, $p < 0.001$) between these two factors (comfort and durability) was positive and high. Comfort is the prime factor that effects the wearability of this material produced. The study found that "Chindi Dari" is well-liked in the area and can aid in the locals' ability to increase their source of income. It is possible to make loose-fitting clothing out of the sample material. According to the study, repurposed rug materials are creative, long-lasting, and environmentally beneficial. There are new opportunities when clothing waste is repurposed to generate fabric.

Keywords: Circular fashion · Fabric rugs · Recycled rugs · Textile recycling · Upcycling textiles

© The Author(s), under exclusive license to Springer Nature Singapore Pte Ltd. 2026
M. Kumar et al. (Eds.): HSFEA 2023, LNCE 899, pp. 168–174, 2026.
https://doi.org/10.1007/978-981-92-3200-0_15

1 Introduction

In the age of mass manufacturing and rapid fashion, there is a growing movement to revive ancient crafts for their cultural relevance as well as their potential to address sustainability concerns. "Our Common Future," report published in 1987 gave the commonly used definition of sustainable development as "development that meets the needs of the present without compromising the ability of future generations to meet their own needs" (Commission on Environment, n.d., page 43). Sustainability in fashion refers to an integrated strategy that aims to reduce damage to the environment and its people when a garment is produced, from the procurement of raw materials to the final disposal of the item. Since textile industry is a major producer of waste that uses the natural resources at almost every stage of production (Juanga-Labayen et al. 2022) textile crafts provide a unique and environmentally friendly way to recycle waste textiles, transforming them into new, functional, and frequently exquisite products. Recycling is a practice which is implied many times in the Indian society of craftmanship. The Indian traditional textile industry is rich in practices that imply the recycle and reuse philosophy. These sustainable practices create a sustainable craft and a skill for the artisans which is an advantage for the environment and the craft community.

Most of the textile waste generated is post-consumer waste which is enters the landfill (Jain and Gupta 2016) is burned which leads to release of harmful chemicals in the atmosphere. The product's life has reduced leading the consumer to buy garments more frequently (Dhir 2021; McNeill et al. 2020). The major advantage of using second hand clothing is the use of water and fossil fuel is reduced. Secondly, the chemical usage in dyeing and finishing processes is reduced. Thirdly, the process of garments ending to landfill and getting burnt is also reduced (Lewis et al. 2017). Compared to simple burning, recycling is a more socially and environmentally responsible choice (Leal Filho et al. 2019). Therefore, repurposing them into a new and useful product is preferred.

The traditional Indian textiles have many craft which repurpose the old textile and convert them into a new one. The Nakshi kantha utilizes three to four layers of old sari are embroidered with silk and cotton threads with simple stitches (Mandal n.d.). The Namda and Gabba carpets of Kashmir are a form of rugs where used woollen felt is repurposed and embroidered in beautiful patterns to form the floor covering (Akhter 2017; Singh and Rani 2021). Applique and patchwork create various patterns from various fabrics where repurposed fabrics are used to create household items and various interior items (Dholakia, n.d.). Similarly, the rugs of Haryana "Panja Durrie" utilize the used fabric strips to form the rugs which are woven on a vertical loom (Singh and Rani 2021).

Uttarakhand also produces rugs from fabric strips known as "Chindi Dari" which are woven on pit loom (Tolia 2018). The warps yarns are installed in the loom while fabric strips work as weft yarn forming a beautiful pattern. From the field study we came across the fact that the number of weavers performing the craft of weaving has reduced drastically. Therefore, work needs to be done for the upliftment of the craft and craftsmen of Uttarakhand. To full fill this aim following objectives were defined. First was to study and document the process of weaving and the second objective was to develop it into a wearable material that can be worn as a fashion garment. A pilot study was done for the

garments produced and the feedback was recorded in the questionnaire. Based on this an analysis results are shared in the results section.

2 Materials and Methods

Literature review: the literature focusing on sustainable rug making process was searched thoroughly on science direct, google scholar and Clarivate using the keywords recycles fabric dari, circular fashion, chindi dari, and textile rugs to develop a theoretical foundation of the research.

Empirical research: the collection and analysis of the primary data was done through interview, and focused group survey with the weavers to understand the problems, challenges, and basic understanding of the craft of chindi Dari weaving process.

Design process analysis: during the investigation it was found that the strips were cut very roughly and wide. There was no measurement done. The major focus was to achieve the longest strip possible from the waste, therefore an inch wide strips were obtained through slash and tear method. The colour scheme depends on the raw material received therefore the weaver generally followed bright complementary and monochromatic colour scheme.

Prototyping and evaluation: to understand the wearability of the fabric produced the garments were made in the three basic styles to understand the drapeability, comfort, texture, uniqueness, and durability of the garments produced. For user testing the garments were given to them for a minimum period of two hours and later a feedback form was filled by them. The volunteers were selected based on the age group 18 year to 35 years (female) of age as in the fashion industry, this range is a huge market area that has a big impact on customer demand (Myers 2014) they are also great influencers and early adopters of fashion. The feedback was further analyzed to assess the wearability of the garments.

3 Result and Discussion

In this study the feedback of the wearability of the garments was evaluated based on comfort, durability, and uniqueness.

A Friedman two-way ANOVA indicated that rankings of comfort varied significantly across the three factors, $\xi_F^F = 8.904$ (corrected for ties), $df = 2$, N − Ties = 32, $p = 0.012$. Follow-up pairwise comparisons with the Wilcoxon Signed Rank test and a Bonferroni adjusted α of 0.017 indicated that comfort (Mean Rank = 1.77) was perceived as significantly more than durability (Mean Rank = 2.31), T = 27, $z = -2.995$ (corrected for ties), N − Ties = 32, $p = 0.003$. This effect can be described as "large", $r = 0.53$.

The difference between the ranked comfort and uniqueness (Mean Rank = 1.92) approached significance ($p = 0.040$, $r = .36$), whereas the difference between the comfort and Durability was clearly not significant ($p = 0.526$) and trivial ($r = 0.011$) (Petter et al. 2014) (Tables 1, 2 and 3).

Our analysis shows that comfort is the top priority among the three factors—comfort, durability, and uniqueness—due to its lower mean rank. This suggests that respondents prioritized comfort when evaluating garments. Furthermore, the relatively higher mean

Table 1. Mean rank of wearability factors

Ranks	Mean rank
COMFORT	1.77
DURABILITY	2.31
UNIQUENESS	1.92

Table 2. Friedman test result of factors

Test statistics[a]	
N	32
Chi-Square	8.904
df	2
Asymp. Sig	0.012

[a]Friedman test

Table 3. Wilcoxon test result of wearability factors

Test statistics[a]			
	DURABILITY–COMFORT	UNIQUENESS–COMFORT	UNIQUENESS–DURABILITY
Z	− 2.995[b]	− 0.635[b]	− 2.054[c]
Asymp. Sig. (2-tailed)	0.003	0.526	0.040

[a]Wilcoxon Signed Ranks Test
[b]Based on negative ranks
[c]Based on positive ranks

rank of uniqueness compared to durability but lower than comfort suggests that uniqueness is positioned between comfort and durability in terms of perceived importance or ranking. Durability, on the other hand, has the highest mean rank and is ranked last among the factors, implying that respondents thought it was less important than comfort or uniqueness. The statistical tests conclude that it is crucial to take comfort, toughness, and originality into account when designing garments and making it wearable. Clothing that are functional need to connect with the user and makes a bold statement in finding a balance between these factors and align with the wearer's preferences. Overall, the garments produced where sustainable, aesthetically appealing, durable and one of a kind in the market.

Affinity mapping was done for the subjective questions where the data was divided into the following categories (Table 4):

Table 4. Affinity mapping of subjective feedback

Style	COMFORT		TEXTURE	AESTHETICS	UNIQUESNESS
	PRO's	CON's			
Vibrant colours	Good and comfortable	Uncomfortable and fashionable product	Thick	Good aesthetics	Unique pattern
Good product	Comfortable and fashionable product	Uncomfortable for long hours	Little rough		Unique design
Loved the design	Very comfortable	Feel can improve			
Pockets are a great add-on					
Gives a fashionable look					

This suggests that the clothing is made with vivid colours and distinctive patterns, which add to its stylish appearance. Although one review claims that wearing the product for extended periods of time is uncomfortable, overall, it is comfortable to wear. This could mean that while it is generally comfy, prolonged use could make it uncomfortable. The clothing falls sturdy because of the texture, which is a little thick and rough, making it appropriate for formal wear in the frigid temperatures.

Numerous studies have examined the advantages of recycling textiles, emphasizing the sustainable and environmental aspects of the practice. Juanga-Labayen et al. (2022) emphasizes the need to improve the technologies and collecting systems, while Huang et al. (2024) emphasizes that how closed loop and open loop recycling systems can be implied to get better recycled products. Rani and Jamal (2018) suggest that textile recycling is beneficial for environment and economic conditions. These studies suggest that recycled fabric can be a sustainable and environmentally friendly option.

The use of Chindi Darri, which was previously a popular material in traditional floor coverings, has declined due to the rise of alternative materials in the flooring business. To restore interest in Chindi Darri, this paper investigates its possible use in trendy clothing and evaluates its viability in this new arena. We wanted to establish the viability of this fashion product by doing a thorough analysis. Our analysis sheds light on its practicality, visual appeal, and overall acceptability in contemporary fashion. Notably, the fabric's great thickness makes it more suitable for colder winter weather conditions fulfilling the functional requirement of the region. To increase comfort levels of the fabric, we recommend using cotton fabric strips as the primary raw material, which improves tactile comfort and makes it more suitable for hot summer conditions. The

garments aesthetics were noteworthy which indicates it has the potential to create its own market. During the study we noticed sourcing raw material was a tedious task and further the process of garment construction involved a lot of precision therefore future study could focus on arranging and segregation of the raw material and developing ways in which it is scalability into garment manufacturing for mass production in the industrial sector can be done. Furthermore, more experimentation with different weaving methods could improve the versatility and quality of these materials, contributing to their wider acceptability and incorporation into the fashion industry.

4 Conclusion

In conclusion, our analysis demonstrates the critical importance of comfort in garment evaluation, as evidenced by its lower mean rank compared to durability and uniqueness. This demonstrates how respondents prioritize wearability when evaluating garments. Furthermore, uniqueness's relatively higher mean rank, which falls between comfort and durability, suggests that it plays an important role in consumer preferences. Durability, despite its importance, ranks last among the factors, indicating that respondents rated it as less important than comfort and uniqueness. These findings highlight the importance of considering comfort, durability, and uniqueness when designing garments. It emphasizes the importance of designing clothing that not only meets functional needs, but also reflects the wearer's preferences and makes a statement.

The feedback provides valuable information about the garment's strengths and areas for improvement. The fabric is praised for its suitability for winter wear, as well as its substantial weight and thickness, which indicate warmth and durability. Also, the garment's style aesthetic receives positive feedback, with its vibrant colours and unique designs drawing praise, particularly for their compatibility with traditional Indian clothing. However, there are some serious concerns about the fabric's texture, which some users find uncomfortable and rough, particularly those with sensitive skin. Addressing this issue could increase the garment's appeal and provide greater comfort for a broader range of wearers. Suggestions for improvement, such as experimenting with softer materials or fine-tuning the fabric's texture over time, provide valuable opportunities for improving the overall user experience.

Despite these challenges, the garment's positive qualities, such as its elegant design and adaptability for colder climes, come through, signalling its potential for continued success with the right modifications.

References

Akhter, M.: The importance of Kashmiri Art and craft. Int. J. Acad. Res. Dev. **2** (2017). www.academicsjournal.com

Petter, A., Kellie, B., Brody, H.: SPSS Statistics Version 22 A Practical Guide, Vol. 22 (2014)

Imperatives, S.: Report of the World Commission on Environment and Development: Our common future. Accessed Feb, vol. 10, no. 42,427, pp. 1–223 (1987)

Dhir, Y.J.: Hazards of fashion and textile waste: approaches for effective waste management. In: Waste Management in the Fashion and Textile Industries, pp. 31–58. Elsevier (2021). https://doi.org/10.1016/B978-0-12-818758-6.00002-8

Dholakia, K.: Appliqué & Patchwork: Traditional Craft of Ornamenting Fabric on Fabric (n.d.). www.Fibre2fashion.com

Huang, X., Tan, Y., Huang, J., Zhu, G., Yin, R., Tao, X., Tian, X.: Industrialization of open- and closed-loop waste textile recycling towards sustainability: a review. J. Clean. Prod. **436** (2024). https://doi.org/10.1016/J.Jclepro.2024.140676

Jain, P., Gupta, C.: Textile Recycling Practices in India: A Review (2016). www.Tjprc.org

Juanga-Labayen, J.P., Labayen, I.V., Yuan, Q.: A review on textile recycling practices and challenges. Textiles **2**(1), 174–188 (2022). https://doi.org/10.3390/Textiles2010010

Leal Filho, W., Ellams, D., Han, S., Tyler, D., Boiten, V.J., Paco, A., Moora, H., Balogun, A.L.: A review of the socio-economic advantages of textile recycling. J. Clean. Prod. **218**, 10–20 (2019). https://doi.org/10.1016/J.Jclepro.2019.01.210

Lewis, T.L., Park, H., Netravali, A.N., Trejo, H.X.: Closing the loop: a scalable zero-waste model for apparel reuse and recycling. Int. J. Fashion Des. Technol. Educ. **10**(3), 353–362 (2017). https://doi.org/10.1080/17543266.2016.1263364

Mandal, R.: Ornamental surface of Nakshi Kantha. Int. Refereed Res. J. **4**(7) (n.d.)

Mcneill, L.S., Hamlin, R.P., Mcqueen, R.H., Degenstein, L., Wakes, S., Garrett, T.C., Dunn, L.: Waste not want not: behavioural intentions toward garment life extension practices, the role of damage, brand and cost on textile disposal. J. Clean. Prod. **260** (2020). https://doi.org/10.1016/J.Jclepro.2020.121026

Myers, G.J.: Designing and selling recycled fashion: acceptance of upcycled second hand clothes by female consumers, age 25 to 65 (2014)

Tolia, P.: The crafts of Uttarakhand, Vol. 1, pp. 300–303 (2018)

Rani, S., Jamal, Z.: Recycling of textiles waste for environmental protection. Int. J. Home Sci. **4**(1) (2018). www.homesciencejournal.com

Singh, S., Rani, J.: Traditional Indian textile techniques used to upcycle and recycle textile waste. Text. Leather Rev., 2623–6281 (2021). www.Tlr-Journal.com. https://doi.org/10.31881/Tlr

Industrial Waste Utilization in Concrete: Towards Sustainable Green Materials for Achieving Net Zero Emissions and Improving Indoor Air Quality

J. S. Sudarsan[1(✉)], Swati Sinha[1], R. Padmapriya[2], and N. Sunmathi[2]

[1] School of Energy and Environment, National Institute of Construction Management and Research (NICMAR), University, Balewadi, Pune, India
ssudarsan@nicmar.ac.in

[2] Department of Civil Engineering, Sathyabama Institute of Science and Technology, Jeppiar Nagar, Chennai, Tamil Nadu, India

Abstract. Concrete stands as the foremost building material globally, prized for its unparalleled strength, durability, and versatility. With India witnessing a surge in monumental construction projects due to globalization, the demand for natural resources escalates, elevating building costs. Concurrently, the burgeoning industries underscore the urgency of managing and disposing of industrial waste to curb environmental pollution and safeguard human health. The imperative to utilize industrial waste emerges as a linchpin for sustainable resource management and mitigating environmental impact. This study highlights the potential of industrial waste as viable substitutes for traditional concrete components like cement and aggregates. Notably, the incorporation of copper industry slags offers dual benefits, bolstering environmental sustainability and operational efficiency across diverse sectors. Additionally, integrating tannery waste used in concrete as a fine aggregate not only cuts down on concrete density but also presents a feasible solution for seismic-prone regions. In the contemporary era, the proliferation of electrical and electronic devices permeates daily life, introducing unparalleled convenience and functionality. However, the swift obsolescence of such devices due to technological advancements fuels a rapid rise in electronic waste, posing significant waste management challenges globally. Recognizing this escalating global waste generation, this research embarks on an innovative waste management initiative. By harnessing various types of waste as alternatives to traditional concrete constituents, such as cement, fine aggregate, and coarse aggregate, this study pioneers a pathway towards sustainable construction practices. Embracing the ethos of the Reduce, Reuse, Recycle (3R) principle, this initiative not only promises enhanced sustainability but also heralds a paradigm shift towards effective waste management strategies. The integration of industrial waste in concrete has profound implications for indoor air quality within buildings. By minimizing the use of traditional materials that emit volatile organic compounds (VOCs), this approach contributes to a healthier indoor environment. The study delves into the mechanisms by which industrial waste additives enhance air quality, reducing harmful emissions and creating spaces conducive to well-being. This research

© The Author(s), under exclusive license to Springer Nature Singapore Pte Ltd. 2026
M. Kumar et al. (Eds.): HSFEA 2023, LNCE 899, pp. 175–190, 2026.
https://doi.org/10.1007/978-981-92-3200-0_16

endeavors to bridge the gap between industrial waste management and sustainable construction, fostering the development of eco-friendly, high-performance concrete materials. Ultimately, this modest initiative signifies a significant leap towards a greener, more sustainable future, where buildings not only stand as symbols of progress but also serve as sanctuaries of clean, healthy air.

Keywords: Industrial waste · Copper slag · Tannery waste · Electronic waste · Volatile organic compounds · 3R principle

1 Introduction

Cement, fine aggregate, coarse aggregate, and water are all materials of the blended substance known as concrete. With the growing population and urbanization, waste management has become a significant problem, particularly in urban areas. To resolve such problems, researchers and industry professionals have investigated ecologically friendly substitutes for concrete production. Copper slag is a substance produced as an industrial by-product as a result of the manufacturing of copper. The world's copper industry is estimated to produce 24.6 million tonnes of slag. Oman produces roughly 60,000 tonnes of copper slag every year in the Sultanate of Oman. Despite the fact that the higher amount of the copper slag produced is employed to make abrasives rather than being recycled or reused. Copper slag is ideal for practice in concrete as a fractional or full spare for aggregates due to a number of physical and chemical characteristics (Al-Jabri et al. 2011). It is currently inconceivable to imagine any construction activity taking place without using concrete. Copper slag, when used as a partial replacement for fine aggregates in concrete, can lead to a reduction in the use of traditional materials that emit volatile organic compounds (VOCs) (Ahmad et al. 2022). Copper slag, being a dense and hard material, can contribute to reducing the generation of dust from concrete surfaces. Dust particles in indoor environments can contribute to respiratory issues and overall discomfort (Suthar et al. 2018; Wu et al. 2010). With fifth place and largest across process add India, the tanning industry is growing as an economic contributor for developing nations. It is necessary to efficiently employ the wastes produced since animal skin products require a large amount of production (Sunmathi et al. 2022a, b). The concrete industry uses e-waste, one of the modern waste products to deal with the salvaging and clearance. Previously, in developed countries. The term "electronic e-waste" refers to apparatus that has been carelessly abandoned, is unnecessary, is out of date, or is damaged. Due to quick technical development and low entry costs, there is an increasing surplus of electronic waste worldwide. E-waste must be disposed of in large quantities each year. Traditional disposal techniques, such as piling waste in landfills, are not ecologically friendly, and adhering to EPA regulations during the disposal process is extremely difficult. Utilizing non-disposable electronic waste taps into an important research field. The inventory of electronic waste is anticipated to reach 146,180 tonnes in 2005, based on this rate of depreciation and India's installed base. This is predicted to get close to 8000 tonnes by 2013. In India, major cities like Delhi, Mumbai, Bangalore, and Chennai are where most e-waste is created. Utilizing waste materials in concrete is a significant step towards achieving sustainable development

goals (Sudarsan et al. 2022). The amount of industrial waste included into concrete has a significant impact on the indoor air quality of buildings (Eštoková et al. 2022). The selection and quantity of industrial waste in concrete formulations is a critical factor in determining the indoor air quality, especially as building methods shift more and more toward environmentally friendly and sustainable materials. Construction materials emitting volatile organic compounds (VOCs) is one of the major elements influencing indoor air quality. When conventional components like cement and aggregates are replaced by industrial waste products, the concrete's emission profile may change. The amount of VOCs emitted into the interior environment is directly impacted by the quantity of industrial waste. This approach helps address environmental challenges, reduces waste, conserves natural resources, and promotes circular economy principles (Phiri et al. 2022; Wrzesińska-Jędrusiak et al. 2023). Waste products can help us reach a number of Sustainable development goals, including Goals 9 and 11 are related to business, creativity, and infrastructure, respectively (*THE 17 GOALS|Sustainable Development*, n.d.). Sustainable consumption and production are goals 12 and 13, respectively. Life on land is goal 15 and collaborations for the goals are goal 17. We can also help create a constructed environment that is more flexible and environmentally friendly.

The exploration of the characteristics of copper slag (CS) has revealed profound insights into how this material influences the qualities of cement, concrete, and mortar. Copper slag, as a by-product of the copper smelting process, possesses unique properties that can significantly enhance the performance and sustainability of construction materials. Shi et al. (2008) from an environmental standpoint, the utilization of CS in concrete offers significant benefits. By diverting CS from landfills, where it would otherwise pose environmental challenges, its incorporation into concrete reduces waste generation and promotes a circular economy approach. This not only aligns with sustainable development goals but also reduces the demand for natural resources, such as sand and gravel, which are often overexploited.

Al-Jabri and Hisada (2009) examined how the use of CS affected HSC. The replacement of copper slag was accomplished in six different quantities. Water usage is reduced by 22% and compression is increased by 20% when FA is completely replaced by CS. It has been discovered that the concrete mix containing copper slag performs better in terms of workability and strength only when combined with the necessary superplasticizer because the strength decreases in the absence of a superplasticizer.

Kanagalakshmi et al. (2015) conducted an experiment using rice husk and copper dust instead concrete made of cement. Depending on the amounts of ingredients, the percentages of RHA and CD were replaced by several percentages. They draw the conclusion that concrete will 40% CD and 20% RHA has demonstrated high comp. strength. RHA replacement up to 20% would not negatively impact influence the mechanical and strength characteristics. RHA and copper dust addition to concrete mix enhanced concrete's mechanical characteristics in relation to compressive strength, which is almost up to 25%. Split tensile with an increase in replacement, strength has increased. Copper dust levels of up to 40% when using fine aggregate.

Manjunatha et al. (2021)**,** conducted experiments to determine the structural features of concrete made up to sixty % Waste Copper Slag by the mass of sand rise the marginal

strength of concrete. The cost of making concrete and the utilization of earth's resources are reduced when WCS is used as an alternate for river sand.

Reddy and Reddy (2020), concluded that copper slag is non-hazardous and is a coarse-grained material with excellent frictional properties. They also discovered that the copper slag's suitability for use in conventional and reinforced earth (soil) retaining walls is assessed based on laboratory studies.

Vasudevan and Raj (2016) examined the effects of replacing the sand in the concrete with textile and tannery sludge This research uses leftovers from the textile and tannery industries, some of which include harmful heavy metals. With M15 grade concrete, an experimental investigation was conducted. The best results were 15% and 20% for replacing textile waste alone, respectively, as well as tannery and textile sludge.

Chen et al. (2023), The residue of fly ash and tanning sludge were utilised as substitutes for cement, while construction debris was used to make regenerated coarse aggregate. Alkali activator was added to the concrete to boost its mechanical properties. Additionally, the numerous characteristics beneath various alkali parallels were thoroughly and deliberately evaluated, and a mechanism for how the evolving microstructure of AA-SFRC affects the material's macroscopic strength was discovered.

Ramesh et al. (2017), conducted experiments thorough laboratory testing, the best mixture of sludge and soil specimens was discovered. According to the study, using 20 and 30% of tannery sludge in the soil gives the soil higher strength and aids in the efficient and environmentally friendly use of tannery sludge. The combination can be used to fill the space across the sub base course in road pavements and the base in supporting loads constructions.

TamilThendral et al. (2019), conducted tests and found that the compressive strength improves when coarse aggregate is replaced with tannery waste up to an additional amount of 10% and decreases with increasing quantities of waste.

Karthikeyan et al. (2014)**,** delved into the effects of substituting tannery sludge for fine aggregate in concrete mixes, uncovering intriguing insights into the mechanical properties of the resulting concrete. Their research revealed that the typical strength of tensile and flexural properties exhibited improvement with the incorporation of tannery sludge as a partial replacement for fine aggregate. This enhancement can be attributed to various factors, including the pozzolanic nature of tannery sludge, which contributes to additional cementitious properties in the concrete matrix. The improved tensile and flexural strengths are particularly advantageous for structures subjected to bending or tensile forces, offering enhanced structural integrity and resistance to cracking. However, as the percentage of tannery sludge in the concrete mix surpassed 15%, a notable decline in compressive strength was observed. This finding underscores the delicate balance required in the utilization of industrial waste materials in concrete formulations. While tannery sludge can confer beneficial properties to the concrete, such as improved workability and reduced water demand, an excessive amount can negatively impact the overall compressive strength of the material. There are a number of reasons why compressive strength decreases as tannery sludge content increases. First off, the tannery sludge's uneven particle size and shape might cause less effective packing inside the concrete matrix, which would lower the material's overall density and strength. Also,

the concrete's compressive strength may be further compromised by the introduction of air spaces or weak zones caused by the organic matter found in tannery waste.

Krishna Prasanna and Kanta Rao (2014), conducted an investigational study employing coarse aggregates made from e-waste with an alternative ratio ranging from 0 to 20%. Similar to this, examples of M30-grade concrete that conform to standards. Both specimens were put to the test in order to learn more about concrete's hardened properties. In the conventional mix, the weight-based e-waste fillings were considered as coarse aggregate. Compressive strength tests were performed on concrete at 7, 14, and 28 days old in order to assess the strength evolution of concrete comprising varied levels of E-waste.

Amiya Akram et al. (2015)**,** examined torn e-plastic and fly ash combined to form two batches, one with only e-plastic and the other with e-plastic and fly ash, to replace some of the coarse aggregates. In one batch, e-plastic is substituted for coarse aggregate in amounts of 5, 10, and 15%. They examine the concrete's flexure and compressive strengths. They discovered that adding E-plastic to concrete made it more ductile, as the specimen failed the flexure strength test without making a sound because it became less brittle, and that compressive strength increases at 10% but declines beyond that.

Balasubramanian et al. (2016) conducted a study on the employment of E-waste in concrete. The annual production of electronic waste accounts for approximately 3–5% of the total amount of waste generated. Utilizing waste in concrete reduces disposal issues and decreases the cost of concrete. He concluded that partial substitution for coarse aggregate is preferable to complete substitution for coarse aggregate in order to achieve concrete-like properties.

Ahirwar et al. (2016) included biodegradable elements from electronic trash into concrete to partially replace fine or coarse particles in industrial building. It has been discovered that using electronic trash as aggregates produces lightweight concrete. In this study, cement was partially replaced by 10, 20, and 30% fly ash, while coarse aggregate was partly supplemented by E-waste from 0 to 30%. It was suggested that using this electronic trash in place of traditional aggregates in concrete would conserve natural resources.

Angure and Maru (2017)**,** explored the viability of by means of fly ash as a substitute of cement and presently produced enormous amounts of trash from electronics as a partial replacement for aggregate (coarse) in the formulation of concrete. M25grade mixture was used for the work. Various cube samplings were cast using e waste and fly ash that extended from 0 to 30% by weight of cement, replacing 5% of the coarse aggregate. After 7, 14, and 28 days of curing, the specimens were examined for compressive strength. The findings were noted and the strength of the reference mix was compared. The study came to the conclusion that while fine aggregate cannot be replaced with e-waste, coarse aggregate may.

2 Materials and Methods

2.1 Cement

Cement plays a pivotal role in modern construction, contributory to the making set-up and houses that form the backbone of societies around the world. The grade used is 43 grade types of cement that comply with IS 269-2015. According to IS 4031 1988 and IS 4032-1985, a physical properties test was conducted and tabulated in Table 1.

Table1. Physical properties of cement

S. No.	Description of test	Results
1	Reliability	30
2	Early setting time	35 min
3	Ultimate setting time	9 h
4	Sp. Gr	3.12
5	Compressive strength (N/mm^2)	45.31
6	Fineness	2.88

2.2 Fine Aggregate

Fine aggregate is a building material that is typically collected of sand, crushed stone or gravel particles smaller than 4.75 mm. It is an important factor of concrete and mortar, serving as a filler material that binds with cement to create a solid and cohesive mixture. Fine aggregate plays a crucial role in provided that workability, strength, and durability to the concrete. It also helps to reduce the amount of cement needed which can lead to cost savings and environmental benefits. Table 2 presents the physical properties of fine aggregate.

Table 2. Physical properties of fine aggregate

S. No.	Description of test	Results
1	Sp. gr	2.60
2	Absorption of water (%)	1.25

2.3 Coarse Aggregate

Coarse aggregate is a construction material that consists of larger particles, greater than 4.75 mm. It is an important module of concrete and is used in conjunction with fine aggregate, cement, and water to create a strong and durable construction material. Coarse aggregate is responsible for providing bulk and strength to concrete. It forms

the structural skeleton of the concrete mixture, contributing to its load–bearing capacity and overall performance. The grouping of coarse and fine aggregates with cement and water creates a composite material that is capable of withstanding various loads and environmental conditions. The physical properties of coarse aggregate are shown in Table 3.

Table 3. Physical properties of coarse aggregate

S. No.	Description of test	Results	
		12.5 mm	20 mm
1	Sp. gr	2.81	2.750
2	Absorption of water (%)	0.49	0.67
3	Flakiness (%)	3.15	5.76
4	Elongation (%)	6.23	8.02
5	Crushing value (%)	15.97	15.97
6	Impact value (%)	15.41	15.41
7	Abrasion value (%)	16.1	16.1

2.4 Copper Slag

Copper slag is a byproduct of copper smelting that has potential use in the housing industry. It was discovered that copper slag concrete had higher tensile and comp. strengths than control concrete. The copper slag is seen in Fig. 1 and its physical characteristics are reported in Table 4.



Fig. 1. Copper slag

Table 4. Physical properties of copper slag

S. No.	Description of test	Results
1	Sp. gr	2.86
2	Hardness	7 Mohr scale
3	Conductivity m S/M	4.56
4	Chloride content	< 0.0003
5	Carbonates	Not detected
6	Sulphates	Not detected

2.5 Tannery Waste

Tannery sludge is a by-product of the leather produced through the process of tanning, which involves treating skins from animals with various chemicals. The method of tanning generates large amounts of wastewater, which contains a variety of substances, both biological and inorganic, such as proteins, fats, collagen, and salts. Tannery sludge can be difficult to dispose of due to the presence of and high organic content of heavy metals and other contaminants. Traditionally, tanneries have disposed of sludge in landfills, which can pose environmental risks such as contamination of groundwater and soil. Figure 2 shows the tannery sludge and the physical properties are listed in Table 5.



Fig. 2. Tannery sludge

Table 5. Physical characteristics of sludge

S. No.	Test	Result
1	Presence	Fine powder
2	Pigment	Grey
3	Smell	Yes
4	Fine	6.54%
5	Absorption of water	1.32%
6	Sp. gr	1.64

2.6 E-waste

The electronic waste consists of superfluous microelectronic devices like computers, smartphones and appliances. Wastes that were intended for disposal were crushed into the coarse aggregates as in Fig. 3 and are used in concrete. Table 6 shows the physical properties of electronic waste.



Fig. 3. Electronic waste

Table 6. Physical properties of E-waste

S. No.	Test	Result
1	Abrasion	3.8%
2	Impact	2.1%
3	Crushing	2.3%

(*continued*)

Table 6. (*continued*)

S. No.	Test	Result
4	Sp. gr	2.3
5	Fineness	2.5
6	Absorption of water	0.04

2.7 Methodology and Mix Proportioning

2.7.1 Methodology

Figure 4 shows the methodology implemented in this project.

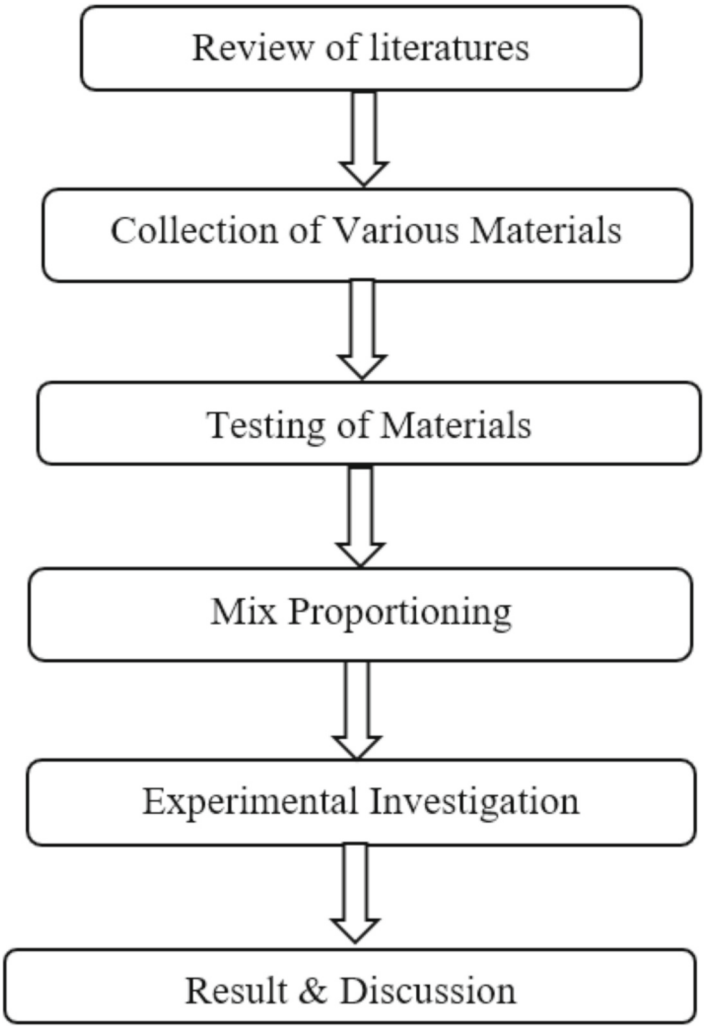


Fig. 4. Methodology

2.7.2 Mix Proportioning

The mix design for M_{20} grade concrete was performed based on the guiding principle for concrete mix design in India IS 10262 (2009). They were performed based on the characteristics of materials available and the workability of concrete. The cement content for M20 grade concrete is 300 kg/m^3, water-cement ratio of 0.6, Fine aggregate 40% of the volume, and coarse aggregate 60% of the volume. The replacement of waste materials is tabulated in Table 7.

Table 7. Mix proportions

Mix designation	Copper slag concrete		Tannery waste concrete		E waste concrete	
	Fine aggregate	Copper slag	Fine aggregate	Tannery waste	Coarse aggregate	E waste
M1	100%	0	100%	0	100%	0
M2	90%	10%	90%	10%	90%	10%
M3	80%	20%	80%	20%	80%	20%
M4	70%	30%	70%	30%	70%	30%

3 Result and Discussion

The mechanical characteristics of the concrete produced by substituting various waste sources for aggregates are discussed. The split tensile strength of concrete was measured using concrete cylinders with dimensions that were 150 mm in round and 300 mm in high, and the flexural strength was measured using concrete prisms with dimensions of 500 mm by 100 mm by 100 mm. Also, since they produce and generate less pollutants, sustainable building materials can result in a better indoor air quality. Using sustainable construction materials has a lot of potential to improve indoor air quality in buildings and has many other advantages that make interior spaces healthier and more comfortable.

3.1 Compressive Strength

The Comp. strength of concrete was found with cubes of 150 mm × 150 mm × 150 mm as per Indian Standards (IS 456 2000). Figure 5 shows the comp. strength of concrete replaced with copper slag. From the graph, it is detected that the maximum fraction of spare of fine aggregate by copper slag is 20%.

Figure 6 displays the concrete's 28-day compressive strength after using tannery sludge in place of fine aggregate. It has been noted that 10% tannery sludge spare of fine aggregate results in the greatest comp. strength. The compressive strength of concrete when coarse material is swapped with electronic trash is shown in Fig. 7. 20% is shown to be the ideal replacement rate.

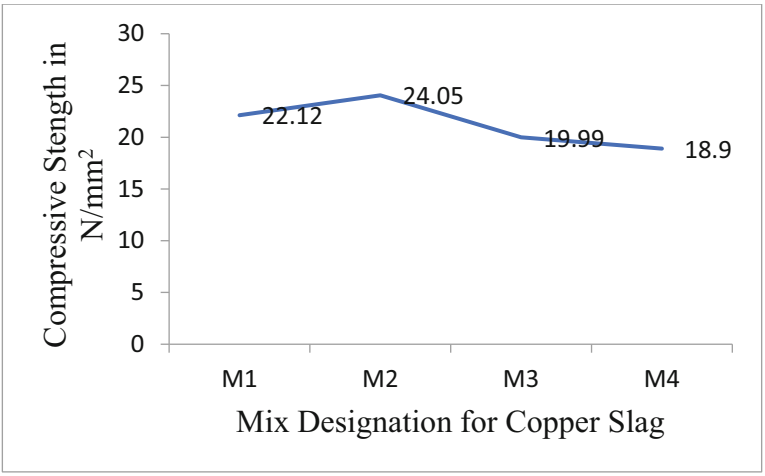


Fig. 5. Comp. strength of concrete with copper slag

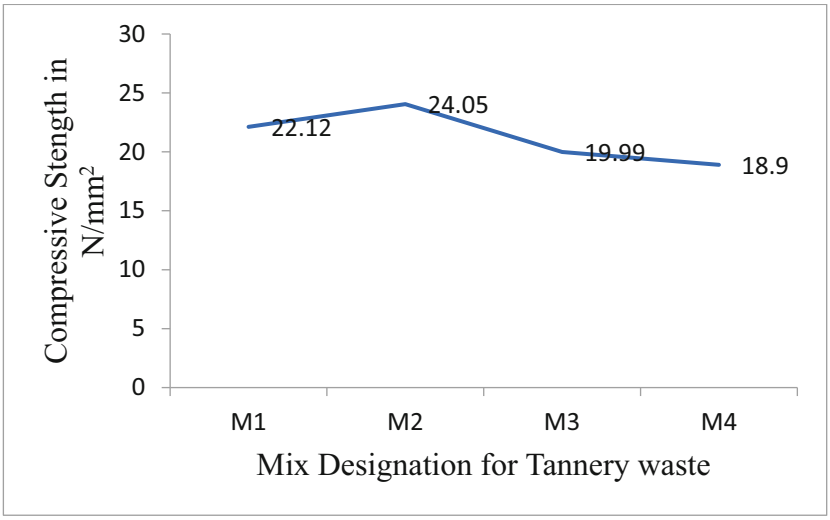


Fig. 6. Comp. strength of concrete with tannery waste

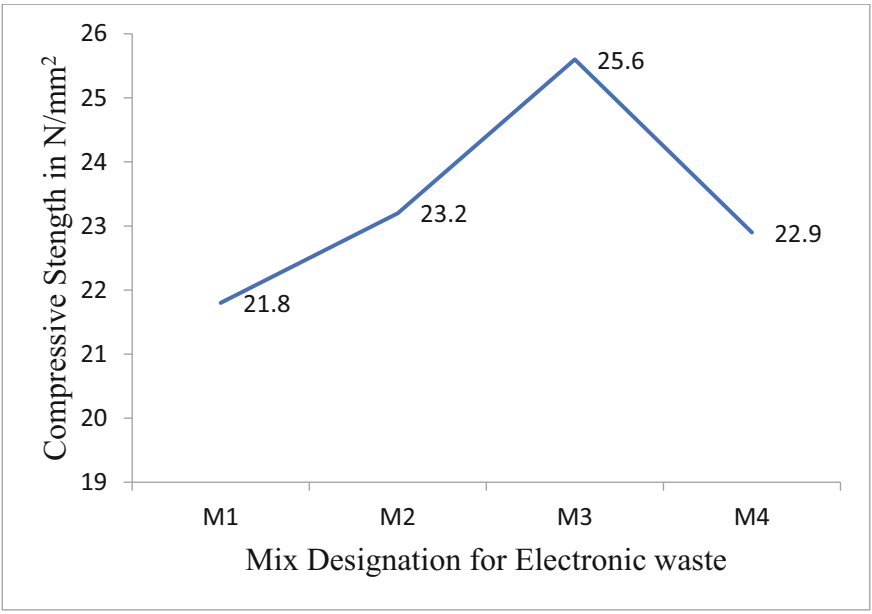


Fig. 7. Comp. strength of concrete with E waste

4 Conclusion

Experimental research on concrete replacement with varied trash in varying percentages reveals improved compressive strength. The comp. strength of the concrete increases once aggregates are replaced by waste materials due to the continued process of hydration. From the comp. strength results, it is found that by utilizing unused materials as a auxiliary for aggregates in concrete, sustainable concrete can be produced.

The enhancement in compressive strength resulting from the utilization of waste materials as aggregate replacements not only speaks to the sustainability of concrete production but also holds implications for indoor air quality. As concrete with waste materials achieves higher compressive strength, it reduces the need for traditional materials that emit volatile organic compounds (VOCs), which are known to deteriorate indoor air quality. This means that buildings constructed with sustainable concrete formulations can provide occupants with improved indoor environments, free from the harmful effects of VOC emissions.

Hence, the research not only demonstrates the feasibility of producing sustainable concrete through waste material utilization but also underscores the potential for creating healthier indoor spaces. By reducing reliance on traditional materials, this approach contributes to the overarching goal of achieving net-zero emissions while simultaneously enhancing the quality of indoor air for occupants.

References

Shi, C., Meyer, C., Behnood, A.: Utilization of copper slag in cement and concrete. Resour. Conserv. Recycl. **52**, 1115–1120 (2008)

Al-Jabri, K., Hisada, M.: Copper slag as sand replacement for high performance concrete. Cem. Concr. Compos. **31**, 483–488 (2009)
Kanagalakshmi, A.S., CarolineSaro, J., Jayashree, V.: Impact of using RHA and CD in replacement of cement for mix. Int. J. Comput. Eng. Res. **05**(02) (2015)
Raj, M., Vasudevan, N.: Reuse of textile and tannery sludge in concrete fine aggregates. Int. J. Sci. Res. Dev. **4**(07), 217–220 (2016)
Krishna Prasanna, P., Kanta Rao, M.: Strength variations in concrete by using E-waste as coarse aggregate. Int. J. Educ. Appl. Res. **4**(2) (2014)
IS 10262:2009: Recommended Guidelines for Concrete Mix Design. BIS, New Delhi
IS 456:2000: Plain and Reinforced Concrete—Code of Practice. BIS, New Delhi
Sunmathi, N., Padmapriya, R., Sudarsan, J.S.: Feasibility study of tannery waste as an alternative for fine aggregate in concrete. In: Sustainable Construction Materials, pp. 397–405. Springer, Singapore (2022)
Akram, A., Sasidhar, C., Mehraj Pasha, K.: E-waste management by utilization of E-plastics in concrete mixture as coarse aggregate replacement. Int. J. Innovative Res. Sci. Eng. Technol. **4**(7), 2319–8753 (2015). ISSN(Online): 2319-8753
Sunmathi, N., Padmapriya, R., Sudarsan, J.S., Nithiyanantham, S.: Optimum utilization and resource recovery of tannery sludge: a review. Int. J. Environ. Sci. Technol. 1–10 (2022)
Reddy, C.N.V.S., Reddy, R.D.K.: Copper slag potential for use as backfill/fill material in conventional and reinforced earth retaining walls. Indian J. Geosynthetics Ground Improv. **9**(1), 46–51 (2020)
Sudarsan, J.S., Vaishampayan, S., Parija, P.: Making a case for sustainable building materials to promote carbon neutrality in Indian scenario. Clean Technol. Environ. Policy 1–9 (2022)
Balasubramanian, B., Gopal Krishna, G.V.T., Saraswathy, V.: Investigation on partial replacement of coarse aggregate using E-waste in concrete. Int. J. Earth Sci. Eng. **09**(3), 285–288 (2016). ISSN 0974-5904
Wu, W., Zhang, W., Ma, G.: Optimum content of copper slag as a fine aggregate in high strength concrete. Mater. Des. **31**, 2878–2883 (2010)
Manjunatha, M., Reshma, T.V., Balaji, K.V.G.D., Bharath, A., Tangadagi, R.: The sustainable use of waste copper slag in concrete: an experimental research. Mater. Today Proc. **47**, 3645–3653 (2021)
Chen, S., Lu, P., Bie, Y., Wang, L., Guo, L.: Mechanical properties and micro mechanism of alkali-activated tannery sludge/fly ash composite cement-based recycled concrete. Constr. Build. Mater.**391**(8) (2023)
Ramesh, S., Mageshkumar, P., Thilagam, S., Nandhini, K.: Utilisation of tannery sludge in building construction. Int. J. Adv. Sci. Eng. **3**(4), 451–454 (2017)
TamilThendral, V., Sachin Anand, K., Shandra Banu, K., Thirumoorthy, B.: Experimental investigation on tannery waste with partial replacement of coarse aggregate in concrete. Int. Res. J. Eng. Technol. **6**(3), 7039–7041 (2019)
Karthikeyan, M., Asha, B., Raja, R.P.: Application of fine aggregate by replacement of tannery dry sludge in concrete. Int. J. Appl. Environ. Sci. **9**, 2805–2815 (2014)
Ahirwar, S., Patidar, V., Malviya, P., Singh, V.K.: An experimental study on concrete by using E-waste as partial replacement for coarse aggregate. Int. J. Sci. Technol. Eng. **3**, 7–13 (2016)
Angure, S.L., Maru, S.: An experimental study on concrete containing e-Waste and fly ash. Int. J. Sci. Technol. Eng. **4**(1), 168–172 (2017)
Ahmad, J., Majdi, A., Deifalla, A.F., Isleem, H.F., Rahmawati, C.: Concrete made with partially substitutions of copper slag (CPS): a state art of review. Materials **15**(15) (2022). https://doi.org/10.3390/MA15155196
Al-Jabri, K.S., Al-Saidy, A.H., Taha, R.: Effect of copper slag as a fine aggregate on the properties of cement mortars and concrete. Constr. Build. Mater. **25**(2), 933–938 (2011). https://doi.org/10.1016/J.CONBUILDMAT.2010.06.090

Eštoková, A., Wolfová Fabiánová, M., Ondová, M.: Concrete structures and their impacts on climate change and water and raw material resource depletion. Int. J. Civ. Eng. **20**(6), 735–747 (2022). https://doi.org/10.1007/S40999-022-00701-8/TABLES/6

Phiri, T.C., Singh, P., Nikoloski, A.N.: The potential for copper slag waste as a resource for a circular economy: a review—part I. Miner. Eng. **180**, 107474 (2022). https://doi.org/10.1016/J.MINENG.2022.107474

Suthar, L., Kansara, P., Gupta, R., Goswami, G.: Pollution due to cement dust. Int. J. Eng. Res. Technol. **2**(3) (2018). https://doi.org/10.17577/IJERTCONV2IS03019

THE 17 GOALS|Sustainable Development (n.d.). Retrieved 16 Dec 2023, from https://sdgs.un.org/goals

Wrzesińska-Jędrusiak, E., Czarnecki, M., Kazimierski, P., Bandrów, P., Szufa, S.: The circular economy in the management of waste from leather processing. Energies **16**(1), 564 (2023). https://doi.org/10.3390/EN16010564



Multiple-Degradation CID:IQ Dataset

Vikas Wasson[1(✉)], Bikrampal Kaur[2], Suniti Dutt[3], and Simarpreet Kaur[4]

[1] Chandigarh University Gharuan, Mohali, India
vikaswasson.cse@gmail.com
[2] CSE, CEC Landran, Mohali, India
[3] NITTTR, Chandigarh, India
[4] ECE, Chandigarh University Gharuan, Mohali, India

Abstract. This work introduces a novel Image Quality Assessment (IQA) dataset designed to mirror real-world scenarios by incorporating diverse and mixed image degradations. Unlike existing IQA datasets that primarily focus on single types of distortion, this dataset encompasses a wide spectrum of real-world challenges, including noise, blur, compression, and colour gamut mappings. This comprehensive approach aims to better reflect the complexity of images encountered in everyday life and addresses the limitations of conventional IQA models. By providing a multifaceted benchmark, this dataset facilitates the development of robust and versatile IQA algorithms, ultimately improving the accuracy and applicability of image quality evaluation in various practical domains.

Keywords: Image dataset · Image quality assessment · Mixed image degradation · Multiple image degradation

1 Introduction

The collection, transmission, and storage of digital media have all increased dramatically in recent years. The Cisco Annual Internet Report (www.cisco.com/c/en/us/solutions/collateral/executive-perspectives/annual-internet-report/white-paper-c11-741490.html) projects that by 2023, around two thirds of the world's population will have access to the Internet. The percentage of people utilizing the Internet worldwide will rise from 51% (3.9 billion users) in 2018 to around 66% (5.3 billion users) by 2023. As a result, there is an increasing need for accurate and efficient criteria for evaluating the image/video quality in order to monitor, preserve, and save the visual media data.

One common belief is that HVS or the Human Visual System is most widely used sensory organ in the body for obtaining information about the external world (Lambrecht et al. 1996). It alludes to the human visual perception that assessment researchers mimic. The image sensor or camera, sometimes referred to as the eye, the transmission path, or optic nerve, and the image data processing unit, or brain, are the main components of the HVS. The primary goal of many imaging applications is to facilitate the perception of the visual data contained in a picture by any human observer. Thus, it is essential to understand the HVS.

© The Author(s), under exclusive license to Springer Nature Singapore Pte Ltd. 2026
M. Kumar et al. (Eds.): HSFEA 2023, LNCE 899, pp. 191–205, 2026.
https://doi.org/10.1007/978-981-92-3200-0_17

The range of image and video handling methods that produce observable replicas of real life includes techniques for acquiring, enhancing, and interacting with images and videos (Chin et al. 1999). Such methods are typically designed as a trade-off among the perceived quality results and the technological resources. As it consistently produces exceptional true scene statistics, it is biased to expect a particular quality level from its digitally apparent representation. However, there are a number of factors that might affect image quality, including taking, sending, and presenting the image or video. The visual material is disturbed by these affecting components, which lowers the perceived quality. This kind of situation is frequently brought about by the visible scene's naturalness being impacted, changing some of its constituent parts. Every unique visual medium goes through a number of processing stages, including capturing and rendering, sending, compressing, and so on. The three processes—capturing, compression, and transmission—that images frequently go through before being seen to end users are shown in Fig. 1.

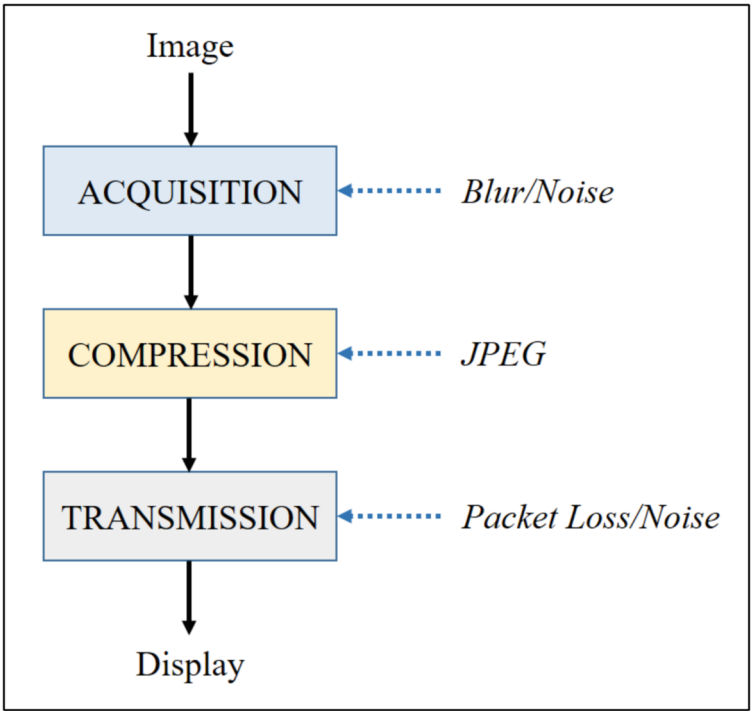


Fig. 1. Three processing stages of visual media

The aforementioned phases have the potential to modify the data and impact its visual quality. All of the aforementioned procedures, as shown in Fig. 1, result in observable artifacts in the images, which lowers the level of satisfaction for users who desire the best possible quality images. Figure 2 illustrates the effect of blurring during image capture.The blur effect of the camera lens or variations in the atmosphere can cause

blurring. The figure shows that when compared to the original images, the Gaussian blurred images are visibly lower quality. Figure 2 clearly illustrates how JPEG compression degrades quality. It is essential to conserve bandwidth and send images with smaller file sizes during transmission. Thus, before transmitting the image, it may be compressed to conserve bandwidth. JPEG compression may greatly shrink the size of an image file, but it also degrades the image quality. When we examine the actual and deteriorated images in Fig. 2, this becomes evident. Figure 2 shows the noise impact during the transmission step. The CID:IQ dataset is the source of all of these images (Liu et al. 2014).

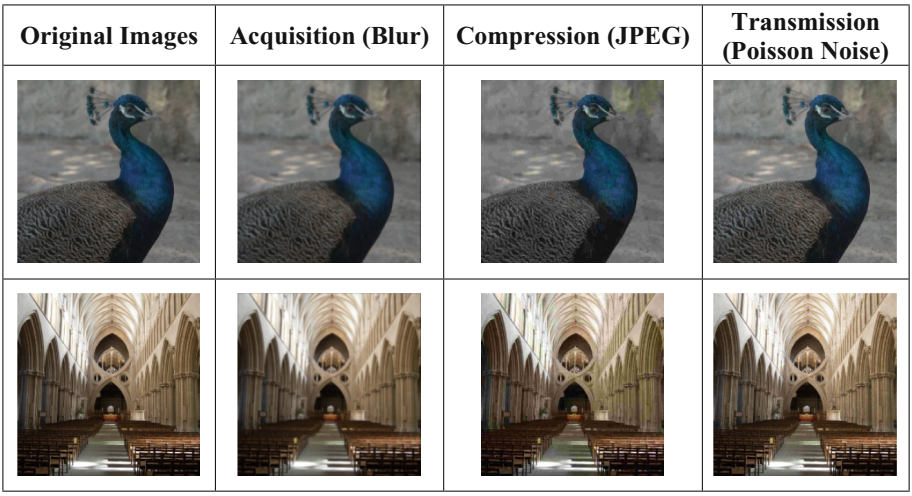


Fig. 2. The effect of blurring during image acquisition, JPEG compression and transmission

The need for images and videos with high digital content has grown significantly over the past few decades. Simultaneously, there is a massive surge in basic image processing processes related to transmission and capture. Before reaching the end consumers, images frequently go through a number of life cycle processing stages, such as capture, transmission, and compression. As a result, the final images may have a variety of distortions, including blur, blocking effects, noise, ringing, etc. An Image Quality Assessment (IQA) measure that continuously checks and aids in improving the quality of these digital images is essential for giving inputs to many practical scenarios using them. Given that an HVS is a digital image's ultimate viewer or end user, the IQA metrics developed must align with the quality standards specified by the HVS system.

With the development of technology comes a growing need to confirm if the most recent technologies can yield images of higher quality than those of the past. IQA techniques may be categorized as: subjective and objective. The former assessment is the process of predicting a quality score using a group of human observers, whereas objective evaluation uses automated computer techniques. While objective evaluation does not always require human assessors, subjective evaluation is carried out by people.

The Objective evaluation might include certain IQ indicators or need the use of measuring apparatus to acquire values.

2 Literature Review

The researchers use multiple IQA datasets for assessing the image quality. The next paragraphs outline the features of certain well-known IQA that are now in use, emphasizing the quantity of photos, their formats and sizes, the kinds of distortions, and the number of subjective assessors:

- IRCCyN/IVC Dataset—The ten control images in the IRCCyN (Institut de Recherche en Communications at Cybernétique de Nantes)/IVC Dataset were created experimentally and comprise four different types of intentional warping: JPEG, JPEG2000, LAR (Locally Adaptive Resolution), blurring, and coding. After each degradation is used at five intensities and optimized to fairly cover all the subjective scales, 185 test images are produced. Every image is stored as a BMP file with a resolution of 512 × 512 (Callet 2005) pixels. The image dataset is strongly supported by the subjective assessments of fifteen observers.
- A popular dataset for evaluating the image quality is the CSIQ (Categorical Image Quality) Dataset, which includes 30 reference pictures and 866 degraded pictures. The thirty reference pictures, which feature people, animals, cities, countryside, and vegetation, were collected from various public domain sites. Thirty reference images are first processed via six distinct distortions at four to five different levels to produce eight hundred sixty-six distorted images. Subjective quality rating scores, or DMOS (Difference Mean Opinion Score), are also included in the dataset. Thirty-five experienced observers who were holding 1920 × 1200 LCDs (Liquid Crystal Displays) at a viewing distance of seventy centimeters were used to get these results (Larson et al. 2010).
- MICT Dataset—The MICT quality evaluation dataset was created by the University of Toyama's MICT (Media Information and Communication Technology) Lab by randomly applying JPEG and JPEG2000 distortions to 14 images. In an experiment, seven different degrees of distortion are applied to 14 reference images, resulting in 168 warped images total—84 compressed by JPEG standard and 84 by JPEG2000 standard. The images are fully colored and stored at 768*512 pixels (http://mict.eng.utoyama.ac.jp/mictdb.html). The subjective quality assessments of sixteen different observers support the dataset as well.
- A57 Dataset—The Cornell University in the United States produced the A57 image collection in an experimental manner. The collection contains three reference images. Three different levels of six different distortions are applied experimentally to every reference image. As a result, 54 distorted images are produced. All images are stored in 512 by 512 pixel grayscale BMP (BitMaP) format. The subjective quality rating results from seven certified observers (Chandler et al. 2007) further validate the dataset.
- Wireless Imaging Quality (WIQ) Dataset—This dataset was created by Radian Communication Group following several experiments conducted at the Western Australian Telecommunications Research Institute. This collection contains twelve reference

pictures. The reference pictures are experimentally degraded by applying five degradation potencies from the DWT (Discrete Wavelet Transform) or Complex Wavelet. Each and every image is captured in the grayscale BMP format with 512 × 512 pixels. This dataset is accompanied with the subjective quality scores that were gathered from 14 observers (Engelke et al 2009, 2010).

- The LIVE Dataset—The LIVE (Laboratory for Image & Video Engineering in USA) dataset for quality evaluation produces 779 warped pictures from 29 reference images using five different degradations: JPG, JPG2000, White Noise, Bit errors, and Gaussian Blur in the JPG2000 data stream. Every image has a colored BMP format. Strong supporting data for the dataset comes from subjective quality assessments, which were gathered as a collection of DMOS scores from 161 different observers (LIVE Image Quality Assessment Dataset Release 2: Sheikh 2006).
- TID2008 (Tampere Image Dataset 2008) Dataset—Twenty-five colored reference photos are included in the TID2008 image quality dataset. Of these 25, twenty-four were obtained from cropping the Kodak dataset, while the twenty-fiveth was created through artificial means by synchronizing the other twenty-four shots. Each image in the TID2008 collection is always 512 × 384 pixels for compatibility with computer screens. There are seventeen distinct types of degradations present in the reference pictures. All degradations are applied experimentally at four different strengths to get a total of 1700 warped images. The dataset is well supported by the 838 observers' subjective quality scores (Ponomarenko et al. 2009).
- TID2013 Dataset—This is an expansion of the TID2008 dataset. Using the dataset's 25 reference photos, 3000 test images were created experimentally. There are 24 different forms of distortion in all the reference photographs, and each type has five levels of distortion. The dataset photographs are also provided together with the MOS subjective quality ratings, which are obtained from experiments with 985 participants from different countries. All of the images in the TID2013 dataset have a fixed size of 512 × 384 pixels in order to be seen on computer displays (Ponomarenko et al. 2015).
- CID:IQ Dataset—The CID:IQ Dataset (Liu et al. 2014) accounts for noise, blurring, compression artifacts, and gamut mapping artefacts; it also forms the basis of this investigation. As the main source of uncertainty in data obtained with the aid of high-performance sensors found in color digital cameras, Poisson noise was utilized for the noise category while JPEG and JPEG2000 compression methods were selected in CID:IQ for the compression artefacts category. Gaussian blur is the selected form of blurring. CIE (Keelan 2002) proposed that two gamut mapping techniques, constant hue minimum E and SGCK gamut mapping, ought to be taken into account when evaluating gamut mapping algorithms in the gamut mapping artifacts domain.

Table 1 summarizes the various image datasets discussed till now.

Table 1. Highlights of standard IQA image datasets

Dataset name	Resolutionof images (pixels	Number of reference Images	Number of distortions	Number of distorted images	Number of Subjective Observers	Formatof Images	Method for Subjective Evaluation
IRCCyN/IVC Dataset (Callet 2005)	512*512	10	5	185	15	BMP	DMOS
CSIQ Dataset (Larson et al. 2010)	512*512	30	6	866	35	PNG	DMOS
MICT Dataset (http://mict.eng.utoyama.ac.jp/mictdb.html)	768*512	14	2	168	16	BMP	RAW
A57 Dataset (Chandler et al. 2007)	512*512	3	6	54	7	Gray	MOS
WIQ Dataset (Engelke et al. 2009, 2010)	512*512	7	5	80	60	Gray	MOS
LIVE Dataset (http://live.ece.utexas.edu/research/quality: Sheikh et al. 2006)	768*512	29	5	779	161	BMP	DMOS
TID2008 Dataset (Ponomarenko et al. 2009)	512*384	25	17	1700	838	BMP	MOS
TID2013 Dataset (Ponomarenko et al. 2015)	512*384	25	24	3000	971	BMP	MOS
CID:IQ Dataset (Liu et al. 2014)	800*800	23	6	690	17	BMP	MOS

3 Choice of CID:IQ Dataset

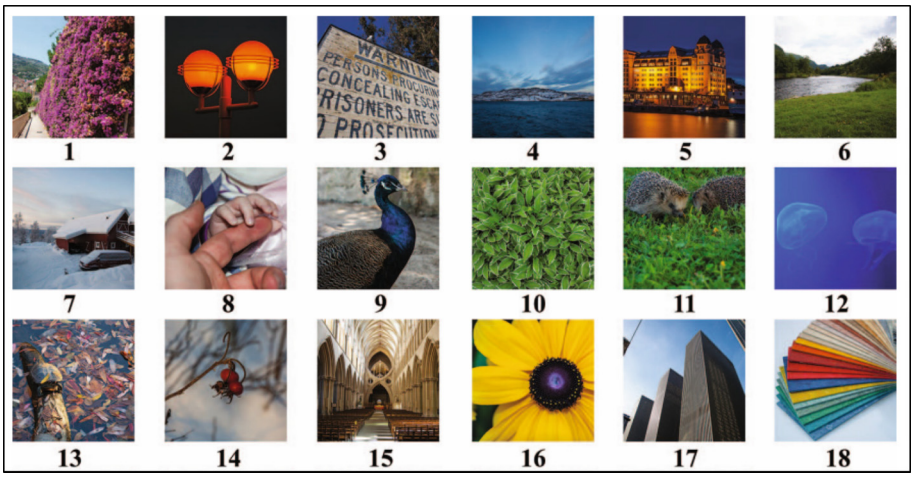


Fig. 3. Reference images in CID:IQ dataset (Liu et al. 2014)

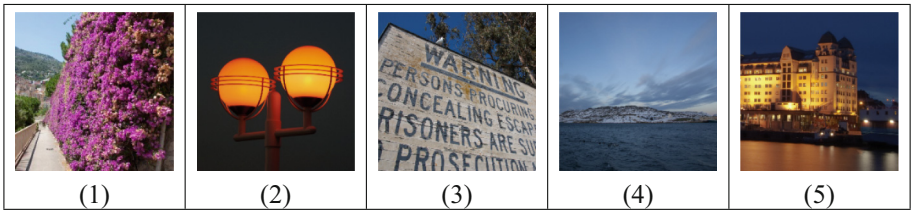


Fig. 4. (1)–(5) CID:IQ dataset: test (reference) images

The CID:IQ dataset (Liu et al. 2014), was chosen for creation of the expanded dataset, which comprises of 690 degraded photos produced by utilizing 23 high-quality reference images. The original pictures of the CID:IQdataset are depicted in Fig. 3. The first five original test photos from the CID:IQ dataset are displayed in Fig. 4 without distortion. These images will be utilized for new dataset creation. In CID:IQ, six distinct distortions are produced by applying the Poisson and Gaussian noises, two gamut mapping degradations (DeltaE and SGCK), and the compressions of JPEG and JPEG2000, over five intensities (from a lower quality degradation intensity to a higher intensity). CID:IQ has the subjective evaluations of 17 observers.

There were many rationales for selecting the CID:IQ dataset:

- To begin with, reference photos are crucial for Full-Reference IQA (FR-IQA). On the other hand, the original images in datasets such as LIVE, IVC, TID2008, etc.

were scanned copies of their negatives. When compared to modern digital photos, this produces images of poor quality.

- Secondly, although having higher quality photos, some datasets, like CSIQ, have the disadvantage of having less color and spatial information (Larson et al. 2010; Anand et al. 2017).
- Furthermore, only a few forms of distortions, such blur and Poisson noise, compression artifacts, etc., are present in the majority of the aforementioned datasets. While these are the most prevalent distortions, one must also take into account color distortions, such as gamut mapping artifacts. Such color degradations are also taken into consideration by the CID:IQ (Liu et al. 2014) dataset.
- Every picture in the CID:IQdataset has a 800 pixels by 800 pixelsresolution. This is because an image's maximum width should be less than 960 pixels in order to display two pictures concurrently on a normal 1920 × 1080 resolution screen (additional pixel width accounts for image border aswell).

The test photos with the six distinct degradations applied at level 1 (lowest deterioration) are displayed in Fig. 5. Figures 5 (1–5) show compressed JPEG images at level 1, Figs. 5 (6–10) show compressed JPEG2000 images at level 1, Figs. 5 (11–15) include Poisson noise, Figs. 5 (16–20) show hazy renditions of the original image, Figs. 5 (21–25) show distorted images using ΔE gamut mapping, and Figs. 5 (26–30) show degraded images using SGCK gamut mapping at level 1.



Fig. 5. (1)–(30) CID:IQ dataset: test (degraded) images

4 Proposed Multiple-Degradation CID:IQ Dataset

Up till now, studies have been conducted to evaluate how individual aberrations affect IQ measures. However, over the course of their capture, compression, and transmission, images experience a variety of distortions in real-world situations. The requirement for a benchmark dataset including test images with various and mixed distortions is the next item to be taken into account, as indicated by the research gaps in the literature. The majority of widely used image quality datasets (Chandler 2013: Zhang 1996) covered in the literature either use one kind of degradation or contain a small number of different forms of distortions, which is seldom the situation in real life. While IQA techniques have been applied on pictures with a certain type of degradation, few applications can generate pictures with many types of distortion at the same time. Consequently, it is important to investigate the effects of mixed and multiple distortions on imaging applications utilized in practical settings.

Since the existing CID:IQ dataset images are affected using a solitary degradation alone, a new dataset is constructed to examine the impact of mixed and multiple distortions. Using reference pictures from CID:IQ collection, experiments are conducted in MATLAB. These reference pictures are degraded with several combinations of distortions, like addition of Poisson noise as well as compression to obtain one collection of multiply degraded pictures, SGCK Gamut mapping distortions as well as compression to obtain a second collection of multiply degraded pictures, Delta E mapping and Gaussian noise and compression to obtain a third collection of multiply degraded pictures, and so on. The multiple-degradation CID:IQ collection is, therefore, a novel dataset that consists of 13 different permutations of mixed and multiple degradations.

Table 2. Multiple-degradation CID:IQ dataset

Multiple-degradation CID:IQ dataset creation						
	Compression (JPEG)	Compression (JPEG2000)	Noise (Poisson)	Noise (Gaussian)	Gamut mapping (SGCK)	Gamut mapping (Delta E)
Multiple_Degraded_Image_1			✓	✓		
Multiple_Degraded_Image_2		✓		✓		
Multiple_Degraded_Image_3		✓	✓			
Multiple_Degraded_Image_4		✓	✓	✓		
Multiple_Degraded_Image_5	✓		✓			
Multiple_Degraded_Image_6	✓			✓		
Multiple_Degraded_Image_7	✓		✓	✓		
Multiple_Degraded_Image_8			✓		✓	
Multiple_Degraded_Image_9				✓	✓	
Multiple_Degraded_Image_10			✓	✓	✓	
Multiple_Degraded_Image_11			✓			✓
Multiple_Degraded_Image_12				✓		✓
Multiple_Degraded_Image_13			✓	✓		✓

The precise combinations of various degradations applied to a picture to produce multiple-degradation CID:IQ dataset is displayed in Table 2. Consequently, this suggested dataset consists of 1495 multiply-degraded images spanning five intensities of degradation (from a lower to a greater degree of quality deterioration) and 23 reference images.

The 13 degraded photos of the recently formed Multiple-Degradation CID:IQ dataset, which was created from images 1 and 3, respectively, of the normal CID:IQ dataset, are displayed in Figs. 6 and 7.



Fig. 6. Original image 1 from CID:IQ dataset and created 13 images of multiple-degradation CID:IQ dataset



Fig. 7. Original image 3 from CID:IQ dataset and created 13 images of multiple-degradation CID:IQ dataset

5 Conclusion & Future Scope

Despite the fact that there are several IQA picture datasets in the literature, they still have the following drawbacks:

- There aren't enough degradations covered by these.
- Unlike real-world issue scenarios, these do not include several or mixed distorted images for experimenting.

MATLAB was utilized for conducting experiments with reference images that were degraded with various combinations of distortions from CID:IQ dataset. The multiple-degradation CID:IQ dataset is a newly created dataset comprised of thirteen different combinations of mixed and multiple distortions.

The majority of currently used IQA metrics are built to rely on grayscale image attributes. Such grayscale IQA metrics frequently underestimate the visual disturbance brought on by chromatic distortions, such as the degradation brought on by tone mapping or colour gamut mapping algorithms, despite their reasonable performance in dealing with traditional degradations (for instance, additive White Noise or Gaussian blur). The current proposed dataset can be used for evaluating the quality of real-world application images including the ones used for medical sciences, agriculture domains other and real-world problems. The proposed dataset is having the potential to examine the effective block-size for implementing intelligent filters for various image processing applications.

References

Cisco annual internet Report—Cisco Annual Internet Report (2018–2023) White Paper (2022) Cisco. Available at: https://www.cisco.com/c/en/us/solutions/collateral/executive-perspectives/annual-internet-report/white-paper-c11-741490.html. Accessed: 14 January 2024

van den Branden Lambrecht, C.J.: A working spatio-temporal model of the human visual system for image restoration and quality assessment applications. In: 1996 IEEE International Conference on Acoustics, Speech, and Signal Processing Conference Proceedings [Preprint]. https://doi.org/10.1109/icassp.1996.547739

Chin, Y.-J., Berger, T.: A software-only videocodec using pixelwise conditional differential replenishment and perceptual enhancements. IEEE Trans. Circuits Syst. Video Technol. **9**(3), 438–450 (1999). https://doi.org/10.1109/76.754773

Liu, X., Pedersen, M., Hardeberg, J.Y.: CID:IQ—a new image quality database. In Lecture notes in computer science, pp. 193–202 (2014). https://doi.org/10.1007/978-3-319-07998-1_22

Camera Image Quality Benchmarking | Wiley Online Books. Available at: https://onlinelibrary.wiley.com/doi/book/https://doi.org/10.1002/9781119054504

Subjective quality assessment irccyn/IVC database. Available at: https://www.semanticscholar.org/paper/Subjective-quality-assessment-IRCCyN-IVC-database-Callet-Autrusseau/b9b1e380bf519f8068fef85eccf8e3ccdb9ebf5a. Accessed 14 January 2024

Chandler, D.M.: Most apparent distortion: Full-reference image quality assessment and the role of strategy. J. Electron. Imaging **19**(1), 011006 (2010). https://doi.org/10.1117/1.3267105

MICT Image Quality Database.: QUALINET Databases (2020). Available at: https://qualinet.github.io/databases/image/mict_image_quality_database/

Chandler, D.M., Hemami, S.S.: VSNR: A wavelet-based visual signal-to-noise ratio for natural images. IEEE Trans. Image Process. **16**(9), 2284–2298 (2007). https://doi.org/10.1109/tip.2007.901820

Engelke, U., et al.: Reduced-reference metric design for objective perceptual quality assessment in wireless imaging. Sig. Process. Image Commun. **24**(7), 525–547 (2009). https://doi.org/10.1016/j.image.2009.06.005

Wireless Imaging Quality (WIQ): Vision dataset Wireless Imaging Quality (WIQ) | Vision Dataset. Available at: https://mldta.com/dataset/wireless-imaging-quality-wiq/

Live Image Quality Assessment Database.: QUALINET Databases (2020). Available at: https://qualinet.github.io/databases/image/live_image_quality_assessment_database/

Sheikh, R., Sabir, M.F., Bovik, A.C.: A statistical evaluation of recent full reference image quality assessment algorithms. IEEE Trans. Image Process 3440 (2006)

Ponomarenko, N., et al.: TID2008—a dataset for evaluation of full-reference visual quality assessment metrics. Adv. Modern Radio Electron. **10**, 30 (2009)

Ponomarenko, N., et al.: Image dataset TID2013: peculiarities, results and perspectives. Sig. Process. Image Commun. **30**, 57 (2015)

Keelan, B.W.: Handbook of Image Quality: Characterization and Prediction. Marcel Dekker, New York (2002)

Saha, A., Jonathan Wu, Q.M.: Full-reference image quality assessment by combining global and local distortion measures. Elsevier Int. J. Sig. Process. **54**, 330 (2016)

Chandler, D.M.: Seven challenges in image quality assessment: past, present, and future research. Int. Schol. Res. Notices (2013)

Zhang, X., Wandell, B.A.: A spatial extension of CIELAB for digital color image reproduction. In: Soc. Inform. Display 96 Digest, San Diego, CA, p. 731 (1996)

Anand, G., Nippani, S.K, Kuchhal, P., Vasishth, A. Sarah, P.: Dielectric, ferroelectric and piezoelectric properties of $Ca_{0.5}Sr_{0.5}Bi_4Ti_4O_{15}$ prepared by solid state technique, Ferroelectrics, p. 516 (2017)

Van den Branden Lambrecht, C. J., Verscheure, O.: Perceptual quality measure using a spatiotemporal model of the human visual system. In: Proceedings of SPIE, the International Society for Optical Engineering/Proceedings of SPIE, 2668, pp. 450–461 (1996). https://doi.org/10.1117/12.235440

Le Callet, P., Autrusseau, F.: Subjective quality assessment IRCCyN/IVC database (2005)

Larson, E.C., Chandler, D.M.: Most apparent distortion: full-reference image quality assessment and the role of strategy. J. Electron. Imaging **19**(1) (2010)

Engelke, U.: Framework for optimal region of interest–based quality assessment in wireless imaging. J. Electron. Imag. **19**(1), 011005 (2010). https://doi.org/10.1117/1.3267097

Author Index

A
Ahluwalia, Divya 128
Anjum, Shahroz 128
Aravind Kumar, A. 1

B
Bansal, Sumit 64
Bhadane, Dimple 117

C
Chavan, Guruprasad Ajay 22

D
Dutt, Suniti 191

G
Goyal, Nishu 117

H
Hothi, Navjot 160

J
Jain, Siddharth 88, 102

K
Kaur, Bikrampal 191
Kaur, Simarpreet 138, 191
Kottangal, Achuthy 49
Kumar, Harmesh 88, 102
Kumar, Rakesh 1
Kumar, Sunil 64, 88, 102

M
Mehta, Charu 1

P
Padmapriya, R. 175
Patidar, Atul Kumar 149

R
Ray, Srishti Sinha 117
Ruchi, 138

S
Sanasam, Jinata 77
Savoikar, Purnanand 22
Saxena, Vandana 32
Sharma, Priyanka 168
Shoeb, Mohammad Ahmad 1
Singh, Rahul Kumar 149
Sinha, Swati 175
Sorum, Neero Gumsar 77
Srivastava, Anushree 32
Srivastava, Atul 32
Sudarsan, J. S. 175
Sunmathi, N. 175

T
Tiwari, Mahesh Kumar 1

W
Wasson, Vikas 138, 191

Y
Yein, Nilakshi 168
Yeole, Niteen R. 10

© The Editor(s) (if applicable) and The Author(s), under exclusive license to Springer Nature Singapore Pte Ltd. 2026
M. Kumar et al. (Eds.): HSFEA 2023, LNCE 899, p. 207, 2026.
https://doi.org/10.1007/978-981-92-3200-0